AN APPROACH TO ERADICATE THE EFFECTS OF ATMOSPHERIC VARIATIONS ON TOTAL STATION DISTANCE MEASUREMENT IN A SURFACE MINE ENVIRONMENT.

The impact of taking measurement through a glass medium

Thomas Busuyi AFENI

Volume I

A thesis submitted to the Faculty of Engineering and the Built Environment, University of the Witwatersrand, Johannesburg, in fulfilment of the requirements for the degree of Doctor of Philosophy in Engineering (Mining)

Johannesburg 2011

DECLARATION

I declare that this thesis is my own, unaided work. It is being submitted for the Degree of Doctor of Philosophy in Engineering in the University of the Witwatersrand, Johannesburg. It has not been submitted before for any degree or examination at any other University.

....

(Signature of candidate)

..........................day of ....(year).....................................

at...

ABSTRACT

Total stations are used extensively for taking geodetic and engineering survey measurements. These measurements are made possible by accurate observation of targeted points. One example is deformation surveys (slope stability monitoring) in mines. Continuous monitoring necessitates sheltering or housing the instrument to protect it against harsh weather conditions that are characteristic of mining environments. This research was carried out to investigate and propagate the effects of atmospheric variations and how these impact on total station observations taken through a shelter (window) glass in a surface mine environment.

Tests and analysis were performed at the University of the Witwatersrand by setting up a total station permanently in a shelter with removable window glass of different properties (thickness, colour and shape). The data collected was subjected to the atmospheric corrections formulae proposed by the instrument manufacturer. The results can be summarized as follows:

- Current formulae for systematic survey error corrections adequately compensate for atmospheric parameters variation during distance measurements when measurements are not taken through glass.

- The research established that the properties of glass matter when taking total station distance measurements through a closed glass. The glass has little or no impact on vertical distance measurements but its impact on horizontal distance measurements increases as glass thickness and tint (colour) increase. The impact remains unchanged after atmospheric corrections formulae are applied which require additional error propagation.

- The research also revealed that glass thickness of less than 3.0 mm has no effect on the accuracy specification limits of the instrument, while a thickness of more than 3.0 mm causes errors in horizontal distances observed through the glass regardless of different angles intersecting the glass.

- There is also positive correlation between the expected error and the colour of the glass.

- The shape of the glass has an impact on distance measurements. However, it is advisable to use only flat glass for total station observation windows; otherwise further research must be carried out to model the impact of the glass shape.

- The distance between the total station and the observation window has no impact on distance accuracy. However, it is advisable to keep the distance between the total station and the observation window as short as practical.

Therefore, distance measurements through any glass medium must either be avoided or the distance must be corrected. If distance must be measured through a glass medium, the properties of the glass material must be carefully considered when selecting the glass for the observation house sheltering the total station.

This thesis develops a systematic error correction formula to remove the impact of glass thickness on distance measurements. A second formula is proposed to cater for the effect of tinted glass on horizontal distance measurements. The formulae are tested on new set of distance readings taken at the University campus and in an open pit mine to evaluate their effectiveness. The results indicate that all horizontal distances measured through glass accurately conform to the accuracy limits specification of the total station after applying the developed glass impact correction formulae. The propagation formulae were also incorporated in software called *Agcomo,* which can be used to propagate total station systematic errors at mines during monitoring surveys. The software performs well in removing both the atmospheric variations impact and the glass properties impact on distance measurements. It has the advantage of performing atmospheric corrections alone or combine atmospheric and glass corrections when the need arises. The propagation formulae were also used to develop nomograms for field observation corrections in lieu of the software programme.

ACKNOWLEDGEMENTS

First and foremost, I want to thank Coaltech Research Association and School of Mining Engineering, University of the Witwatersrand for funding this research project. I am heartily grateful to my supervisor, Professor Frederick Cawood, whose encouragement, supervision and support from the preliminary to the concluding level enabled me to develop a better understanding of this research. It would have been next to impossible to write this thesis without his help and guidance. Thanks for giving me the privilege to learn under you.

I would like to thank Thapelo Agus who assisted me in the coding aspect of the *Agcomo* software developed in this thesis. I also want to express my appreciation to Professor Jean Rueger for his contribution in the literature aspect of the thesis. The members of staff of the School of Mining Engineering have contributed immensely to my personal and professional growth at Wits. I am especially grateful to Professor Richard Minntt and Professor Huw Philips for their moral and financial support when things were tough during the initial stage of my PhD program. I would like to acknowledge David Wilson - my professional fellow – as well as Naani Mphathiwa and Sanisha Naidoo for helpful discussions. I also want to thank the entire staff of Geosystems Africa in Midrand, for their technical services and relevant discussions on total station survey instruments.

My time at Wits was made enjoyable in large part due to the many friends and colleagues that became part of my life. I am grateful to Jide Popoola, Kayode Osasan, Isaac Popoola, Victor Akinbinu, James Adewumi, Gafar Oniyide and all the members of Dominion Family Church pastorate for the wonderful times we shared.

Finally, it is a pleasure to thank my parents for all their love and encouragement. I also owe my deepest gratitude to my loving, supportive, encouraging and patient wife Kemi and my loving children Ifeoluwa, Gbolahan and Boluwatife for their support and prayers at all time. Above all, I thank the Omnipresent God, for answering my prayers and for giving me the strength to complete this program.

DEDICATION

“When you pass through the waters, I will be with you; And through the rivers, they shall not overflow you. When you walk through the fire, you shall not be burned, Nor shall the flame scorch you”.

Isaiah 43:2

This work is dedicated to the Almighty God and my loving kids Ifeoluwa, Gbolahan and Boluwatife.

TABLE OF CONTENTS

LIST OF FIGURES

LIST OF TABLES

ABBREVIATIONS

ABL	Atmospheric boundary layer
Agcomo	Atmospheric and glass corrections model
ALR	Adiabatic lapse rate
ASCE	American Society of Civil Engineers
ASCII	American Standard Code for Information Interchange
ATR	Automatic target recognition
CADD	Computer aided design and drafting
CM	Chamber of mines
CMC	Chamber of mines corner
CSIR	Council for Scientific and Industrial Research
DALR	Dry adiabatic lapse rate
DGN	Design
EDM	Electronic distance measurement
EGL	Guide light
ELR	Environmental lapse rate
FA	Free atmosphere
FI	Far-infrared
Geo	Geomos
GeL	Genmin laboratory
GL	Ground layer
GPS	Global positioning system
HD	Horizontal distance
Hz	Horizontal angle
IAG	International Association of Geodesy
IPTS-1948	International Practical Temperature Scale-1948
IR	Infrared radiation
ISO	International Organization of Standardization
ITS-90	International Temperature Scale-1990
IUGG	International Union of Geodesy and Geophysics
JHB	Johannesburg
LCD	Liquid crystal display
MALR	Moist adiabatic lapse rate
MIR	Middle-infrared
NIR	Near-infrared
Oreg	Oregon
PBL	Planetary boundary layer
PC	Personal computer
POB	American Journal Point of Beginning
PS	Power search
RB	Reference beacon
RL	Reflectorless total station
RSV	Remote surveying vehicle
RTS	Robotic total station
SALR	Saturated adiabatic lapse rate
SL	Surface layer
SR	Short-range
SREATM	Short range EDM atmospheric temperature model

SSD	Sum of squares of deviation
STAM	Simple two-layer atmospheric model
TB	Transfer beacon
TTM	Turbulent transfer model
UV	Ultraviolent
V	Vertical angle
VD	Vertical distance
WALR	Wet adiabatic lapse rate
WITS	University of the Witwatersrand
XIR	Extreme-infrared

SYMBOLS

c	Velocity of light in the medium
$\Delta t^{'}$	Flight time of pulse
t_R	Time of departure of pulse from the emitter gate of the instrument
t_E	Time of arrival of returning pulse at receiver gate of the instrument
C_t	Temperature correction
K	Coefficient of expansion.
Δt	Difference between the standard and field temperatures
t_s	Standardization temperature
t_f	Field temperature
α	Coefficient of thermal expansion of steel
L_f	Measured length obtained in the field,
f	Frequency of the signal
λ	Wavelength of the signal in a medium
d	Corrected distance
m	Metre
mb	Millibar
°C	Degree Celsius
%	Percentage
d'	Measured distance as appeared on the screen of the total station
n	Refractive index
c_0	Velocity of light in a vacuum
N	Refractive number or refractivity
N_{go}	Group refractivity of standard air
N_g	Group refractivity at prevailing atmospheric condition
T	Absolute temperature
t	Dry bulb temperature
P	Atmospheric pressure
e	Partial water vapour pressure
t_w	Wet bulb temperature
E	Saturation water vapour pressure
σ	Wave number
$^{'}f$	Partial pressure of water vapour in torr
$n_{tp^{'}f}$	Refractive index of moist air and dry air
n_{tp}	Refractive index dry air
M_a	Molar mass of dry air
M_w	Molar mass of water vapour
R*	Gas constant
x_w	Molar fraction of water vapour in moist air
ρ_a	Density of dry air
ρ_{axs}	Density of dry air at 15°C

ρ_w	Density of water vapour component of moist air,
ρ_{ws}	Density of pure water vapour at 20^{o}C, 1333 Pa and x_w =1
n_{go}	Group refractive index of standard air
n_{gws}	Group refractive index of air with water vapour at standard condition
cf	Correction factor as stated in equation
N_L	Group refractivity of visible and near infrared waves in ambient moist Air (i.e. refractivity of light waves),
n_L	Corresponding refractive index
h	Relative humidity
ΔD_1	Atmospheric correction
n_{ref}	Reference refractive index
C_1	First velocity correction
d_i	Distance corrected for zero and scale error
C_2	Second velocity correction
R_m	Mean radius of curvature of the spheroid
k	Coefficient of refraction
C_3	Correction for the curvature of the path of the beam
R	Radius of the earth
d_1, d_2, and d_3	Corrected distances
d_r	Distance measured with red laser (HeNe)
d_b	Distance measured with blue laser (HeCd)
A	Coefficient, dependent on wave length, pressure and water vapour pressure
d_{mw}	Microwave distance
φ	Angle of incidence of the rays (measured from the normal to the glass surface).
n_G	Refractive index of the window material
q	Specific humidity
θ	Potential temperature
θ'	Angle of incidence of the RTS with respect to the surface normal of the glass
θ_g	Angle of refraction within the glass
sd_i	Slope distance between the RTS and the glass
hd_i	Horizontal distance between the RTS and the glass
sd_g	Slope distance within the glass or distance travelled by the RTS beam through the glass
H	Heat flux,
τ	Adiabatic lapse rate
u_*	Friction velocity in cm/sec;
C_p	Specific heat of air at constant pressure;
ρ	Air density;
k	Von Karman's constant (with value of 0.4 – its dimensionless);

g	Acceleration due to gravity
U	Wind speed measured at instrument height
h_i	Instrument height in cm
z_o	Surface roughness parameter
$\underline{R}$	Net radiation –heat transfer at earth surface to the air
G	Heat flow into the ground
F	Evaporation flux i.e. latent heat lost through evaporation.
η	Bulk aerodynamical coefficient
u_h	Wind speed at height h (h = 1.5 or 2.0 m) above the surface in cm/sec
D_h	Wet-bulb depression at height h, in ^oK
D_s	Wet-bulb depression at the earth surface in ^oK
S_{dw}	Downward short wave radiation (0.3 µm to 4 µm)
S_{uw}	Upward short wave radiation
L_{dw}	Downward long wave radiation
L_{uw}	Upward long wave radiation
S_w	Net short wave radiation
L_w	Net long wave radiation
e_A	Partial water vapour pressure in mbar at dry-bulb temperature
E_A	Saturation water vapour pressure in mbar applicable to the dry-bulb temperature
q_{SLA}	Saturation specific humidity for dry-bulb temperature at height
M	Effective molecular weight of the air (=28.9644 x 1.293 kg/m^3)
R^*	Universal gas constant
dx	Integration variable along the chord

k_r	Refraction coefficient (i.e. 0.15)
Z_A and Z_B	Zenith distance in radian
$\hat{y}$	Systematic error correction for glass thickness (m); and
x	Glass thickness
k'	Combined correction factor for atmospheric variation and glass thickness effect
$\hat{y}'$	Systematic error correction for glass colour
x'	Glass colour or glass tint level
k''	Combined correction factor for atmospheric variation and glass colour effect

CHAPTER ONE

1.0 INTRODUCTION

'*Mine surveying is as essential to prudent mining operations as is the employment of skilled labour to win minerals from the earth. The technical expertise needed to accomplish this task varies with the complexity of the mining operation and the desire of the mine management to comply with regulations and good mining practice' (Solomon, et al., 1992 as compiled by Hartman, et al., 1992).*

1.1 THE THEORY OF DISTANCE MEASUREMENT

The nature of the surveying profession requires surveyors to fulfil certain legal, regulatory and/or accuracy requirements for their clients. They will classically strive to do so in an optimally cost-effective way and with the most appropriate equipment for the job at hand. This work, in most cases, requires a good understanding of and confidence in the instrumentation employed. Clients want value for money and assurance that the products of survey services deliver quality. Legislative authorities and public companies require assurance that the services rendered conform to globally accepted rules of best practice. Today, however, ease and speed of modern survey instruments result in a tendency to assume measurements are free from errors. This assumption is, of course, simply not true. Instrument verification, testing and calibration are as important today as what they were in the past (Martin, 2007). As a matter of fact, the high technological level of such equipment requires high-level skills for understanding the operation and on-board processing of survey measurements.

Distance measurement is the most fundamental of all surveying operations. Several methods of distance measurement are available; the preferred method depends on the level of accuracy required in the measurement. Surveyors have used various means to measure distance between two points in the past. These means include using parts of the human body[1], pacing[2],

---

[1] Rough estimates of distances can be made by eye, which estimates are based on experience in observing commonly used dimensions such as inch, foot and yard, etc. (Brincker & Minnick, 1995)

[2] Although pacing and time on horseback are crude methods of distance measurement, they can be used as an aid. Pacing requires no equipment. Experienced pacers can measure distances of 30 m or longer to a precision of 1:100 on a level terrain (Brincker & Wolf, 1984)

odometer[3], tacheometry (stadia reductions)[4], chains, measuring tapes[5] and electronic distance meter (EDM). Of these methods, measuring tapes and EDM are commonly used by surveyors today (Brinker & Wolf, 1984). However, no matter which method is used, there are only three basic types of distance that can be measured: slope distance, horizontal and vertical distance (while the slope distance can be measured directly, the horizontal and vertical distances are not measured directly, but derived from projections on the horizontal or the vertical planes). The factors that determine which distance is required depend on the purpose of the survey work. Distances can be measured and set out in one or two ways:

- Direct (contact with the ground) distance measurements (also called mechanical distance measurements) for example, using a tape or chain.
- Indirect (above the ground surface) measurement using optical equipment, for example, optical distance measurements or EDM.

Schofield and Breach (2007) confirmed Brinker and Wolf's statement above by saying "*the basic methods of measuring distance are, at the present time, by taping or by electromagnetic (or electro-optical) distance measurement known as EDM".*

Optical distance measurement or EDM provides significant savings in time compared to direct distance measurements because the terrain between the terminal points of the distance to be measured is of relevance only in exceptional cases. The method has high measuring speed, considerable range and high accuracy, in addition to being independent of local conditions. EDM allows measurement of lines that are difficult to access and can also measure accurately a longer distance than any other distance measuring instrument. It permits measurement of distance with precision. The accuracy of EDM is 1:10,000 to 1: 100,000 (Wirshing, *et al.*, 1985). However, a good organisation of the work and a well-functioning field crew are necessary. The two ways in which distance can be measured are illustrated in Figure 1.1 below:

---

[3] This method is easy to use and very fast, although not as accurate as using a tape measure. It is a good method of rough-checking distance measurement made by other methods. A precision of 1:200 may be expected, with greater precision on a smooth road surface (Brincker & Minnick, 1995).
[4] Tacheometry is a surveying method used to quickly determine the horizontal distance to and elevation difference to a point. A precision of 1:500 could be achieved with reasonable care (Brincker & Wolf, 1984).
[5] The act of using a measuring tape is called taping. The accuracy of taping is 1:1000 to 1: 5000. (Wirshing, *et al.*, 1985).

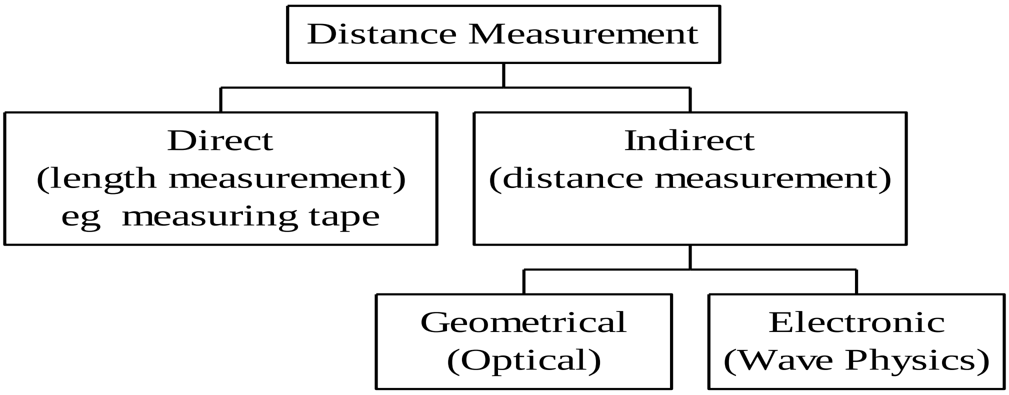

Figure 1.1: Distance measurement ways (Source: Wirshing et al, 1985).

Deumlich (1982) stated that *"the accuracy of distance measurements depends on the instruments and the methods used"*. The accuracy of the various methods of distance measurement is summarised in the table 1.1 below:

Table 1.1: Accuracy of geodetic distance measuring instruments

Instrument or Auxiliary Device	**Accuracy**
Pacing	1:50 up to 1:100
Measuring wheel, odometer	1:100 up to 1:500
Field Dividers	1:1000
Tape with alignment poles	1:1000 up to 1:3000
Rolled measuring tape	1:3000
Steel tape, fully supported with temperature and slope corrections	1:10000
Measuring rods (horizontal)	1:10000
Stadia (up to 250 m)	1:300
Stadia with wedges (up to 200 m)	1:5000
Double image tacheometer with rotating wedges (up to 200 m)	1:5000
Double image tacheometer with half lenses (up to 1000 m)	1:1000
Subtense bar and theodolite (up to 150 m without auxiliary base)	1:5000
Microwave distance meters (up to 50 km)	1:300,000
Electro-optical distance meters (up to 50 km)	1:100,000
Electro-optical distance meters for short range (up to 3 km)	1:300,000
Electro-optical precision distance meters (up to 3 km)	1:1,500,000

Source: Deumlich (1982)

This research will explore EDM accuracy in greater detail as performed by a total station surveying instrument.

In addition to mine surveyors, geomatics practitioners, engineers and developers, regulatory authorities use various parts of the surveying process in contributing to the conceptualization, design, actualization and monitoring of engineering and land development projects. Mine surveying requirements are as follows:

- Accuracy;
- Functionality;
- Integration with other methods and software;
- Productivity; and
- Ease of use.

These requirements are to ensure that the activities required by surveying processes that contribute to the project are done properly and accurately. Today, a wide variety of tools are available to the surveyor to accomplish these activities. It is no longer a matter of just having a transit, tape and dumpy level on hand. The tools themselves overlap the required functionality in some respects. It is incumbent on the surveyor to do the analysis, synthesis and integration to most effectively use the resources at hand. When the surveyor's toolbox is integrated properly, it is possible to optimize the tool to the application.

The quest for surveying precision and advancement in technology led to evolution and improvement of many instruments. Total station and Global Positioning System (GPS) are two recent survey instruments that were developed as a result of the advancement in technology and the search for precision in survey measurements (or for achieving a given specification). Equipment and methodology must be chosen to ensure that the requirements above are achieved. GPS and EDM are not free from error[6]. Several types of errors may occur and knowledge of their importance and propagation is essential in understanding the limitation of the techniques of measurement. Errors can be classified as follows:

Mistakes: These mistakes are sometimes called gross errors or blunders, often resulting from fatigue, inexperience or carelessness on the part of the surveyor. Any types of mistakes (ranging from miscounting the number of tape lengths when measuring a long distance to

[6] There are three sources of errors: people (personal errors), instrumental and natural (see Schofield & Breach, 2007 for details)

transposing numbers when booking) can occur at any stage of a survey, that is when observing, booking, computing or plotting. Such mistakes would obviously have a very damaging effect on the results if not detected. Mistakes are significant and, therefore, great care must be taken to prevent them (Schofield & Breach, 2007). It is possible to reduce the number of mistakes by following a strict and well-planned observing procedure. In practice, mistakes should never go undetected and should be eliminated.

Systematic Errors: These errors are also known as cumulative errors that magnify under constant conditions (McCormac, 1983). Systematic errors arise from sources that act in a similar manner on observations. The method of measurement, the instruments used and the environmental conditions at the time of measurement (i.e. temperature, barometric pressure and relative humidity) must all be considered. These errors are of vital importance in activities that consist of adding together a succession of individual observations, such as traversing. Systematic errors are not revealed by taking the same measurement again with the same instrument. The only way to check for systematic error adequately is to re-measure the quantity by an entirely different method using different instruments under different conditions (Bannister, *et al.*, 1998). Schofield and Breach (2007) concluded that systematic errors conform to mathematical and physical laws; thus appropriate corrections can be computed and applied to reduce their effects. It is doubtful, however, that all systematic errors can be entirely eliminated, largely due to the inability to obtain an exact measurement of the quantities involved. A typical example is the difficulty of obtaining an accurate refractive index throughout the measuring path of EDM distances, which is one of the major focus areas of this research work. Consequently, systematic errors are the most difficult to deal with and, therefore, they require very careful consideration prior to, during and after the survey.

Random Errors: All those discrepancies which remain after mistakes and systematic errors have been removed are known as random errors. If a quantity is measured many times with the same instrument in the same way, and if all sources of systematic error have been removed, it is unlikely that all results will be identical due to limitations of instruments and observers. Random errors should be small and there is no procedure that will compensate for or reduce any single error. The size and sign of any random error is unpredictable. Although the behaviour of one observation is unpredictable, the behaviour of a group of random errors becomes predictable which mean that the larger the group, the more predictable is its behaviour. For this reason, random errors are often analysed using statistical analysis of many results.

1.2 PROBLEM STATEMENT

With the advent of new generation EDM instruments for surveying, surveyors perhaps do not pay sufficient attention to the effects of atmospheric conditions under which they are carried out. These effects are unlike the past when chains and steel tapes were used and the environmental impacts were more visible in the results. The general belief is that the instrument will compensate for the effects that the variation in atmospheric conditions may pose on their readings. This belief is risky, since the instrument is like a computer; it needs human inputs in order to function well. Even when some surveyors want to pay attention to the effects of atmospheric variation on their instrumental readings they are confronted with complex equations and input parameters. Also it is general mine survey practice to mount the total station inside a protective cool shelter and take the observations through a window (covered with glass) for security reasons and fear of not wanting to expose the instrument to harsh weather conditions. This practice has its own side effects on the accurate performance of the instrument. In this research, the effects of atmospheric parameters – temperature, pressure and humidity variations on total station distance measuring was examined, also the effects of glass with varying properties was investigated. Therefore this research would benefit the mining industry, equipment vendors and research institutes. It will also contribute to making mines a safer environment if employed during continuous surveys to monitor mine slope stability or ground movement.

1.3 RESEARCH QUESTIONS

The research would address the following questions:

a. What are the effects of atmospheric variations on total station surveying instruments?
b. Which of the two types of total station EDMs (reflector and reflectorless) is affected most by these variations during distance measurement and why?
c. How effective are the atmospheric correction techniques provided by the manufacturer of the instrument?

d. What are the effects of mounting the instrument inside shelter and taking observations through a glass window?
e. Is it possible to generate any new method of dealing with atmospheric variations corrections to total station distance observation on surface mines given the circumstances under which measurement are recorded?

1.4 AIM AND OBJECTIVES OF THE RESEARCH

The aim of the research was to investigate the effects of atmospheric variations on total station distance measurement in a surface mine environment.

The objectives of the research were as follows:

a. to compare and analyse the distance measurement at varying atmospheric variations using two different methods (reflector and reflectorless) associated with total station instruments;
b. to investigate the appropriateness of current systematic error formulae for surface mines operating in environments of extreme temperature and pressure variations; and
c. to accumulate data to develop a new method to compensate for or eradicate the effects of taking observations through glass at the mine site during the deformation monitoring process alongside the general refractive index formulae.

1.5 EXPECTED CONTRIBUTION TO KNOWLEDGE

- The research would contribute to knowledge in the area of error monitoring and corrections in total station distance measurement;
- It would reveal the effectiveness of current equations generated by past authors on effects of atmospheric variations corrections, since most of these experiments were based on laboratory experiments and not on the field (mine).
- It would provide additional method(s) of dealing with atmospheric variation corrections for total station distance measurements that are more relevant to the mine survey.
- It would result in an improvement of the standard operating procedure on the use of EDM during mine surveys.
- It would allow for accurate uninterrupted monitoring data at surface mines

1.6 LAYOUT OF CHAPTERS

Chapter 1 provides the general introduction to the study. It contains background to the theory of distance measurement, introduction to measurement errors, problem statement, research questions, aim and objectives of the research, expected contribution to knowledge and a preview of the chapters in this thesis.

Chapter 2 discusses at what a total station surveying instrument is, the type of total station, specifications, mode of operation, areas of application and associated errors. The chapter also considers atmospheric variations and the distance measuring instrument; refraction and the most prominent formulae for refractive index correction in total station readings.

Chapter 3 explains the part of the atmosphere that is relevant to this study, that is the troposphere. It describes the turbulent zone and the effect of this zone on total station readings. The chapter also describes conservative parameters that are connected with the atmosphere and total station. The available atmospheric models - TTM, SREATM and STAM are discussed in this chapter.

Chapter 4 expounds on the materials used during this research. It highlights the importance of calibration of surveying instruments and discusses the pre-delivery calibration carried out on the new total station procured for this research. The chapter also explains how field data was gathered to test the validity of existing equations and models for refractive index correction.

Chapter 5 elaborates on data acquisition and processing to determine the likely impact of glass thickness on distance measurement so as to isolate the glass thickness impact from the atmospheric corrections formulae. The chapter isolates atmospheric corrections formulae from glass thickness impacts; in addition, it establishes the impact of the glass thickness on distance measurements.

Chapter 6 discusses data acquisition and processing to determine the likely impact of glass colour (tint level) on distance measurement so as to isolate the glass colour impact from the atmospheric correction formulae. The chapter also investigates the impact of the glass shape on distance measurements and the optimum distances with which the total station can be to the observation window.

Chapter 7 points the steps taken to develop systematic error correction formulae that combine corrections for atmospheric variations and impacts of observation glass.

Chapter 8 validates the systematic error correction formulae or approach to compensate for both atmospheric variations and glass impacts using data generated at the university campus and at an open pit mine. The chapter discusses procedures taken to write a computer programming and develops nomograms in conformity with the result validation.

Chapter 9 presents the general conclusions of the work. Various suggestions for future research, in relation to the glass colour impact presented in this thesis, are also made.

The Appendix contains the list of materials (tables, figures and write-ups) that are relevant to the development of this thesis.

1.7. CONCLUSION

The background to this study has shown that there are three basic types of distance that can be measured, namely: slope, horizontal and vertical distances. The accuracy depends on both the instruments used and the applied methods. The evolution in distance measuring methods has resulted in better accuracy. However, irrespective of the instrument and/or method used, surveying work is subjected to certain error. Hence, it is paramount for surveyor to know how to eliminate or reduce error sources and types.

Therefore the next chapter of this study will discuss the typical total station surveying instrument, its areas of application and its associated errors. The chapter will then expounds on the literature on atmospheric systematic error corrections typical of a surface mine environment.

CHAPTER TWO

2.0 TOTAL STATION SURVEYING INSTRUMENT AND BASIC CONCEPT OF REFRACTION

Chapter one discussed the introduction to theory of distance measurement and its associated errors. This chapter reviews total station surveying instruments, their mode of operation, associated errors, areas of application, the impact of refraction on total station distance measurements and the effect of glass on beam of Light

2.1 TOTAL STATION SURVEYING INSTRUMENT

The most difficult part of surveying operation is distance measurement, but the introduction of EDM instruments has revolutionized this (Bannister, *et al.*, 2008). EDM equipment became commercially available after Word War-II and has since then become very important to the surveying, navigation and scientific communities. Since the introduction of EDM, the instrument components, such as size and power consumption, have been reduced. The precision and speed of measurement have also improved. Because of redesigning EDM equipment to make it smaller, it made good sense to merge EDM and theodolite[7] functions in a single instrument. This redesign resulted in the development of telescopes that can precisely measure horizontal angles, vertical angles and distances to targets. Such combinations are electro-optical hybrids called "total station".

Whyte and Paul (1997), described a total station as a special-purpose instrument resembling a theodolite but capable of measuring both angles and distances by electronic methods. The instrument is now widely used for all forms of linear measurement where distances exceed a tape length with an increased speed and accuracy.

[7] A theodolite is an instrument for measuring both horizontal and vertical angles as used in triangulation networks. The name theodolite was invented by Leonard Digges in 1571 (Bannister *et al*, 1998).

According to Eiteljorg (1994), "*a total station is a combination of electric transit*[8] *(theodolite) and EDM"*. This device would enable the user to determine angles and distances from the instrument to the point to be surveyed just like the old transit and tape. Taping distance with all its associated problems has been rendered obsolete for all baseline measurement. Distance can now be measured easily, quickly and with great accuracy, regardless of terrain conditions.

Before total stations were invented, surveyors used the Tellurometer to measure distances and a theodolite (transit) to measure angles. The first EDM instrument is known as "Tellurometer". The first model of Tellurometer known as the "Micro-Distancer M/RA 1" was introduced in 1959. It was invented by Dr. Travor Lloyd Wadley of the Telecommunications Research Laboratory of South African Council for Scientific and Industrial Research (CSIR). The Tellurometer emits an electronic wave while the remote station re-radiates the incoming wave in a similar wave of more complex modulation, and the resulting phase shift was a measure of the distance travelled. The results show on a cathode ray tube with circular sweep. The instrument can penetrates haze and mist in daylight or darkness and has distance measurement range of 30 – 50 km, but can extend up to 70 km. The Tellurometer has high accuracy distance measurements over geodetic distances, but it is also useful for second order survey work, especially in areas where the terrain is rough and/or the temperatures extreme (Wright & Sturman, 2008).

The combinations of theodolite, EDM and microprocessor created the ability of electrically making simultaneous slope distance, horizontal distance, horizontal and vertical angles measurements. The measured distances and angles may be used to calculate the coordinates of actual positions (easting- X, northing – Y and elevation –Z) of surveyed points, or the position of the instrument from known points, in absolute terms using trigonometry and

[8] A transit is basically a telescope with cross-hairs for sighting a target; the telescope is attached to scales for measuring the angle of rotation of the telescope (normally relative to north as 0 degrees) and the angle of inclination of the telescope (relative to the horizontal as 0 degrees). After rotating the telescope to aim at a target, one may read the angle of rotation and the angle of inclination from a scale. The electronic transit provides a digital read-out of those angles instead of a scale; it is both more accurate and less prone to errors arising from interpolating between marks on the scale or from mis-recording. The readout is also continuous; so angles can be checked at any time (Eiteljorg, 1994).

triangulation. The data may be downloaded from the total station to an external computer and application software will generate a map of the surveyed area (Eiteljorg, 1994).

The first total stations were the Zeiss Reg ELTA 14 (released in 1970) and the AGA Geodimeter 700 (released in 1971). These instruments were large and heavy. Paper tape (like in telex machines) and cassette tapes (audio) were used for data recording. A second generation of instruments was released around 1978 by Hewlett-Packard, Wild (now called Leica) and Zeiss. Zeiss ELTA 2 being the first total station with slide-in memory modules (RAM) for data recording. Today all manufacturers of surveying instruments produce total stations because they allow the three-dimensional coordination of points from single instrument set-up (Rueger, 2003).

The American Journal Point of Beginning (POB) illustrated the trends in the purchasing of surveying instruments. In 1983, the journal listed 11 fully electronic tacheometers (total stations) while 68 different models were listed in 1994. It became obvious that total stations were replacing stand-alone theodolite and stand-alone EDM (Rueger, 2003).

Hartman et al, (1992), described the rapid development and widespread availability of electronic devices (total stations) for the direct measurement of distance. The adaptability of the instrument to mine surveying presented problems due to: its relative light weight, portability, a beam of infrared or visible light that would be reflected back to the transmitter by a suitable reflector and produce a distance reading directly without the need for data conversion by the operator. Figure 2.1 illustrates the main component of a total station.

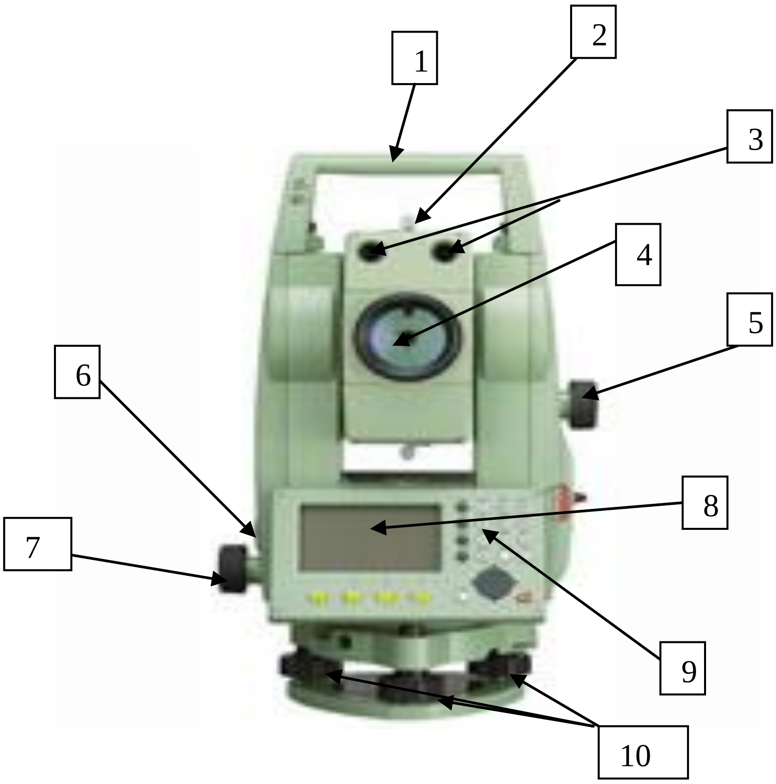

1 – Integrated, removable handle
2 – Quick sight
3 – Point guide
4 – Optical lens
5 - Vertical image adjuster
6– USB A and mini connector
7 – Horizontal image adjuster
8 – Digital screen
9 – Key pad
10 – Level screws

Figure 2.1: Photograph of a Total Station - Leica TPS800 Series (Source: Leica Geosystem).

A combination of electronic theodolite and EDM instruments allow surveyors to find the ‘space vector’ from the instrument to a distance target. Weber and Lazowick (1984) summarized the advantages of total station as follows:

> *“the introduction of total station with data recording and computer plotting capability has been an innovative advancement in the surveying industry. When a total station is connected to an electronic data recorder, field information can be quickly gathered and used to generate maps and plans in the office. Though, the application of this system is similar to conventional surveying procedures, the capability of the system exceed most traditional methods employed by surveyors. The ease of manipulation of the field data to a final product makes the system ideal for boundary, topographical and local survey”.*

Most modern total station surveying instruments measure angles by means of electro-optical scanning of extremely precise digital bar-codes etched on rotating glass cylinders or discs within the instrument. High precision total stations are capable of measuring angles down to 0.5 arc-second (1/7200 degrees). A typical example of this is the Leica TCA 2003 instrument. Low price "construction grade" total stations can generally measure angles to 5 or 10 arc-seconds; examples are: Pentax R-326EX, Sokkia T610, Topcon GPT-3000LW and Leica Builder 17.

Measurement of distance is realized with modulated microwave or infrared carrier signal, generated by a small solid-state emitter within the instrument's optical path, and bounced off from the object to be measured. The modulation pattern in the returning signal is read, interpreted and displayed by the onboard computer in the total station. The distance is determined by sending out and receiving multiple frequencies, and determining the integer number of wavelengths to the target for each frequency. Most total stations use a purpose-made glass prism as the reflector for the EDM signal, and can measure distances out to a few kilometers, but some instruments are "reflectorless", and can measure distances to any object that is reasonably light in colour, up to a few hundred meters. Examples are Leica TCR 705, TPS 400 and Pentax R-300NX. A typical example of a reflectorless total station (RL) is shown in Figure 2.2.

Figure 2.2: Leica TCR 705 Reflectorless Total Station (Source: Leica Geosystems online product site).

A typical Total Station (EDM component) can measure distances accurately to about 3 millimetres or 1/100th of a foot. The ability to measure to a reflector or even without reflector is one of the criteria used to group the instruments into two types (reflector user types and reflectorless types). Also the types of operations that can be performed on the instruments can be used to separate them into three types:

Manual Total Station: Both distance measuring and angle measuring make use of the same telescope optics (coaxial). Slope reduction of distances is done by optically reading the vertical angle (or Zenith angle) and keying it into an on-board calculator or any pocket calculator. Horizontal angles are read optically.

Semi-Automatic Total Station: Contains a vertical angle sensor for automatic reduction of distances (without keying in a slope angle). Horizontal angles are read optically.
Automatic Total Station: Both horizontal and vertical are read electronically for use with slope distances in a data collector or internal computer

Total stations went through a sort of 'psychological slump' (in the minds of users and manufacturers) when GPS grew in popularity in the late 1980s (Paiva, 2006). However, total station technology has not only continued to exist, it has been invigorated through several add-on innovations. The first was to motorize the horizontal and vertical movements so that the instrument could "reverse face" automatically. The next innovation to be added was target detection and acquisition. Finally, with the addition of a wireless (usually radio, but sometimes infrared) interface, it has become what a profession refers to as 'robotic'[9]. The modern total stations called 'robotic' (Robotic Total Station – RTS) allow the operator to control the instrument from a distance via remote control. Examples are the Trimble 5600DR and Leica TPS 1200 Professional. Such robotic total station eliminates the need for an assistant staff member to hold the reflector prism over the point to be measured. The surveyor holds the reflector him/herself and controls the total station instrument from the observed point. An automated monitoring survey system using a robotic total station removes the manual repetition factor from the survey. The robotic system is "taught" the sequence of measuring to each of the monitoring points and continues measuring at pre-set intervals. Thus the human element is removed from the task including the probability of human error (Thomas, 2003).

[9] A total-station may be called robotic if it is able automatically to follow a prism moving through 3D space; key to this feature is the communication link between base-station and prism pole (Key & Lemmens, 2008).

It is not uncommon to see some total stations with GPS interface which combines these two technologies to make use of the advantages of both (GPS - line of sight not required between measured points; Traditional Total Station - high precision measurement especially in the vertical axis compared with GPS) and reduce the consequences of each technology's disadvantages (GPS - poor accuracy in the vertical axis and lower accuracy without long occupation periods; Total Station - requires line of sight observations and must be set up over a known point or within line of sight of 2 or more known points). Figure 2.3 shows the combination of total station and GPS called "smart station"

Figure 2.3: The combination of Total Station and GPS – Smart Station (Source: Hill, 2005)

2.2. SPECIFICATIONS

Many brands of total stations are available in the market today. The six major manufacturers of total stations are presented in Table 2.1 below.

Table 2.1: Manufacturers of total station surveying instrument

Product	**Manufacturer**
Leica (Wild)	Leica Geosystem, part of the Hexagon Group Sweden
Sokkia	Sokkia Co. Ltd, Japan
Trimble	Trimble Navigation Ltd, Sunnyvale, California, USA
Pentax	Pentax Industrial Instruments Co. Ltd, Tokyo Japan
Topcon	Topcon Europe B.V., Japanese Multinational Company, Capelle, Netherland
Spectra Precision	Spectra Precision, Westminster, USA

Source: www.directindustry.com

The specification of total stations varies from one manufacturer to the other. It also depends on the types (whether reflector – using infrared radiation IR, non reflector user - reflectorless RL, or with both technology – reflector/reflectorless) of the total station in use. For this research, a Leica total station TCR1201+ was used. The specification presented in Table 2.2 is primarily for that of Leica Geosystem products TPS1200+ series. The Leica TCR1201+ used for this research belongs to this series. Therefore, the entire relevant technical specification and system features of the TCR1201+ type is highlighted in blue colour in the Table as shown below:

Table 2.2: **Leica TPS1200+ technical specifications and system features**

Models and options							
	TC	TCR	TCRM	TCA	TCP	TCRA	TCRP
Angle measurement	•	•	•	•	•	•	•
Distance measurement (IR-mode)	•	•	•	•	•	•	•
Distance measurement (RL-mode)		•	•	•	•	•	•
Motorized			•	•	•	•	•
Automatic target recognition (ATR)				•	•	•	•
Power search (PS)					•		•
Guide light (EGL)	°	°	°	•	•	•	•
Remote control unit/Radio handle	°	°	°	°	°	°	°
GUS74 Laser guide				°		°	
Smart station (ATX1230+ GNSS)	°	°	°	°	°	°	°
Key: • = standard ° = optional							

Angle measurement		**Type 1201+**	**Type 1202+**	**Type 1203+**	**Type 1205+**
Accuracy	Hz, V	1” (0.3 mgon)	2” (0.6 mgon)	3” (1 mgon)	5” (1.5 mgon)
	Display resolution:	0.1” (0.1 mgon)	0.1” (0.1 mgon)	0.1” (0.1 mgon)	0.1” (0.1 mgon)
Method	absolute, continuous, diametrical				
Compensator	Working range:	4’ (0.07 gon)	4’ (0.07 gon)	4’ (0.07 gon)	4’ (0.07 gon)
	Setting accuracy:	0.5” (0.2 mgon)	0.5” (0.2 mgon)	1” (0.3 mgon)	1.5” (0.5 mgon)
	Method:	centralized dual axis compensator			

Distance measurement (IR-mode)		
Range	Round prism (GPR1):	3000 m
(average atmospheric conditions)	360^0 reflector (GRZ4):	1500 m
	Mini prism (GMP101):	1200 m
	Reflective tape (60 mm x 60 mm):	250 m
	Shortest measurable distance:	1.5 m
Accuracy/Measurement time	Standard mode:	± 1 mm + 1.5 ppm/typ. 2.4 s
	Fast mode:	± 3 mm + 1.5 ppm/typ. 0.8 s
	Tracking mode:	± 3 mm + 1.5 ppm/typ. < 0.15s
	Display resolution:	0.1 mm
Method	Special phase shift analyser (coaxial, visible red laser)	

Table 2.2: Leica TPS1200+ technical specifications and system features continues...

Distance measurement (RL-mode)	
Range	Pinpoint R400: 400 m/ 200 m (Kodak gray card: 90% reflective / 18% reflective)
(average atmospheric conditions)	Pinpoint R1000: 1000 m/ 500 m (Kodak gray card: 90% reflective / 18% reflective)
	Shortest measurable distance: 1.5 m
	Long Range to round prism (GPR1): 1000 m – 7500 m
Accuracy/Measurement time	Reflectorless < 500 m: ± 2 mm + 2 ppm / typ. 3 – 6 s, max. 12 s
	Reflectorless > 500 m: ± 4 mm + 2 ppm / typ. 3 – 6 s, max. 12 s
	Long range: ± 5 mm + 2 ppm / typ. 2.5 s max. 12 s
Laser dot size	At 30 m: approx. 7 mm x 10 mm
	At 50 m: approx. 8 mm x 20 mm
Method	Pinpoint R400/R1000: System analyser (coaxial, visible red laser)

General data	
Telescope	**Laser plummet**
Magnification: 30 x	Centring accuracy: ± 1.5 mm at 1.5 m
Free objective aperture: 40 mm	Laser dot diameter: ± 2.5 mm at 1.5 m
Field of view: 1^{0}30' (1.66 gon) / 2.7 m at 100 m	**Endless drives**
Focusing range: 1.7 m to infinity	Number of drives: 1 horizontal / 1 vertical
Keyboard and Display	**Battery (GEB221)**
Display: ¼ VGA (320*240 pixels), graphic LCD, colour, illumination, touch screen	Type: Lithium-ion Voltage: 7.4 V
Keyboard: 34 keys (12 function keys, 12 alphanumeric keys) illumination	Capacity: 4.4 Ah
Angle display: 360^{0} ' ", 360^{0} decimal, 400 gon, 6400 mil, V%	Operating time: typ. 5 – 8 hr
Distance display: meter, int. Ft, int. Ft/inch, US ft, US ft/inch	**Weight**
Position: face I standard / face II optional	Total station: 4.8 – 5.5 kg
Data storage	Battery (GEB221): 0.2 kg
Internal memory: 256 MB	Tribrach (GDF121): 0.8 kg
Memory card: Compact Flash cards (256 MB)	**Environmental specifications**
Number of data records: 1750 / MB	Working temperature range: -20^{0}C to +50^{0}C
Interfaces: RS232, Bluetooth, Wireless – Technology (optional)	Storage temperature range: -40^{0}C to +70^{0}C
Circular Level	Dust / water (IEC 60529): IP54
Sensitivity: 6' / 2 mm	Humidity: 95%, non-condensing

Source: Leica Geosystems TPS 1200+ Series Brochure

2.2.1. Classification of EDM

EDM instruments are classified according to the type and wavelength of the electromagnetic energy generated or according to their operation range. In survey work, most instruments use infra-red radiation[10] (IR). The accuracies required in distance measurement are such that the measuring wave cannot be used directly due to its poor propagation characteristics. To overcome this, the measuring wave is superimposed on high-frequency waves called carrier waves. This superimposition can be done in three ways:

1. Amplitude modulation of the carrier wave;
2. Frequency modulation of the carrier wave; and
3. Impulse modulation of the carrier wave

These three ways are described with the aid of Figures 2.4, 2.5 and 2.6.

1. Amplitude modulation of the carrier wave

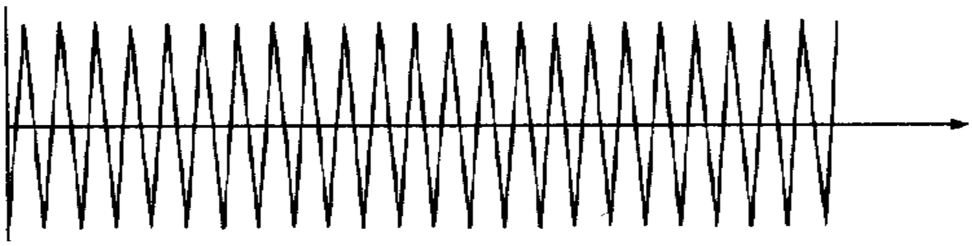

Figure (a): High-frequency carrier wave

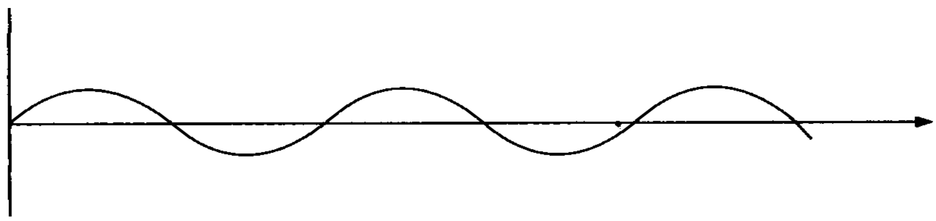

Figure (b): Low-frequency carrier wave

[10] IR has wavelengths of 0.8-0.9µm transmitted by gallium arsenide (GaAs) luminescent diode, at a high constant frequency (Schofield & Breach, 2007)

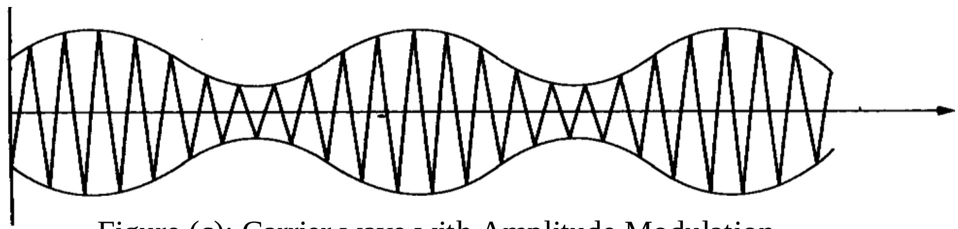

Figure (c): Carrier wave with Amplitude Modulation

Figure 2.4: Amplitude modulation of the carrier wave

2. Frequency modulation of the carrier wave

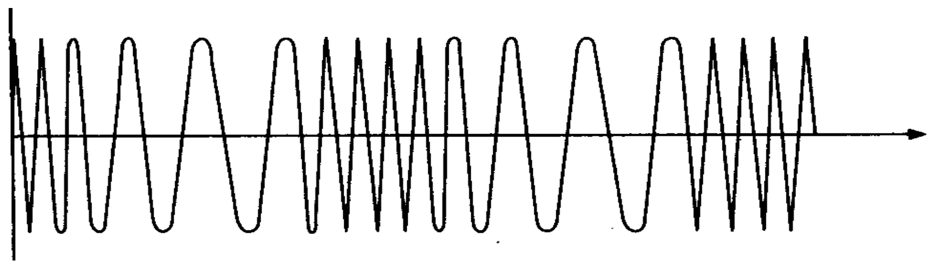

Figure 2.5: Frequency modulation of the carrier wave

3. Impulse modulation of the carrier wave

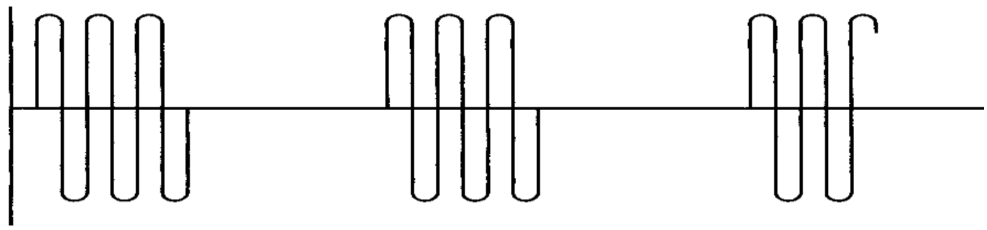

Figure 2.6: Impulse modulation of the carrier wave

The type of modulation used in electro-optical total station is amplitude modulation (Figure 2.4) in which the measuring wave is used to vary the amplitude of the carrier wave. The carrier wave used in an electro-optical instrument is either visible light (RL mode) or infra-red - IR (prism user mode), since these wavelengths are readily transmitted through the atmosphere without suffering severe attenuation[11]. Thus the carrier wave develops the necessary measuring characteristics and maintains the high-frequency propagation characteristics that can be measured with the requisite accuracy. In addition, light and infra-red can be controlled using small components such as mirrors and lenses so that a high collimated beam is transmitted by the instrument (Price & Uren 1989).

2.3. MODE OF OPERATION

The total station transit allows the surveyor to focus on a special reflective tape stuck to a surface or on a prism mounted on a stake. The EDM then aims at the target with a beam of near infrared light. The light bounces back; the EDM measures time elapsed and then calculates the distance travelled by the beam in thousandths of a metre. A data collector either built into the total station or attached to it can then send the site readings to an external computer. The computer-aided design and drafting (CADD) software translates the information into accurate field drawings and contour maps for various engineering and other usage (MacDonald, 2001). Figure 2.7 shows the principle of total station distance measurement.

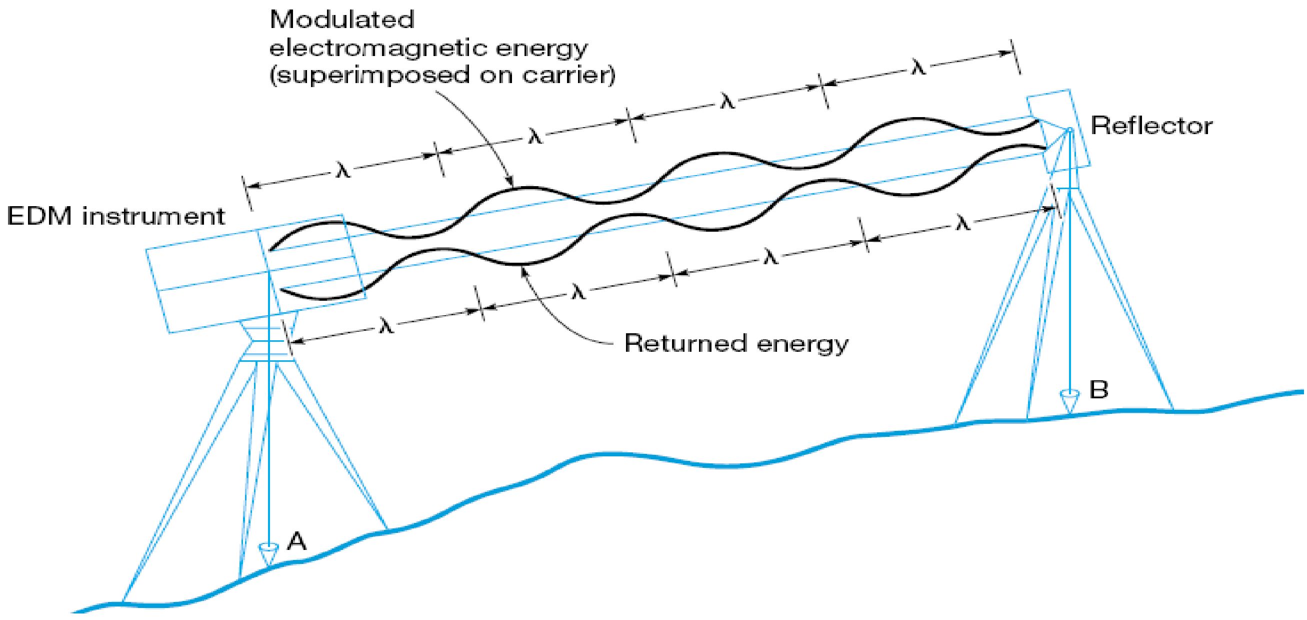

Figure 2.7: **Principle of total station distance measurement using reflector** (Source: Ghilani & Wolf, 2008)

[11] Reduction of signal strength during transmission is called attenuation. Scattering of light wave or intensity gives rise to an attenuation of the incident light in addition to the absorption (Bergmann *et al* 1999).

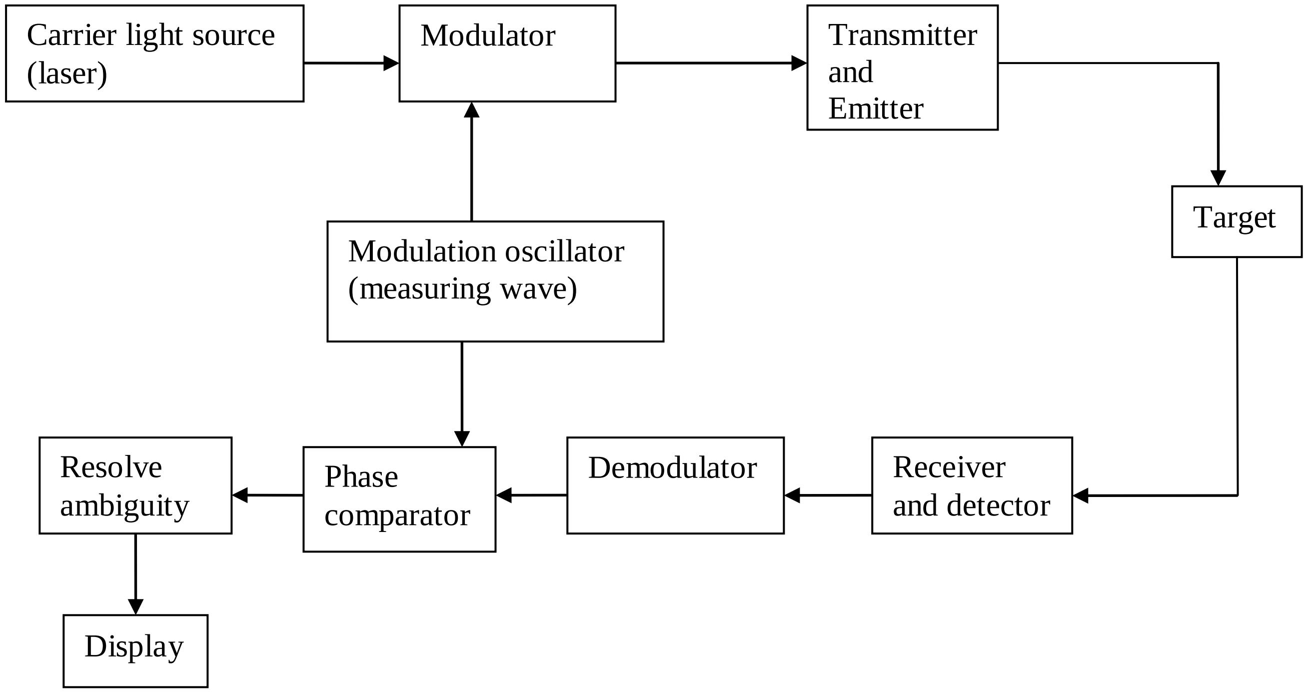

Figure 2.8: Schematics of EDM system (Price & Uren, 1989)

The Figure 2.8 illustrates the schematics of EDM system. The carrier light source of the instrument generates and sends the beam of light to modulator. As soon as the beams of light reach the modulator, they are modulated and, in the process, the modulation oscillator senses the light wave before the modulator sends the beams of light to the transmitter. The transmitter then sends the light beams to the reflector (prism or target) through open air (the atmosphere). The light beam is finally reflected back through the atmosphere to the instrument receiver/detector. The receiver sends it to the demodulator and from there to the phase comparator. The phase comparator compares the received light wave to the signal received from modulation oscillator initial measuring wave. The comparator then sends the differences to the resolve ambiguity section where the calculation is done and the result displayed on the total station screen. The displayed reading can be stored on the instrument memory and later downloaded to computer for further process. Figure 2.9 shows the total station data field to finish flow chat illustration while figure 2.10 shows its diagrammatic representation

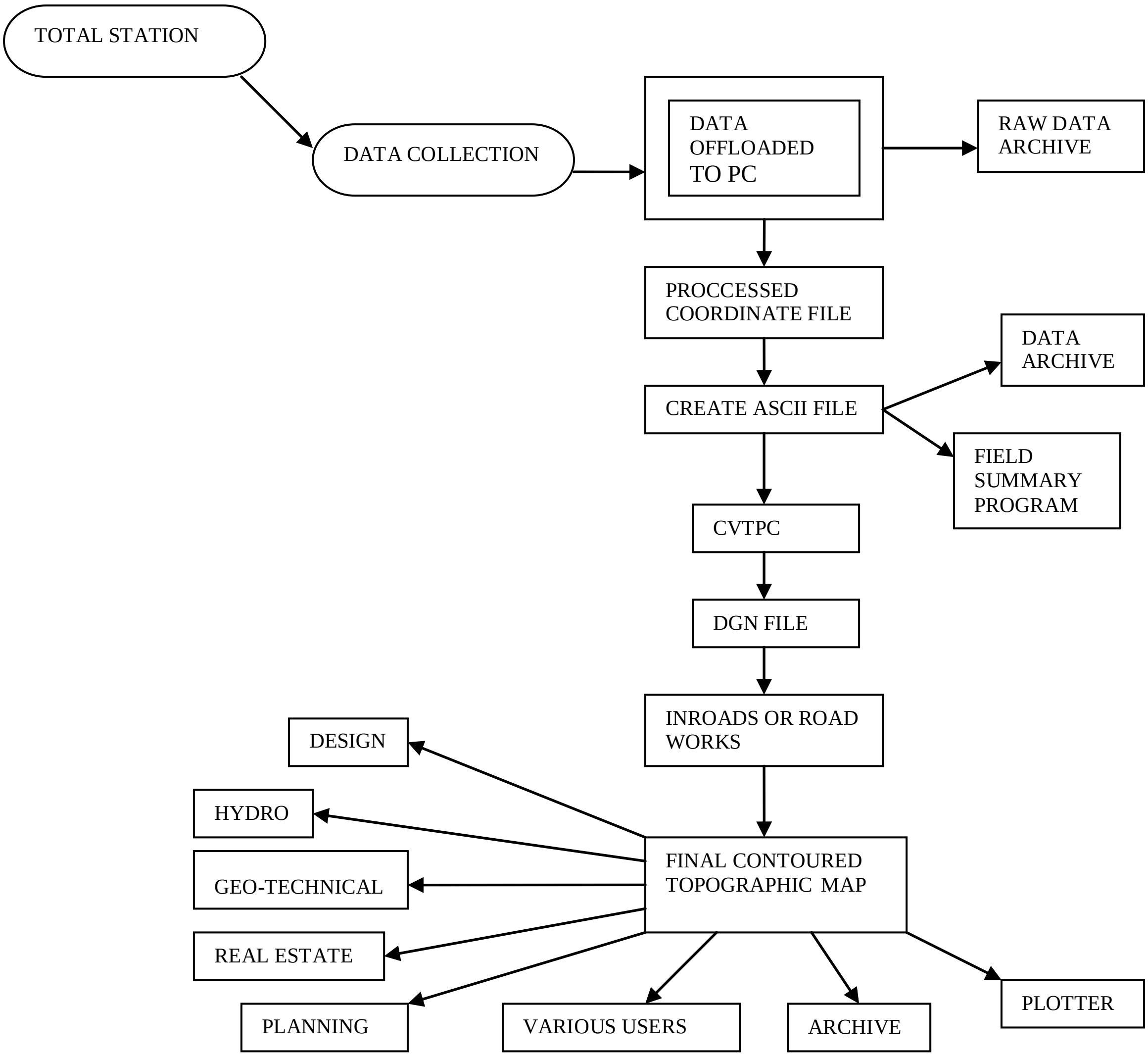

Figure 2.9: **Total station data – field to finish** (Source: ASCE, 1999)

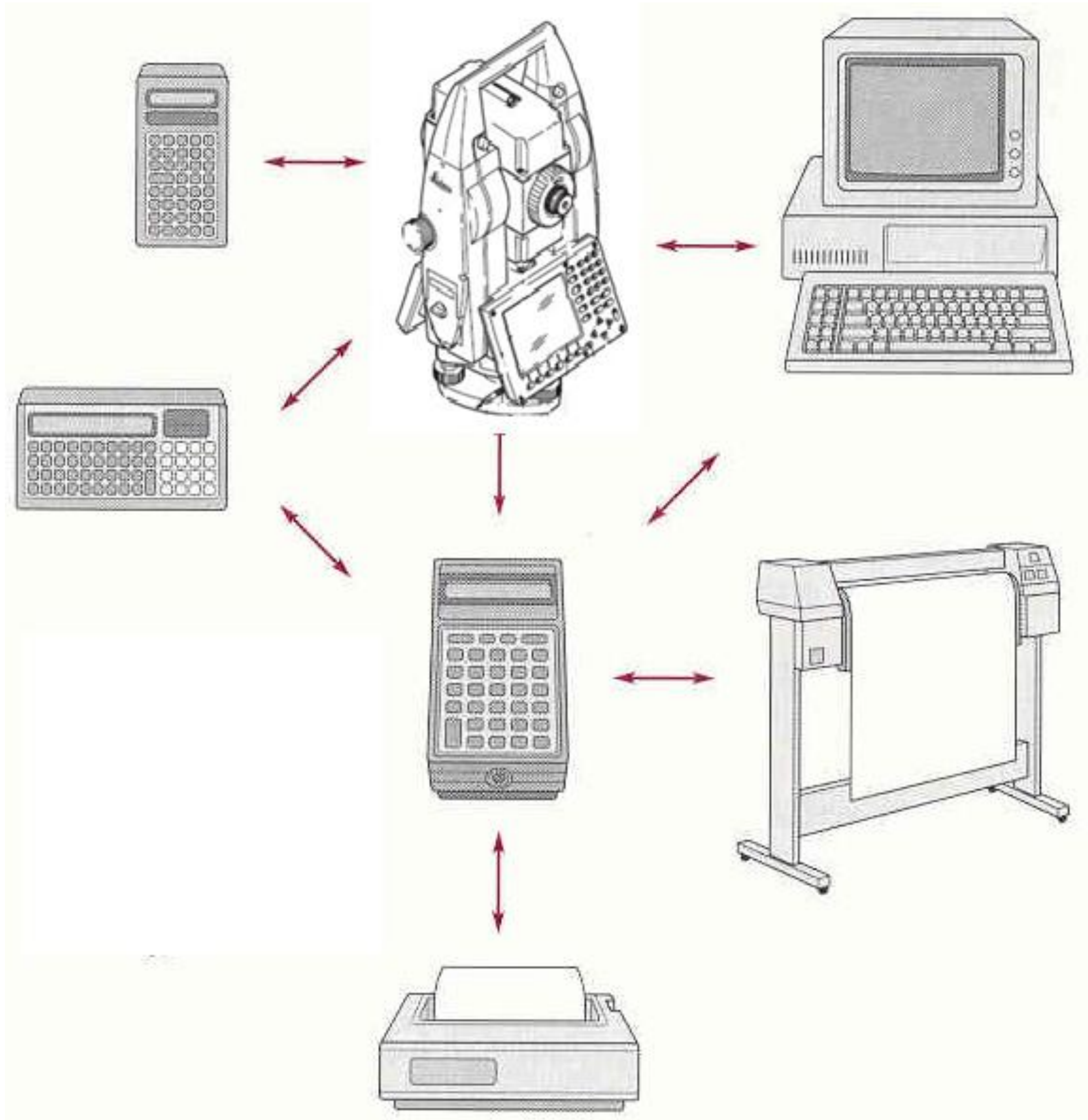

Figure 2.10: **Diagrammatic representation of total station data - field to finish** (Source: SÖNMEZ, 2005).

2.4. AREA OF APPLICATIONS

The areas of application of total station instruments continue to expand. An overview of the electronic total station and some of its uses have been provided by Philpotts *et al.*, (1997), and Schlische and Ackermann, (1998). This section describes some of the applications: namely, application in mining, geology, engineering surveying, road and safety surveys and archaeology surveys, just to mention a few.

2.4.1. Mining Surveys

The total station is the primary survey instrument used in many mining applications at both surface and underground mines. In underground surveys as the development drifts[12] are driven, a total station is used to record the absolute location of the tunnel walls (stope), ceilings (backs), and floors. This data is then downloaded into a CADD environment, and compared to the designed layout of the tunnel. At regular intervals, the survey party will set up stations made of small steel plugs drilled into the walls or the roof. The plugs are established in sets. For wall stations, two plugs are set up in opposite walls, forming a line vertical to the drift. When the survey squad wants to set up the total station in a drift, they use a set of stations to locate the total station. The use of total station for correlation survey for shaft deepening in underground mine was described by Bahuguna, (2003).

Cruden and Masoumzadeh (1987) explained that the recent development in total station have made reliable remote monitoring of rock slope movements possible. Observation of slope movements in surface mines can now be reliably extrapolated to predict slope failure and the slope movements can be treated as ‘another mining problem’.

Coggan *et al* (2001) described the use of total station to generate essential spatial data to produce production plans, undertake initial hazard appraisal of excavated slopes, perform slope face geometry profiling and provide spatial data for blast design purposes and monitor slope stability of identified critical excavations.

The increasing use of servo-driven electronic total stations in the mining industry due to their high survey efficiency and accuracy was discussed by Ding, *et al.*, (1998). Fully automatic total stations (also referred to as survey robots) have been developed to automate field deformation surveys. When the instrument is properly set up, it is automatically capable of finding prisms, taking the observation and storing the readings (angles, distances and coordinates readings). Therefore, much less human involvement is required in the field. This

[12] Drift mining is a method of subsurface or underground mining that involves cutting an opening horizontally into the side of a mountain or hillside to access a mineral seam. The result is the creation of a drift, a tunnel dug and driven directly along a horizontal path to the seam (Ritchiewiki).

is a great advantage as manual observations are usually repetitive, labour-intensive and time consuming.

Jobling-Purser (2006) explained the use of remote surveying vehicle (RSV) fitted with RL to carry out surveying work in hazardous mining areas. The RSV fitted with RL would help to conduct a non-contact survey, thereby eliminating the risk of exposing personnel to any hazardous areas in a mine.

2.4.2. Geology Surveys

The use of total station surveying instrument as a new basic tool for various geological surveys including mapping surface - faulting and hazards was recorded by Lavine, *et al.*. (2003) in confirmation with various publications of other geologists (such as Philpotts, *et a.,.et al.* 1997; Schlische, *et al.*, 1997; Wallace, *et al.*, 1996; Bulut & Tudes, 1996).

Feng, *et al., (2001)* discussed the use of total station to replace compass directions for measuring magnitude of fracture orientation at exposed rock faces. Ground deformation monitoring of potential landslide using total station surveying instruments was discussed by Moss, *et al.*, (1999) and Haentjens, (1992). Total stations made the use of plane table surveying and alidades for mapping obsolete. Its usage in topographic survey and for measuring the directions/velocities of steams flow was discussed by Keim *et al.*, (1999) and Philpotts *et al.*, (1997). Digital landscape modeling of small stream channels with a total station was also described by Keim *et al.*, (1999).

2.4.3. Engineering Surveys

EDM devices are extensively used in the construction industry nowadays. The early instruments, which were capable of very precise measurement over very long distances, were large, heavy, complicated and expensive. Technological advancement has provided lighter, smaller, simpler and less expensive models (Roberts, 1995).

The new instruments offer many advantages including accuracy, productivity and interconnectivity. Owing to the advantages offered by the instruments, many construction companies are now readily adopting the use of these instruments in their businesses (Arumala, 2000). The total station instrument has shown itself to be very useful for planning new construction and for providing quick measurements to difficult to reach or inaccessible surfaces (Gaudreault, *et al.*, 2004). Engineering applications of total station for monitoring of high rise buildings (Rueger, 1994) and stability of water storage dams (Signoret & Borelli, 1992; Rueger, 1994a).

MacDonald (2001) recorded the use of total station instruments during highway and bridge construction work and other construction sites due to the rugged nature of these instruments.

Geodetic methods have been used over the last decades for structure monitoring. Recent developments allow total stations to track, make measurements of distances and angles to a moving target (target in motion) and to store data automatically. It has been demonstrated that RTS can be used for dynamic deformation monitoring of structures in certain circumstances with good results (Cosser, *et al.*, 2003).

Slow–deforming structures, such as dams, require sub-millimetre to millimetre-level accuracy to monitor wall displacement. Although such precision may be achieved with GPS under certain conditions, from an accuracy perspective, it is not always the preferred method. To effectively monitor such structures, GPS should be supplemented with geotechnical sensors and high-accuracy total stations (El-Rabbany, 2002).

The use of total station for monitoring bridges and structural deformation has been explained by many other authors, including Merkle and Meyers, 2004; Hill and Sippel, 2002; Kuhlmann and Glaser, 2002; and Leica Geosystems, 2002). Landslide monitoring based on geodetically derived distance changes (Stiros, *et al.*, 2004).

2.4.4. Road Safety Surveys

Total stations are also used for police crime scene investigations, private accident re-constructionists and insurance companies for the measurement of accident scenes. Such accurate measurements are downloaded into modelling software to recreate the accident in a 3D environment in order to have better interpretation of what happened at the time of the accident (Philpotts, *et al.*, 1997, Sechlische & Ackermann, 1998).

2.4.5. Archaeology

Cultural heritages should be preserved for future generations; therefore, it is imperative to keep records of such sites. This task is challenging because of the process and equipment involved which is usually expensive. Rick (1996) wrote:

> *"Because of dropping prices, increasing reliability and numbers of features, and decreasing weight, total stations are increasingly likely to enter the archaeologist's toolkit. For mapping of all kinds, the additional speed and accuracy offered by total stations demand our attention. The reduced error rate, greater annotation potential, and higher efficiency of electronic data transfer contribute to timely, successful data processing. For local area surveys, total stations could be quite useful in place of or in conjunction with GPS instruments".*

Only recently has the reflectorless total station opened an alternative door for cultural heritages recording. The use of total station to collect data on cultural heritage and using 3D modelling to generate the image on computer have been discussed in many publications on archaeology and total station (Yildiz, *et al.*, 2007; Hirst, 2006, and Lehtonen, 2005).

Haddad and Ishakat (2007) carried out a comparative measurement study using a 3D laser scanner and reflectorless total station on the slots of El-khazneh at Petra in Jordan. Their results indicated that the difference in the measurement was within the range of 0.2 cm to 2 cm. However, the authors concluded by saying that the accuracy of laser scanning cannot reach that of geodetic instrument (reflectorless total station) and cannot provide the possibility to increase accuracy through larger image scales.

Modern architecture or contemporary architecture can be quite difficult to survey. Most of the time, a survey is done to support an analytical view that has been constructed for a conservation or restoration project. Since contemporary or modern architecture, generally, does not call for these types of interventions, the case history of surveys of modern buildings is extremely limited. However, the architecture of the modern movement is beginning show the effects of the passing of time, since reinforced concrete, the basis of many buildings, is not as durable as originally believed. The survey of the modern architecture of Giardino delle Scultire in Biennale Italian Pavillon was carried out using Total Station – Leica TCA 2003 (Balletti, *et al.,* 2005).

2.4.6. Factors influencing the use of total stations

The factors that influence the use of total stations are as follows:

- A clear line-of-sight between the instrument and the measured points is essential;
- The precision of the instrument is dependent on the raw repeatability of the direction and distance measurements;
- A well-defined measurement point or target/prism is required to obtain optimal precision and accuracy; and
- The accuracy of the direction and distance measurement is subject to a number of errors and the correct field procedures.

2.5. ERRORS IN TOTAL STATION DISTANCES

Many users labour under the general misconception that total stations automatically correct distances for errors and that the distance displayed is perfect. Unfortunately, this is not the case. According to Wolf and Ghilani (1997), the most important aspect of surveying is to bear in mind that no measurement is exact - that is all measurements always contain errors. The elimination of errors requires that correct surveying procedures be followed. Surveying measurements are subject to systematic and random errors as discussed in chapter one.

The main factor which distorts the results of distance measurements using total station is the change in the atmospheric conditions of the field where measurements are being carried out. A variation of 1^0C in the air temperature causes about 1ppm error in the measurement. Similarly, an error of 0.1 inches (3.386 mb) in pressure affects the measured distance by 1ppm, as does an elevation difference of 100feet (30.48 m). Such errors are insignificant for topographic surveys but can be significant for boundary surveys (Buckner, 1998).

Hoffman (2006) reported that temperature plays a major role in the measurement accuracy of a laser scanner surveying instrument. He affirmed that the wavelength of a laser varies with temperature and, as a result, it is essential that any laser scanner be carefully temperature controlled and compensated for such variations. Examples of harrow errors that are common to total stations are as follows:

- Centring errors: the centring of an optical tribrach over a survey point. Although surveyor attempts to centre the optical plummet exactly, the tribrach that is slightly off centre will cause a centring error; and

- Reading and pointing errors: the reading and pointing of a total station. Surveyors do their best to align and read the instrument. In reality, the instrument may be pointing slightly left or right.
- Levelling error: The levelling bubble in the total station must be exactly in the level circle before it can be said that the instrument is levelled. In reality it may not; it may be off the circle by 5%.

Also errors in total stations may results from imperfections in the design, construction, and adjustment. Some of these imperfections are as follows:

- Eccentricity of the instrument;
- Calibration of total station surveying instruments;
- Plate levels out of alignment;
- Level line of sight is out of adjustment; and
- Collimation errors.

Typical examples of these errors are represented in the figures 2.11 to 2.13 below:

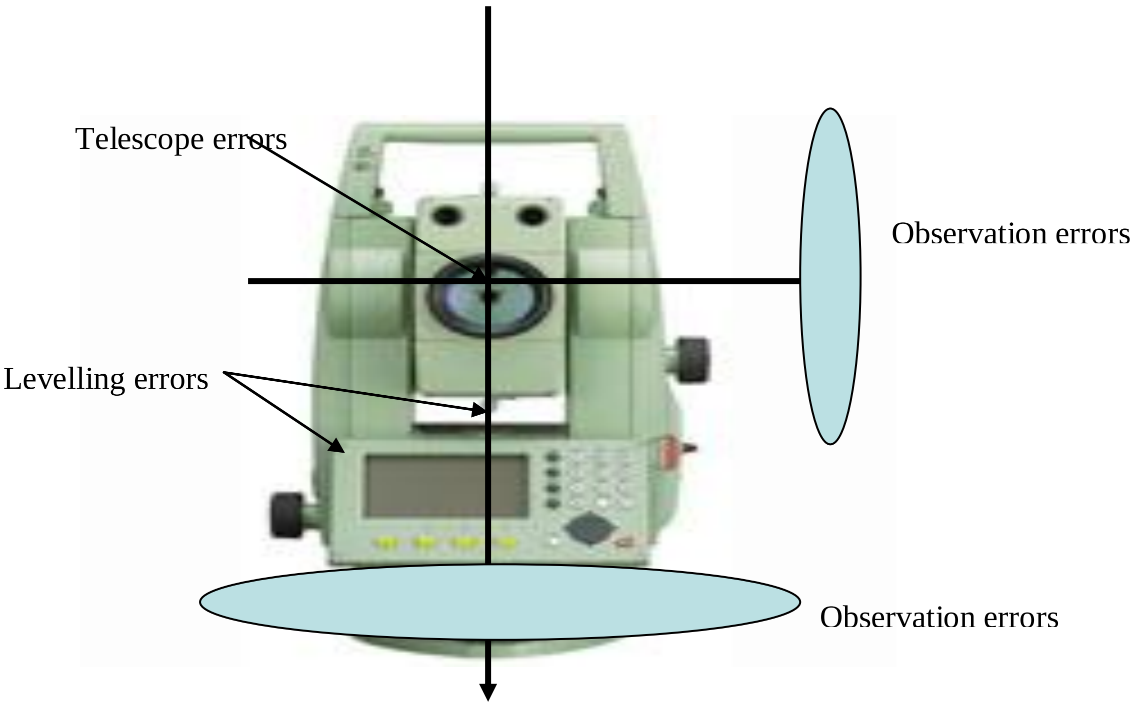

Figure 2.11: **Total station errors**

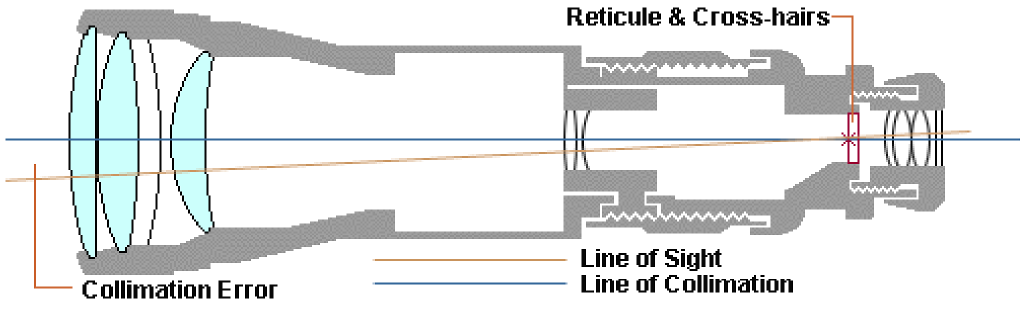

Figure 2.12: Collimation error

Figure 2.13: Plate bubble error

Table 2.3 shows overview of measuring instruments in surveying and their error limit.

Table 2.3: Overview of measuring instruments in surveying and their error limit

Method	Results	Typical Range	Typical Precision
Precision tape	Δdistance	<30 m	± 0.5 mm/30 m
Fixed wire extensometer	Δdistance	<10 – 80 m	± 0.3 mm/30 m
Rod for crack opening	Δdistance	<5 m	± 0.5 mm
Offsets from baseline	ΔH, ΔV	<100 m	± 0.3-3 mm
Surveying triangulation	ΔX, ΔY, ΔZ	<300-1000 m	± 5-10 mm
Surveying traverses	ΔX, ΔY, ΔZ	Variable	± 5-10 mm
Geometrical levelling	ΔZ	Variable	± 2-5 mm/km
Precise geometrical levelling	ΔZ	Variable	± 0.2-1 mm/km
Total station (EDM)	Δdistance	Variable (usually 1-14 km)	± 1-5 mm, +1-5 ppm
Terrestrial photogrammetry	ΔX, ΔY, ΔZ	Ideally < 100 m	± 20 mm from 100 m
Aerial photogrammetry	ΔX, ΔY, ΔZ	H_{flight} < 500 m	10 cm
Clinometer	Δα	± 10^0	$0.01\text{-}0.1^0$
GPS	ΔX, ΔY, ΔZ	Variable (usually <20 km)	± 5-10 mm + 1-2 ppm

*Note: 1 ppm means one part per million, or one additional millimetre per kilometre of measured line (Source: Gili *et al*, 2000).

This research aims to investigate the effects of atmospheric parameters (pressure, temperature and humidity) variations and the impact of observation house (measurement through the observation house window covered with glass) on total station distance measurement in a surface mine environment (i.e. to investigate what are the likely effects of atmospheric parameters variations on the light beam when it leaves the instrument transmitter and travels in an open space (air) to the reflector and from the reflector back to the open space (air) before getting to the instrument receiver; also what are the likely effects of the glass properties on the light beam). During the movement of the light beam in an open space, the speed of the light must have been affected by variations in the atmospheric parameters. However, the magnitude of these variations depends on the conditions of the atmospheric parameters.

2.6. ATMOSPHERIC VARIATIONS AND DISTANCE MEASURING INSTRUMENTS

Newcomen *et al* (2003) mentioned climatic conditions such as wind, snow, rain, dust and atmospheric refraction as contributing factors to total station survey errors. Although, these factors cannot be controlled, their effects on the accuracy of the survey can be reduced.

In distance measurement, most of the instruments are standardized at a temperature that does not conform to tropical regions which can experience temperatures of 36^{0}C or more. In order to make things work, correction must be performed on the readings recorded at the end of the day. Tapes are usually standardized at 20^{0}C. Any variation above or below this temperature will cause the tape to expand or contract giving rise to systematic errors. The difficulty of obtaining the true temperature of tape resulted in the use of invar[13] tapes (Schofield, 1993). Schofield suggested the equation below for temperature correction when using tape:

$$C_t = KL\Delta t \quad \text{…} \quad 2.1$$

where:

C_t is the temperature correction (^{o}C)

K is the coefficient of expansion.

For steel K= 11.2 ×10^{-6} per ^{o}C and for invar (nickel-steel alloy) K= 0.5 ×10^{-6} per ^{0}C

L is the measured length (m)

Δt is the difference between the standard and field temperatures (^{o}C) = ($t_s - t_f$).

Other authors have different equations for temperature corrections in tape, Khurmi and Gupta, 2003; Ganic and Hicks, 2002; proposed the following:

$$C_t = \alpha(T - T_s)L_f \quad \text{…} \quad 2.2$$

where:

C_t is temperature correction in ^{0}C or ^{0}F

α Is the coefficient of thermal expansion of steel; α = 6.45 ×10^{-6} ppm/ ^{0}F or 11.6 ×10^{-6} ppm/ ^{0}C

T is the temperature at which measurements are made, ^{0}F or ^{0}C

T_s is the temperature at which tape is standardized, ^{0}F or ^{0}C

L_f is the measured length obtained in the field, m.

If an aluminium body is used, α = 23 ×10^{-6} ppm/ ^{0}C or 12.3 ×10^{-6} ppm/ ^{0}F

[13] Invar is a nickel-steel alloy with a very low coefficient of expansion

The effects of the prevailing atmospheric conditions (temperature, pressure and relative humidity) on the new EDM (total station, or GPS) is similar to the influence of temperature variations when measuring distances with steel tape as discussed earlier above. Variations in temperature cause an expansion or contraction of the tape from its standardized length, which, if not corrected, will result in a systematic error in the measured distances. Similarly, variations in atmospheric conditions from those which are assumed by the total station will cause an increase or reduction in the measuring wavelength or the speed of light and lead to a systematic error, if a correction is not applied. The total station is standardized at a specific reference refractive index[14].

Whyte and Paul (1997) also mentioned that EDM results are directly affected by the atmospheric conditions prevailing at the time of measurement and the greater the distance the greater the effect. Many researchers in the past have published on the possible ways of correcting the effects of prevailing atmospheric conditions on short range and long range EDMs, but the relevance of such corrections to total station when used in a mine environment (a place with harsh weather conditions) still remains an area of research worldwide among the Geodesists and Mine Surveyors. Figure 2.14 below shows the relationship between the operator, the instrument (total station and prism/reflector) and the atmosphere:

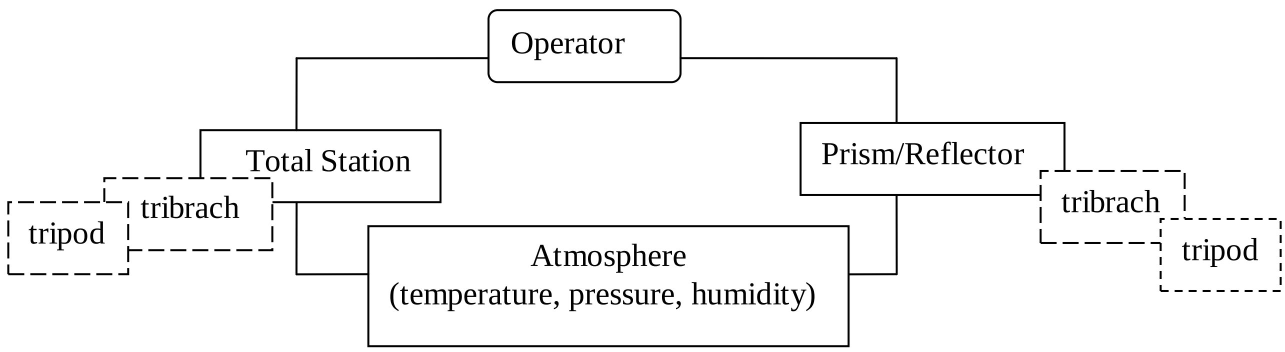

Figure 2.14: Relationship between the operator, the instrument and the atmosphere

[14] Refractive index is a function of atmospheric temperature, pressure and humidity. The reference refractive index is usually defined as: 20°C temperature, 1013.25mb pressure or 760 mmHg. This means that any deviation from that standard atmospheric condition will create small errors (much like they do in a steel tape) that are proportional to scale (larger for longer distances). As a rule of thumb, every 1°C deviation from standard temperature and every 3.5mb deviation from the standard pressure will produce errors of 1 ppm respectively (Anderson & Mikhail, 1998).

From figure 2.14 above, the operator can adjust the total station and the prism/reflector to his or her desired status before taking distance measurements. The atmospheric parameters variations can cause a default to the signal sent by the total station to and from the prism before the operator receives the result of such observation on the screen of the total station. This is a clear indication that the operator has no control over the prevailing atmospheric condition. Therefore, something must be done to remove or compensate for this default in the final reading or result.

2.7. BASIC CONCEPT OF REFRACTION

A beam of radiation moving from one point (point **A**) to another (point **B**), would follow a simple path if conditions were ideal. The reality is that conditions deviate slightly from ideal, especially in a mine environment, which is surrounded by many factors, such as frequent vibration (from blasting operation), dust (from drilling, blasting and loading operation) and variation in mineral compositions. The composition of the ore/mineral deposit has an impact on the extent the beam of the light can travel and, therefore, on the distance that can be measured. These factors, coupled with atmospheric variations, cause the beam to follow a more complicated path when travelling between the two points A and B. To minimize the time of travel, it is necessary to quantify the deviation of the true path from the ideal.

The indirect method of distance measurement using either electro-optical or electromagnetic wave (which are based on any of the following methods: time of flight pulse, phase comparison, and interferometer) relies on the fact that the velocity of propagation (light or radio waves) is finite and requires this propagation velocity to be accurately known. The velocity of light waves in the atmosphere is dependent on the refractive index of the atmosphere. This velocity is not constant but is dependent on the state of the atmosphere. The refractive index is also dependent upon the wavelength of the particular type of light under consideration. Thomas (2011) noted that the effect of atmospheric variations is critical when using total station for measuring distances. The author recommended that the atmospheric parameters (ambient temperature and barometric pressure) should be measured simultaneously during continuous distance measurements operations because the density of the atmosphere between the instrument station, the reference station and the target station can affect the velocity of the signal emitted by the EDM. If the atmospheric conditions are not compensated for, then the accuracy of a measured distance can be adversely affected as the atmospheric conditions change.

Significant research has been carried out on this particular problem. Rueger (1998) discussed the history of refractive index formula, and Young (2007) gives the chronology of past publications on refractivity of air. However, refraction uncertainties are not of great importance for common survey measurements, but in the case of mine surveying where accuracy and precision is of importance (especially when using total station for slope deformation monitoring), refraction tends to be or is the major problem.

2.7.1. Propagation of Electromagnetic (Light) Waves

The relationship between the frequency (the number of wave crests that pass a certain point in a given amount of time) and wavelength for electromagnetic waves (or of the signal) is given by Rueger (1996) as follows:

$$\lambda = \frac{c}{f} \quad \text{...} 2.3$$

$$f = \frac{c}{\lambda} \quad \text{...} 2.4$$

where:

f = frequency of the signal, Hz

λ = wavelength of the signal in a medium, m

c = velocity of light in a medium, m/sec

The inverse connection between wavelength and frequency means that as wavelengths increase, frequency decreases. Because the rate of recurrence of a photon[15] or electromagnetic wave is directly proportional to the energy of the photon or wave, the higher the frequency of the photon or wave, the greater the energy state of the photon or wave. As a result of this, the shorter wavelength blue light within the visible spectrum is more active than longer wavelength red light.

[15] Photon is a discrete bundle of electromagnetic (or light) energy. Photons are always in motion and, in a vacuum, have a constant speed of light to all observers, at the vacuum speed of light (more commonly just called the speed of light) of c = 2.998 x 10^8 m/s (Jones, 2009).

The mode and velocity of propagation of electromagnetic (light) waves are dependent to some extent on the frequency of the signal (which is constant value and independent of the medium) and the nature of the earth's atmosphere. The total station surveying instruments are capable of measuring path lengths to a very high degree of accuracy in many cases, but this information cannot be fully utilised unless the nature of that path is understood. Since the range of frequencies used in the various instruments is very wide, the mode of propagation also differ widely. Rueger, (1996) presented a table that shows the range of frequencies and wavelengths in use:

Table 2.4: Frequency spectrum for electromagnetic waves

Classification	Symbol	Wavelength λ (m)	Frequency f (Hz)
Light waves:			
X-rays		1.6×10^{-11}- 6.6×10^{-8}	$1.9 \times 10^{19} – 4.5 \times 10^{15}$
Ultraviolent	UV	$1.4 \times 10^{-8} – 3.6 \times 10^{-7}$	$2.2 \times 10^{16} – 8.3 \times 10^{14}$
Visible light	VL	$3.6 \times 10^{-7} – 7.8 \times 10^{-7}$	$8.3 \times 10^{14} – 3.8 \times 10^{14}$
Infra-Red	IR	$7.8 \times 10^{-7} – 3.4 \times 10^{-4}$	$3.8 \times 10^{14} – 8.8 \times 10^{11}$
Radio waves:			
Extra High Frequency	EHF	$1 \times 10^{-3} – 1 \times 10^{-2}$	$3 \times 10^{10} – 3 \times 10^{11}$
Super High Frequency	SHF	$1 \times 10^{-2} – 1 \times 10^{-1}$	$3 \times 10^{9} – 3 \times 10^{10}$
Ultra High Frequency	UHF	$1 \times 10^{-1} – 1 \times 10^{0}$	$3 \times 10^{8} – 3 \times 10^{9}$
Very High Frequency	VHF	1 – 10	$3 \times 10^{7} – 3 \times 10^{8}$
High Frequency	HF	$10 - 10^{2}$	$3 \times 10^{6} – 3 \times 10^{7}$
Medium Frequency	MF	$10^{2} - 10^{3}$	$3 \times 10^{5} – 3 \times 10^{6}$
Low Frequency	LF	$10^{3} - 10^{4}$	$3 \times 10^{4} – 3 \times 10^{5}$
Very Low Frequency	VLF	$10^{4} - 10^{5}$	$3 \times 10^{3} – 3 \times 10^{4}$
Extra Low Frequency	ELF	$10^{5} - 10^{6}$	$3 \times 10^{2} – 3 \times 10^{3}$

Source: Rueger, (1996)

Radio waves are not in use in the main Leica total station surveying instruments that was used to carry out this research, except in their radio system for communication (i.e. auxiliary part). Only infra-red and visible light are used in the Leica total station. The infra-red part of the spectrum is further divided into three, namely:

i. Near-infrared NIR (wavelength is 0.76 μm – 3.0 μm),
ii. Middle-infrared MIR, Far-infrared FI and
iii. Extreme-infrared XIR.

The NIR has propagation characteristics which are close to those of visible light and these characteristics facilitate its use both in optical communication systems and EDM. According to Rueger, (1996), "*electro-optical EDM instruments typically use NIR radiation of 800 to 900 nm wavelength or red HeNe laser light of 633nm".*

Burnside (1991) states: "*All the various methods of propagation other than the direct wave are the results of reflection, diffraction, or refraction of the wave caused by variations in the refractive index of the troposphere*".

2.7.3. Refractive Index

The effect of the refractive index of the atmosphere on distances measured through it by EDM (total station) is well established. There has always been a problem in actually determining the value of the refractive index so that the corrections can be applied to allow for its effect (Iliffe & Dodson, 1987). The availability of more precise total station surveying instruments on the market nowadays necessitate accurate determination of refractive index of the atmosphere for the achievement of their full potential.

According to Bonsch and Potulski (1998), *"the ultimate precision of a measured length value is often limited by the uncertainty of the actual value of the refractive index of air".* Accurate knowledge of the refractive index of air is essential to geodetic surveying, where overall uncertainties of approximately 1 part in 10^7 are sought. The refractive index should be known to a few parts in 10^8. The velocity of propagation of the electromagnetic or electro-optical wave used for distance measurement is dependent on the medium in which it is propagated.

Using EDM, the measurement of distance is obtained by measuring the time of propagation of the electromagnetic or electro-optical waves through the atmosphere as earlier stated (see section 2.3 above). While the velocity of these waves in a vacuum (c_o) is known, the velocity will be reduced depending on the atmospheric conditions through which the waves travel at the time of measurement. Therefore knowledge of the refractive index (n) of the prevailing atmosphere is necessary in order to apply a correction for velocity to the measured distance. The relationship between the distance measured, d', the refractive index and the corrected distance d is given as (Scofield & Breach, 2007):

$$d = \frac{d'}{n} \quad \text{.......} 2.5$$

where:

d = corrected distance (m)

d' = measured distance (m)

n = refractive index

The relationship between the propagation of velocity of wave in vacuum and that in the medium is described as refractive index, n, (Rueger, 1996):

$$n = \frac{c_0}{c} \quad \text{.......} 2.6$$

where:

n = refractive index of a medium (air)

c_0 = velocity of light in a vacuum

c = velocity of light in a medium

The refractive index of air is a function of:

- the gaseous composition of the atmosphere, which is very nearly a constant;
- the amount of water vapour pressure in the atmosphere;
- the temperature of the gaseous mixture;
- the pressure of the gaseous mixture; and
- the frequency of the radiated signal.

EDM equipment is standardized under certain conditions of temperature and pressure that may differ to conditions where the equipment is being used. This difference implies that even on low-order surveys, the measurement of temperature and pressure is important. The refractive index is related to wavelength via the Cauchy equation:

$$n = A + \frac{B}{\lambda^2} + \frac{C}{\lambda^4} \quad \text{.......} 2.7$$

where:

A, B and C are constants relative to specific atmospheric conditions

λ = vacuum wavelength (μm)

The values of constants A, B, and C can be determined by fitting the equation to measure refractive indices at known wavelength. Usually it is sufficient to use two terms for equation 2.7 above:

$$n = A + \frac{B}{\lambda^2}$$

A table of coefficients for common optical material is shown below:

Table 2.5: Coefficients for common optical materials

Material	A	B (μm^2)
Fused silica	1.4580	0.00354
Borosilicate glass BK7	1.5046	0.00420
Hard crown glass K5	1.5220	0.00459
Barium crown glass BaK4	1.5690	0.00531
Barium flint glass BaF10	1.6700	0.00743
Dense flint glass SF10	1.7280	0.01342

Source: Jenkins and White (1981)

To execute a correction in parts per million (ppm), the refractive number or refractivity (N) is used:

$$N = (n-1)\times 10^6 \qquad \text{......2.8}$$

There are two techniques for the determination of the refractive index of air: the index can either be measured directly by means of an air refractometer or it can be calculated from measured values of the air parameters, such as pressure, temperature, humidity and possibly carbon (iv) oxide, CO_2 content. Several authors have published their own equations for calculating refractive index of air, for example Barrel and Sears, (1939), Edlen, (1966) and Ciddor, (1996). These equations are discussed in the next section.

2.7.4. Barrel and Sears Equation for Refractive index of Air

Barrell and Sears (1939), described the refractive index, n for visible and near-infrared modulation radiation under standard atmospheric condition (0^oC temperature, 1013.25 hPa pressure and dry air with 0.03% CO_2). However, it is the refractive index of the modulated beam, not the carrier that is required; hence the use of group refractive index where:

$$N_{go} = A + \frac{3B}{\lambda^2} + \frac{5C}{\lambda^4} \quad \text{.........} 2.9$$

and therefore for group velocity in standard air with λ in µm, where constants A, B. and C are given as: A = 287.604, B = 1.6288 and C = 0.0136. By substitution for these constants in equation 2.9, we have:

$$N_{go} = (n_{go} - 1) \times 10^6 = 287.604 + \frac{4.88640}{\lambda^2} + \frac{0.06800}{\lambda^4} \quad \text{.........} 2.10$$

The above equation 2.10 is accurate to ±0.1 ppm at wavelength between 560 and 900µm. To accommodate the actual atmospheric conditions under which the distances are measured, equation 2.10 was modified by Barrel and Sears (Scholfield & Breach, 2007)

$$N_g = \frac{N_{go} \times Q \times P}{T} - \frac{V \times e}{T} \quad \text{.........} 2.11$$

where:

N_{go} = group refractivity of standard air

N_g = group refractivity at prevailing atmospheric condition

T = absolute temperature K, or (^oK) = 273.15 + t

t = dry bulb temperature in ^oC

P = atmospheric pressure

e = partial water vapour pressure

with P and e in hPa, Q = 0.2696 and V = 11.27 (i.e. $N_g = \frac{0.2696 N_{go} P}{T} - \frac{11.27e}{T}$)

with P and e in mmHg, Q = 0.3594 and V = 15.02 (i.e. $N_g = \frac{0.3594 N_{go} P}{T} - \frac{15.02e}{T}$)

The value for e can be calculated from:

$$e = E - 0.000662 \times P \times (t - t_w) \qquad \text{2.12}$$

where: t = dry bulb temperature

t_w = wet bulb temperature

E = saturation water vapour pressure.

The saturation water vapour pressure E can be calculated using:

$$\log E = \frac{7.5 t_w}{t_w + 237.3} + 0.7857 \qquad \text{2.12a}$$

If only the dry bulb temperature t is available as commonly used in most field works nowadays, e can be calculated as follows:

$$e = \frac{Eh}{100} \qquad \text{2.13}$$

where:

$$E = 10^{\left(\frac{7.5 \times t}{237 + t} + 0.7858\right)} \qquad \text{2.13a}$$

2.7.5. Edlen Equation for Refractive Index of Air

Edlen (1966) saw the need to improve the Barrel and Sears equations and standards above and carried out new experiments aiming at reducing the uncertainty associated with the works of Barrel and Sears to about ± 5 x 10^{-8}. This led him to derive an improved dispersion formula for standard air, as shown below:

$$(n-1)_s \times 10^8 = 8342.13 + \frac{2406030}{(130 - \sigma^2)} + \frac{15997}{(38.9 - \sigma^2)} \qquad \text{2.14}$$

where:

σ = wave number in μm^{-1} (the reciprocal of the vacuum wavelength i.e. ($\frac{1}{\lambda}$)

Edlen also derived equation for the dependence of refractivity on temperature and pressure based on theoretical considerations:

$$(n-1)_{tp} = (n-1)_s \times \frac{0.00138823P}{(1+0.003661t)} \quad \ldots\ldots\ldots\ldots\ldots\ldots\ldots\ldots\ldots\ldots\ldots\ldots\ldots\ldots 2.15$$

where:

P = atmospheric pressure in torr

t = atmospheric temperature in °C

$(n-1)_s$ is given by the dispersion formula for standard air in equation 2.14

In order to accommodate the effects of CO_2 and water vapour, he combined Erickson's dispersion data for water vapour with Barrel and Sears' absolute measurement to obtain an equation for difference in refractive index of moist air:

$$(n_{tpf} - n_{tp}) = -f(5.722 - 0.0457\sigma^2) \times 10^{-8} \quad \ldots\ldots\ldots\ldots\ldots\ldots\ldots\ldots\ldots\ldots\ldots 2.16$$

where:

$(n_{tpf} - n_{tp})$ = difference in refractive index of moist air and dry air

f = partial pressure of water vapour in torr.

The above equation given by Edlen is valid for visible radiations and normal atmospheric conditions.

Birch and Downs (1993) carried out an experiment to update Edlen's equation for refractive index of air due to availability of improved data on density of air, refractivity of water vapour, new measuring scale for temperature and increase in the CO_2 content of normal laboratory air. These effects result in a discrepancy of typically 1 x 10^{-7}. He also reported that the consequent revision of the equation brings the agreement between calculation and experiment within an experimental uncertainty of ± 3 x 10^{-8}. In the process of conversion of temperature scale from IPTS-1948 (International Practical Temperature Scale-1948) to the ITS-90 (International Temperature Scale-1990), they made a sign error which led to Birch and Downs (1994) correcting the updated Edlen equation for refractive index of air. The equations are as follows:

$$(n-1)_{tp} = \frac{P(n-1)_s}{96095.43} \times \frac{\left[1+10^{-8}(0.601-0.00972t)P\right]}{(1+0.0036610t)} \quad \ldots\ldots\ldots\ldots\ldots\ldots 2.17$$

where $(n-1)_{tp}$ is the refractivity of air at a temperature t (^oC) and atmospheric pressure P (Pa) and $(n-1)_s$ is given by a revised dispersion equation:

$$(n-1)_s \times 10^8 = 8342.54 + \frac{2406147}{130-\sigma^2} + \frac{15998}{38.9-\sigma^2} \qquad \text{……………….………2.18}$$

For the difference in the refractive index of moist air, containing a partial pressure f of water vapour (Pa) and dry air at the same total pressure, the following revised expression was presented by Birch and Downs:

$$n_{TPf} = n_{TP} - f\left(3.7345 - 0.0401\sigma^2\right)\times 10^{-10} \qquad \text{…………………..…………2.19}$$

The above new formulae were expected to have an uncertainty of ±1 x 10^{-8}, over the wavelength range 350 – 650 nm,

2.7.6. Ciddor Equation for Refractive Index of Air

Ciddor (1996) noticed limitations in Birch and Downs' updated Edlen equation for refractive index of air and concluded that the study was restricted to conditions likely to occur in a controlled laboratory. He used various existing equations to generate a better and more effective one for each parameter of atmospheric air. He tried and analysed these parameters one by one:

He defined standard air as dry air at 15^oC, 101.325 Pa and with 450 ppm CO_2 content as suggested by Birch and Downs above. However, instead of using Edlen's equation like Birch and Downs, he used Peck and Reeder (1972) because the later equation covered data over the wavelength range 230 – 1690 nm as against Edlen, Birch and Downs' wavelength range of 350 to 650 nm. He arrived at the following equations for the refractivities of standard air at 15^oC, 101.325 Pa and 0% humidity, with 450 ppm (n_{as}) or x_{CO_2} ppm of CO_2 (n_{axs}):

$$(n_{as}-1)10^8 = \frac{k_1}{\left(k_0-\sigma^2\right)} + \frac{k_3}{\left(k_2-\sigma^2\right)} \qquad \text{………………………………………2.20}$$

$$(n_{axs}-1) = (n_{as}-1)\left[1 + 0.534\times 10^{-6}\left(x_{c0_2}-450\right)\right] \qquad \text{……………………………..2.21}$$

where:

k_0, k_1, k_2, and k_3 are constants. Based on the experiment carried out by Peck and Reeder the following values were assigned to these constants:

$k_0 = 238.0185\ \mu m^{-2}$; $k_1 = 5792105\ \mu m^{-2}$; $k_2 = 57.362\ \mu m^{-2}$; $k_3 = 167917\ \mu m^{-2}$;

For water vapour at standard air:

$$(n_{ws}-1)10^8 = cf\left(w_0 + w_1\sigma^2 + w_2\sigma^4 + w_3\sigma^6\right) \quad \text{.........................2.22}$$

where:

cf = 1.022 (which is the correction factor)

$w_0 = 295.235\ \mu m^{-2}$; $w_1 = 2.6422\ \mu m^{-2}$; $w_2 = -0.032380\ \mu m^{-4}$; $w_3 = 0.004028\ \mu m^{-6}$;

For density of moist air and its components, he gives the equation below:

$$\rho = \frac{PM_a}{ZR^*T}\left[1 - x_w\left(1 - \frac{M_w}{M_a}\right)\right] \quad \text{.........................2.23}$$

where:

M_a = molar mass of dry air, kg/mol; P = total pressure, Pa

M_w = molar mass of water vapour, kg/mol; T = temperature, ^oK;

R* = gas constant, J $mol^{-1}K^{-1}$ and

x_w = molar fraction of water vapour in moist air, ppm

Using the above equations, Ciddor generates a phase refractive index:

$$n_p - 1 = \frac{\rho_a}{\rho_{axs}}(n_{axs}-1) + \frac{\rho_w}{\rho_{ws}}(n_{ws}-1) \quad \text{.........................2.24}$$

where:

ρ_a = density of dry air component, Pa; ρ_{axs} = density of dry air at 15°C, 101325 Pa and $x_w = 0$, using equation 2.24 above.

ρ_w = density of water vapour component of moist air, using the same equation 2.24; ρ_{ws} = density of pure water vapour at 20°C, 1333 Pa and x_w =1.

He finally derived the following equations for group refractive index of air (n_g):

$$(n_{go}-1)10^8 = \left[\frac{k_1\left(k_0+\sigma^2\right)}{\left(k_0-\sigma^2\right)^2} + \frac{k_3\left(k_2+\sigma^2\right)}{\left(k_2-\sigma^2\right)^2}\right] \quad \text{.........................2.25}$$

where:

n_{go} is the group refractive index of standard air

k_0, k_1, k_2, and k_3 are constants as described above in equation 2.18

$$(n_{gws}-1)10^8 = cf\left(w_0 + 3w_1\sigma^2 + 5w_2\sigma^4 + 7w_3\sigma^6\right) \quad \ldots\ldots\ldots\ldots 2.26$$

where:

n_{gws} is the group refractive index of air with water vapour at standard condition

cf = correction factor as stated in equation 2.22 above.

w_0, w_1, w_2, and w_3 are constants as given above in equation 2.22

2.7.7. IAG, 1999

At their 22nd General assembly, the International Association of Geodesy (IAG, 1999) resolved that for group refractive index of air for EDM to be better than 1 ppm with visible and near infrared wave in the atmosphere it should be computed using the computer procedure of Ciddor, 1996. This resolution is an indication that Ciddor equations remain one of the best for the new generation of electronic distance measuring equipment.

However, the body also adopted the following closed formulae for computation of the group refractive index in air for EDM to within 1 ppm with visible and near infrared waves in the atmosphere:

$$\left.\begin{array}{l} N_L = (n_L - 1)10^6 = \left(\dfrac{273.15}{1013.25}\dfrac{N_{go}P}{T}\right) - \dfrac{11.27e}{T} \\ \quad \text{or} \\ N_l = 0.2696 N_{go}\dfrac{P}{T} - 11.27\dfrac{e}{T} \end{array}\right\} \quad \ldots\ldots\ldots\ldots 2.27$$

where:

N_L = the group refractivity of visible and near infrared waves in ambient moist Air (i.e. refractivity of light waves),

T = temperature in Kelvin (ITS-90), T = 273.15 + t, t = temperature °C

P = total pressure in hPa

e = partial water vapour in hPa and

n_L = the corresponding refractive index

N_{go} = group refractivity of standard air (CO_2 = 0.0375%, T = 273.15, P = 1013.25 hPa and e = 0.0 hPA) as shown in equation 2.10 above.

For group refractivity, N_{go} of standard air:

$$N_{go} = (n_{go} - 1) \times 10^{-6} = 287.6155 + \frac{4.88660}{\lambda_0^2} + \frac{0.06800}{\lambda_0^4} \quad \ldots\ldots\ldots\ldots\ldots\ldots 2.28$$

For phase refractivity:

$$N_{ph} = (n_{ph} - 1) \times 10^{-6} = 287.6155 + \frac{1.62887}{\lambda_0^2} + \frac{0.01360}{\lambda_0^4} \quad \ldots\ldots\ldots\ldots\ldots\ldots 2.29$$

The difference in equation 2.29 and Barrel and Sears (1939) equation 2.10 arises from change in CO_2 content from 0.0300% (300 ppm) to 0.0375% (375 ppm). That is, multiplication of all constants given in Barrel and Sears formula with a factor 1.000,040,07 (derived from the results of Ciddor's formulae for wavelength of 650 nm and 850 nm at 0^oC, 1013.35 mb, 0% relative humidity and CO_2 contents of 375 ppm) convert equation 2.10 to equation 2.28.

2.7.8. Leica Geosystem

The manufacturer of the total station (TCR 1201+) surveying instrument used a modified version of Barrel and Sears formula to generate the index n for IR and visible red laser EDM presented in table 2.6.

Table 2.6: Refractive index for IR and visible red laser EDM

Type	Index n	Carrier wave (nm)
Infra-red EDM	1.00028305	780
Visible red laser	1.0002859	670

Source: Leica TPS 1200 Users manual

The figures in the table 2.6 above are valid under the following atmospheric conditions: Air pressure P = 1013.25 mb, Air temperature t = 12^0C and Relative air humidity h = 60%.

Since the conditions in the field differ from the above atmospheric conditions, the manufacturer proposed the following formulae for index n corrections:

For infra-red EDM:

$$\Delta D_1 = 283.05 - \left[\frac{0.29196P}{(1+\alpha.t)} - \frac{4.126\times 10^{-4} h}{(1+\alpha.t)}.10^x. \right] \text{..............................2.30}$$

For visible red laser:

$$\Delta D_1 = 285.93 - \left[\frac{0.29493P}{(1+\alpha.t)} - \frac{4.126\times 10^{-4} h}{(1+\alpha.t)}.10^x. \right] \text{.............................2.31}$$

where:

ΔD_1 = atmospheric correction, ppm

P = air pressure, mb

t = air temperature, ^{0}C

h = relative humidity, %

$$\alpha = \frac{1}{273.15}$$

$$x = \left[\left(\frac{7.5t}{237.3+t} \right) + 0.7858 \right]$$

The index n in the table 2.6 above were derived from IUGG (International Union of Geodesy and Geophysics), 1963 recommended equation for reducing refractive index in EDM to ambient conditions with a recommended IAG 1999 formula for group refractivity N_{go}:

$$\left.\begin{aligned} N_{go} &= (n_{go}-1)\times 10^{-6} = 287.6155 + \frac{4.8866}{\lambda_0^{\,2}} + \frac{0.06800}{\lambda_0^{\,4}} \text{....a} \\ n_L &= 1 + \left(\frac{n_{go}-1}{1+\alpha.t}.\frac{P}{1013.25} \right) - \left(\frac{4.125\times 10^{-8}}{1+\alpha.t} e \right) \text{...............b} \end{aligned}\right\} \text{................2.32}$$

When the figures for the atmospheric parameters given above (i.e. Air pressure P = 1013.25 mb, Air temperature t = 12°C and Relative air humidity h = 60%) were used with the equation after N_{go} was derived using equation 2.28. It yielded 1.00028305 and 1.0002859 for infrared EDM (with λ = 0.780) and visible red laser EDM (with λ = 0.670) respectively.

Expansion of equation 2.32b above with 273.15 would leads to the final form of interpolation formula shown in equation 2.27.

2.8. ERROR ANALYSIS

The effects of errors in the variables t, p, and e (i.e. atmospheric parameters- temperature, pressure and water vapour pressure) on the derived quality N_g (group refractivity) may be analysed by their partial differentials. For a temperature t of 12°C, a pressure p of 1013.25 mb, a partial water vapour pressure e of 8.4 mb and carrier wave λ of 670 nm is given by a manual of Leica Geosystem for total station TPS 1200. Differentiation of equation 2.27 gives:

$$\left.\begin{aligned} \frac{\partial N_L}{\partial T} &= -\left(\frac{273.15}{1013.25}\frac{N_{go}P}{T^2}\right)+\frac{11.27e}{T^2} \\ \frac{\partial N_L}{\partial P} &= \frac{273.15}{1013.25}\frac{N_{go}}{T} \\ \frac{\partial N_L}{\partial e} &= -11.27\frac{1}{T} \end{aligned}\right\} \qquad \text{.......................... 2.33}$$

By inserting the value of carrier wave λ of 670 nm (0.670 µm) in equation 2.28 to get N_{go} and the result derived from with other values T (t+273.15), p and e in equation 2.32, the table below is obtained:

Table 2.7: Sensitivity of Group Refractivity N_g to meteorological parameters (T = 285.15°K, P = 1013.25 mb, e = 8.4 mb with instrument carrier wave λ = 0.670 µm)

Visible Light and Infrared Light		
$\frac{\partial N_g}{\partial T}$	$\frac{\partial N_g}{\partial P}$	$\frac{\partial N_g}{\partial e}$
1 unit/°K or 1unit/°C	0.28 unit/mb	0.04 unit/mb

The significant of the equation 2.34 above can be summarized as follows:

1. An error of 1°C affects refractive index and distance measured by 1 ppm
2. An error of 1 mb affects refractive index and distance measured by 0.28 ppm or ≈ 0.3 ppm
3. Also, an error of 1 mb affects refractive index and distance measured by 0.04 ppm

The above facts show that temperature T has a great impact on light wave movement followed by pressure P, while water vapour pressure e has a little impact on the light wave path or movement. Therefore, e needs not to be known accurately especially when working on short-range distance measurement. Nevertheless, when working on the long-range distance measurement, every atmospheric parameter plays vital roles (Rueger, 1996).

However, it has been established by using differentiation that water vapour pressure has more effects (e is a critical parameter) on microwave. According to Rueger (1996), the effect 1 mb of e on refractive index and distance is as high as 4.66 ppm when a microwave instrument is used.

2.9. ORDER OF APPLICATION OF REDUCTIONS

The order in which corrections/reductions are applied to total station distance reading varies from one user or professional to another, but what is certain is that corrections must be done to the field readings. The corrections/reductions applicable to distances measured with total station surveying instrument can be separated into the following categories:

a. Corrections which depend on the instrument which is known as internal error corrections are categorised into three categories:
    - The scale error (internal scalar error);
    - The cyclic error (Internal cyclic error); and
    - The additive constant which is also called zero error or index error.

All the three errors can be corrected by calibration. Therefore, the results of calibration or pr-delivery tests carried out on the new total station procured for this research work are important to the research work and is discussed and analysed in one of the chapters of this research write-up.

b. Corrections which depend on the atmospheric conditions. These corrections are the basis of this research work and are discussed in detailed in the next section.
    - First velocity correction;
    - Second velocity correction; and
    - Correction for curvature of the total station - EDM beam.

c. Geometrical reductions - These reductions/corrections entail the following:
   - Correction for inclination at mean height;
   - Reduction to sea level;
   - Reduction from chord at sea level to arc at sea level; and
   - Reduction of the ellipsoid arc to the projection distance.

2.10. ATMOSPHERIC DEPENDENT CORRECTIONS

As stated earlier above, three corrections need to be carried out on total station distance measurement readings, prominent among them are atmospheric-dependent corrections. The atmospheric-dependent corrections are further divided into three as listed in section 2.9b.

2.10.1 First Velocity Correction

The EDM component of the total station has its nominal or reference refractive index stated as (n_{ref}). The figure or value assigned is based on an assumed standard atmosphere and the vacuum wavelength of the carrier. Therefore, any distance displayed is correct only if the atmospheric conditions under which the instrument is being used correspond to the condition under which the instrument was standardized by its manufacturer. The field condition under which the total station is being used in most cases varies widely from the manufacturer's standardized condition.

Any deviation from the standard atmospheric conditions given by the manufacturer of the total station leads to error in distance measured with the instrument. This error must be corrected using the first velocity correction as given below (Rueger, 1996):

$$C_1 = d'\left(n_{ref} - n\right) \qquad 2.34$$

where:

C_1 = First velocity correction

d' = measured distance as indicated or displayed on the total station digital screen

n_{ref} = reference or nominal refractive index. The value of this varies from one total station model to another (it is usually given by the manufacturer of the total station in the manual that accompanies the instrument)

n = refractive index of air or atmosphere around the field where the total station is being used (as derived from any of the above equations for calculating refractive index of air). It is also known as group refractive index in the above equations (i.e. n_g)

The corrected distance d_1 is given as follows (Rueger, 1996):

$$d_1 = d' + C_1 \quad \text{...2.35}$$

Where d_1 is the distance corrected for zero and scale error.

2.10.2 Second Velocity Correction

The first velocity corrections above are computed based on atmospheric parameters observations made at instrument and reflector stations. The means of both values are used to calculate the group refractive index, n_g used in the equation for the first velocity correction. However, an error is introduced if the mean first velocity correction of both stations is used without a further small correction, called the second velocity correction.

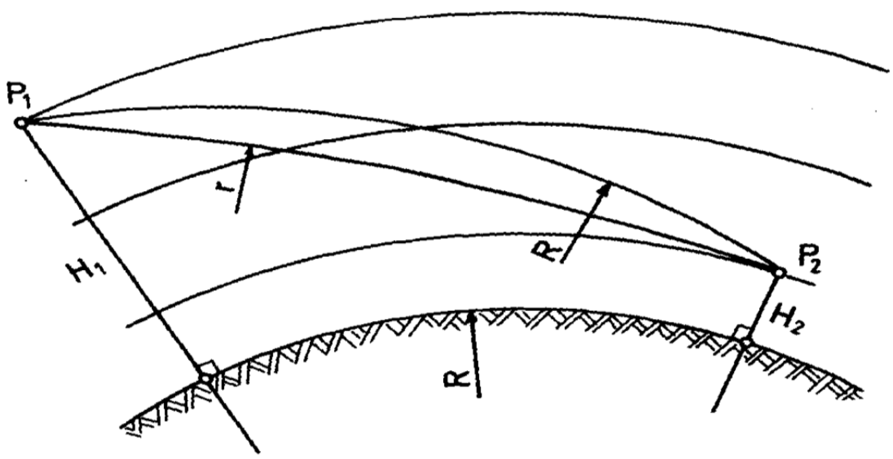

.

Figure 2.15: **Total station wave paths in a spherically layered atmosphere.**

In practice, it can be assumed in measurements between ground points (let say P_1 and P_2 as indicated in the figure 2.15 above) that the refractive index of air layers nearest the ground varies in linear manner according to the height. In figure 2.15 above, the mean refractive index $n=\frac{1}{2}(n_1+n_2)$ would be correct for the upper curve with a radius R but not for the actual wave path below it having a radius r, assuming a spherically layered atmosphere on a sphere (Rueger, 1996). Assuming linear vertical gradients of temperature and pressure, the correct refractive index for the actual wave path would be:

$$n=\frac{n_1+n_2}{2}+\Delta n \quad \text{......} 2.36$$

where:

$$\Delta n=(k-k^2)\frac{d'^2}{12R^2} \quad \text{......} 2.37$$

The second velocity correction may be written as:

$$C_2=-d'\Delta n \quad \text{......} 2.38$$

By substituting for equation 2.36 in equation 2.37; the equation for second velocity correction becomes:

$$C_2=-(k-k^2)\frac{d'^3}{12R^2} \quad \text{......} 2.39$$

Where:

C_2 = the second velocity correction

R = the mean radius of curvature of the spheroid along the line.

k = the coefficient of refraction ($k=\frac{1/r}{1/R}=\frac{R}{r}$; the $1/r$ is the curvature of ray path while $1/R$ is the curvature of spheroid)

k varies from place to place and from time to time. Therefore, it must be estimated every time that the total station distances are measured. Researchers in the past assigned 0.13 to k (Angus-Leppan, 1962; Brunner & Fraser, 1977). Angus-Leppan (1962) stated that the coefficient k is taken as a constant +0.13 for South Africa. It must be emphasised that this figure is not applied to specific areas.

However, this coefficient can be estimated for a specific area on the earth's surface using simultaneous reciprocal vertical angles observed at the ends of a line of known length or by measuring vertical angles along a line of known (or measurable) length for which the elevations of the end points are known with sufficient accuracy (Albanis, 1993).

The corrected distance d_2 is:

$$d_2 = d_1 + C_2 \qquad \text{2.40}$$

2.10.3 Correction for Curvature of the Line of Sight

During a survey exercise (distance measurement between two points P_1 and P_2), the light waves propagate by the EDM portion of the total station do not follow a straight line. The defects resulted from vertical gradient of refractive index ($\frac{dn}{dH}$, where H is the midpoint of the upper curve, which is the mean height $\frac{H_1 + H_2}{2}$ of the terminals P_1 and P_2 as shown in figure 2.16) that have a curve path. This necessitates reduction in the length of the arc to that of the chord:

$$C_3 = -k^2 \frac{d_2^{\ 3}}{24R^2} \qquad \text{2.41}$$

According to Hopke (1964), d_1 is nearly the same as d_2. Therefore, equation 2.42 may be approximated to:

$$C_3 = -k^2 \frac{d_1^{\ 3}}{24R^2} \qquad \text{2.42}$$

where:

C_3 = correction for the curvature of the path of the beam

k = coefficient of refraction

R = radius of the earth

The corrected distance d_3 is:

$$d_3 = d_2 + C_3 \qquad \text{2.43}$$

where:

d_3 = the spatial chord

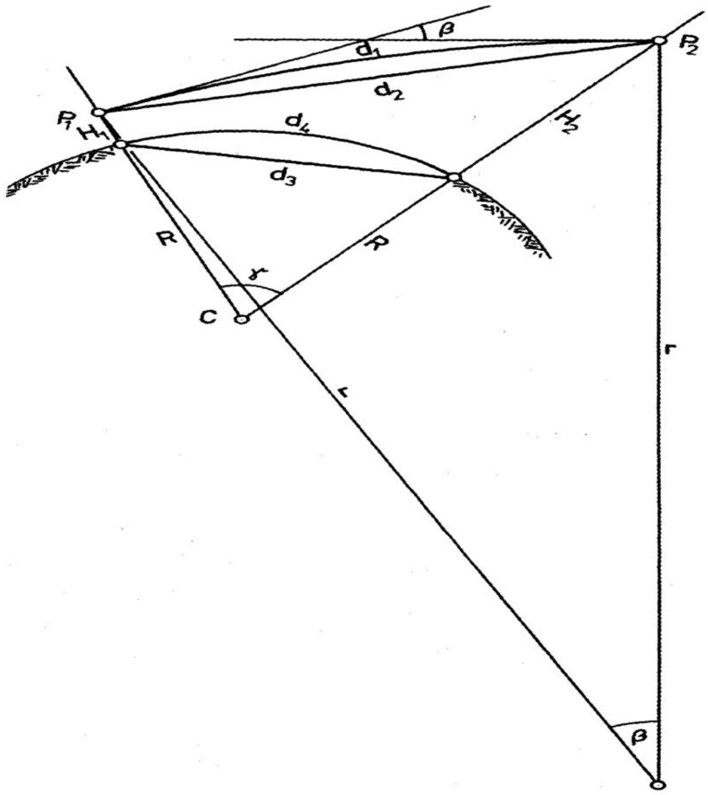

Figure 2.16: Correction for path curvature

The reduction from chord at sea level to arc at sea level is:

$$C_4 = \frac{d_1}{24R^2} \qquad 2.44$$

The corrected distance is:

$$d_4 = d_3 + C_4 \qquad 2.45$$

The combination of C_2, C_3 and C_4 (equations 2.39, 2.42 and 2.44 above) results in the following overall correction (Rueger, 1996):

$$-\left(k-k^2\right)\frac{d_1^{\,3}}{12R^2} - k^2\frac{d_1^{\,3}}{24R^2} + \frac{d_1^{\,3}}{24R^2} = \left(1-k\right)^2\frac{d_1^{\,3}}{24R^2} \qquad 2.46$$

Using k = 0.13 as suggested by Angus-Leppan (1962), the above equation 2.46 becomes:

$$\frac{d_1^{\ 3}}{32R^2} \qquad \text{...2.47}$$

Since the radius of the earth is known (6.38 x 10^6 m), assuming the value of d_1 is 1000m, then equation 2.47 above results in correction of about 0.77μm (0.77 x 10^{-3} ppm). Generally, if equation 2.46 above is differentiated with respect to k, it can easily be found that for a variation of k between -0.4 to +0.4, the correction is affected from 1 x 10^{-3} ppm to 3 x 10^{-3} ppm. This is the main reason why only first velocity correction is important in a short-range distance (up to 1 km) measurement. Exceeding this range of distance measurement all the three corrections must be considered especially when long-range distance is involved.

2.11 ALTERNATIVE APPROACH

Attempts to solve the problem of refraction are not limited to equations or formulae generation alone. There have been attempts to solve the refraction problem instrumentally. The first of such attempts resulted in the production of the Kern ME 3000 (Mekometer). This instrument employed a standard cavity that sampled the air surrounding the instrument and adjusted the measuring frequency accordingly, thus compensating for the refractive index (and the change in it) at the instrument station (Iliffe & Dodson, 1987). Nowadays, all the new generation total stations are designed to employ the same principle. The principle did not solve the problem because the mean refractive index along the line differs from that at the instrument station.

A second approach has led to the development of an instrument using two beams with different carrier frequencies (for example, red and blue laser beams). Such an instrument makes use of the frequency dependence of the refraction effect and by a combination of the two measurements allows a first-order refraction correction to be made. The distance is derived from the equation:

$$d = d_r - A(d_b - d_r) \qquad \text{...2.48}$$

where:

d_r = distance measured with red laser (HeNe)

d_b = distance measured with blue laser (HeCd)

A = coefficient, dependent on wave length, pressure and water vapour pressure (approximately 21 for HeNe + HeCd lasers)

Although the two-colour arrangement eliminates a considerable part of the uncertainty of refractive index, the distance has to be measured with at least 20 times higher resolution than finally required, because of the factor 21 involved. Due to the limitation of the systems, only distances of more than 500 to 1000 m can be measured. The maximum range is 10 – 15 km during the evening period (Rueger, 1980a).

The three-colour instruments reduce even further the residual effects of the uncertainty of atmospheric parameters. The distance equation is as follows:

$$d = d_r - A(d_b - d_r) - B(d_{mw} - d_r) \qquad 2.49$$

where:

A = 20 approximately

B = 0.02 approximately

d_{mw} = microwave distance.

The essential drawbacks of all hitherto existing instruments with two- or three-carrier wavelengths are as follows:

- Using carrier wavelengths having little separation results in a very small difference in optical dispersion.
- This leads to the need for an extremely high resolution which in the prior art cannot be realized under field conditions.
- The alternative for using carrier wavelengths that are widely spaced, according to the prior art, requires a high instrumental effort inasmuch as the requirements for controls, switching, *et cetera* are different between the two wave-length regions.
- The instruments to be realized when using carrier wavelengths that are widely spaced do not meet the requirement of surveying technology, especially with respect to their weight and ruggedness.

The third solution would be to build an atmospheric model into a microprocessor inside the EDM so that a refraction correction can be calculated from meteorological data supplied to or measured by the instrument (Iliffe & Dodson, 1987).

2.12 THE EFFECT OF GLASS ON BEAM OF LIGHT

The effect of the shelter glass on the beam generated by the total station during monitoring with RTS from transfer beacon shelter is called refractive effects and it is based on Snell's law. This law expresses the relationship between the angles of incidence and refraction, when a light ray passes through a boundary between two different isotropic media, namely air and glass, as regards to this study. Ostdiek and Bord (2008) simplified the whole process by saying, "a light ray is bent toward the normal when it enters a transparent medium (e.g. glass or water) in which light travels more slowly. It is bent away from the normal when it enters a medium in which light travels faster". Based on Snell's theory, the beam from the RTS passes through the air inside the total station shelter (transfer beacon shelter) and strikes the shelter glass window at an angle of incidence θ' with respect to the surface normal. It refracted and passed through the glass at angle θ_g with respect to the surface normal. The beam is slowed down when passing through the glass, because the refractive index of the glass n_g is greater than the refractive index of the air n_a. When the beam emerges from the glass, it refracted once more so that its angle with respect to the surface normal is again θ and also resumes its original speed. Figure 2.17 below demonstrates the whole scenario.

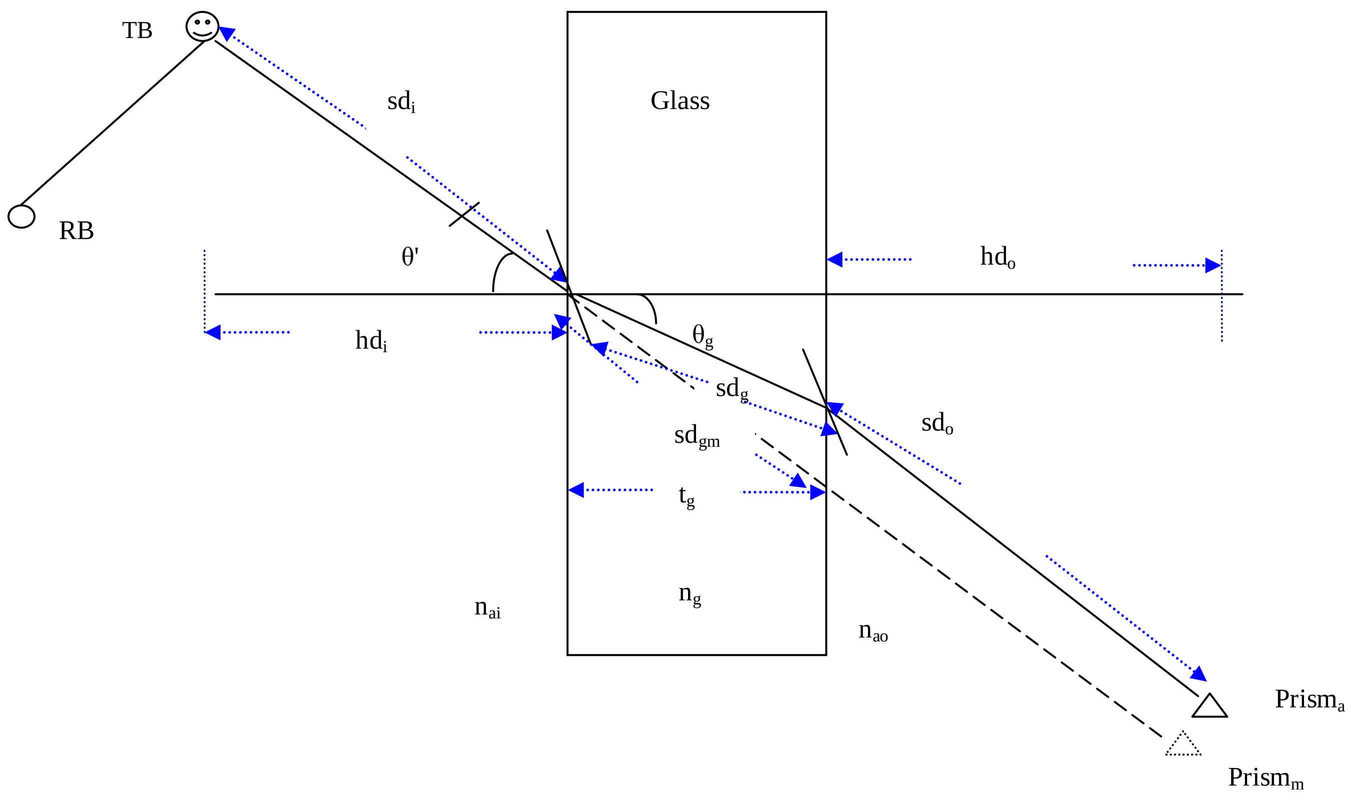

Figure 2.17: Effect of plane glass on light beam.

Where:

TB is the transfer beacon upon which the RTS is mounted inside the shelter;

RB is the reference beacon (control point) for orientation;

θ' is the angle of incidence of the RTS with respect to the surface normal of the glass;

sd_i is the slope distance between the RTS and the glass;

hd_i is the horizontal distance between the RTS and the glass;

n_{ai} is the refractive index of air inside the shelter;

θ_g is the angle of refraction within the glass;

sd_g is the slope distance within the glass or distance travelled by the RTS beam through the glass;

sd_{gm} is the slope distance that would be measured by the RTS through the glass

t_g is the thickness of the glass;

n_g is the refractive index of the glass;

n_{ao} is the refractive index of air outside the shelter;

sd_o is the slope distance between the glass and the target, the prism, that is being monitored, while hd_o is the corresponding horizontal distance; and

$Prism_m$ is the measured prism position, while $Prism_a$ is the actual prism position.

Mathematically, the total slope distance would be:

$$sd_{total} = sd_i + sd_g + sd_o \quad \ldots\ldots 2.50$$

(where $sd_g = \dfrac{t_g}{\cos(\theta_g)}$; and $\theta_g = \sin^{-1}\left[\sin(\theta) \times \dfrac{n_a}{n_g}\right]$)

While horizontal distance would be:

$$hd_{total} = hd_i + t_g + hd_o \quad \ldots\ldots 2.51$$

Consequently, the actual coordinate of the prism would be:

$$Prism_a\,(Y_a) = (sd_i + sd_o).\sin(\theta) + sd_g.\sin(\theta_g); \text{ and } Prism_a\,(X_a) = (sd_i + sd_o).\cos(\theta) + sd_g.\cos(\theta_g) \quad \ldots\ldots 2.52$$

However, all the above quantities are hardly taken into account, nor are their values known when computing the position of the prism relative to the RTS position. The measured coordinate values that are displayed on the RTS screen are usually computed from:

$$\left.\begin{array}{l} Prism_m\ (Y_m) = (sd_i + sd_{gm} + sd_o).\sin(\theta);\ \text{and}\ Prism_m\ (X_m) = (sd_i + sd_{gm} + sd_o).\cos(\theta) \\ \text{I.e.}\ Prism_m\ (Y_m) = sd_{total}.\sin(\theta)\ \text{and}\ Prism_m\ (X_m) = sd_{total}.\cos(\theta) \end{array}\right\} \quad 2.53$$

(where $sd_{gm} = sd_g \times \frac{n_g}{n_{ao}}$)

If the join between the TB and RB is calculated, and the direction from TB to the prism is known by using RB for orientation, for instance $\alpha_{tb\text{-}p}$, the above equation 2.53, can be re-written as:

$$\left.\begin{array}{l} Prism_m\ (Y_m) = [(hd_i + t + hd_o).\sin(\alpha_{tb\text{-}p})] + Y_{TB};\ \text{and}\ Prism_m\ (X_m) = [(hd_i + t_g + \\ hd_o).\cos(\alpha_{tb\text{-}p})\ ] + X_{TB} \\ \text{i.e.}\ Prism_m\ (Y_m) = [hd_{total}.\sin(\alpha_{ts\text{-}p})] + Y_{TB}];\ \text{and}\ Prism_m\ (X_m) = [hd_{total}.\cos(\alpha_{tb\text{-}p})] + \\ X_{TB}. \end{array}\right\} \quad ..2.54$$

where:

$\alpha_{tb\text{-}p}$ is the direction of prism from the instrument station TB; and

Y_{TB} and X_{TB} are the coordinates of instrument station TB or the transfer beacon.

The displayed coordinate on the screen of the RTS are based on equations 2.53 and 2.54. According to Lutes (2002), this is based on the assumptions that:

a. the glass is perfectly flat on both sides;
b. the inside and outside surfaces of the glass are parallel;
c. the glass molecules are pure, i.e. without bubbles in the inner structure of the glass
d. the glass refractive index is uniform;
e. the refractive index of air inside the shelter is identical to that outside of the shelter; and
f. the refractive index of the air is uniform.

Practically, the above assumptions are not attainable. Therefore, there is need to examine the effect of the shelter glass on the quality of distances measure with a total station setup in a transfer beacon shelter.

2.13 REMARKS ON VALIDITY OF ATMOSPHERIC CORRECTION FORMULAE WHEN TAKING READING THROUGH GLASS

Accurate determination of the group refractive index of the air along the line of sight (the light wave path) is required for an accurate distance measurement. The general practice of taking the atmospheric parameters (temperature, pressure and water vapour pressure) at both terminals (instrument station and reflector) and using the means in group refractive index equations can only give good results for low accuracy surveying total station lines. This method may not function well in a surface mine environment where a little displacement (or little mm shift in distance) counts considerably during slope stability monitoring exercise. However, this method may work under a dry day and a cloudy sky with a moderate wind blowing.

The question now is that: Are these conditions attainable in a mine and to what extent will the practice of using the mean of atmospheric parameters readings taken at both terminals provide an accurate value for the line path average?

The first part of the above question is, in capitals, NO. In answering the second part, the following factors must be considered:

- How long is the distance to be measured (the length of the line)?
- The prevailing atmospheric conditions
- How straight is the surface (terrain) where the work is being done (i.e. the nature of topography beneath the wave path or line)?

Although the act of using terminals atmospheric readings is economic, the above question must be fully satisfied and must be at the back of the mine surveyor's mind that the economic gain cannot supersede the life and the cost of equipments that can be lost due to slope failure in a surface or an underground mine. Therefore, proper modelling or extrapolation of atmospheric parameters must be considered.

Finally, empirical research and IAG (1999) recommended equations for refractive index corrections, but there is no consideration for impacts of taking measurements through a glass (window) barrier. Only three movements of light rays were considered, that is from the total station telescope (transmitter) to the atmosphere and from there to the reflector (or target) back to the total station telescope (receiver) through the atmosphere. In the new area of investigation that this research is based on, five movements of light ray were considered, that is from the total station telescope (transmitter) to window glass through atmosphere, from there to atmosphere again before getting to the target (reflector). This procedure can be summarised as shown in figures 2.18 A and B below:

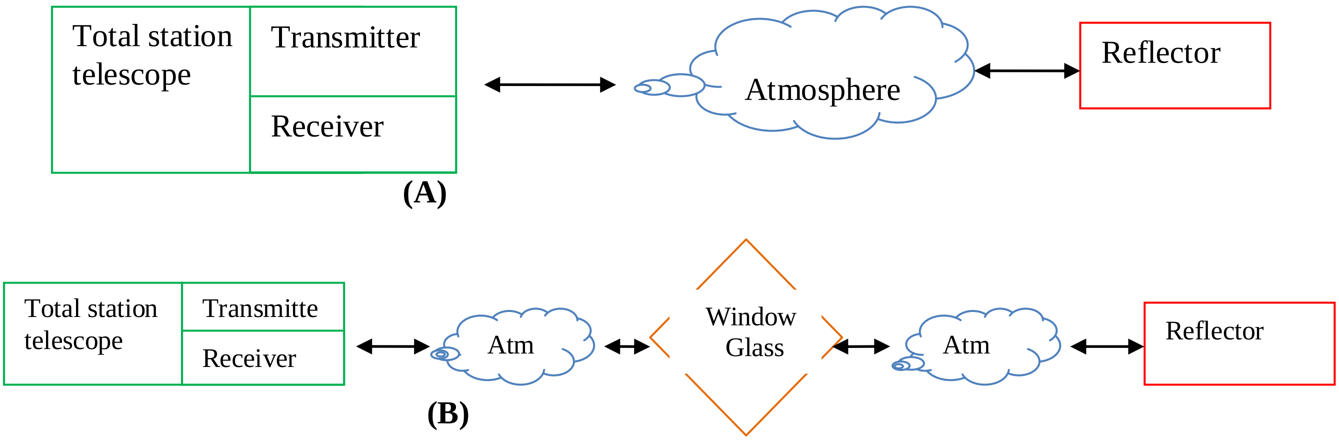

Figure 2.18: A - Movement of light ray during survey exercise with no barrier and B - with barrier

When measuring angles through windows, the glass sheet acts as a plain parallel plate. The effects of parallel plates on line of sights are known from precise levelling. The parallel shift q caused by a parallel plate of thickness t_i can be computed from (Rueger, *et al* 1994):

$$q = \left(\frac{n_G - 1}{n_G}\right) \times t_i \tan\varphi \qquad 2.55$$

where:

φ = angle of incidence of the rays (measured from the normal to the glass surface).

n_G = refractive index of the window material (n_G=1.5 for glass and acrylic glass e.g. Perspex).

However, real windows differ from parallel plates in so far as the glass is not perfectly flat and does not have parallel faces. The effects of window glass imperfections can only be established through experiment (Rueger, *et al*. 1994).

This research investigated the effect of this middle (window) barrier on the total station reading during distance measurement to confirm whether manufacturer of total station atmospheric corrections formulae (which is a modified version of empirical researcher as well as the IAG, 1999 recommended corrections), cater for the anomalies that this middle barrier might cause on the total station distance measurements. The following properties of glass were considered:

- Glass thickness;
- Glass colour; and

- Shape of glass.

2.13. CONCLUSION

The chapter reviewed the total station surveying instrument, its areas of application and the formulae to correct systematic error resulting from atmospheric variations. It also gave the steps of the corrections and the alternative approaches that could be used. It concluded that another systematic error was potentially introduced when EDM measurements were taken through a glass, which is typical for continuous survey monitoring because of fear of theft or damage to instruments. The remainder of this thesis considers the issue of taking distance measurements through a window glass via the atmosphere.

The next chapter discusses what an atmosphere is and the likely effects of atmosphere on the path of beam generated during total station survey. It also discusses the various atmospheric models commonly employed in the past for refraction correction during distance measurement with EDM.

CHAPTER THREE

3.0 THE ATMOSPHERE AND THE ATMOSPHERIC MODELS

The chapter discusses the part of the atmosphere (the troposphere) that is relevant to this study. It also describes the turbulent zone and the effect of this zone on total station readings and provides the formulae for correcting EDM measurements for atmospheric conditions by stating the available atmospheric models - TTM, SREATM and STAM.

3.1. INTRODUCTION

Atmospheric variation is the limiting factor for the accuracy and precision of single wavelength EDM (i.e. for microwaves, infrared and visible light). Owens (1968) declared that one of the main limitations to the accuracy of geodetic measurements is the uncertainty in the average propagation velocity of the radiation due to the inhomogeneity of the atmosphere.

The main source of error in the refraction correction is the difference between the observed temperature and the average temperature over the length of line. The typical line of sight extends from one high point in the topography to another and lies in between, at a height above the surface. Since there is considerable temperature variation with height above the surface, measurements at the end points (terminals measurement) are not representative (Angus-Leppan, 1972).

According to Angus-Leppan (1979), *"the atmospheric effects on geodetic observations place a limit on their accuracy".* Variation in refractivity (refractive index) arise through variations in the temperature (T), pressure (P) and water vapour pressure (e) part of the lower atmosphere as shown in chapter two of this report (see section 2.7). Fraser (1979) also affirmed this in his statement: "the accuracy attainable with EDM (total station) techniques, for both light and microwave instrument, is still limited by shortcomings in the adequate modelling of integral refractivity prevailing over the wave path at the time of observation". Standard total station procedures involve sampling these atmospheric (or meteorological) parameters at each end point of the EDM line, usually at the instrument height. In electro-optical EDM, the principal shortcoming in refractivity modelling arises mainly due to the measured endpoint temperatures being unrepresentative of the mean air temperature over the wave path. In the EDM error analysis, as shown in section 2.8 of chapter two, the water vapour pressure (e) has a negligible effect, while the pressure (P) is subject to regular variations and hence is adequately modelled by the mean of the terminal meteorological readings (as shown in Table 2.7).

According to Angus-Leppan and Brunner (1980), "the *variations of pressure with height are regular. For light wave EDM, unlike microwave EDM, water vapour pressure changes have only insignificant effects. So, for pressure and humidity, the mean of end point measurements is sufficiently representative"*. The mean of end points temperature readings is representative only when the atmospheric structure (conditions) is neutral (i.e. neither stable nor unstable) Also, Wilkins (2004) pointed out that the temperature gradients crossing the line of sight could cause problems with the apparent direction to the target being observed by bending the light rays.

The theoretical foundation for the study of turbulence and the development of a set of approximation equations was introduced by Priestly in 1965 (Panofsky & Dutton, 1984). However, atmospheric turbulence in geodesy has been taken into account in atmospheric modelling only since 1977. Investigations have indicated that the accuracy of EDM, as reflected by the accuracy of determining a representative mean value of refractivity from the endpoint meteorological measurements, is closely related to the thermal stability of the atmospheric boundary layer at the time of observation. In the present context, optimum meteorological conditions are those in which the measured endpoint temperatures can be transformed via atmospheric models into representative mean value for the EDM wave path. Significant research on atmospheric models as regards EDM surveying instrument was carried out by three researchers:

A. Turbulent Transfer Model (TTM) was proposed by Brunner and Fraser (1977). The model is only applicable for a long-range EDM lines when an unstable turbulent regime has developed in the lower atmosphere. The model is not applicable in neutral or stable atmospheric conditions.

B. Angus-Leppan and Brunner (1980), described the Short Range EDM Atmospheric Temperature Model (SREATM) for unstable, neutral and stable thermal stratifications.

C. Fraser (1981) proposed a Simple Two-layer Atmospheric Model (STAM) for electro-optical EDM reduction. The model is applicable when the thermal state of the lower atmosphere is either unstable, near-neutral or weakly stable.

This chapter discusses the atmosphere, its basic theory as it affects EDM distances (micrometeorology) and the analysis of these three atmospheric models mentioned above.

3.2. THE ATMOSPHERE

The atmosphere is a non-homogeneous system in which properties are sensitive to changes in altitude - pressure, temperature, humidity, wind direction and wind speed. A vertical profile of the atmosphere reveals that the earth's atmosphere is divided into several layers. Each layer may be defined in a number of ways:

- The mode in which the air temperature varies through it;
- The gases that comprise it; or
- Its electrical properties.

Three variables – air pressure, air density and air temperature - play important roles in the description of the earth's atmosphere.

Air Density: Air molecules are held near the earth by gravity. This strong, unnoticeable force pulls down the air above and squeezes air molecules together. This causes their number in a given volume to increase (i.e. the more the air above a level, the greater the compressed effect). Since air density is the amount of air molecules in a given space (volume), it follows that air density is greatest at the earth's surface and decreases as one moves up into the atmosphere. Figure 3.1 shows a clear expression of air density variation with altitude. It illustrates that, because the air near the surface is compressed, air density normally decreases rapidly at first, then more slowly as one moves farther away from the earth surface.

Air Pressure: Air molecules have weight; this weight exerts a force upon the earth. The quantity of force exerted over an area of surface is called atmospheric pressure or air pressure. As one climbs in elevation, less air molecules are above one; for this reason, atmospheric pressure always decreases with increase in height. Like air density, air pressure decreases quickly at first, then more gradually at higher levels. Figure 3.1 shows variations in both air density and air pressure with increase in altitude.

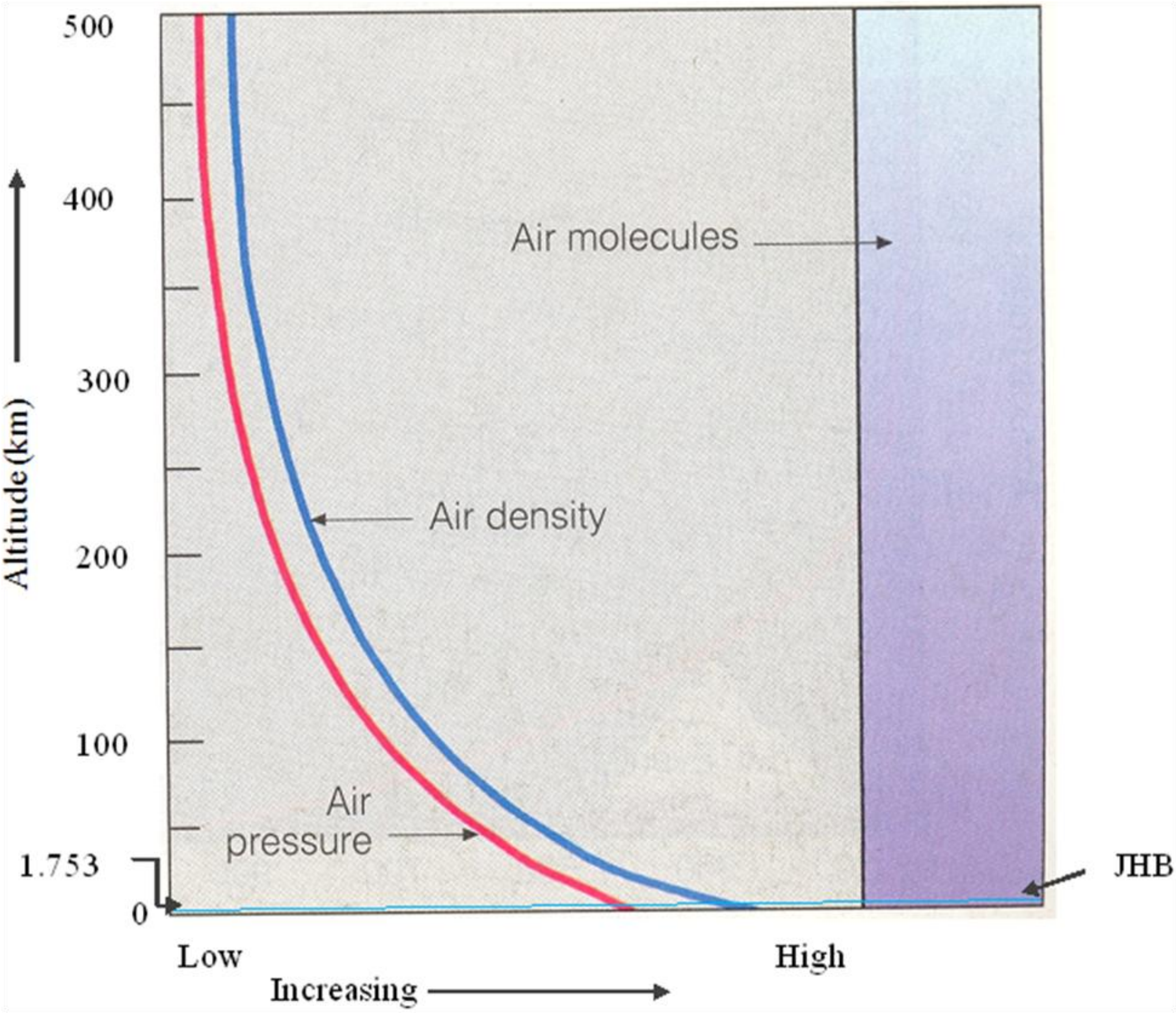

Figure 3.1: Variations in both air density and air pressure with increase in altitude (source: Ahrens, 1993).

Air Temperature: Air temperature has a more complicated vertical profile compared to air density and pressure discussed above. It generally decreases from the earth's surface up to an altitude of about 11 km (Ahrens, 1993). This diminishing in air temperature with increasing height is due primarily to the fact (discussed further in section 3.3.2) that sunlight warms the earth's surface and the surface in turn, warms the air above. This main portion in the Figure 3.1 above that is relevant to this research lies between altitude 1.650 km and 1.80 km. The research was carried out in Johannesburg (JHB) which is situated in the centre of the Highveld, at an elevation of 1,753 metres (5,751 ft), latitude 26º08' South and longitude of 28º14' East. Johannesburg is on the south side of the famous ridge called the 'Witwatersrand'.

The University where this research was carried out is named after this ridge. The region receives an annual rainfall of 760 millimetres (30 in), and has a maximum midwinter average temperature of 19^{0}C. The average temperature varies from 4^{o}C in winter to 26 (or a little above 26^{o}C) in summer. Temperature variation within a day can be as much as 13^{o}C as shown in Figure 3.2 below.

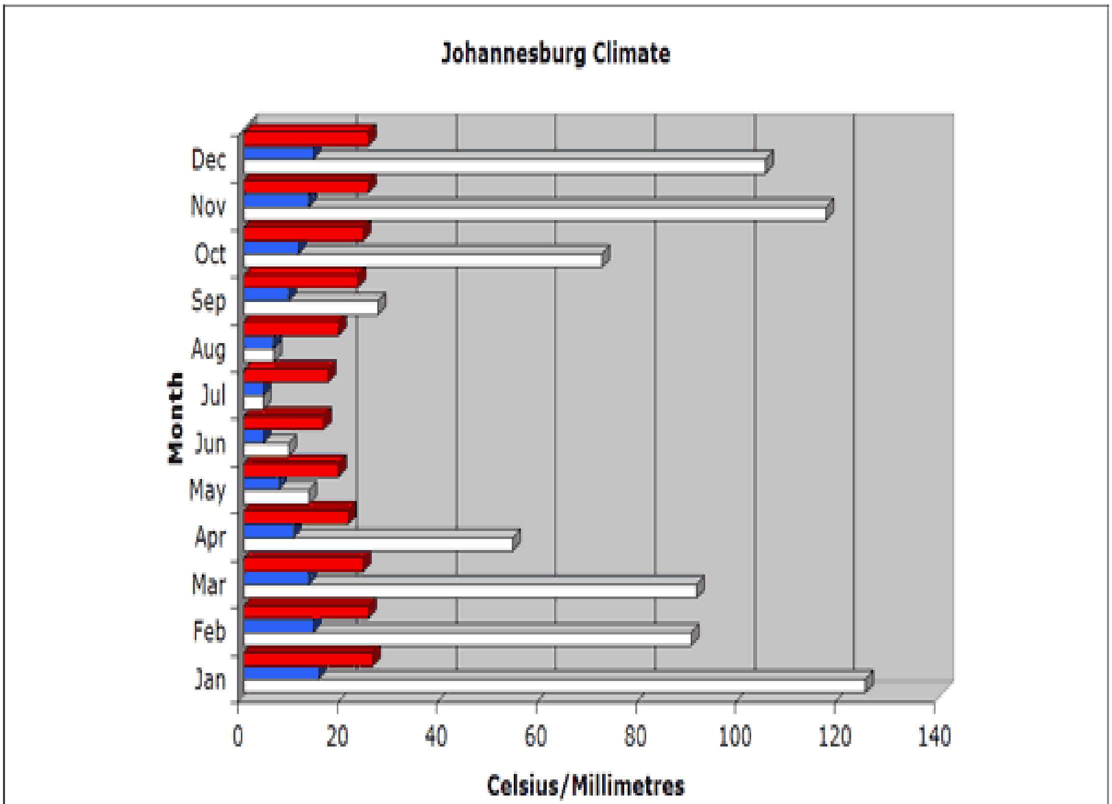

	Jan	Feb	Mar	Apr	May	Jun	Jul	Aug	Sep	Oct	Nov	Dec
Max Temp	26	25	24	21	19	16	17	19	23	24	25	25
Min Temp	15	14	13	10	7	4	4	6	9	11	13	14
Precipitation	125	90	91	54	13	9	4	6	27	72	117	105

Figure 3.2: **Graphical representation of Johannesburg climate** (Source: Safari now)

The altitude of Johannesburg above the sea level (i.e. 1.753 km) keeps the average summer temperature below 30^{0}C. In winter, for the same reason, the night temperature drops to freezing point, in some places even lower. The average atmospheric pressure in Johannesburg is 810 mb as shown in the Figure 3.3.

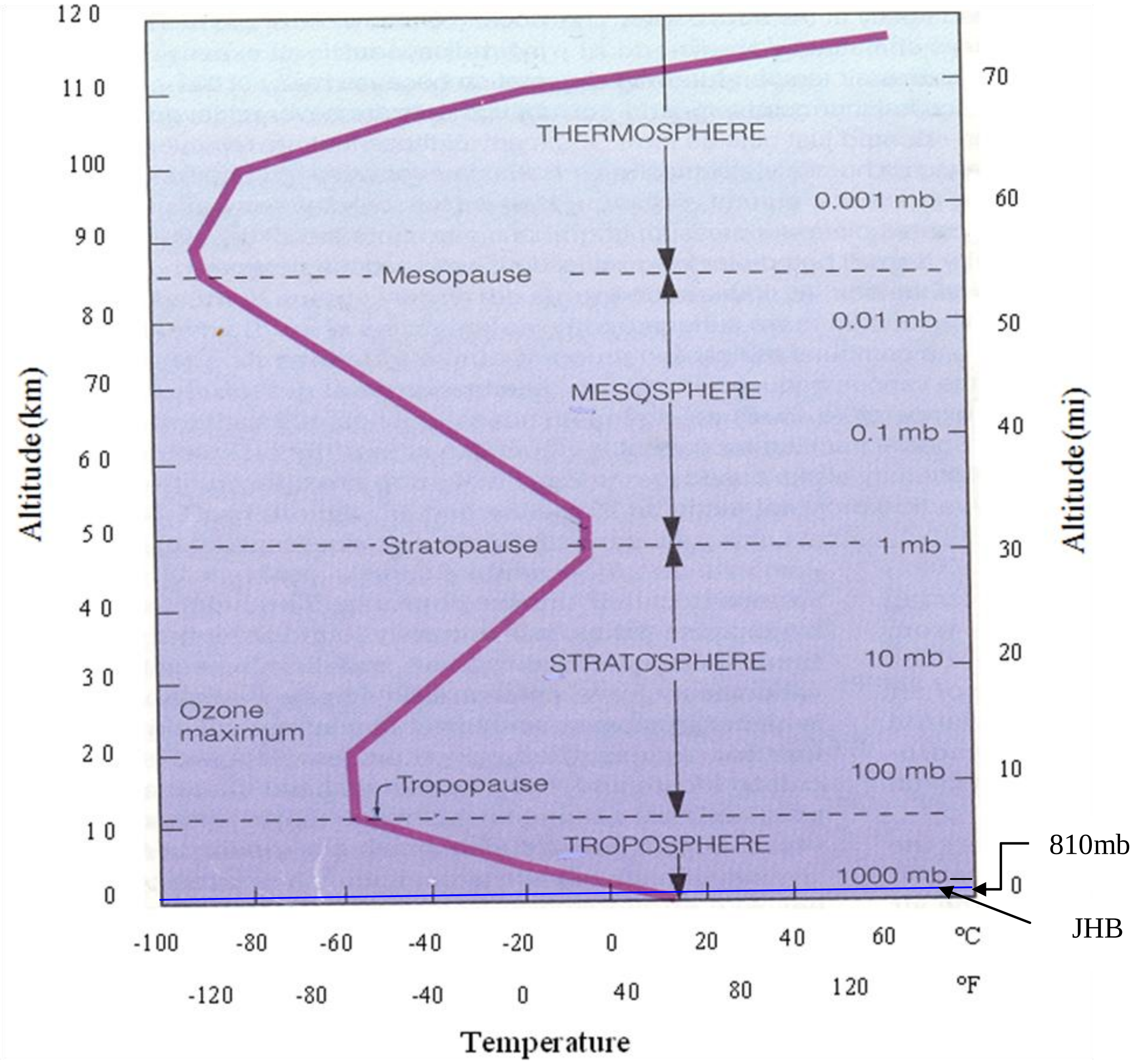

Figure 3.3: **Changes in temperature and pressure with altitude** (Source: Ahrens, 1993)**.**

The earth's atmosphere can be grouped into three zones – lower, middle and upper zones. The lower atmosphere is made up of the troposphere, while the middle comprises the stratosphere and mesosphere. The upper atmosphere consists of the thermosphere and the exosphere respectively. The **troposphere** is the only relevant part of the atmosphere that can influence this research therefore the discussion focuses on it.

3.2.1 Troposphere

The troposphere is the most active zone of the atmosphere with pronounced wind motion, rich in moisture and temperature decreasing with increase in the altitude. Its size varies according to latitude, ranging from 7 km at the poles up to 20 km at the equator. It is in this portion of the atmosphere that most of the weather patterns occur. The word troposphere is derived from Greek "tropos" meaning "turning" or "mixing"; The term reflects the fact that turbulent mixing plays an important role in the troposphere's structure and behaviour. Most of the phenomena associated with day-to-day weather occur in the troposphere. In the troposphere, properties also vary as a function of the altitude with respect to the earth surface due the layered nature of the atmosphere. Figure 3.4 shows the layers of the earth atmosphere.

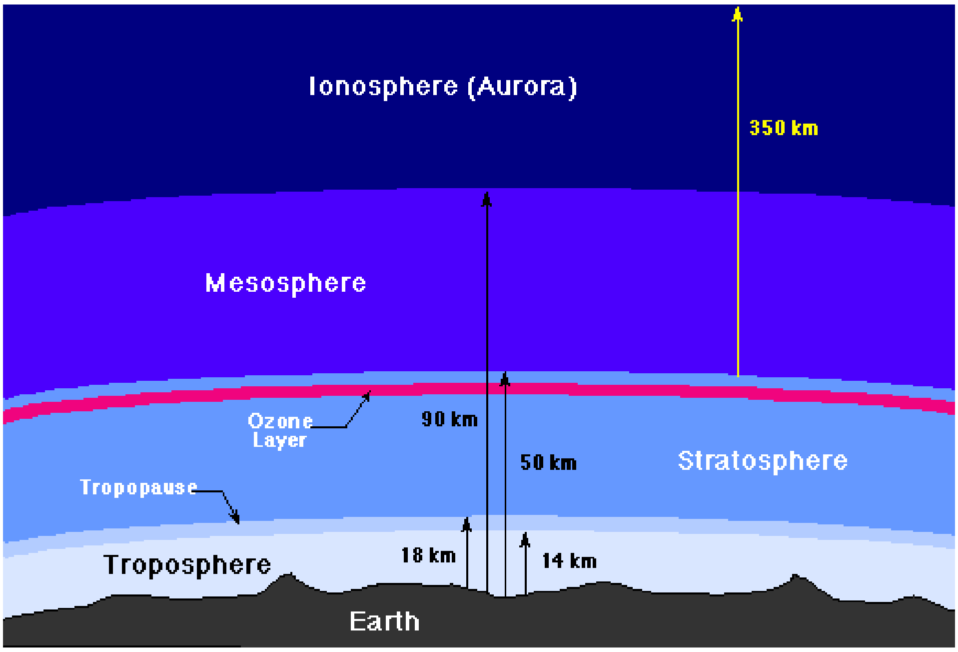

Figure 3.4: Layers of the earth's atmosphere (Source: Astronomy 161 online Lecture)

The border between the troposphere and stratosphere is called the tropopause – this region is known for temperature inversion (Danielson *et al*, 2003). The tropopause caps the troposphere and at this region, the temperature is stable or near stable.

The layered nature and the sensitivity of the non-homogeneous atmosphere to different variables create the turbulent fluctuations in the refractive index of the atmosphere. It also causes phase fluctuations in the travelling wavefront. Figure 3.5 below illustrates the distortions in response to the changes of refractive index in the atmosphere.

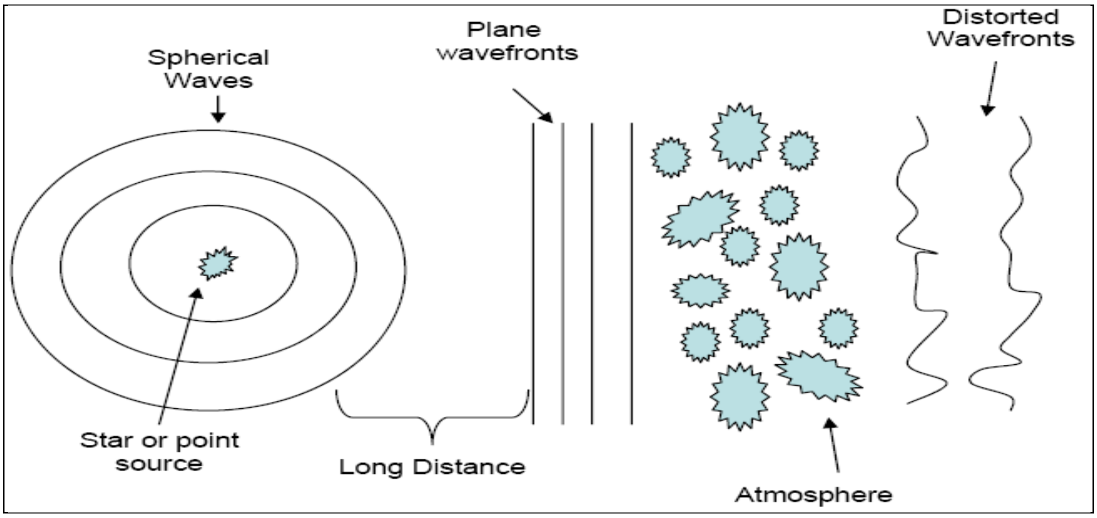

Figure 3.5: Representation of light from a point source travelling through the atmosphere (Source: Font Jiménez, 2006)

3.3. MICROMETEOROLOGICAL BACKGROUND

The above stated models in section 3.1 are based on micrometeorological properties. Micrometeorology deals with the exchange of heat (energy) mass and momentum occurring between the atmosphere and the earth's surface, including the subsurface medium. The energy at or near the surface over a short duration (say hourly) is an important aspect of the different types of energy exchange involved in the earth-atmosphere-sun system (Arya, 2001). Vertical distributions of meteorological variables, such as temperature, wind and humidity as well as trace gas concentrations and their role in the energy balance near the surface also affect micrometeorology. In addition to short-term averaged values of meteorological variables, more or less random fluctuations of the same in time and space around their respective average values are of considerable interest in the development of the above-mentioned models. The statistics of these so-called **turbulent** fluctuations are intimately related to the above-mentioned exchanged processes and hence constitute an integral part of micrometeorology or boundary-layer meteorology.

According to McLaren (1990) in his report on the monitoring of an unstable slope in North East of Portland Dorset, *"distances along the monitoring lines are measured with EDM, a device which uses polarized light and is stated to be capable of measuring distances up to 500 m with accuracy of the order of 1 in 1 million or better".* He identified a number of micrometeorological factors that can affect the accuracy and significance of the measurement made in the field, namely:

a. Factors affecting the accuracy of measurements

The accuracy of measurements can be affected by variations in the refraction of polarised light due to:

i. A change in altitude along the line of sight;

ii. Different types of surface and terrain beneath the line of sight; and

iii. Atmospheric turbulence caused by wind blow over rough ground.

b. Factors affecting the significance of the measurements made.

Change in the distance measured between two particular points on different occasions may result from:

i. Change in temperature – the expansion or contraction of the materials upon which survey stations are mounted; and

ii. Change in moisture content – causing shrinkage or swelling of cohensive soils around survey stations.

The three models (TTM, SREATM and STAM) mentioned in section 3.1 deal with the accuracy matter, as listed in (a) above.

3.3.1. Turbulent Zones

Within the troposphere, the bottom layer, which is in contact with the surface of the earth, is called the atmospheric boundary layer (ABL), sometimes referred to as the ground layer (GL) or planetary boundary layer (PBL). It varies 1-2 km and is typically turbulent in the daytime (Panofsky & Dutton, 1984). This is the area where the atmosphere experiences surface effects through vertical swap of momentum, heat and moisture. Johannesburg at an altitude 1.753 km typically experiences this condition. On a typical day there is always a breeze in Johannesburg. The horizontal forces of friction with the Earth's relief, acting on the air movement that would keep the balance of the wind between the Coriolis[16] force and the horizontal pressure gradient, modify the displacements and the exchanges of energy and mass within a layer thick of about 1500 m. The surface layer, where the interactions between the

[16] Coriolis force is a force that acts to change direction of a moving body to the right in Northern Hemisphere and to the left in the Southern Hemisphere (Persson, 1998). A great circle can be used to understand motion on a rotating sphere (Mclntyre, 2000).

surface and the wind are at the strongest has a thickness of about 30 m. In the layer, the ground-air friction is stronger, the wind shear generates mechanical turbulence that exceeds the buoyant forces, and in addition, a differential temperature is present due to warming during day time and cooling during night time. Temperatures in the boundary layer are affected by the specific heats of soil and air by energy transfer processes that result in turbulence status of the layer. Above the ABL is the free atmosphere (FA) where the effect of the surface friction on the air motion becomes less important. The dynamics are more complicated and turbulence depends on wind shear and gravity waves. The surface layer (SL) contributes greatly to atmospheric turbulence. The importance of the contribution of the turbulence in the ABL is significant, in the order of 60% found in different observatories (Tokovinin, *et al.*, 2005). Figure 3.6 shows a simple diagram of turbulent zones in the atmosphere:

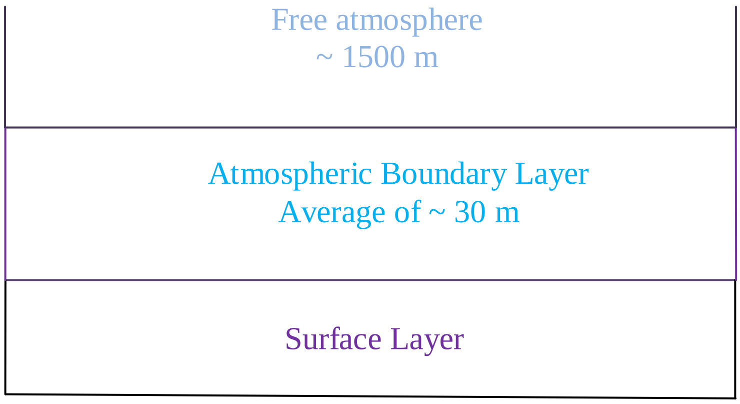

Figure 3.6: Turbulent zones in the atmosphere

Effect of turbulence

Turbulence[17] refers to the apparently chaotic nature of many air flows, which is manifested in the form of irregular, almost random fluctuations in velocity, temperature and scalar concentrations around their mean values in time and space (Arya, 2001). It is difficult to define turbulence, but it is fairly easy to recognise its presence.

Turbulence research has customarily focused on the structure of the turbulent boundary layer over relatively smooth and homogeneous surfaces. In the atmosphere, the underlying surface, however, is almost always rough, and in recent years, the interests and efforts of boundary layer (BL) researchers have been increasingly directed toward

[17] Turbulence is air flow filled with turmoil (Panofsky & Dutton, 1984)

problems of surface-atmosphere interaction over ‘complex’ surfaces. At the base of such research lies the fundamental difficulty that the well-established homogeneous SL relationships, used to describe the mean and turbulence properties, collapse in regions of inhomogeneity because several assumptions underlying their derivation are invalid. Comprehensive field studies of atmospheric turbulence over rough and inhomogeneous environments in general are difficult to accomplish and, as a result, are limited in scope. However, a consistent picture of flow and scalar transfer is emerging, based on carefully conducted observations over a wide range of complex surfaces such as crops and forests (Kaimal & Finnigan 1994).

Atmospheric turbulence is always manifested in the form of gustiness of winds[18], so that gustiness is regarded as a simple measure of turbulence strength or intensity. The motions in the ABL are almost always turbulent. In the surface layer, turbulence is more or less continuous, while it may be intermittent and patchy in the upper part of ABL and is sometimes mixed with internal gravity waves.

Atmospheric turbulence spans a huge range of scales. Turbulent currents are important elements in the global circulation, in synoptic weather systems, in regional circulations, in severe storms, in clouds, in the ABL and in plant canopies. In its large-scale limit, atmospheric turbulence approaches two-dimensionality, while its smaller-scale forms are inherently three-dimensional (Wyngaard, 1992). In the atmosphere, the flow near the ground is almost always turbulent up to a height of 1 km or more in the daytime over the land and up to 100 m or so over the land at night. This effect may be up to a few hundred metres over the sea or ocean. At larger heights, turbulence occurs in cumulus cloud systems and in layers with strong changes in average wind speed or direction (Albanis, 1993).

Panofsky and Dutton (1984) stated the three main reasons why atmospheric scientists (Astrologists and Meteorologists) and engineers are concerned with the properties of turbulence as cited below:

a. Turbulence creates spatial and temporal variations of refractive index (n) and thus leads to scattering of electromagnetic and acoustic radiation;

[18] Gustiness of winds is the difference between the scalar and vector wind speeds, that is, contributed by boundary layer large eddies, convective precipitation and cloudiness (Zeng, *et al.*, 2002)

b. Turbulence imposes forces on buildings, towers, aeroplanes and other structures; and

c. Turbulence mixes air with different properties and creates fluxes of important physical quantities.

3.3.2 Conservative Parameters

The atmosphere is not isothermal; in reality, air temperature falls fairly with increasing altitude. In ski resorts, the temperature is expected to drop by about 1 degree per 100 metres of upward movement. This depends on three important properties of air. The first significant property is that air is transparent to most, but by no means all, of the electromagnetic spectrum. In particular, nearly every infrared radiation, which carries heat energy, passes straight through the lower atmosphere and heats the ground. In other words, the lower atmosphere is heated from beneath, not from above. The second important property of air is that it is continuously in motion. In fact, the lower 20 kilometres of the atmosphere (the so-called troposphere as shown in Figure 3.3 above) are fairly thoroughly mixed. One may think that this would mean that the atmosphere is isothermal. However, this is not the case because air is a very poor conductor of heat.

Within the atmosphere, the mean pressure at any point is hydrostatic. Thus when a parcel of air is displaced upward, it moves into a region of lower pressure where it expands and cools. If there is no exchange of sensible heat between the parcel and the environment during this movement, the process is adiabatic, with the extent of cooling being in accordance with the dry adiabatic lapse rate (Fraser, 1979; Augus-Leppan & Brunner, 1980).

An adiabatic atmosphere can be linked to a packet of air which is being swirled around in the atmosphere. It is expected to always remain at the same pressure as its environs; otherwise it would be automatically be unstable. It is also likely that the packet moves around too quickly to effectively exchange heat with its surroundings, since air is a very poor conductor of heat and heat flow is consequently quite a slow process. Therefore, to a first approximation, the air in the packet is adiabatic. In a *steady-state* atmosphere, it is normal that as the packet moves upwards, expands owing to the reduced pressure, and cools adiabatically, its temperature always remains the same as that of its immediate surroundings. Any quantity that does not change with either time or displacement during an adiabatic process is termed a **conservative parameter**.

In atmospheric models there are two conservative parameters that play important roles in the study of potential refractivity:

a. **Specific humidity (q)** can be utilized in tracing the motion of water vapour in the atmosphere. q is defined as the fraction of the mass of water vapour to the mass of moist air containing the vapour and can be calculated from the expression below:

$$q = 0.622\frac{e}{p} \quad \text{...} 3.1$$

where:

q = specific humidity, which is dimensionless;

e = partial pressure of water vapour in mbar; and

p = atmospheric pressure in mbar.

b. The **potential temperature** (θ) is more important than q. θ of the air mass or parcel is defined as that temperature which it would take up (or assume) if brought adiabatically (i.e. with no exchange of heat) from its altitude down to a standard pressure of 1000 mbar (Fraser, 1979; Augus-Leppan & Brunner, 1980; Jacobson, 2005). In order to relate the absolute temperature T with the potential temperature θ, first law of thermodynamics of adiabatic processes is used as follows (Iliffe & Dodson, 1987; Abahamid *et al.*, 2004):

$$\theta = T\left(\frac{1000}{p}\right)^{0.286} \quad \text{..} 3.2$$

where:

θ and T are the potential temperature and the absolute temperature respectively in $^{\circ}$K respectively; and

p = the air pressure in mbar.

Equation 3.2 indicates that the potential temperature gradients $\frac{\partial \theta}{\partial h}$ are due only to heat exchange and not to pressure variation. Therefore, the temperature gradients must be predicted to a sufficient accuracy to deduce the temperature of the air through which the light travels.

Atmospheric Stability

The tendency of the atmosphere to oppose or enhance vertical motion and thus turbulence is termed stability. Atmospheric stability is certainly a complex theory; stability in the atmosphere is usually described in terms of lapse rates[19]. Lapse rates come in two general ways; the Environmental Lapse Rate (ELR) and the Adiabatic Lapse Rates (ALR). The latter comes in two ways of its own: The Dry Adiabatic Lapse Rate (DALR) and The Saturated Adiabatic Lapse Rate (SALR) sometimes called the Wet Adiabatic Lapse Rate (WALR) and sometimes it is also called the Moist Adiabatic Lapse Rate (MALR). The ELR is the actual disparity in temperature with height at a certain time and place. It varies from place to place, time to time and has no fixed rate (Steve, 2009).

Properties of the atmosphere are to some extent determined by its stability or resistance to change. Close to the ground, atmospheric stability changes frequently between **Stable,** and **Unstable**. Change in air temperature relative to height is a major factor for predicting atmospheric stability. From the earth's surface to around 11 km, the temperature decreases with altitude. This occurs because atmosphere is being heated by conduction current from the warm earth. Incoming solar emission is absorbed by and heats up the earth, which in turn warms the adjacent atmosphere. The farther one travels away from the warm earth, the colder the air becomes. In standard circumstances, the lapse rate is about 3.5°F for every 1,000 feet. The actual lapse rate varies from day to day and time to time (Esser, 1998).

Investigations carried out by Brunner and Fraser (1977) have shown that the accuracy of EDM, as reflected by the accuracy of determining a representative refractivity value is closely related to the thermal stability condition in the portion of the atmospheric boundary layer through which the wave propagates. In examining different thermal stratifications – neutral, stable and unstable – the concept of conservative parameters discussed in 3.3.2 above proves useful as these parameters can be utilized in tracing variations in the atmosphere that

[19] The rate at which temperature decreases with height or as altitude increases is called lapse rate (Ahrens, 1993)

arise through other than adiabatic processes. The term “stability” in this context refers to the behaviour of small parcel of air when moved upward or downward from an initial position, with no exchange of heat. When the parcel of air has adjusted to the pressure at the new height, its density compared with the surrounding air either tends push it back down or to drive it further upward. This simple act is used to describe the conditions of atmosphere at any point in time as follows:

When the density of the air parcel matches its surrounding air in its new position, **Neutral conditions** are experienced. The condition is characterized by zero potential temperature gradients in the vicinity of the ground (i.e. $\frac{\partial \theta}{\partial h} = 0$) and also correspond to zero heat flux, H from the ground to air (i.e. H = 0). In neutral or adiabatic conditions, no buoyancy forces are called into play and there is no heat transfer. A near zero potential temperature gradients is usually found during the two daily transaction periods, which in ideal conditions, occur a short time after sunrise and a short time before sunset. In the atmospheric surface layer, the neutral stratification within the transition periods is typically a short-term phenomenon rarely exceeding periods of more than a few tens of minutes. Nevertheless, adiabatic conditions may also prevail in special circumstances as follows:

i. when the cloud cover is very thick and there is a moderate or high wind; and
ii. during the transition periods between stable and super adiabatic conditions.

When the temperature decreases slowly with increased altitude, the actual lapse rate is low and the atmosphere **stable**. Also when the air parcel has been pushed back toward its initial position, the atmosphere is stable**.** The **stable conditions** are characterized by positive potential temperature gradients (i.e. $\frac{\partial \theta}{\partial h}$ is +ve) and also correspond to negative heat flux (i.e. H is –ve). An air parcel moving upwards will, after its pressure has adjusted, be cooler and denser than its surroundings and will tend to return downward. These types of atmospheric conditions are generally found on clear nights when the temperature inversions form as a result of ground cooling.

Wherever there the drop in temperature with height is greater than the adiabatic rate, the atmosphere is **unstable**. In an unstable atmosphere, the temperature decreases rapidly with increased altitude, the actual lapse rate is high and the atmosphere unstable. Also when the air parcel tends to move further upwards from the initial position, the atmosphere is unstable. The **unstable conditions** are characterized by negative potential temperature gradients (i.e. $\frac{\partial \theta}{\partial h}$ is –ve) and also correspond to positive heat flux (i.e. H is +ve). The conditions occur when the earth's surface is strongly heated by incoming short wave solar radiation. Consider a sunny day; the atmosphere is heated by contact with the ground over which it passes, which is in turn heated by radiation from the sun, either directly or diffused through the cloud. The parcel of air will be cooled and hence the air above it will be denser. Its buoyancy, therefore, tends to keep it moving upwards. Unstable stratification is typically encountered in the atmospheric surface layer during clear daytime periods. The researcher is of the opinion the above characteristics of lower atmosphere prompted Angus-Leppan (1972) to write that: "*the features of atmospheric temperatures in the lowest few hundred metres are well known. The chief variations are with height above surface, time of the day and season of the year*". Table 3.1 summarizes the characteristics of stable and unstable weather conditions.

Table 3.1: Characteristics of stable and unstable weather

Weather condition	**Stable**	**Unstable**
Turbulence	Smooth	Bumpy
Clouds	Stratus, layered	Cumulus, heaped
Precipitation	Steady	Showery
Visibility	Good	Poor
Surface winds	Steady	Gusty
Icing	Rime, continuous	Clear/mixed, intermittent

Source: Williams, (2003).

Field determination of the prevailing temperature gradient usually involve the measurement of $\frac{\partial T}{\partial h}$ and not $\frac{\partial \theta}{\partial h}$. Close to the ground, the distinction between the two gradients is minor and the relationship between these qualities is given as follows (Angus-Leppan & Web, 1971):

$$\frac{\partial \theta}{\partial h} = \frac{\partial T}{\partial h} + \tau \qquad \text{............3.3}$$

where

τ = adiabatic lapse rate (τ = -0.00977 $^{\circ}$C/m or $^{\circ}$K/m)

The explicit relationship between the potential temperature gradients and heat flux would be discussed in TTM and SREATM.

3.4 TURBULENT TRANSFER MODEL

The TTM was proposed by Brunner and Fraser (1977) as an atmospheric model for long-range EDM reduction which is applicable only during the periods when an unstable turbulent regime has developed in the atmospheric boundary layer. These conditions are typically encountered on clear sunny days between 10.00 and 15.00 hours. The model requires the determination of some additional parameters, namely net radiation, heat flux into the ground, evaporation and wind speed. In developing TTM, the following are essential: Obukhov length, unstable potential temperature profile and sensible heat flux.

3.4.1 Obukhov Length (L)

The interface height or scale length called Obkhove length (L) is essential when considering atmospheric turbulence. It can be represented as follows (Webb, 1964; Brunner & Fraser, 1977):

$$L = \frac{-u_*^3 C_p \rho \theta}{kgH} \quad \text{..3.4}$$

where :

u_* is the friction velocity in cm/sec;

C_p is the specific heat of air at constant pressure;

ρ is the air density;

θ is the potential temperature in ^{o}K;

k is Von Karman's constant (with value of 0.4 – its dimensionless);

g is the acceleration due to gravity (980.7 cm/sec^2); and

H is the heat flux in mW/cm^2

Rueger (1984), defined friction velocity (u_*) as follows:

$$u_* = \frac{kU}{\ln(h_i / z_0)} \text{...}3.5$$

where:

U is the wind speed measured at instrument height in cm/sec;

h_i is the instrument height in cm; and

z_o is the surface roughness parameter in cm (see Table A.1 - Appendix A)

The sign of L varies with atmospheric conditions, that is in unstable conditions it is negative (H is positive), in stable conditions, it is positive (H is negative) and in near – neutral conditions, L becomes infinitely large. Panofsky and Dutton (1984) assigned – 10 m to L on a strong convective days with upward heat flux (i.e. positive H). At night when stable conditions do exist, L is positive and small. In pure turbulence, when H tends to be extremely small; L approaches infinity.

3.4.2 Unstable Potential Temperature Profile

Dodson and Zaher (1985) identified three regions of different physical behaviour with associated different potential temperature gradients which can be defined in terms of L and their physical nature in terms of convective processes. Figure 3.7 shows a typical profile of potential temperature in unstable conditions:

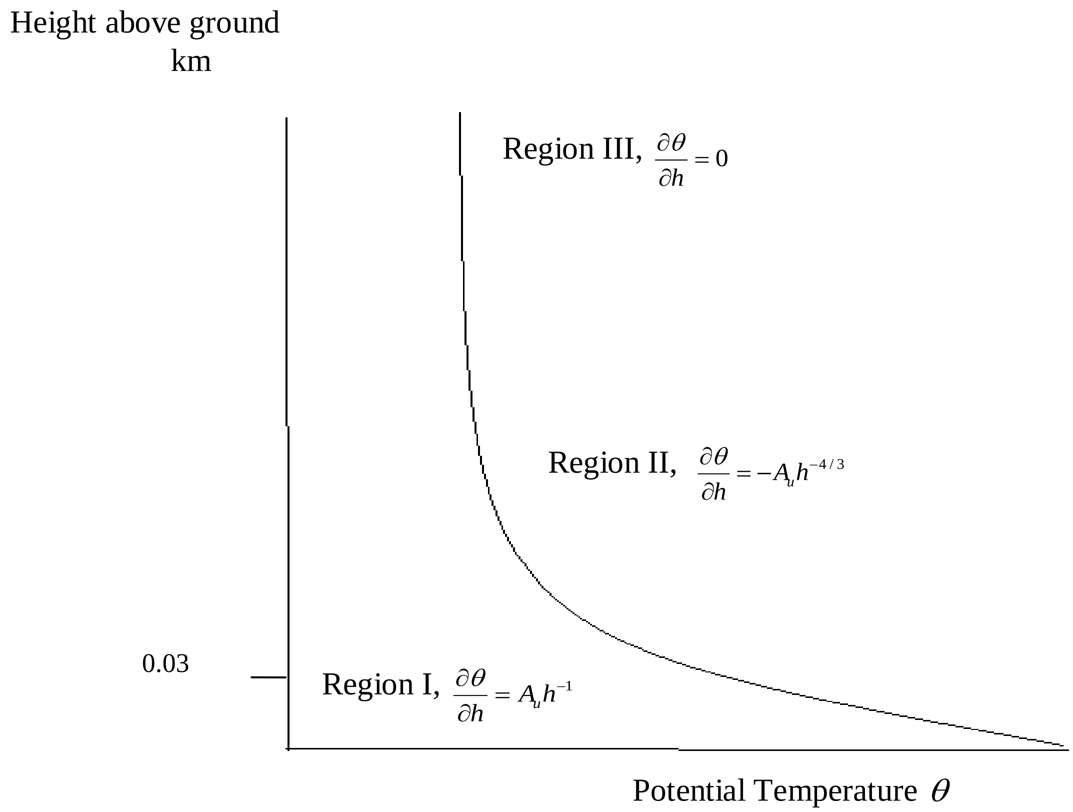

Figure 3.7: A typical profile of potential temperature in unstable conditions (Source: Brunner and Fraser 1977)

- Region I called forced convection occurs when wind passes over a rough surface. In accordance with well known logarithmic formula in micrometeorology, the prevailing temperature gradient within the region is given as:

$$\frac{\partial\theta}{\partial h}=A_u h^{-1} \qquad (3.6)$$

The upper limit of region I is given as (Brunner and Fraser, 1977):

h = 0.03L

- Region II is called free convection. It is caused by density differences within moving air. The potential temperature gradient of the region can be expressed as follows:

$$\frac{\partial\theta}{\partial h}=-A_u h^{-4/3} \qquad (3.7)$$

where:

$$A_u = \left[\frac{H^2 \theta}{(C_p \rho)^2 g} \right]^{1/3} \quad \text{...3.8}$$

The region has a limit range of:

0.03L< h < L

- Region III is called Quasi-free convection. The region depends on thermal up-currents from region II. The mean potential temperature gradient at this region is considered to be near-zero, because of the adiabatic conditions which prevail.

$$\frac{\partial \theta}{\partial h} = 0 \quad \text{..3.9}$$

The region limit is defined as: L< h < 10L

From the above discussions, only region I and II create the surface layer tagged with unstable conditions while region III is termed the adiabatic layer. According to Brunner and Fraser (1977), the profiles of temperature within region I have limited applications in geodesy, as most geodetic measurements are generally above this region. Most meteorological measurements are made for the purpose of determining refractive index and coefficient of refraction within region II.

3.4.3 Sensible Heat Flux

Sensible heat flux H is difficult to measure directly; for the empirical determination of upward sensible heat flux the energy balance equation can be applied (Fraser, 1981):

$$H = (\underline{R} - G) - F \quad \text{...3.10}$$

Where:

$\underline{R}$ is the net radiation –heat transfer at earth surface to the air

G is the heat flow into the ground

F is the evaporation flux i.e. latent heat lost through evaporation.

Another approach to the solution of equation 3.10 above is called combined method (Slatyer & Mcilroy, 1961; Angus-Leppan & Webb, 1971). In this formulation, the upward heat flux is expressed as:

$$H = A(\underline{R} - G) - C_p \rho \eta u_h (D_h - D_s) \quad \text{...3.11}$$

where:

A is a term whose value is dependent on the value of the gradient of saturation specific humidity with temperature (A is given in Table A.2 - Appendix A)

η is the bulk aerodynamical coefficient (see Table A.3 - Appendix A)

u_h is wind speed at height h (h = 1.5 or 2.0 m) above the surface in cm/sec

D_h is the wet-bulb depression at height h, in ^oK

D_s is the wet-bulb depression at the earth surface in ^oK

The net radiation R received by the earth's surface is simply obtained as:

$$\left.\begin{aligned} R &= (S_{dw} - S_{uw}) + (L_{dw} - L_{uw}) \\ &= S_w + L_w \end{aligned}\right\} \quad \text{...3.12}$$

where:

S_{dw} is downward short wave radiation (0.3 μm to 4 μm)

S_{uw} is upward short wave radiation

L_{dw} is downward long wave radiation

L_{uw} is upward long wave radiation

S_w is net short wave radiation ($S_w = S_{dw} - S_{uw}$)

L_w is net long wave radiation ($L_w = L_{dw} - L_{uw}$)

All the above defined parameters are used in the development of TTM

3.4.4 Development of TTM

Brunner and Fraser (1977) developed the TTM for unstable conditions (sunny or daytime) using heat processes which govern temperature profile. They end up introducing formulae for the reduction of visible light and IR radiation. Figure 3.8 shows a schematic representation of TTM for an electro-optical EDM**.** It clearly illustrates the physical significance of L. Within the unstable surface layer (h < L), the gradient of potential temperature varies in accordance with equation 3.7 above.

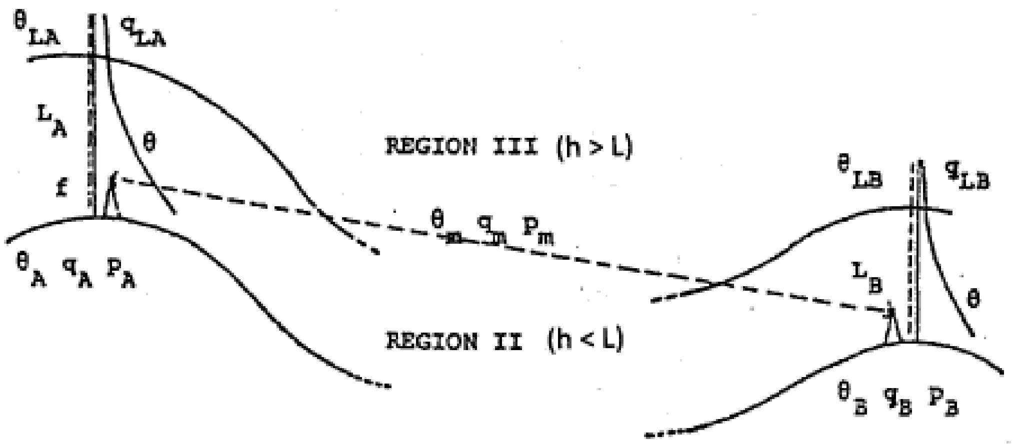

Figure 3.8: A schematic representation of TTM for an electro-optical EDM line (Source: Brunner & Fraser 1977)

Meteorological measurements (P, T, and e) for EDM are normally taken at the height of the instrument which is well within region II of the unstable turbulent region. By considering the parameters at station A (instrument station as shown in Figure 3.8 above), the potential temperature (θ_{LA}) at the Obukhov scale height (L_A) will be:

$$\theta_{LA} = \theta_A + \int_{hA}^{LA} \left(\frac{\partial \theta}{\partial h} \right) dh \quad \text{.......} 3.13$$

where:

h_A is the height at which temperature T_A is obtained

The essence of the TTM is contained in the following equation by substituting equation 3.7 into equation 3.13:

$$\theta_{LA} = \theta_A + 3A_{uA}\left(L_A^{-1/3} - h_A^{-1/3}\right) \qquad 3.13$$

The specific humidity (q_{LA}) at the Obukhov height (L_A) is calculated from the equation (Brunner 1977):

$$q_{LA} = h_u q_{SLA} \qquad 3.14$$

where:

$$h_u = \frac{e_A}{E_A} \qquad 3.15$$

where:

e_A is the partial water vapour pressure in mbar at dry-bulb temperature

E_A is the saturation water vapour pressure in mbar applicable to the dry-bulb temperature

q_{SLA} is the saturation specific humidity for dry-bulb temperature at height (L_A). This can be calculated from the equation below (Atkinson, 1981):

$$q_{SLA} = 0.622\frac{E_{LA}}{P_{LA}} \qquad 3.16$$

where:

E_{LA} is the saturation water vapour pressure in mbar

P_{LA} is the atmospheric pressure in mbar measured at L_A

$$P_{LA} = P_A \exp A \qquad 3.17$$

Where:

P_A is the atmospheric pressure at the height of instrument in mbar

$$\left.\begin{aligned} A &= -\left[\frac{gM(h_2 - h_1)}{R^* T_A}\right] \\ \text{Or} \quad A &= -3053.697\left(\frac{L_A}{T_A}\right) \end{aligned}\right\} \qquad \text{..........3.18}$$

where:

g is the acceleration due to gravity in m/sec^2

M is the effective molecular weight of the air (=28.9644 x 1.293 kg/m^3)

R^* is the universal gas constant (i.e. 8.31432 joules/^{o}K mol)

h_1 is the height of instrument in m

h_2 is h_1 + Obukhov length in m

Similarly for the terminal B (reflector station), θ_{LB} and q_{LB} can be calculated using the same steps as in terminal A above.

Therefore in estimating the mean conditions (θ_m, q_m) for the ray path, the following equations were given by Brunner and Fraser (1977):

$$\left.\begin{aligned} \theta_m &= \frac{\theta_{LA} + \theta_{LB}}{2}, \\ q_m &= \frac{q_{LA} + q_{LB}}{2} \end{aligned}\right\} \qquad \text{..........3.19}$$

EDM reduction formula for TTM

The Figure 3.8 above shows clearly that the short portion of the path length at the terminals lie in region II, while the chord (AB) lies in the region III. With the computed values of

θ_m, q_m using equation 3.19 above, and P_m which is taken as the mean of the endpoint pressure measured [i.e. $P_m = (P_A + P_B)/2$] for convenience sake, the corrected spatial chord distance S can be computed to a sufficient accuracy from the observed EDM wave path length d_r using the formula (Brunner & Fraser, 1977):

$$S = d_r + (130q_m - 1.944N_{go})\theta_m^{-1}.10^{-6}\int_0^S P^{0.714}dx - \frac{A_u^3 k_r^{\ 2}}{24R^2} \quad \text{....................................3.20}$$

where:

N_{go} is the group refractivity

dx is an integration variable along the chord

k_r is the refraction coefficient (i.e 0.15)

R is the radius of the spheroidal section along the line (i.e. 6371 km)

As an alternative to applying equation 3.20, which has the advantage of being an integration along the known chord, it is possible to first compute the mean refractivity N_m for the wave path based on the values of θ_m, q_m and P_m. This value is then substituted into the standard EDM reduction formula (Rueger, 1980):

$$S = d' + (N_{ref} - N_m)d_1.10^{-6} + (k_r^{\ 2} - 2k_r)\frac{A_u^3}{24R_E} \quad \text{..3.21}$$

where:

d' is the instrument readout distance (i.e $d_r = d.n_{ref}$). n_{ref} is the reference refractive index.

3.5 SHORT-RANGE EDM ATMOSPHERIC TEMPERATURE MODEL (SREATM)

Angus-Leppan and Brunner (1980) developed a new atmospheric model for short-range EDM line (line with a maximum length of 3 km, a maximum slope of 10^0 and a ground clearance of 100 m and aim at an accuracy of ±0.5 ppm). Different equations are proposed for unstable (sunny days) and stable (nights) conditions. Three additional parameters must be evaluated in the field on the basis of diagrams. Another two must be measured or estimated: wind speed and elevation angle of the sun. A rough profile of the line must also be known. The model accounts for the difference between the reference (also called nominal) refractive index (n_{ref}) of the instrument and the integral refractive index along the path of the measurement.

3.5.1 Development of SREATM

In a typical EDM line between two points (for example, A and B), measurements of temperature, pressure and humidity are taken at a standard reference height, h_r, (e.g. 1.5 m or 2.0 m) above the surface. Figure 3.9 shows a schematic representation of how meteorological parameters on the EDM line (AB) are taken.

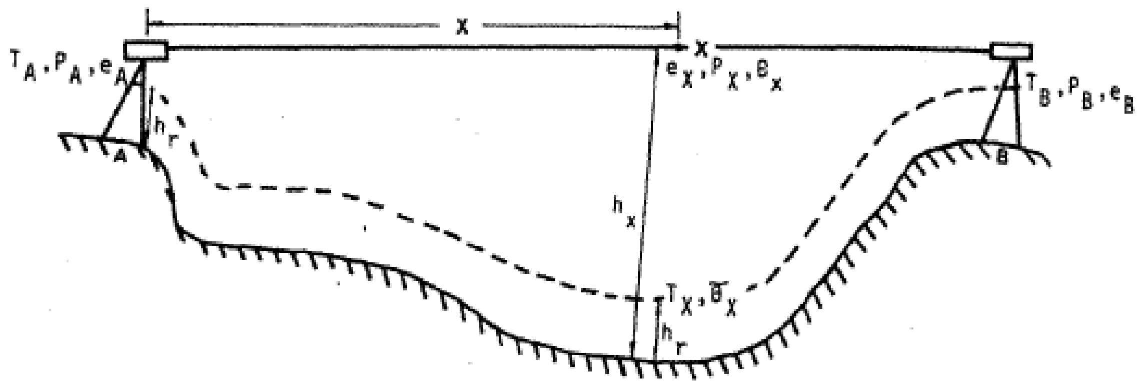

Figure 3.9: A schematic representation of SREATM for an electro-optical EDM line
(Source: Angus-Leppan & Brunner 1980)

The model assumes that along the surface, which extends at reference height h_r (parallel to the ground as shown in Figure 3.9 above), the potential temperature $\tilde{\theta}$ varies linearly between A and B. Atmospheric temperatures are measured at stations A and B (i.e. instrument station and reflector station), using equation 3.2 above, potential temperature $\tilde{\theta}_A$ and $\tilde{\theta}_B$ can be calculated. The temperature $\tilde{\theta}_x$ below the point at distance x from A is linearly interpolated between $\tilde{\theta}_A$ and $\tilde{\theta}_B$.

Therefore, at an arbitrary point on the cord AB, θ_x for distance x from point A is:

$$\theta_x = \tilde{\theta}_x + \Delta\theta_x \text{...} 3.22$$

where: $$\Delta\theta_x = \int_{h_r}^{h_x} \left(\frac{\partial \theta}{\partial h} \right) dh \text{...} 3.23$$

By substituting equation 3.2 into equation 2.27, the refractivity for visible or near infrared waves (NL) in ambient moist Air (i.e. refractivity of light waves) can be rewritten as follows:

$$N_L = \left(1.944 N_{go} - 81.1 \frac{e}{p} \right) \frac{P^{0.714}}{\theta} \text{..} 3.24$$

For a point at distance x along cord AB, the equation 3.24 above becomes:

$$N_L = \left(1.944 N_{go} - 81.1 \frac{e_x}{p_x} \right) \frac{P_x^{0.714}}{\left(\tilde{\theta}_x + \Delta\theta_x \right)} \text{..} 3.25$$

To carry out the reduction:

For the reduction of an EDM observation d_r to the chord distance S:

$$\left. \begin{aligned} \Delta S &= d_r - S \\ &= 10^{-6} \left(\int_0^S N_L - N_{ref} \right) dx \end{aligned} \right\} \text{..} 3.26$$

Substitute equation 3.25 into equation 3.26, we have:

$$\Delta S = 10^{-6} \int_0^S \left[\left(1.944 N_{go} - 81.1 \frac{e_x}{P_x} \right) \frac{P_x^{0.714}}{\theta_x + \Delta\theta_x} - N_{ref} \right] dx \text{...............................} 3.27$$

At this point, the mean values of the meteorological parameters P_m, T_m and e_m are introduced at reference height hr at the terminals A and B (see Figure 3.9 above):

$$\left.\begin{aligned} P_m &= \frac{1}{2}(P_A + P_B) \\ T_m &= \frac{1}{2}(T_A + T_B) \\ e_m &= \frac{1}{2}(e_A + e_B) \end{aligned}\right\} \qquad \ldots\ldots\ldots\ldots\ldots\ldots\ldots\ldots 3.28$$

If the integral in equation 3.27 is expand in a Tylor series about mean values P_m, T_m and e_m and if P_x, T_x and e_x are average over their distribution, ΔS becomes:

$$\Delta S = 10^{-6} S(N_m - N_{ref}) - 10^{-6} \frac{N_m}{T_m} \int_0^S \Delta\theta_x dx \ldots\ldots\ldots\ldots\ldots\ldots 3.29$$

where:

N_m is the mean refractivity derived from Barrel and Sears formula (see equation 2.11)

$$N_m = \frac{1}{T_m}(0.2696 N_{go} P_m - 11.25 e_m) \ldots\ldots\ldots\ldots\ldots\ldots 3.30$$

Neutral conditions:

Under neutral conditions, the sensible heat flux is near zero and the mean potential temperature gradient will also be zero.

Therefore:

$$\Delta\theta_x = 0 \ldots\ldots\ldots\ldots\ldots\ldots\ldots\ldots 3.31$$

Equation 3.30 is therefore reduced to ΔS_{neu}, the correction for neutral conditions is:

$$\Delta S_{neu} = 10^{-6} S(N_m - N_{ref}) \ldots\ldots\ldots\ldots\ldots\ldots 3.32$$

Unstable conditions:

At heights above 1.0 m, the mean potential temperature gradient can be expressed as region II Figure 3.8.

$$\theta_x = \theta'_x + 3A_u\left(h_x^{-1/3} - h_r^{-1/3}\right)\text{...}3.33$$

The EDM reduction formula for unstable conditions can therefore be derived by substituting equation 3.33 into equation 3.29:

$$\Delta S_{un} = \Delta S_{neu} + 3\times10^{-6} A_u S\left(\frac{N_m}{T_m}\right)\left[h_r^{-1/3} - \frac{1}{S}\int_0^S h_x^{-1/3}.dx\right]\text{........................}3.34$$

The factor A_u is average A_u calculated from parameters measured at terminals A and B using equation 3.8.

Stable conditions:

These conditions prevail mainly at night when there is typically an inversion layer and the sensible heat flux is negative. Therefore the potential temperature can be derived from similarity theory:

$$\frac{\partial\theta}{\partial h} = \frac{A_s}{h}\left(1 + 5\frac{h}{L}\right)\text{...}3.35$$

Where:

L is the Obukhov length as expressed in equation 3.4 above.

The coefficient A_s is given as:

$$A_s = -\frac{H}{C_p\rho k u_*}\text{ ....}3.36$$

Consequently, the potential temperature $\Delta\theta_x$ difference can be computed as:

$$\Delta\theta_x = -A_s\left[\ln\left(\frac{h_x}{h_r}\right) + \frac{5}{L}\left(h_x - h_r\right)\right]\text{....................................}3.37$$

The EDM reduction for stable conditions can be achieved by substituting equation 3.37 into equation 3.29 as follows:

$$\Delta S_{st} = \Delta S_{neu} + 10^{-6}\left(\frac{N_m}{T_m}\right)A_s S\left[\left(\ln h_r + 5\frac{h_r}{L}\right) - \frac{1}{S}\int_0^S\left(5\frac{h_x}{L} + \ln h_x\right)dx\right] \text{.........3.38}$$

3.6 THE SIMPLE TWO-LAYER ATMOSPHERIC TEMPERATURE MODEL (STAM) FOR ELECTRO-OPTICAL EDM

Fraser (1981) proposed the STAM because the earlier two atmospheric models, TTM and SREATM, required determination of some micrometeorological parameters which are not usually measured during EDM survey (e.g. sensible heat flux). The model requires that the endpoint meteorological measurements and refraction coefficient over the wave path be known. Also the model is applicable only when the thermal state of the lower atmosphere is either unstable, near stable or weakly stable. Figure 3.10 shows a schematic representation of two-layer atmospheric model for a typical EDM line (Fraser, 1981):

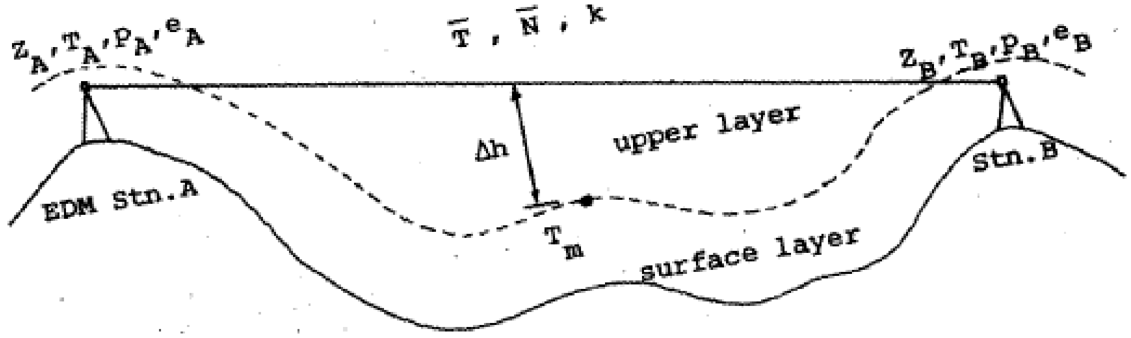

Figure 3.10: A schematic representation of STAM for an electro-optical EDM line (Fraser, 1981)

3.6.1 Development of STAM

The figure shows $\bar{N}$ *and* $\bar{T}$ as the true representative refractivity and temperature values for the EDM wave path, whereas, T_m is the mean of the measured endpoint temperature T_A and T_B. Δh is the integral vertical separation between the base of the upper layer and the wave path. k_r which stands for refraction coefficient can be determined from the end point zenith distance observations and apply the following equation:

$$k_r = 1 - (Z_A + Z_B - 3.143)\frac{R}{d_r} \quad \text{.....3.39}$$

where:

Z_A and Z_B are the zenith distance in radian;

R is the radius of the spheroidal section of along the wave path; and

d_r is the measured distance in m.

The mean refractivity value for the EDM wave path can be determine using Barrel and Sears (1939) formula as stated in equation 3.30 above.

The parameters T_m and N_m are not the true representatives of the path. Therefore the true temperature $\bar{T}$ is determined from vertical extrapolation of the mean value T_m via the simple two-layer temperature model:

$$\bar{T} = T_m + \frac{dT}{dh}.\Delta h \quad \text{.....3.40}$$

The vertical temperature gradient ($\frac{dT}{dh}$) can be expressed with sufficient accuracy as a function of refraction coefficient using the formula (Brunner, 1977):

$$\frac{dT}{dh} = \frac{T_m k_r}{503 P_m} - 0.0342 \quad \text{.....3.41}$$

Fraser (1981) neglects terms involving water vapour pressure (which is negligible in light wave as shown in section 2.8, table 2.6 of chapter 2 of this report) and integrate equation 3.30 above with respect to temperature:

$$-\Delta N = 0.2696 N_{go} \frac{P_m}{T_m}.dT \quad \text{.....3.42}$$

A combination of equation 3.21, 3.41 and 3.42 yield the required expression for the chord distance correction ΔS in terms of the refraction coefficient k_r; the mean temperature and pressure (T_m and P_m); the mean height parameter Δh; and the spatial chord distance S:

$$\Delta S = \left(5.360 \times 10^{-4} k_r - \frac{9.22 \times 10^{-3} P_m}{T_m^2} \right) \Delta h S . 10^{-6} \text{ ....3.43}$$

3.7 APPLICATION TO THIS STUDY

All the conditions for which the models discussed in this chapter were developed must be considered for total station measurements at mines, because data is continuously acquired day and night (i.e. data is acquired during stable, weakly stable, neutral, near-neutral and unstable atmosphere). EDM measurements by the new total stations that are currently available in the market are less affected by most parameters upon which the models were developed with the exception of the major atmospheric parameters, for example temperature, pressure and humidity, due to technological advancement. Besides, there are good sensors that can capture accurately the air density, temperature, pressure and humidity in the troposphere (where the effect of turbulence is predominant during the day time) that are relevant to this study. The three models (TTM, SREATM and STAM) discussed in this chapter deal with possible ways of overcoming the effects of atmospheric parameters variation and terrain where the measurements is carried out.

In order to achieve this, Geodetic Monitoring System (GeoMos) Digital Terrain Model (DTM) Meteorological (meteo) sensor was procured for capturing air temperature and pressure and communicating the readings to a PC through a cable connection. The GeoMos meteo sensor is more accurate and sensitive in capturing atmospheric parameters than the old-fashioned standalone thermometer and barometer. It also permits meteorological network modelling over measurement area. In addition to this, three Oregon Scientific weather sensors (forecasters) were procured to adequately capture the atmospheric parameters along the line-of-sight correctly. Inaccurate capturing of atmospheric variations along line-of-sights is the basis for which the three models were developed. During slope monitoring at mines, the maximum monitoring distances with total stations are almost always less than 3 km. The true representative of atmospheric parameters can be achieved under this condition irrespective of the terrain where the measurements is carried out.

3.8 CONCLUSION

The chapter discussed the various effects of atmosphere on EDM distance measurements and the three commonly used atmospheric models (proposed by past researchers) to reduce these effects. However, these atmospheric models require many input parameters to be measured, which question their practicality during slope stability monitoring. Alternative approaches to refraction correction (as stated in section 2.11 of chapter two) are the preferred propagation methods nowadays. In accordance with this, the instrument procured for this research (Leica TCR 1200) has an inbuilt temperature, pressure and humidity compensator for automatic error propagation. In addition and as a check to these in-built corrections, the GeoMos accessories installed detected any change in atmospheric parameters and communicated such changes to a computer through a cable connection. As a further check, three Oregon scientific weather instrumentations were also procured for collecting additional data.

The next chapter will discuss the need for calibration and pre-delivery calibration carried out on the new total station procured for this research by the Leica Geosystems (i.e. the supplier of the new instrument). Furthermore, the campus observation procedures are discussed.

CHAPTER FOUR

4.0 TOTAL STATION CALIBRATION AND SITE PREPARATION FOR CAMPUS OBSERVATIONS

In order to examine the likely impact of the atmospheric parameters variation on distance measurement as discussed in chapter three, this chapter discusses the pre-delivery test carried out on the new total station procured for this research. In addition, it expounds on the considerations for data collection.

4.1. CALIBRATION

The accuracy of EDM instruments is derived from an internal reference frequency source, that is a crystal oscillator. Crystal oscillators can wear out over time and with use. Exposure to harsh environments can also upset delicate calibrations of the reference frequency source. Therefore, EDM instruments should be regularly calibrated against known distances (Talbot and McCusker, 2003).

Routine verification of the measuring accuracy of EDM instruments (total stations) is very important. Such verification is of particular concern to contractors to meet the instrument accuracy requirements for a given contract (Dzierzega & Scherrer; 2002). Verification is concerned with the determination of instrument errors, which can then be used to monitor the performance of the instrument (Manual of Survey Practice).

The periodic calibration aims to minimize systematic errors and to determine the highest achievable precision using the instrument (US Army, 2002). Bossler (1984) noted that EDM instruments should be calibrated annually and frequency checks made semi-annually. Becker, *et al* (2000), Greenway (2000), Heiste (2001) and Zeiske (2001) discussed the International Organization of Standardization (ISO) specifications for testing the surveying instruments and they concluded that it is necessary to create uniform, universally-recognized standards for test procedures that can be applied in the field without excessive effort. They also remarked that the issue of standardization is gradually becoming more important for surveyors and other professionals. Becker (2001) stated that the objective for the standards is to indicate field procedures to be followed and the professionals should bear in mind that the achievable precision for a given surveying instrument used together with its supportive equipment has to be determined.

4.1.1 Methods of Calibration

There are two methods for calibrating EDM, the laboratory method and the field method. For field calibrations, the EDM must be calibrated over a series of distances representative of the range of the instrument known as the baseline[20]. These baselines are designed to generate a statistically accurate determination of the errors in the EDM (Paiva, 2006). The verification method involves the measurement of a set of subdivision on the EDM base to determine the existence and magnitude of any errors present (WAG, 2009). The length of the baseline ranges from 500 to 1400 m (Buckner; 1998), so the field method is suitable for determination of the scale error. The engineering manual of the US army (2002) stated that establishing a calibration baseline and keeping it in good order can be expensive and time consuming when maintenance is considered. For the laboratory calibration, a series of distances ranging from 5 to 100 meters must be measured. Sometimes, it may be necessary to mount some of the reflectors outside of the laboratory (Dzierzega and Scherrer; 2002). During pre-delivery calibration described in this chapter, a laboratory calibration with all targets set inside the laboratory was used.

4.1.2 Reasons for Pre-delivery Calibration or Test

Precise measurements with total stations assume that all instrument axes are entirely perpendicular to each other. Also, the RL EDM reference laser beam, the ATR zero point, and the line-of-sight should coincide precisely. Unfortunately, these requirements are never perfectly fulfilled. Even with great care when manufacturing the instrument, small deviations from the target position of the different components occur. Also during the normal working life of the instrument, small movements inside the instrument can occur. There are various possible reasons for this:

1. Result of temperature changes, as every material expands and contracts with temperature;
2. Shocks (e.g. during transportation);
3. Long storage periods; and
4. Stress during normal use.

[20] A baseline is a permanently marked distance, the length of which is known to be precise and accurate. It consists of a minimum of four marked monuments, all in a straight line over uniformly slope terrain (Buckner; 1998).

- Temperature variations: Most equipment is manufactured in Europe and the equipment is standardised, based on the European atmospheric conditions. To make the equipment work effectively in Africa (a region with predominantly harsh weather), it has to be calibrated to make the equipment acclimatise to typical African atmospheric conditions

- Shocks: In the course of transporting the equipment to Africa, various means of transportations (air, water and land) may be involved. None of these transportation means is shock or vibration free. The shock or vibration in the course of transportation may alter the internal assemblage of the equipment, hence the need for pre-delivery calibration.

- Long storage: Most equipment is not immediately purchased after manufacture, due to high cost and other factors. Therefore whenever new survey equipment is bought, it needs to be pre-delivery calibrated to make sure that the equipment meets the manufacturer's specifications.

- Stress during normal use: During field usage after pre-delivery calibration, especially in engineering projects of high precision, the instrument should be calibrated at least twice a year, or before and after each important project, following special procedures (Skyttner, 2002).

Small deviations can result in measurement errors which are greater than the specified accuracy of the instrument. These deviations can happen with every instrument, regardless of whether they are mechanical or electronic, and are independent of the manufacturer. For most electronic instruments, the main deviations can be determined during pre-delivery test or by the users. This procedure is called **calibration**. Generally, total station may be calibrated for a number of reasons. The most important ones are as follows: (Rueger, 1996):

- Quality control
  - At time of purchase
  - Periodically thereafter
- Improvement of accuracy
- Legal metrology.

The quality control measurements at the time of purchase have to establish if the total station fulfils the manufacturer's specifications. The three points, temperature changes, shocks and long storage periods, discussed above come under this heading. The quality control measurements that should be carried out periodically thereafter may be due to the fourth point - stress during normal use. All these quality control measurements are a necessity rather than an option. They are essential if the specified accuracy of a total station is to be realized.

Extensive calibrations may be carried out on the new total station to improve its accuracy to job-at-hand specification. However, the cost of extensive calibrations should always be compared with cost of hiring or purchasing a new total station with better accuracy specifications.

The requirement for legal metrology may also be a reason for calibrating total station. The requirements of legal metrology necessarily differ from country to country.

4.1.3 Pre-delivery Calibration of a new Total Station

A pre-delivery calibration was carried out on a new total station bought for research purposes – Leica TCR 1201 model (this type of total station belongs to TPS 1200+ series). The machine was procured by the School of Mining Engineering, University of the Witwatersrand purposely for this PhD research project on likely impacts of atmospheric parameters variation and norms of taking observations through a window (covered with glass) on the quality of data generated during slope monitoring using a total station surveying instrument.

The School decided to buy TCR 1201 type of total station because the nature of the research required high precision and accuracy. The attributes of the TCR 1201 model total station are presented in Table 2.2 of Chapter two: high accuracy angle measurements (Hz, V; 1" or 0.3 mgon) and precise long-range distance measurements backed by automatic fine pointing and fast reliable reflector location (i.e. 3 km to a single prism and accuracy superb of 1 mm + 1.5 ppm). It has intuitive interface, power data management, on-board routines and programs, easy viewing of entire surveyed area and immediate access to all measured data.

The pre-delivery calibration was carried out at the Geosystems African laboratory, located at Midrand in Johannesburg, South Africa. The laboratory is appropriately equipped for calibration testing with reflectors mounted on the sides and corners of the laboratory (see figure 4.1). For complete discussion of the pre-delivery calibration see Afeni and Cawood 2010 (see appendix B.2 of appendix B)

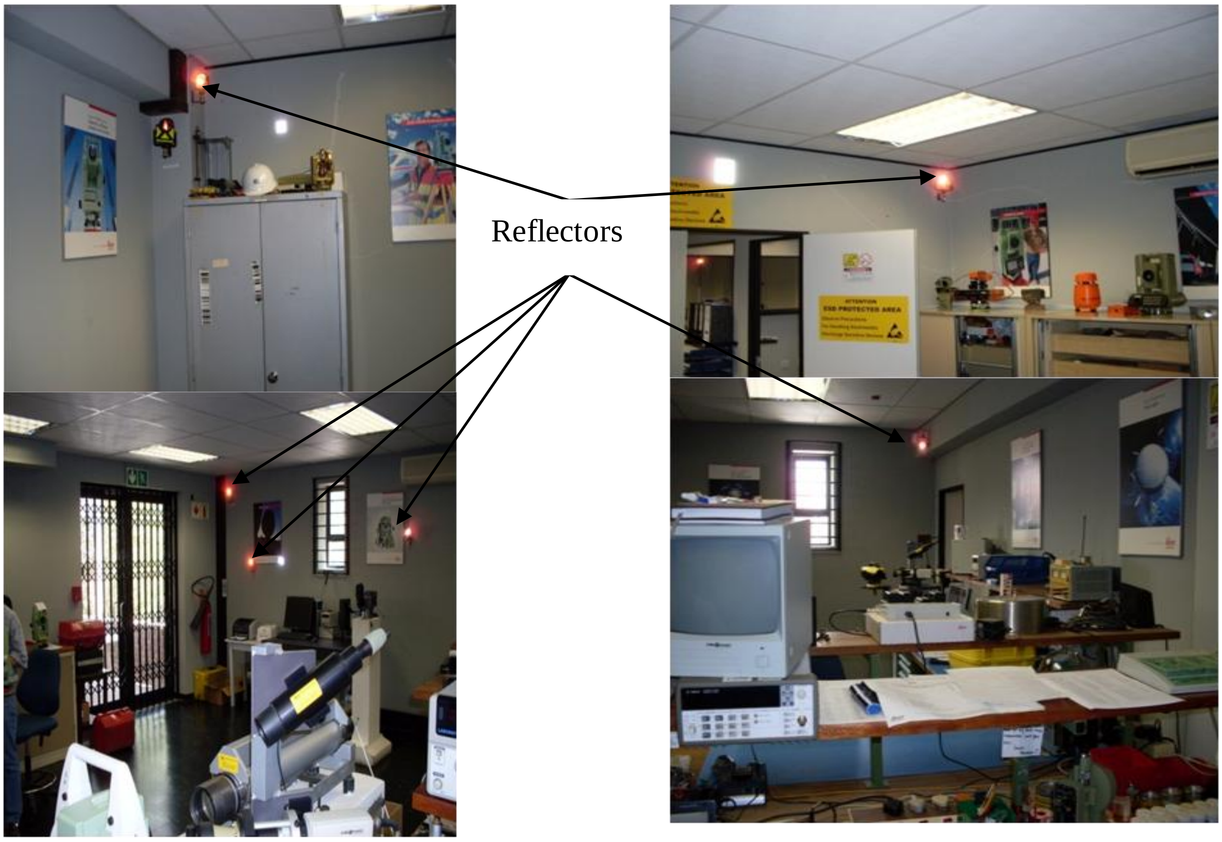

Figure 4.1: Reflectors on the laboratory corners and walls

The pre-delivery calibration of the new TCR 1201 was carried out using computer software purposely designed for calibration exercise. However, the software has sixty eight (68) steps or operations to be followed when carrying out full calibration on total station survey instruments. Because the TCR 1201 was new, only some of these steps were carried out during the pre-delivery calibration. The selected operations are steps 23 to 28, 29 to 30, 31 to 37, 44 to 47 and 66 (see Appendix B.1 of Appendix B).

The collimation and tilting axis error test

The steps 23 to 28 catered for collimation and tilting axis errors. The calibration steps were carried out using the appropriate collimation testing equipment. The total station was mounted in such a way that its optical lens was at the same height with that of the collimation calibrator as shown in figure 4.2. Both the collimation testing equipment and the total station were connected to a computer laptop for data exchange between the three. The collimation testing equipment senses the tilting axis reading of the total station with the help of the software and displays it on the screen of the laptop. Adjustment can be made if the error exceeds the manufacturer specification. The adjusted data is communicated back to the total station under test with the help of cables from the computer laptop to the total station.

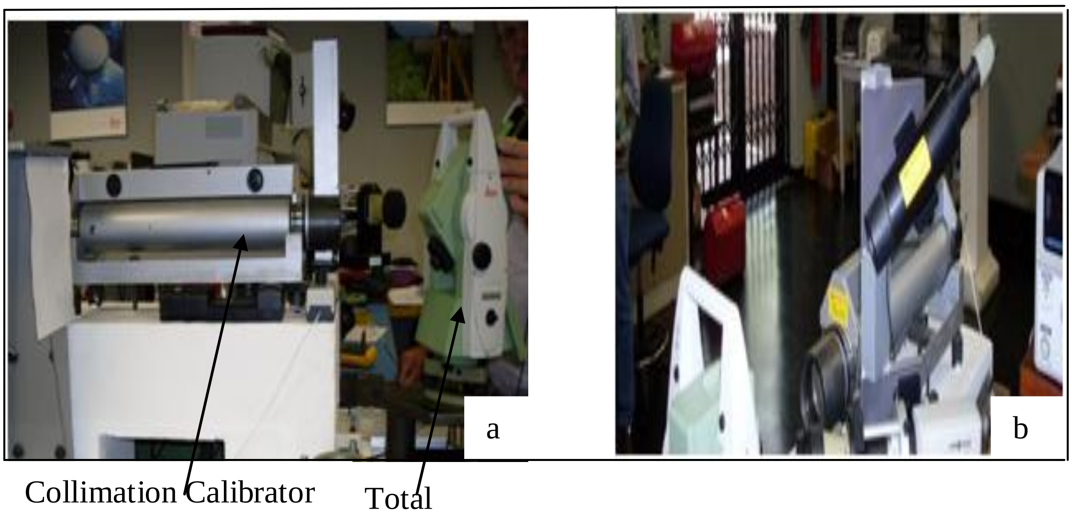

Figure 4.2: Collimation calibrator (a - shows side view; b – shows front view)

Steps 29 to 30 deal with sensing the frequency and power consumption of the new total station. The frequency sensor connected to a frequency calibrator as shown in figure 4.3 was placed on the optical lens of the new total station and the frequency was displaced digitally on the frequency calibrator equipment. Adjustment could be made via the connection between the frequency calibrator and the software. Also to examine the power consumption rate of the new total station, a power sensor was connected to a meter reader (figure 4.4 shows the digital electric signal level meter), the current (energy) consumption of the total station was displayed on the meter. The displayed power consumption reading was then compared with the specification given by the manufacturer to see if there was significant deviation. If there was a discrepancy between the two, adjustments could be made to make the reading conform to the manufacturer's specifications.

Figure 4.3: Frequency calibrator Instrument

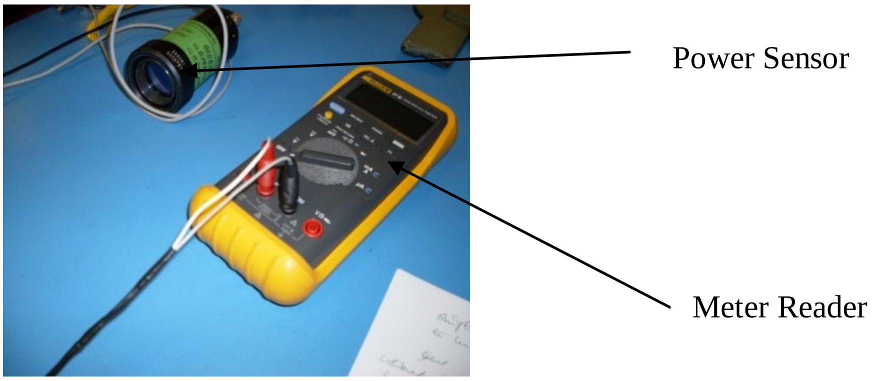

Figure 4.4: Power sensor and meter reader

Dynamic and distance test

According to Zeiske (2001), "*the first stage in system evaluation is determining the level of consistency that can be achieved by the total station per measuring circle. This will give a good indication of the instrument performance in real-world conditions as opposed the factory – certified instrument ratings that does not reflect the changing atmospheric effects encountered in practice*". Steps 44 to 46 entail dynamic testing, short-range (SR) distance and distance after power on. To achieve these, measurements were taken to a known distance, in the case of this exercise – distance was measured to one of the reflectors hung on the wall of the laboratory several times. The distance readings displayed on the total station screen. These readings were compared after each reading to check consistency in the displaced readings when observations were made to the same target at different time intervals.

Finally, any alteration or upgrades made during any of the above steps were uploaded to the total station via the calibration software. Figure 4.5 shows a laptop connected to various calibration tools.

Figure 4.5: Computer laptop with connection cables to other calibration instruments

4.1.4 Result and Discussion

The results of the pre-delivery test carried on the new total station in most cases were within the limits specified by the manufacturer and developer of the calibration software. All the steps required for full calibration exercise and the selected ones of these steps (reason for selection and not carrying out all the steps being that the total station under consideration was new) are presented in Appendix B.1. The result of the pre-delivery calibration carried out on the new total station TCR 1201 using the 68 steps calibration software showed that the instrument collimation error was -000.00056, which is within the limit stated under step 23 (collimation infinity -000.0006). Also the tilting axis error of the new total station was found to be 000.00042 which conformed with a tilting axis error of 000.0004 as required under step 24 of the software. The V coarse index and L coarse index of the instrument were 004.22328 and -002.54576 respectively, which are also within the limits of 004.2233 and -002.5458 stated under step 25. The T coarse index of the new total station was -000.75843.This also conformed with -000.7854 as stated under step 25. Lastly, the distance measurements readings shown in 45 and 46 of the appendix indicated consistency in the distance measured with the new total station under test.

4.2 SITE PREPARATION FOR CAMPUS OBSERVATIONS

The steps taken to establish the control points (reference points) that were used for the campus monitoring survey setups are discussed in this section. These setups were used for the data collection.

4.2.1 Pre-Survey Works

Traverse survey works were carried out from known control points (C1, C3, C8 and TOL) around Chamber of Mines (CM) building located in West Campus area of the University of the Witwatersrand to an observation station (a point beside a window located inside an office on the third floor within the three-story Chamber of Mines building – window station, WS) and set a new control point around this station (A1, A2, A4, A5, CMC1, CMC2 and CMC3). The three monitoring targets (Leica mini prism, Leica circular prism and sticker) were located on the wall of Genmin Laboratory (GeL) just directly opposite the observation station window.

These traverses were carried out to assign coordinates to the office observation station and to have an idea about the coordinates of the monitoring targets (placed on short-distance monitoring point). Table 4.1 shows the list of coordinates of the known control points and the newly established points (see appendix B.3 for detail pre-survey work carried out in preparation for campus observation). The plan of the control points is shown in figure 4.6.

Table 4.1: List of control survey

Point	Y	X	Z	Remarks
C1	97208.460	2898355.735	1760.246	Original control stations
C3	97289.097	2898387.391	1759.902	
C8	97259.071	2898384.736	1760.082	
TOL	97364.920	2898217.700	1801.510	
A1	97299.313	2898406.436	1760.146	New control stations
A2	97316.332	2898407.950	1759.496	
A4	97322.067	2898402.412	1758.500	
A5	97315.816	2898412.004	1759.660	
CMC1	97287.773	2898404.975	1760.900	
CMC2	97285.010	2898425.534	1760.901	
CMC3	97286.662	2898425.768	1760.859	
WS	**97286.071**	**2898412.590**	**1777.623**	Research stations
Mini prism	97325.812	2898398.076	1766.650	
Circular prism	97325.812	2898398.076	1766.147	
Sticker	97325.812	2898398.076	1765.646	

Source: Pre-survey data

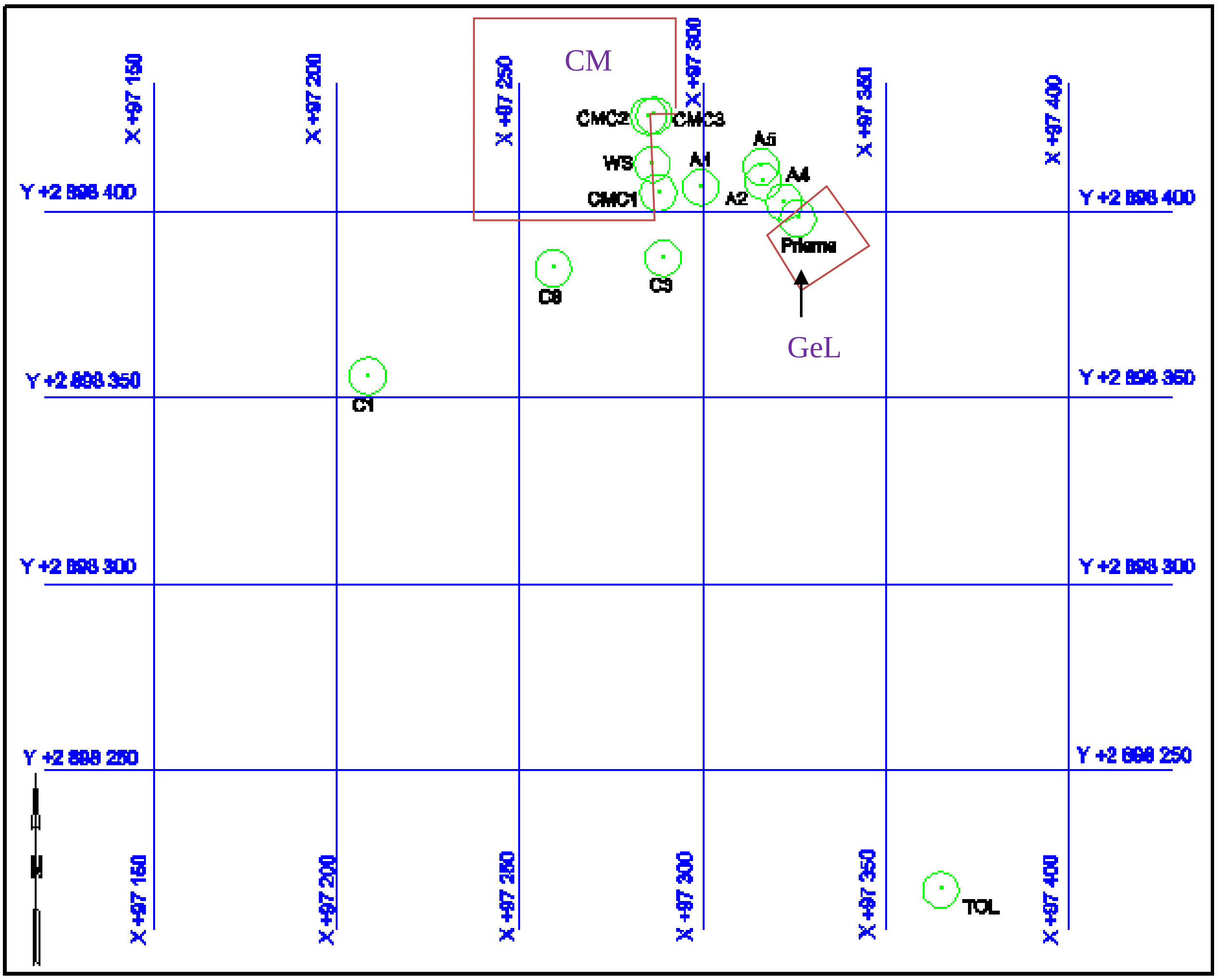

Figure 4. 6: Plan showing geometry of survey control points

4.2.2 The Campus Observation Station Beacon Construction

The observation station beacon/bracket was attached to a wall near a window inside an office assigned for the purpose of this research work. The beacon was made of iron bar with dimensions 20 x 200 mm (top and base part) and 40 x 560 mm (middle part). The beacon was designed and constructed in such a way that it allowed forced centring to eliminate zero error. It was constructed in the School workshop using iron bars and was fixed to the office window wall with the help of three (3) mounting bolts with expanding shield. The designs of the beacon/bracket and pictorial view of the mounting bolt are shown in figures 4.7 and 4.8 below:

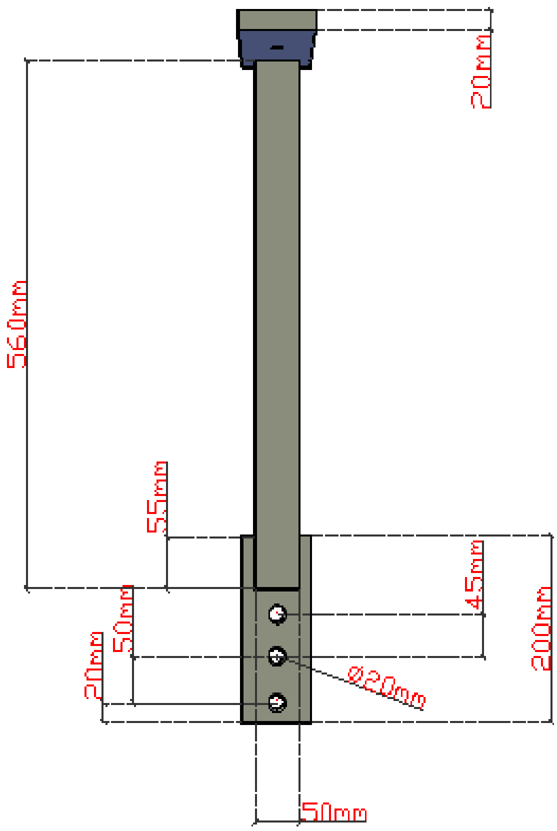

Figure 4.7a: Front view of the beacon

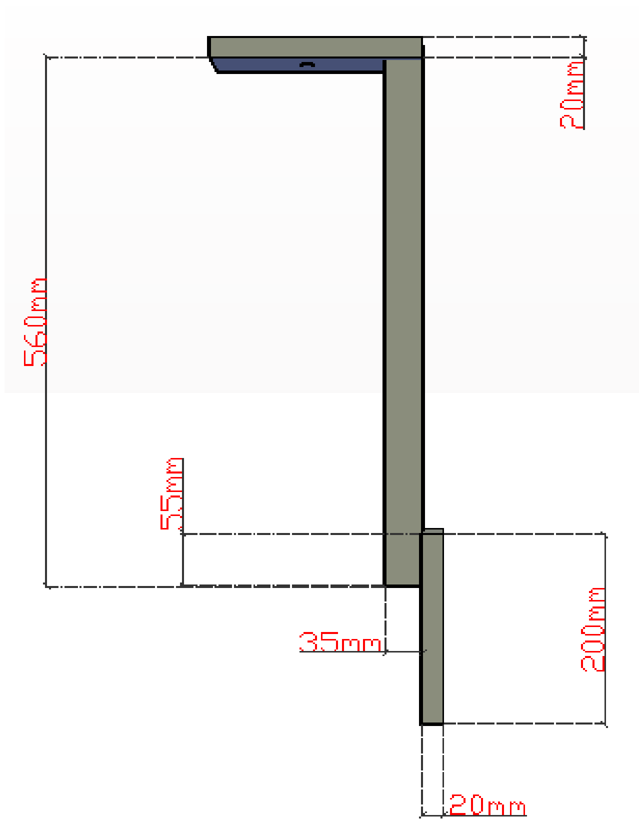

Figure 4.7b: Right view of the beacon

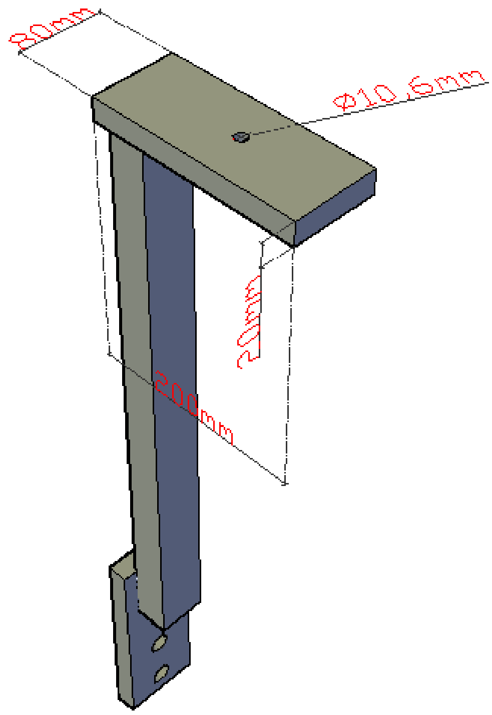

Figure 4.7: The beacon

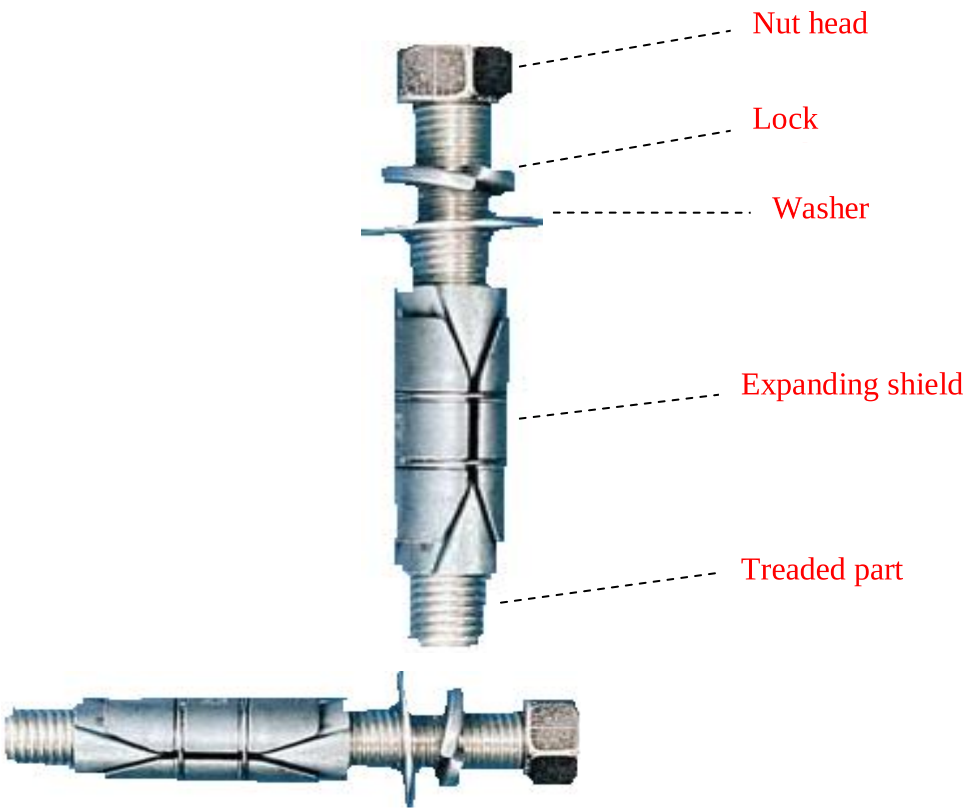

Figure 4.8: Mounting bolt with expanding shield

4.2.3 The Campus Monitoring Target

The target was designed using three targets (namely: Leica mini prism, Leica circular prism and sticker) fixed on a plank in such a way that the centre of the two prisms are aligned with that of the sticker to make the entire three have the same horizontal distances. The figure 4.9 summarizes the construction of the campus observation target.

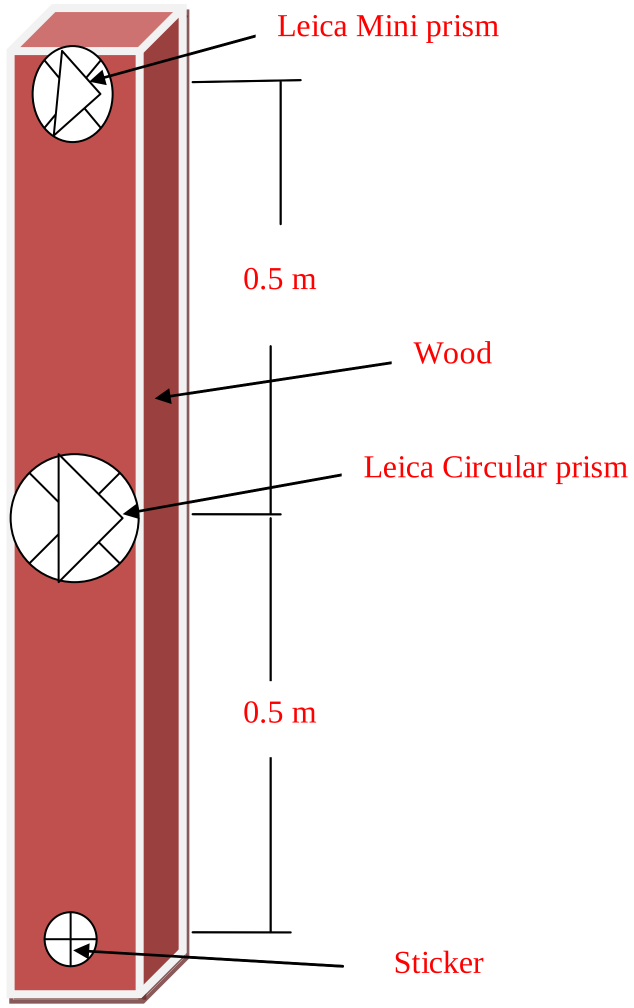

Figure 4.9: The target construction for campus observation

4.2.4 Measurement of Atmospheric Parameters

The atmosphere of the earth is a system whose parameters change and fluctuate significantly. The unsteady state of the atmosphere has a severe impact on geodetic measurements (for example, measurement of distance with a total station), if they are not taken into consideration. The distribution of temperature, pressure, humidity and their turbulent fluctuations must be known in order to determine the refractive index of the boundary layer, which is significant for the correction of errors in geodetic measurements due to atmospheric effects.

Propagation of electromagnetic waves in the air is disturbed by the turbulence of the atmosphere. One of the consequences is the scintillation of the wave, which is the result of fluctuations of temperature, moisture, pressure and their interactions.

The extent and precision required in the measurement of atmospheric parameters depends largely on the total station instrument type, its internal accuracy, the distance accuracy required, the length to be measured and the purpose for which the observation/job is meant for (Rueger, 1996). In this study where high precision is desired, two types of atmospheric parameters sensor were used: Geodetic Monitoring System (GeoMoS) Digital Terrain Model (DTM) meteorological (meteo) sensor and Oregon Scientific weather forecaster.

GeoMoS DTM meteo sensor

The instrument has a DTM meteo sensor (combined pressure and temperature sensor) that measures both temperature and pressure and communicates the data to a PC (with GeoMoS analyser software installed on it) through a cable that runs from the base of the sensor to the computer central processing unit. The connection is shown below:

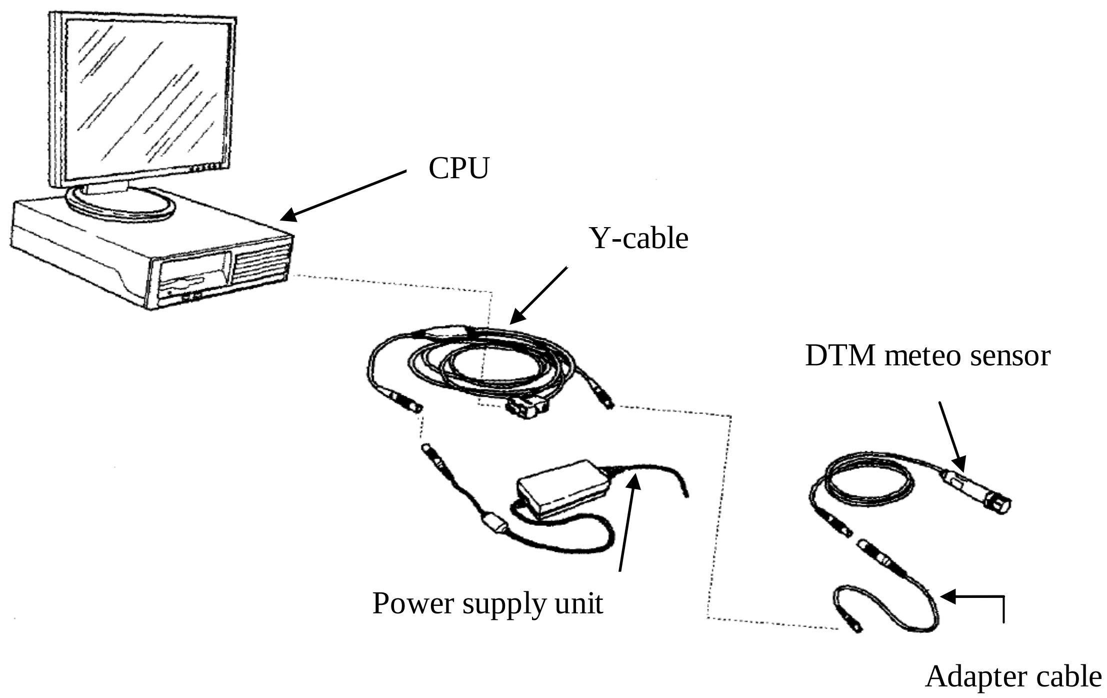

Figure 4.10: Setup of Meteo sensor (Source: Geosystems)

For this particular research, the DTM meteo sensor was permanently placed inside a station constructed purposely to house it. This structure was needed because when the sensor was placed outside without a cover during the test-running experiment/installation, the intensity of direct sunlight affected its readings. By having it in the open, solar radiation will naturally heat the outer surfaces of the sensor ultimately giving temperature unrealistic readings, and possibly causing premature failure of the sensor. To solve this latter problem, a device/compartment that shrouds the sensor called a **Stevenson Screen** (weather station) was constructed in the School workshop.

The sensor work with GeoMoS software is called “monitor”. It can record both variations in temperature and pressure at any particular time interval (the timing can be programmed to a desired interval) and it can also plot the graph of these variations against time. All the results can be viewed on the PC. The figure 4.11 shows the constructed weather station that housed the DTM meteo sensor:

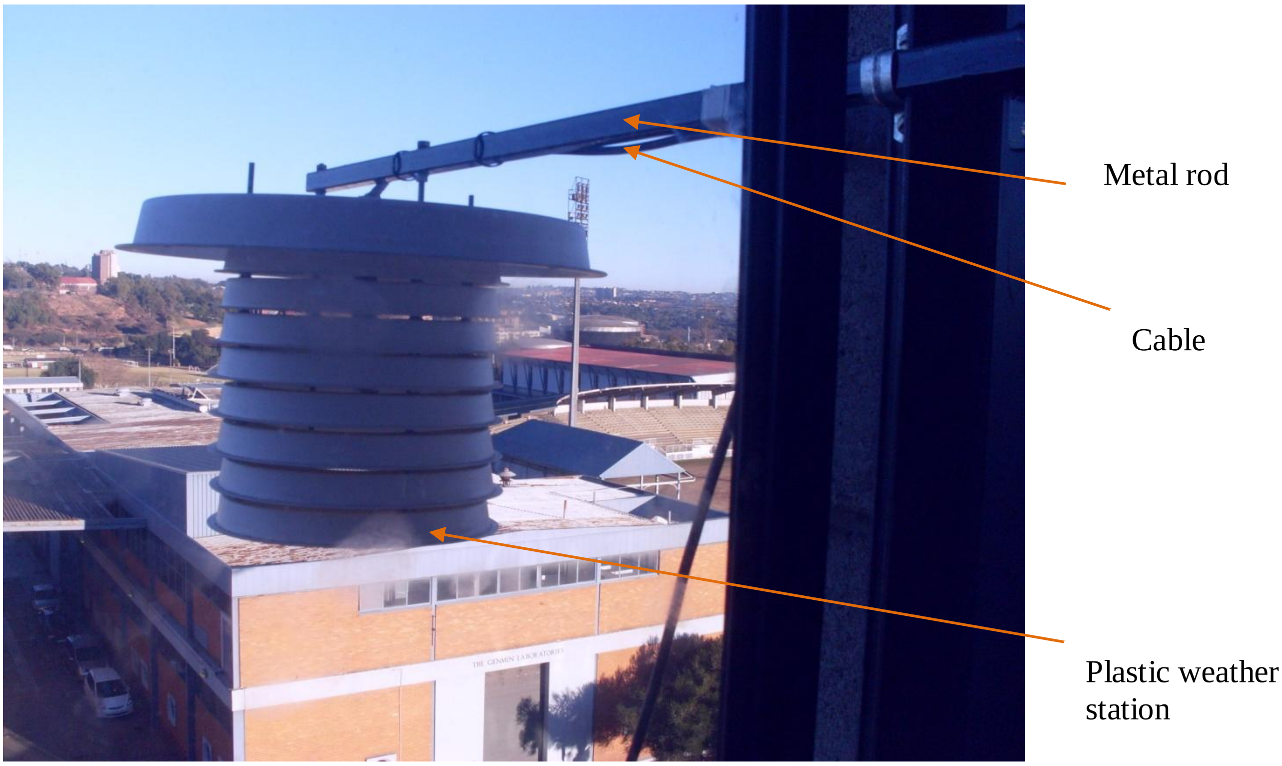

Figure 4.11: Weather station and the DTM Meteo sensor

The construction of the weather station in the figure 4.11 above is based on the Stevenson screen kit design (The Stevenson screen kit design steps are shown in Appendix B.4). Due to the inability of the DTM meteo sensor to read humidity, which is one of the atmospheric parameters needed for this research and the need to measure the office/monitoring station atmospheric parameters, three (3) Oregon Scientific weather forecaster (Model: BAR916HG) were procured.

Oregon scientific weather forecaster

The forecaster consists of a main unit and one thermo/hygro remote sensor RTGR328N. The weather information is displayed on a liquid crystal display (LCD) screen, using comprehendible weather forecasting symbols; these include current barometric pressure reading, ultraviolent (UV) index reading, indoor/outdoor temperature, and humidity. Figure 4.12 shows the main unit of Oregon scientific weather forecaster.

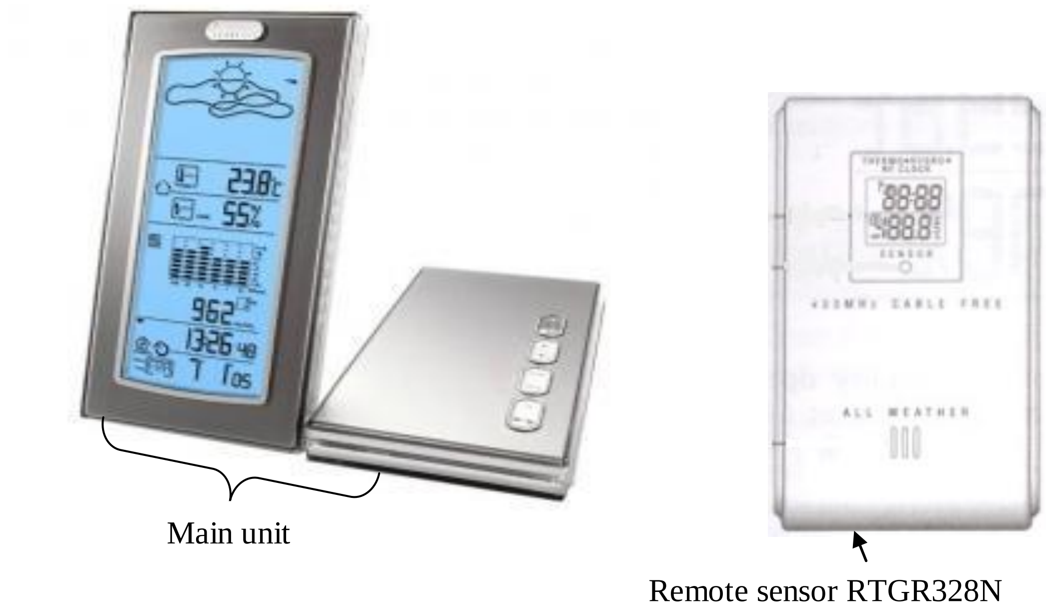

Figure 4.12: Oregon scientific weather forecaster (Source: Oregon scientific user manual)

The above main unit was the indoor component; it received continuous weather updates from an outdoor thermo/hygro remote sensor RTGR328N through a radio signal format (European Union Data Collection Framework - EU-DCF, or United Kingdom Microwave Frequency Standard - UK-MSF). The main unit has ability to receive signals every minute from up to five (5) different outdoor sensors which can be as far as 70 m away and store the received data in different channels (1-5). The received data can be read on the main unit by pressing the channel button. Twenty-four (24) hours history of weather data can be accessed on the main unit by pressing the history button. In the same way, hourly data can be accessed by pressing the memory button. Both the main unit and the sensor are powered by Lithium AAA batteries (The main unit uses 4 batteries of 1.5 volts while the sensor uses 2 batteries of 1.5 volt each). For the purpose of this research, three Oregon wireless weather forecasters were used. One was stationed permanently inside the observation room and two were spaced outside at predetermined interval along the wave path. All three weather instruments were calibrated before use.

4.2.5 Glass and Window Frame.

The glass used in this research work was ordered from PG glass manufacturer. Five (5) clear float glass panes of thickness **2mm, 3mm, 4mm, 5mm and 6.38mm** with dimensions **0.787 m** by **0.590 m** and a refractive index of **1.52** were used in this research. The frame was constructed with normal aluminium in natural colour. The frame was made in such a way that it could be easily dismantled and re-assembled at the free edge to provide easy way of changing the glass to a desire glass thickness at a particular point in time. The frame was also installed in such a way that it could be opened at varying angles. Figure 4.13 shows the window frame with glass and the total station mounted on the beacon.

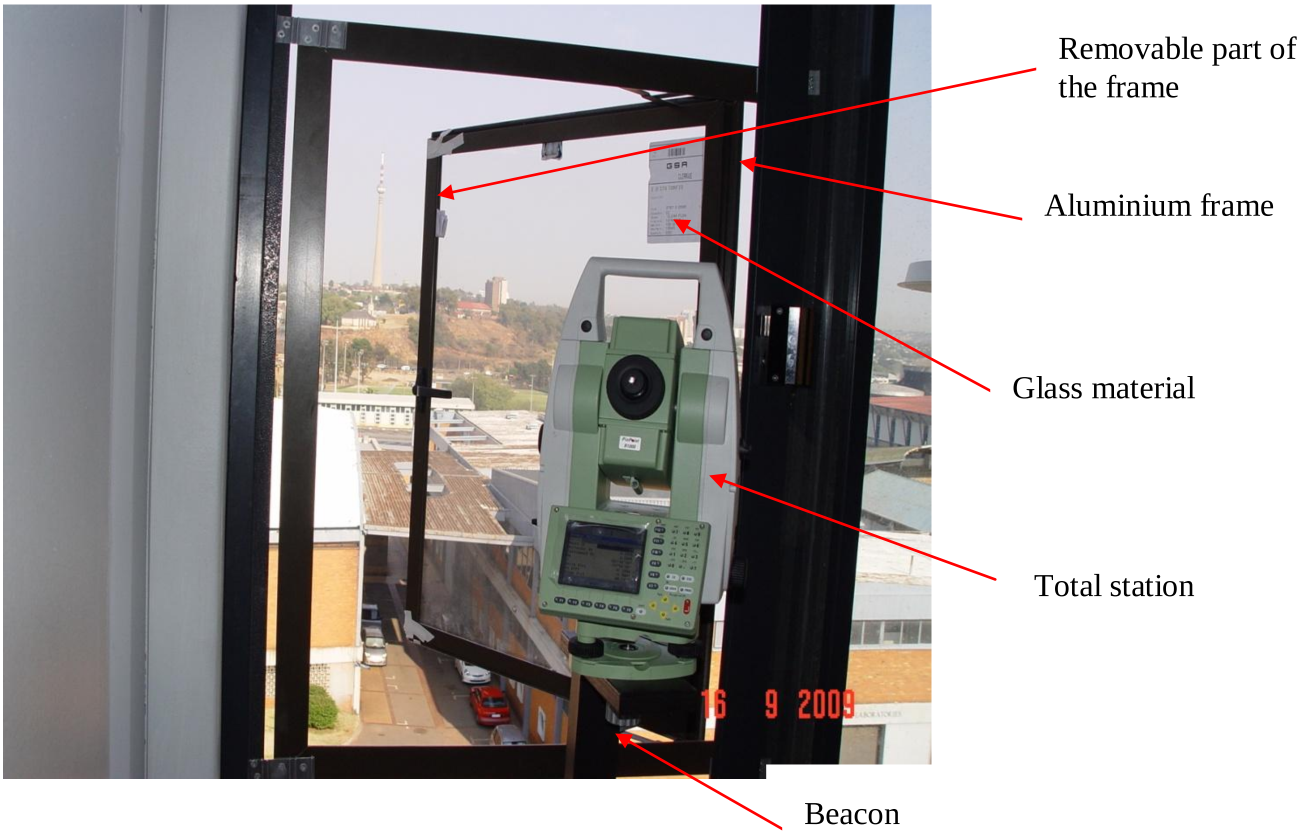

Figure 4.13: Window frame and total station

4.3 OBSERVATION/DISTANCE MEASUREMENT

The total station was mounted on the top of the beacon (as shown in Figure 4.13) and levelled. Before starting any measurements with the total station, the atmospheric part per million (ppm) correction of the instrument was turned off to avoid double atmospheric correction as a result of GeoMoS activation. The instrument was orientated using an established reference point. Figure 4.14 shows the target hung on Genmin Laboratories metal pillar.

Figure 4.14: Target attached to Genmin Laboratories metal pillar

Distances were then measured to each of the three targets (Leica mini prism, Leica circular prism and sticker): first, when there was no glass in place and second, when the glass was placed at different angles (45^o, 60^o and 90^o) to the total station telescope. It must be noted that the instrument automatically corrects the distance measured for prism error and all that is needed is that the operator should enter the corresponding prism constants from the machine manufacturer configured corresponding prism constants (for example, Leica circular prism is 0.0 mm, Leica mini prism is 17.5 mm and sticker represents reflectorless is 34.4 mm respectively) before embarking on distance measurement to the prisms. Readings were taken on an hourly basis from 6:00am to 6:00pm daily. The measurements were taken as fast as possible (maximum period of 5 minutes) to ensure that the total time taken in measuring distances did not straddle adverse conditions. Also, the atmospheric parameters were recorded each time (on an hourly basis) before embarking on distance measurement. These were carried out using each glass type for three days. A total of 15 days were used for taking both the distance, angular and atmospheric parameters readings. The distance measurement to the targets in the first position started on 29 August and ended on 12 September 2009. The targets were later moved further away in order to resemble a typical surface mine environment. The same procedures followed in the first 15 days were repeated. The distance measurements to the targets in the second position started on 6 October and ended on 20 October 2009. Figure 4.15 shows the map of campus observation station, target stations and line-of-sights. The measurement sequence with the total station is presented in a flow chart presented in Figure 4.16.

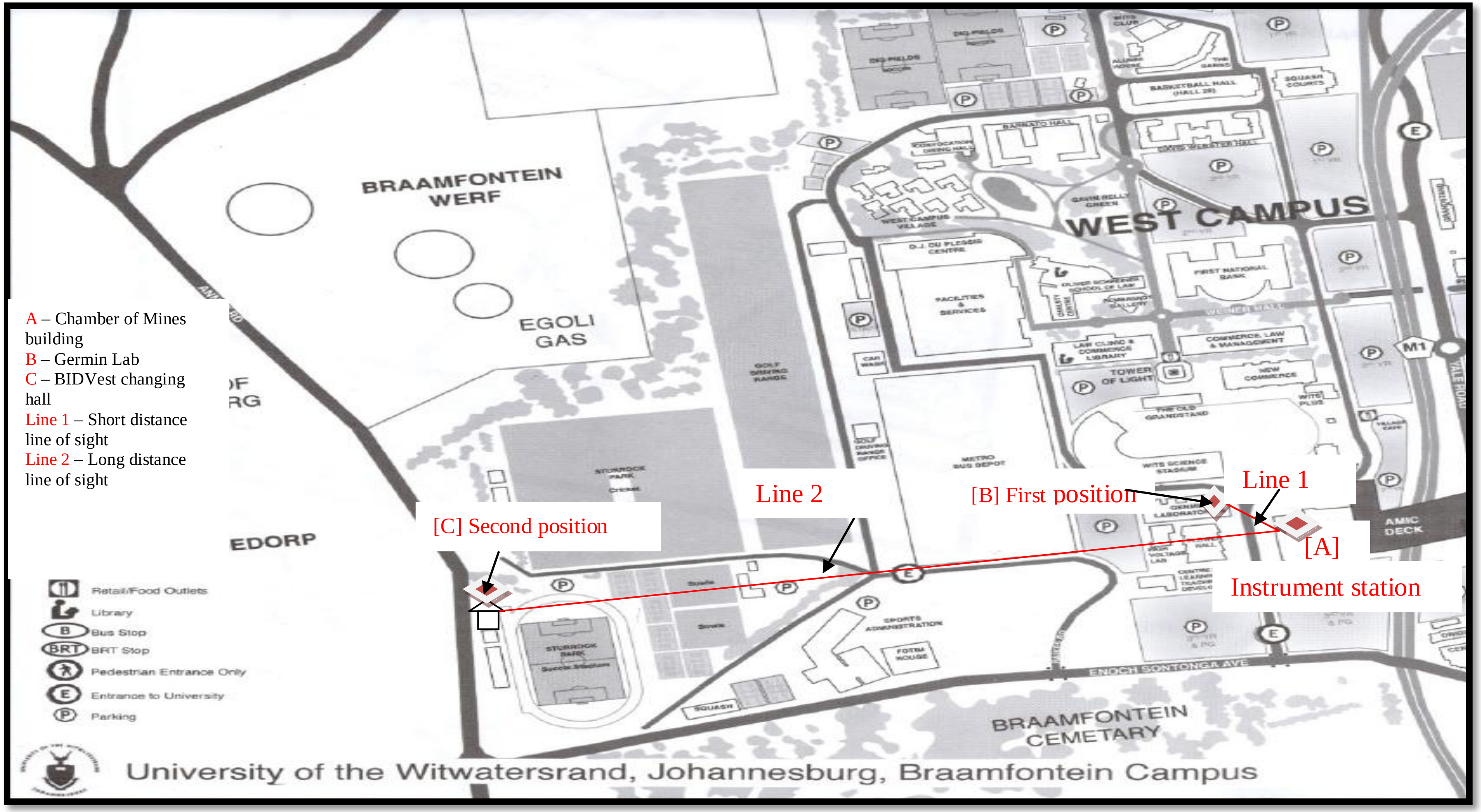

Figure 4.15: Map showing campus observation stations (Source: WITs map)

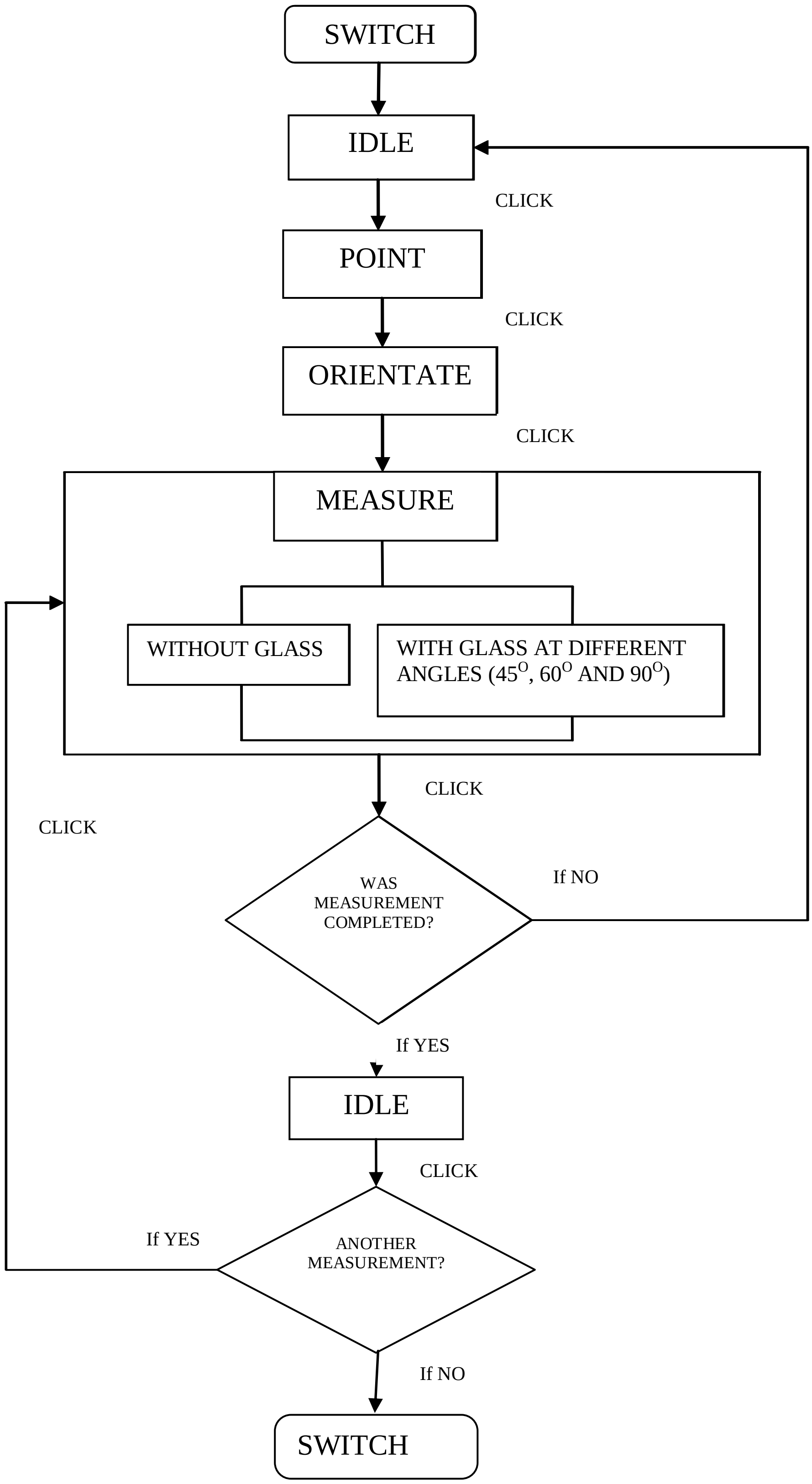

Figure 4.16: The TCR 1201 total station measurement circle

Based on the outcome of the analyses of short- and long-distance monitoring, two tinted (dark- and light-tinted) 3.0 mm thick glass panes were procured in addition to the 3.0 mm clear float (non-tinted) glass used in the previous tests. Each of the three glass types was used for three days over the long distance. Distances were measured to each of the three targets (Leica mini prism, Leica circular prism and sticker) without glass and with glass at different angles (30^o, 45^o, 60^o and 90^o).

All the measured distances were recorded and corrected for atmospheric corrections using the atmospheric correction formulae given by Leica Geosystems (the manufacturer of the Leica TCR +1201 used for this research) listed in equations 2.30 and 2.31 in chapter two (repeated below for clarity purpose):

For infra-red EDM:

$$\Delta D_1 = 283.05 - \left[\frac{0.29196P}{(1+\alpha.t)} - \frac{4.126\times10^{-4}h}{(1+\alpha.t)}.10^x \right] \quad \text{.......... 2.30}$$

For visible red laser:

$$\Delta D_1 = 285.93 - \left[\frac{0.29493P}{(1+\alpha.t)} - \frac{4.126\times10^{-4}h}{(1+\alpha.t)}.10^x \right] \quad \text{.......... 2.31}$$

where:

ΔD_1 = atmospheric correction, ppm

P = air pressure, mb

t = air temperature, ^{0}C

h = relative humidity, %

$$\alpha = \frac{1}{273.15}$$

$$x = \left[\left(\frac{7.5t}{237.3+t} \right) + 0.7858 \right]$$

The two equations above give the following equations for atmospheric corrections after expansion of second term with 273.15 (1/0.003661) and when put into consideration the display distance reading on the total station screen d':

For infra-red EDM (IR):

$$C_1 = \left[283.05 - \frac{79.7489P}{(273.15+t)} + \frac{11.27e}{(273.15+t)} \right].10^{-6}d' \quad \text{.......... 4.1}$$

For visible red laser (RL):

$$C_1 = \left[285.93 - \frac{80.5601P}{(273.15+t)} + \frac{11.27e}{(273.15+t)} \right].10^{-6} d' \quad \text{..........4.2}$$

where:

$$e = \frac{10^{x} h}{100}$$

i.e. $$e = \frac{10^{\left[\left(\frac{7.5t}{237.3+t}\right)+0.7858\right]} h}{100}$$

The above two equations 4.1 and 4.2 were used to correct the impact of atmospheric variations on the distances measured on an hourly basis to each of the three targets (Leica mini prism, circular prism and sticker). The atmospheric corrected distances were recorded for further analysis.

4.4 CONCLUSION

The chapter discussed the reasons for pre-delivery calibration of total station instruments and the pre-delivery calibration performed on the new total station procured for this research. The key parameters examined during the pre-delivery calibration were also explained.

Site preparations for campus observations and the methodologies used in campus data collection were provided in detail. The next chapter examine the analysis of the data collected.

CHAPTER FIVE

5.0 DATA ANALYSIS AND PROCESSING TO INVESTIGATE THE IMPACT OF GLASS THICKNESS ON DISTANCE MEASUREMENTS

Chapter four discussed the preparation for data collection for the purpose of this research. This chapter explains the measurements analysis and the processing carried out on the data collected to ascertain the impact of glass thickness on distance measurements.

5.1 DISCUSSION ON DATA COLLECTED

The collection of data for thickness analysis started on 29 August, 2009 and ended on 20 October 2009. The date, 29 August 2009, marked the beginning of distance measurements to each of the three targets when the targets were placed on short-distance monitoring points. On the first three (3) days, 2.0 mm glass was used, after which 3.0 mm, 4.0 mm, 5.0 mm and 6.38 were used each for three (3) days. During each of these days, the distance readings recorded followed the same pattern. The distance readings captured were high in the morning (6 am – 10 am) when the air temperature was low while the humidity was high and began to drop as air temperature increased/decreased in humidity, then began to increase as air temperature reduced/increased in humidity in the evening period (3 pm – 6 pm). The variations in outside average daily temperature ranged between 5.5°C and 7.0°C, while the average daily pressure variation ranged between 3 mb and 7.9 mb. The change in average daily humidity was as high as 39.8% during the short-distance monitoring. The distance readings showed a positive response to the glass barrier. The distance readings when there was no glass in place were low compared to distance readings when there was glass in place. The effect of the angle position of the glass on distance readings was negligible. However, the distance readings with glass increased with the increase in the glass thickness. The distance measurement during the short-distance monitoring was about 42 m. The horizontal distance readings to the two prisms (mini and circular) were closer when compared to the horizontal distance readings to the sticker. However, the vertical distance readings to each of the targets were different because the targets were not at the same height. They were 0.5 m apart. As a result of this, discrepancies in vertical distance readings to each of the target were expected. The 0.5 m gap between the targets manifested in the vertical readings recorded (i.e. mini prism -11.88, circular prism -12.38 and sticker -12.88). The data collection from the short-distance monitoring point ended on 12 September 2009 which marked the third day of using 6.38 mm glass. The targets were later moved to the long-distance monitoring point.

The targets were placed on a long-distance monitoring point which was about 626.5 m from the instrument station (i.e. office window station - WS). Distance measurements to the each of the three targets during long distance monitoring began on 6 October 2009. In the first three (3) days, 2.0 mm glass was also used after which 3.0 mm, 4.0 mm, 5.0 mm and 6.38 were used each for 3 days. The variations in outside average daily temperature ranged between 4.4°C and 6.7°C, while the average daily pressure variations ranged between 4.1 mb and 5.8 mb. The average daily humidity was as high as 50.7% during the long-distance monitoring. The distance readings captured during long-distance monitoring also followed the same pattern as the distance readings during short-distance monitoring: high distance readings in the morning, slightly lower in the afternoon and high again in the evening. The distance readings also increased with increased glass thickness. The HD readings to the two prisms (mini and circular) were also close when compared to HD readings to the sticker. The VD readings to each of the three targets also varied by 0.5 m which accounted for the gap between each target in the wooden structure that housed them. Distance readings to the two prisms could be achieved without glass and with glass irrespective of the glass angle to the total station telescope but distance readings could only be measured to the sticker when there was no glass and when there was glass at angle 60°. All other glass angles resulted in error notification by the total station. The data collection from the long-distance monitoring point ended on 20 October 2009 which marked the third day of using 6.38 mm glass. All the data acquired during the glass thickness impact tests are presented in the raw observation data book (see appendix C.1).

5.2 ANALYSIS OF CAMPUS OBSERVATIONS

The analysis of the atmospheric conditions that were encountered during the campus distance measurements (the atmospheric parameters readings which were used to correct the measured distances for atmospheric corrections) is presented in appendix C.2.

In analyzing the campus distance measurements, the hourly (6:00 to 18:00) readings were subjected to a variability test. Standard deviations were calculated and used to measure the variability or diversity in the daily distance readings. The method helped to ascertain how much variation or dispersion occur with the hourly distance readings from the average daily distance reading (i.e. the mean). The results of the standard deviation are presented in appendix C.3 (see table C.2 of appendix C.3).

The standard deviation of HD and VD hourly readings during short and long distance measurements were very low (i.e. within 2.0 mm before atmospheric corrections and below 1 .0 mm after atmospheric corrections). The results were the same for HD and VD measurements to both mini and circular prisms. The only few exceptional cases were in HD and VD measurements to the sticker during long distance monitoring. This clearly revealed that visible red laser light is more affected by atmospheric variations as distance measurement increases (nevertheless, the standard deviation of the daily distance readings the sticker were a little above 2.0 mm after atmospheric corrections). The results presented in appendix C.3 revealed that the hourly distance readings per day were very close to the mean (i.e. the daily average distance readings). It also revealed the efficiency and sensitivity of the total station TCR 201+ used in the data collection. This is an indication that the hourly distance measurements were well observed without outliers. Based on these findings, the hourly daily readings were reduced to average daily distance readings to reduce the bulk volume of daily acquired data.

The data acquired on distance measurements were subjected to graphical analysis to confirm the effectiveness of the atmospheric corrections formulae given in the total station instrument manual (as stated in equations 2.30 and 2.31 of chapter 2 and modified in chapter 4 equations 4.1 and 4.2 of this report) in reducing/removing the impact of the glass medium on the measured distances. In order to achieve these objectives, the accuracy specifications given in the instrument manual were used to set the confidence limits[21] (i.e. upper limit and lower limit) in the graphs. These accuracy specifications were: ±1 mm + 1.5 ppm, when using IR mode; ±2 mm + 2 ppm when using RL mode to measure distances less than 500 m; and ±4 mm + 2 ppm when using RL mode to measure distances greater than 500 m. The analysis of the data is presented in two headlines, namely: horizontal distance (HD) and vertical distance (VD) analysis.

[21] These are the limits within which it can be said with a given degree of confidence that the true value (true distance – in case of this research) lies. (Bannister *et al.*, 1998).

5.3 HORIZONTAL DISTANCE (HD) ANALYSIS

The HDs were analyzed in two ways, that is, HD before atmospheric corrections and HD after atmospheric corrections. Figure 5.1 and 5.2 show the results of HD analysis for short- and long-distances monitoring to the three targets without glass. The HDs were corrected for prism constant and scale factor but not for atmospheric corrections.

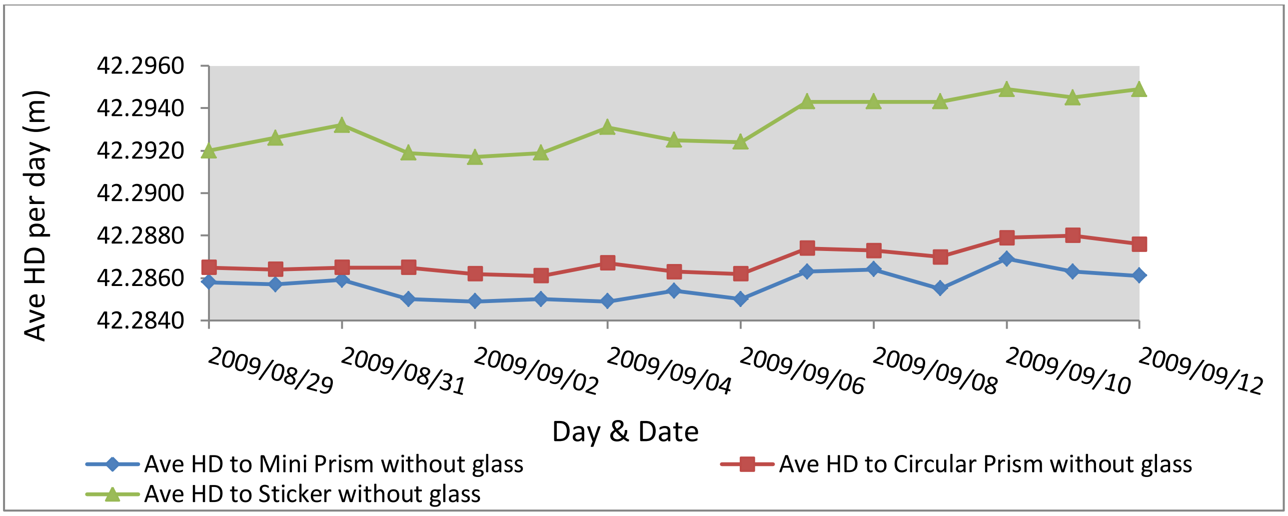

Figure 5.1: Average daily HDs before atmospheric correction (short-distance)

Figure 5.1 shows the graph of average daily HD measurements to the three targets during short-distance monitoring. The graph shows average daily HD measurements to the sticker with the highest values range followed by the average daily HD measurements to the circular prism, while the average daily HD measurements to the mini prism has the least values range. The average daily HD measurements to the mini prism ranged between 42.2849 m and 42.2869 m; that of circular prism range between 42.2861 m and 42.2880 m; while the average daily HD measurements to the sticker ranged between 42.2917 m and 42.2949 m.

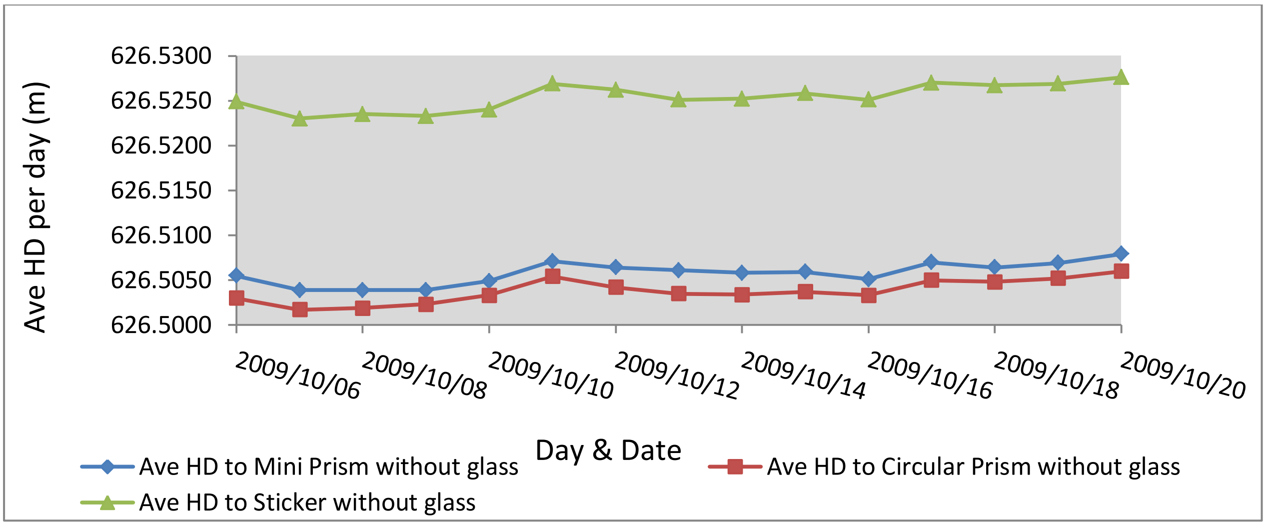

Figure 5.2: Average daily HDs before atmospheric correction (long-distance)

Figure 5.2 shows the graph of the average daily HD measurements to the three targets during long-distance monitoring. The graph shows average daily HD measurements to the sticker with highest values' range followed by average daily HD measurements to the mini prism and the average daily HD measurements to the circular prism with the least values' range. The average daily HD measurements to the circular prism ranged between 626.5017 m and 626.5060 m; that of mini prism ranged between 626.5039 m and 626.5079 m; while the average daily HD measurements to the sticker ranged between 626.5230 m and 626.5276 m. The only difference in figure 5.1 and figure 5.2 is the change in the position of mini and circular prism. The sticker positions in the two graphs remain unchanged.

Figures 5.3 and 5.4 show the results of HD measurements to the three targets during short- and long-distances monitoring after atmospheric corrections. During atmospheric corrections, the atmospheric parameters measured with Oregon atmospheric sensors and the GeoMoS DTM meteo sensor (**simply referred to as GeoMoS in this analysis report**) were applied separately to the daily HD readings to see the discrepancies that may arise from using two different systems (unlike the Oregon instrument the GeoMoS has no humidity sensor). Surprisingly, the impact of the humidity sensor lacking in the GeoMoS was negligible in the final results. The HD measurements corrected for atmospheric variations using GeoMoS atmospheric parameters and HD measurements corrected for atmospheric variations using Oregon atmospheric parameters were too close to each other. The effect of the humidity was below 1.0 mm and 2.0 mm during short- and long-distances monitoring as revealed in figures 5.3 and 5.4.

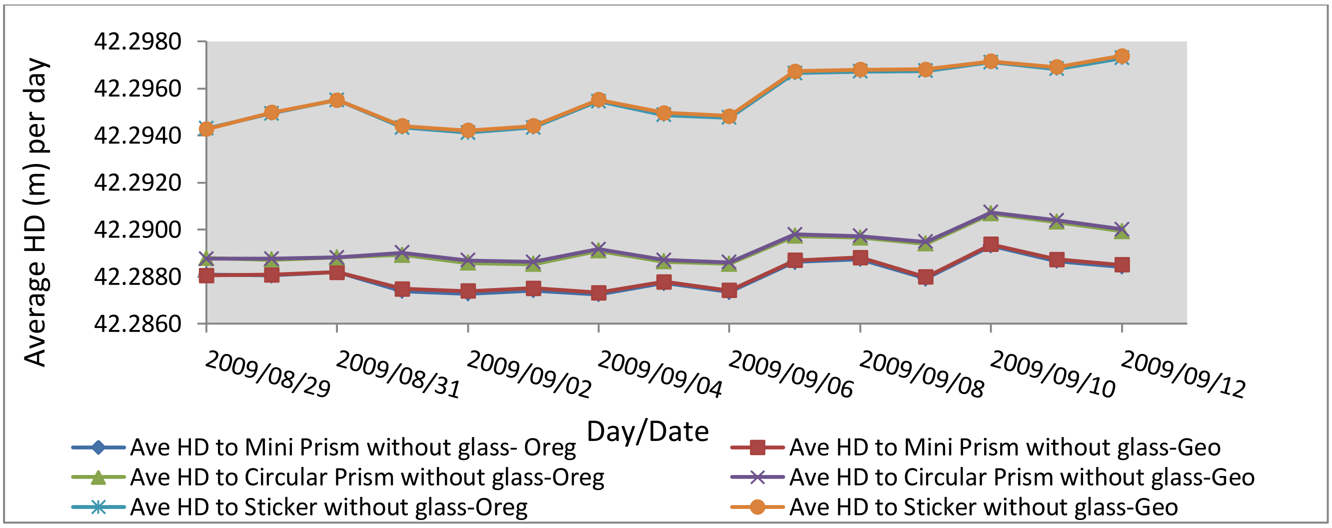

Figure 5.3: Average daily HDs after atmospheric corrections (short-distance)

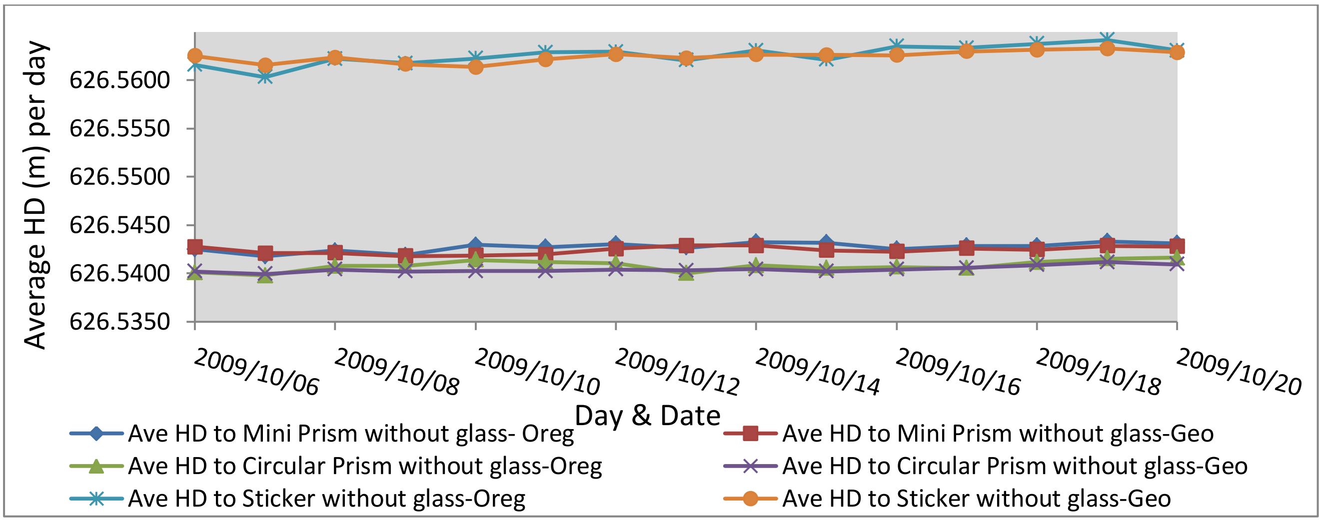

Figure 5.4: Average daily HDs after atmospheric corrections (long-distance)

The two graphs show no difference despite using atmospheric data from the two different systems (GeoMoS meteo sensor and Oregon scientific weather sensor). The use of average outside Oregon (Oreg) and GeoMoS (Geo) atmospheric measurements in the correction only was due to the closeness in the two instrument readings and the fact that the inside atmospheric parameters were fairly constant during the monitoring periods. Therefore, in subsequent atmospheric corrections, the GeoMoS parameters would be used because it is the widely used sensor in most mines visited before the commencement of this research work. To make the total station adapt to the room atmospheric conditions, the machine was usually installed and switched on for about 45 minutes before the commencement of the daily measurements.

In order to examine the likely impact of the glass medium on the HD measurements to the three targets during short- and long-distance monitoring and the effectiveness of the atmospheric corrections formulae in reducing or removing the glass impact, the HD measurements to each target were analyzed separately (HD before and HD after atmospheric corrections).

5.3.1 Glass Impact on HD Measurements before Atmospheric Correction during Short Distance Monitoring

The result of the average daily HD measurements to the Leica mini prism before atmospheric corrections during short-distance monitoring is presented in figure 5.5. The corresponding results when monitoring to the circular prism and the sticker are presented in figure 5.6 and 5.7.

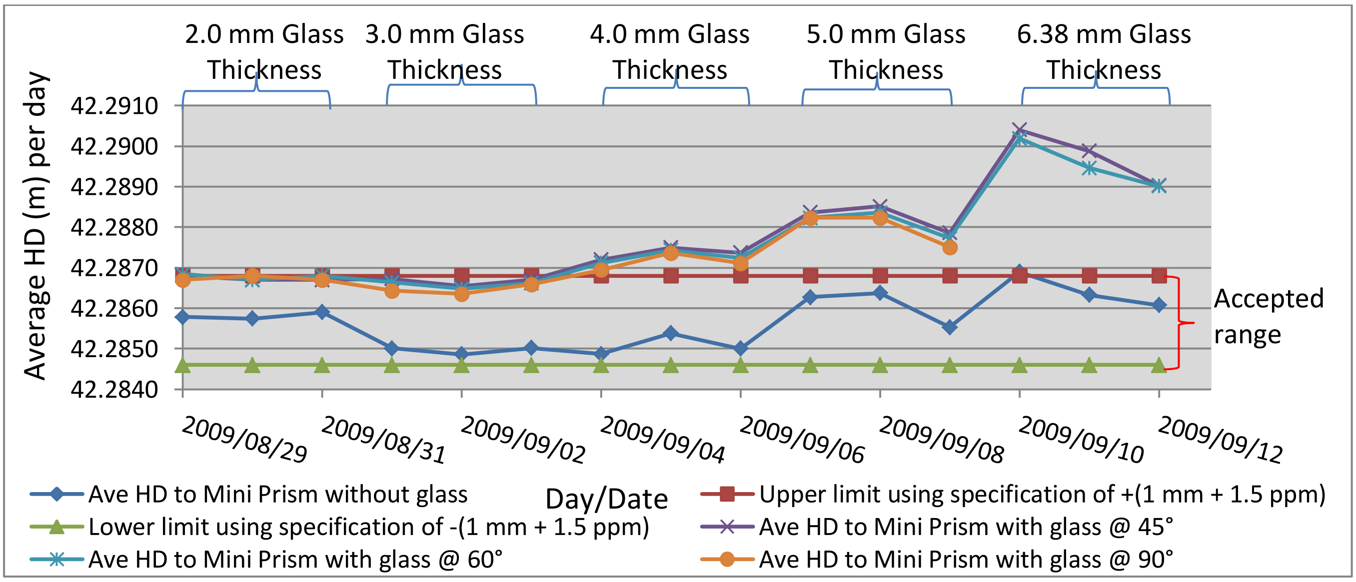

Figure 5.5: Average daily HDs before atmospheric corrections using mini prism as target (short-distance)

Figure 5.5 reveals that 2.0 mm and 3.0 mm glass thickness have little or no impact on accuracy in all the different angles (45^o, 60^o and 90^o) tested. The graph also shows a proportional increase in the variations between HDs without glass and HDs with glass at varying angles in 2.0 mm, 3.0mm and 4.0 mm glass thickness. The impact range between 0.0010 m and 0.0012 m (i.e. 0.2 mm variation in HD readings with glass) when 2.0 mm glass was used; it ranged between 0.0014 m and 0.0017 m (0.3 mm variation) when 3.0 mm glass was used; The impact caused by 4.0 mm glass ranged between 0.0020 m and 0.0024 m (0.4 mm variation); 5.0 mm glass impact ranged between 0.0019 m and 0.0023 m (0.4 mm variation); while the impact caused by 6.38 mm glass ranged between 0.0029 m and 0.0035 m (0.6 mm variation). The graph shows a proportional increase in HD with an increase in glass thickness at different angles up to 4.0 mm glass which changed when 5.0 mm glass and above were used. It also shows that the angle at which the measurement is taken through the glass does not affect the accuracy of the measurement provided the glass thickness is less than 3.0 mm.

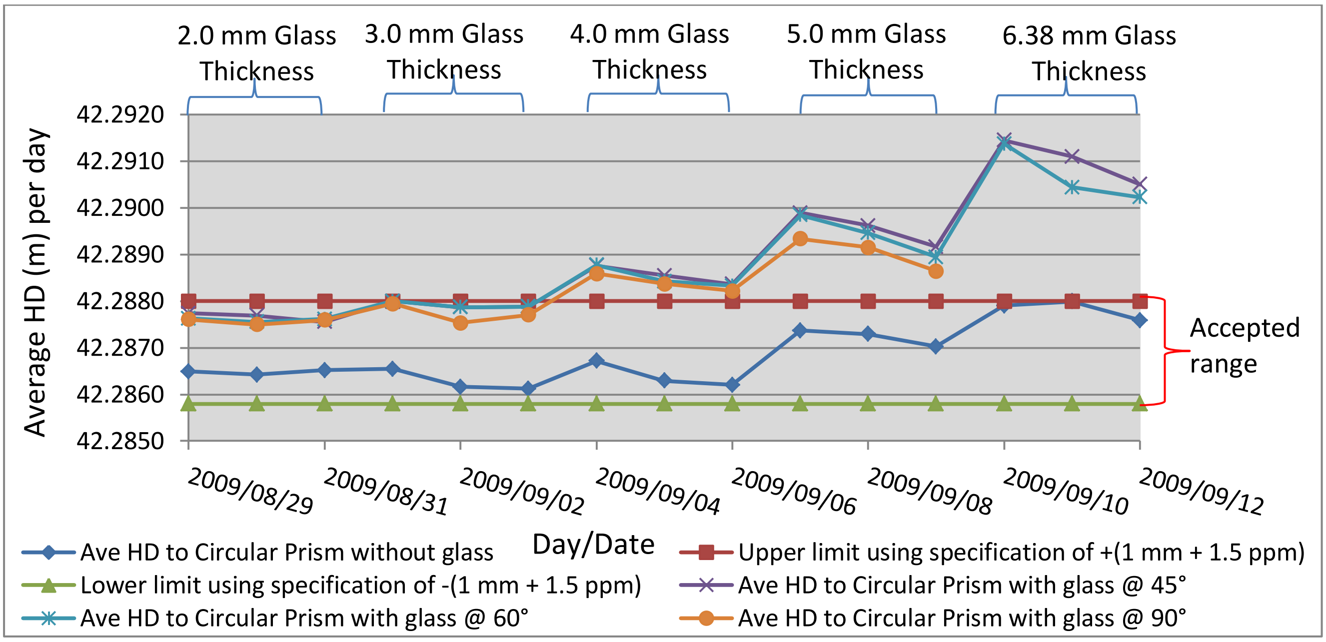

Figure 5.6: Average daily HDs before atmospheric corrections using circular prism as target (short-distance)

The results of short-distance monitoring to the Leica circular prism is presented in Figure 5.6. The graph is similar to Figure 5.5; it also reveals that glass thickness of 2.0 mm and 3.0 mm had no impact on accuracy specification at different angles tested. The graph shows proportional increase in the variations between HDs without glass and HDs with glass at varying angles. The graph reveals that when 2.0 mm glass was used, the impact ranged between 0.0011 m and 0.0013 m (i.e. 0.2 mm variation in HD readings with glass); 0.0014 m and 0.0018 m (0.4 mm variation) when 3.0 mm glass was used; 0.0019 m and 0.0023 m (0.4 mm variation) when 4.0 mm glass was used; the impact ranged between 0.0016 m and 0.0025 m (0.9 mm variation) when 5.0 mm glass was used; while the impact caused by 6.38 mm glass ranged between 0.0024 m and 0.0031 m (0.7 mm variation). The graph also shows an increase in HD with increase in glass thickness.

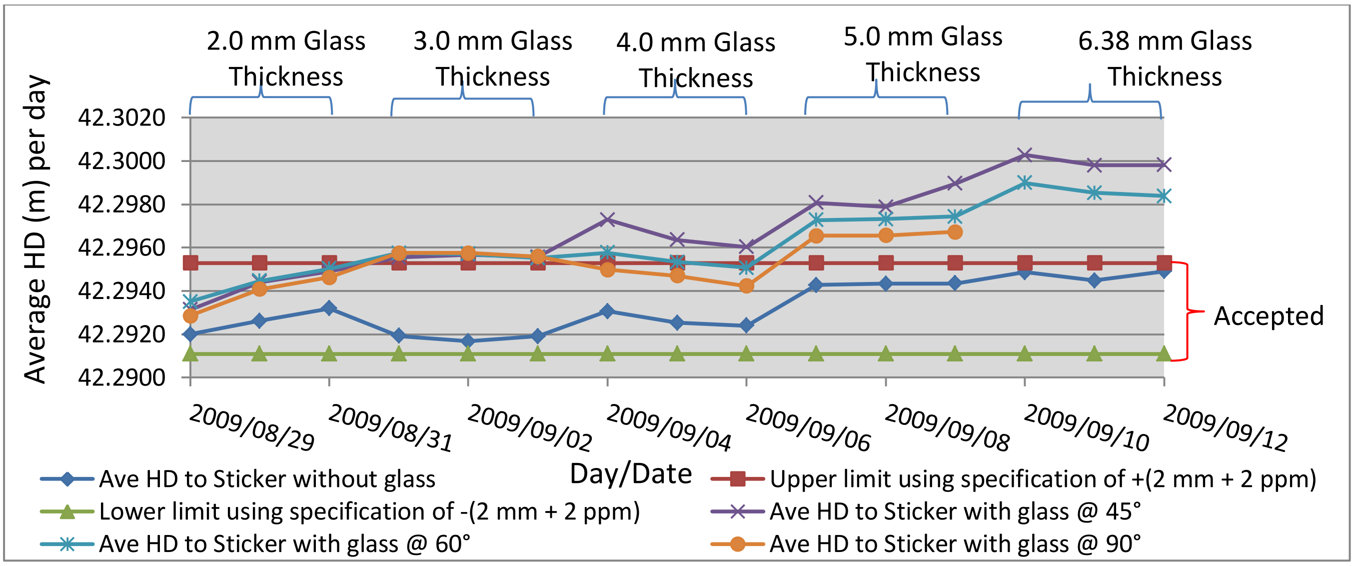

Figure 5.7: Average daily HDs before atmospheric corrections using sticker as target (short-distance).

The graph of the average daily HD measurements to the sticker before atmospheric corrections shown in figure 5.7 reveals that only glass thickness 2.0 mm had no impact. All other glass thickness (3.0 mm, 4.0 mm, 5.0 mm and 6.38 mm) had an impact on accuracy. The graph also shows an inconsistent increase in variation between HDs without glass and HDs with glass at different angles. This inconsistency may be as a result of the red laser rays that are supposed to actualize the measurement being reflected back by the glass medium (appendix C.3 - Figure C.3.1 shows the picture of the black board and Figure C.3.2 shows the picture of reflected ray captured on the black board during one of the monitoring exercises). The impact ranged between 0.0009 m and 0.0018 m (i.e. 0.9 mm variation) when 2.0 mm glass was used; 0.0036 m and 0.0041 m (0.5 mm variation) when 3.0 mm glass was used; 0.0018 m and 0.0042 m (2.4 mm variation) when 4.0 mm glass was used; the impact caused by 5.0 mm ranged between 0.0022 m and 0.0046 m (2.4 mm variation); while 6.38 mm glass impact ranged between 0.0035 m and 0.0054 m (1.9 mm deviation). The graph reveals that the increase in HD with increase in glass thickness differs at varying glass angles when glass thickness 3.0 mm and above were used.

5.3.2. Glass Impact on HD after Atmospheric Corrections during Short-Distance Monitoring

As stated earlier, only graphs of the atmospheric corrections using GeoMoS sensor would be presented since there was little or no difference in the final results achieved when GeoMoS and Oregon sensors readings were used separately with the atmospheric corrections formulae.

The result of the average daily HD measurements to the Leica mini prism after atmospheric corrections using atmospheric parameters captured with GeoMoS is presented in Figure 5.8. The corresponding results when monitoring to the Leica circular prism and the sticker are presented in Figures 5.9 and 5.10.

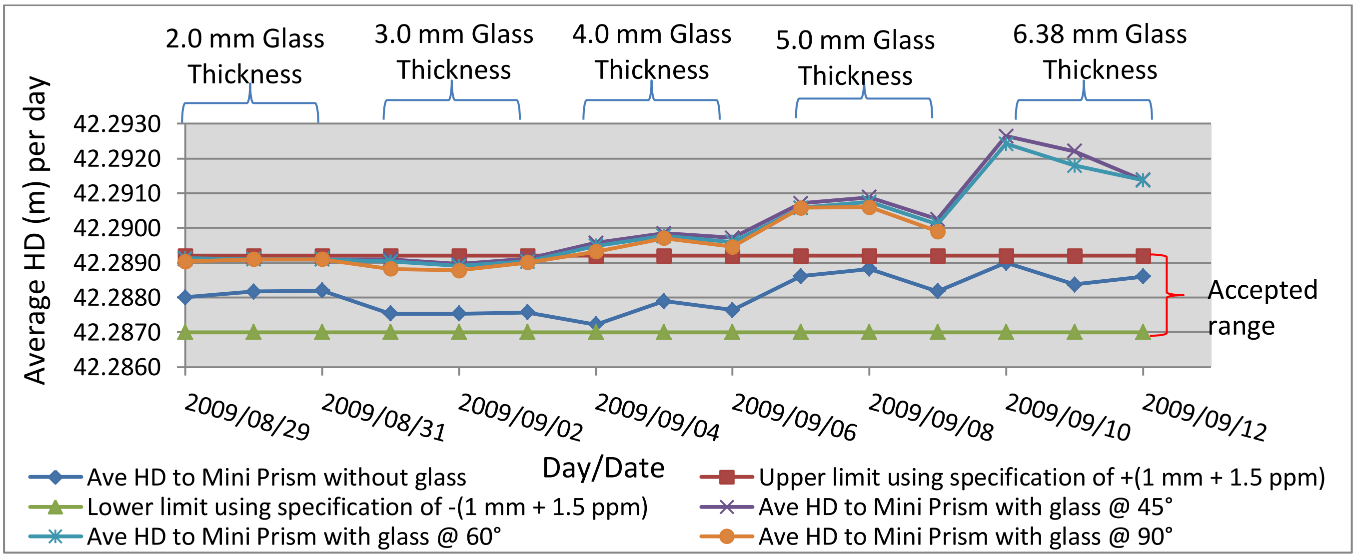

Figure 5.8: Average daily HDs after atmospheric corrections using mini prism as target (short-distance)

Figure 5.8 shows the result of the average daily HD measurements to the mini prism after atmospheric corrections. The graph is similar to the graph of the average daily HD measurements to the mini prism before atmospheric corrections presented in Figure 5.5. The only difference is that the effects of atmospheric parameter variations have been removed. The impact caused by the glass thickness at different angles is virtually the same. When 2.0 mm glass was used, the impact ranged between 0.0011 m and 0.0012 m; 3.0 mm glass impact ranged between 0.0014 m and 0.0017 m; the impact ranged between 0.0020 m and 0.0024 m when 4.0 mm glass was used; it ranged between 0.0019 m and 0.0023 m when 5.0 mm glass was used; while 6.38 mm glass impact ranged between 0.0029 m and 0.0035 m. The graph shows a proportional increase in HD with increase in glass thickness at different angles.

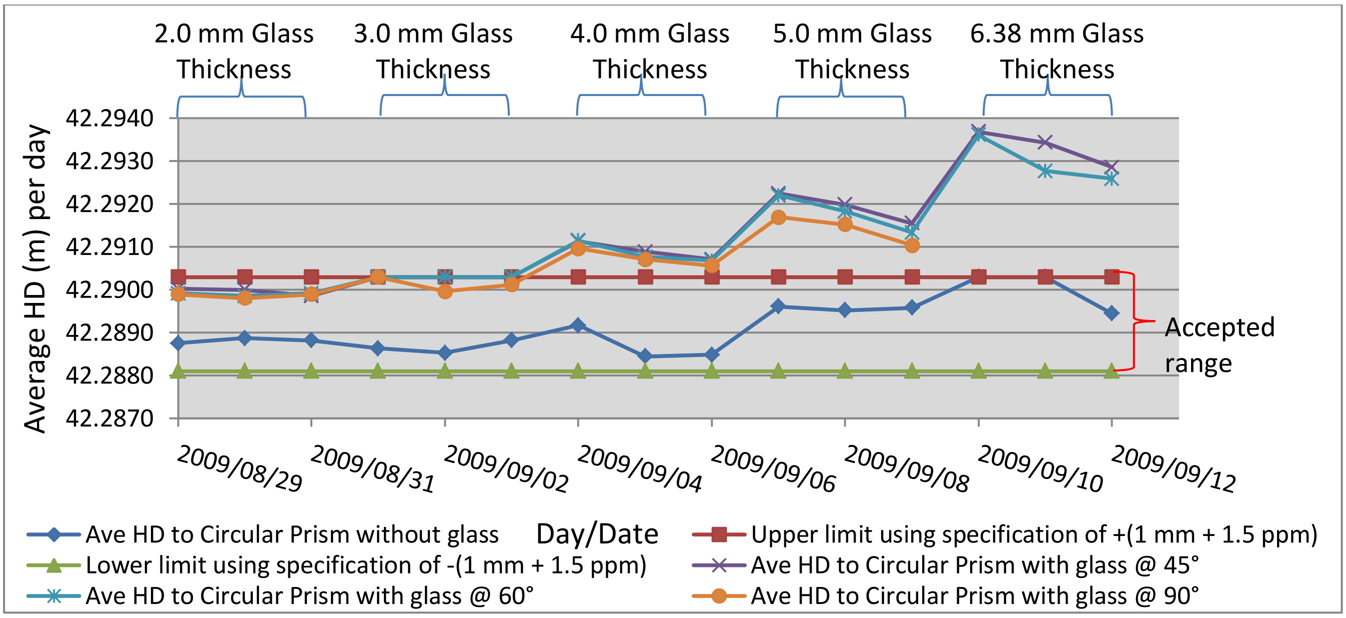

Figure 5.9: Average daily HD after atmospheric corrections using circular prism as target (short-distance)

Figure 5.9 shows the average daily HD measurements to the Leica circular prism after atmospheric corrections. The graph also reveals that glass thickness above 3.0 mm has an effect on accuracy. The impact ranged between 0.0011 m and 0.0013 m (i.e. 0.2 mm variation in HD readings with glass at different angles) when 2.0 mm glass was used; 0.0014 m and 0.0017 m when 3.0 mm glass was used; 0.0019 m and 0.0023 m when 4.0 mm glass was used; 0.0019 m and 0.0025 m when 5.0 mm glass was used; while the impact ranged between 0.0024 m and 0.0031 m when 6.38 mm glass was used.

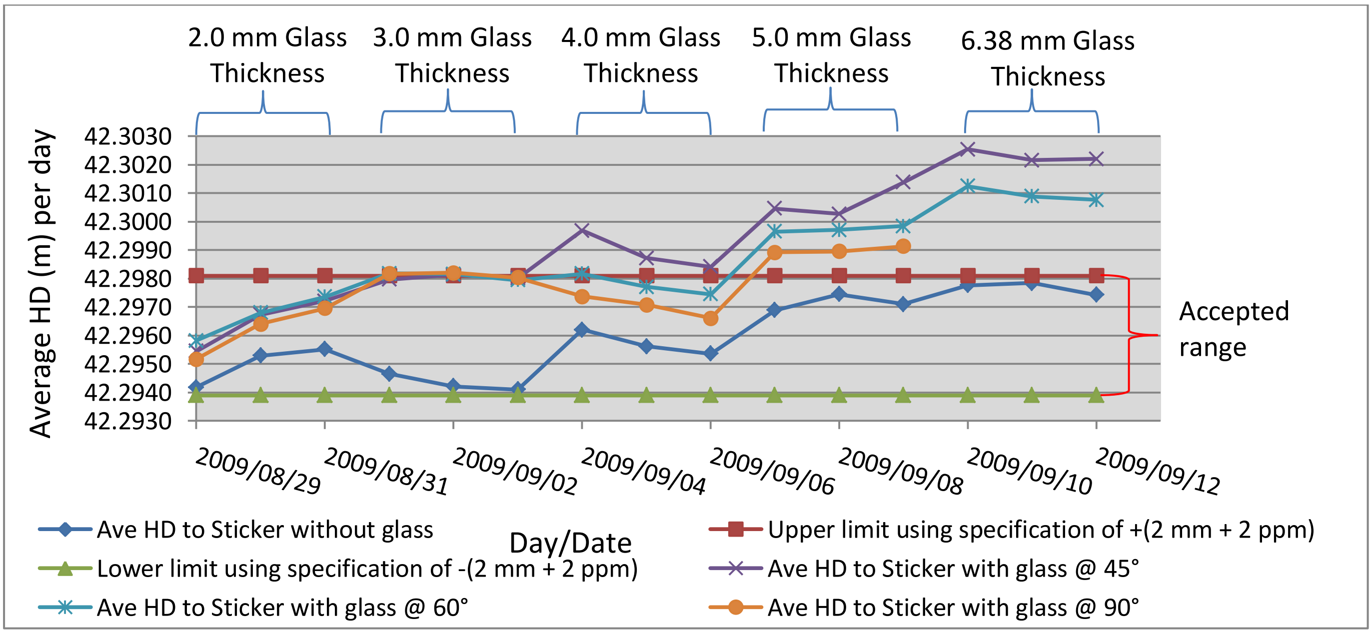

Figure 5.10: Average daily HD after atmospheric corrections using sticker as target (short-distance)

Figure 5.10 shows the average daily HD to sticker after atmospheric correction. The graph shows an impact range between 0.0009 m and 0.0018 when 2.0 mm glass was used; 0.0036 m and 0.0041 m when 3.0 mm was used; 0.0019 m and 0.0036 m when 4.0 mm was used; 5.0 mm glass caused impact range between 0.0026 m and 0.0046 m on HD measurements; while the impact caused by 6.38 mm glass on HD measurements ranged between 0.0035 m and 0.0054 m. The graph shows an inconsistent increase in HD with an increase in glass thickness at varying glass angles after 3.0 mm glass thickness.

5.3.3 Glass Impact on HD before Atmospheric Correction during Long-Distance Monitoring

The result of the average daily HD measurements to the Leica mini prism before atmospheric corrections is presented in Figure 5.11. The corresponding results when monitoring to the Leica circular (circ) prism and the sticker are presented in Figure 5.12 and 5.13.

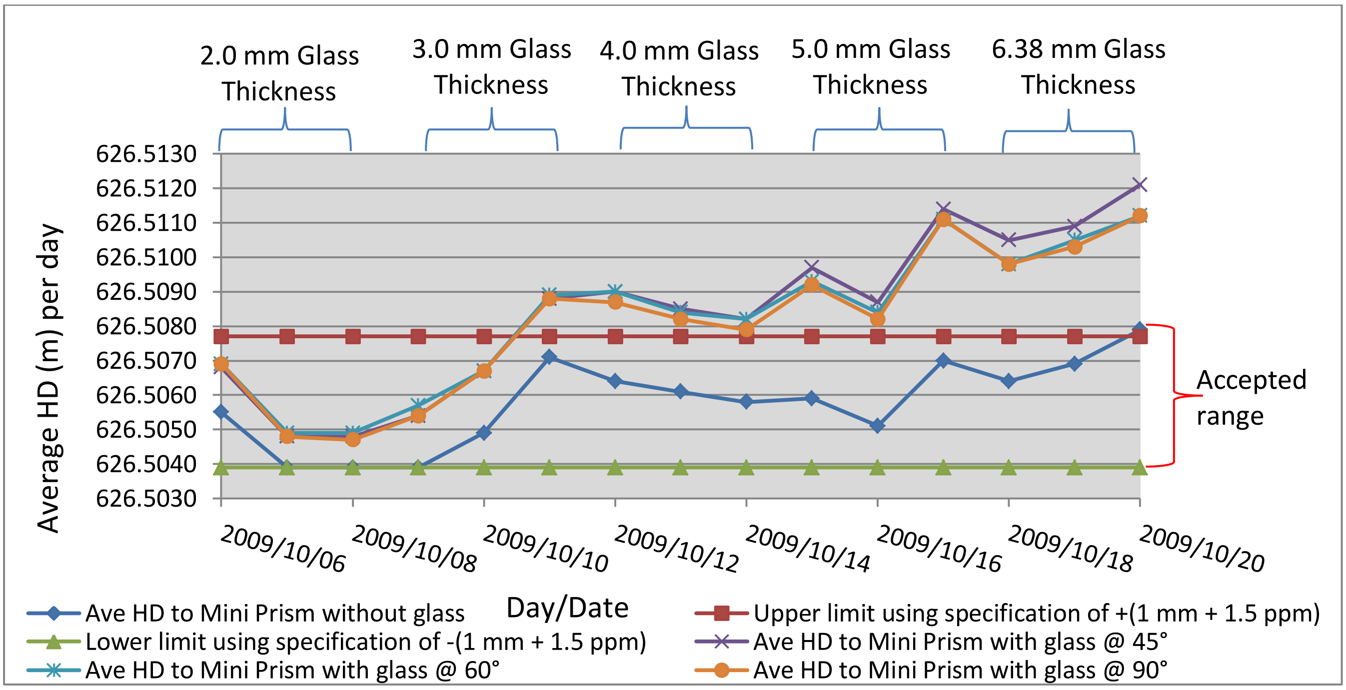

Figure 5.11: Average daily HD before atmospheric corrections using mini prism as target (long-distance)

Figure 5.11 shows the graph of the average daily HD measurements to the mini prism before atmospheric corrections during long distance monitoring. The graph shows proportional variation when 2.0 mm and 3.0 mm glass thickness were used. There are noticeable incoherent variations in HDs when 4.0 mm glass thickness and above were used at varying angles. Although there was little difference in HDs with glass at different angles when 4.0mm glass thickness was used, a noticeable variation in HDs with glass at varying angles started to occur when 5.0 mm glass and above were used. The graph shows that glass thickness of 2.0 mm and 3.0 mm had little or no impact on accuracy. It reveals that the impact of the glass medium on the HD readings when 2.0 mm glass thickness was used is between 0.0009 m and 0.0013 m (i.e. 0.4 mm variation in HD readings with glass); the impact ranged between 0.0015 m and 0.0019 m (0.4 mm variation) when 3.0 mm glass was used; 0.0021 m and 0.0027 m (0.6 mm variation) when 4.0 mm glass was used; 0.0031 m and 0.0045 m (1.4 mm variation) when 5.0 mm glass was used; while the impact caused by 6.38 mm glass ranged between 0.0032 m and 0.0042 m (1.0 mm variation). The graph shows an increase in HD with an increase in glass thickness.

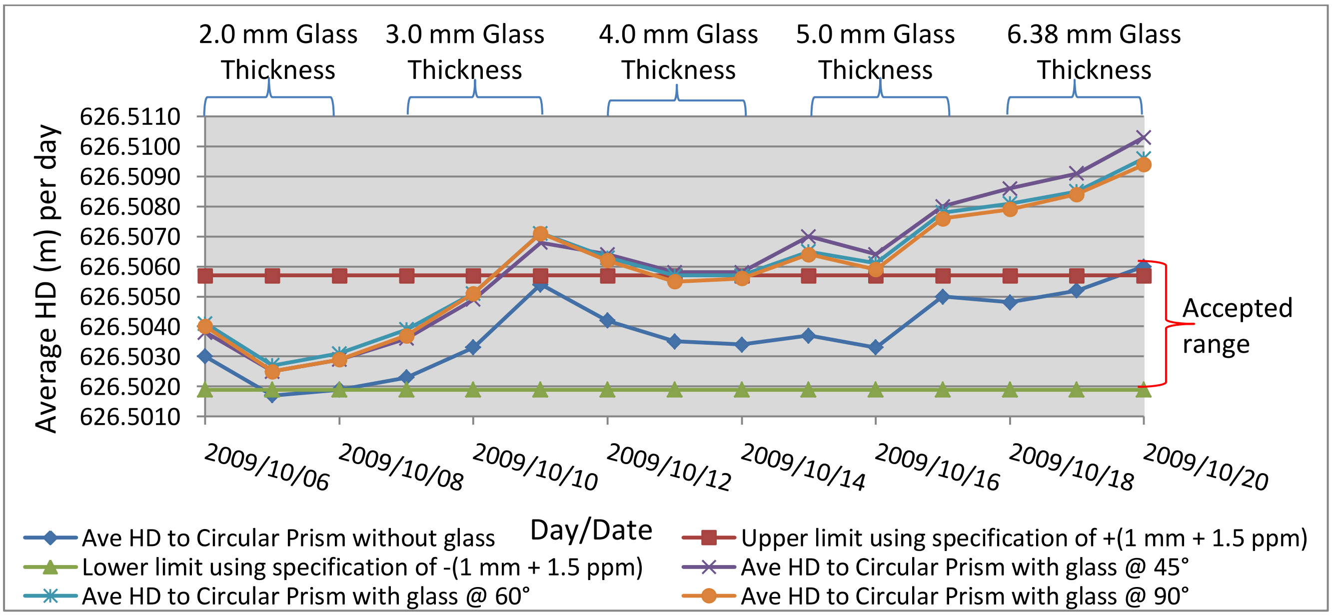

Figure 5.12: Average daily HD before atmospheric corrections using circular prism as target (long-distance)

Figure 5.12 is similar to Figures 5.11 above. The graph shows no variation in HDs with glass at different angles up to 4.0mm glass thickness but noticeable variations in HDs with glass at varying angles started to occur when 5.0 mm glass and above were used. The graph reveals that the impact caused by 2.0 mm glass thickness on HD readings ranged between 0.0008 m and 0.0012 m (i.e. 0.4 mm variation in HD readings with glass); it ranged between 0.0013 m and 0.0018 m (0.5 mm variation) when 3.0 mm glass was used; 0.0019 m and 0.0024 m (0.5 mm deviation) when 4.0 mm glass was used; the impact caused by 5.0 mm glass thickness ranged between 0.0026 m and 0.0033 m (0.7 mm variation); while 6.38 mm glass impact ranged between 0.0031 m and 0.0043 m (1.2 mm variation). The graph also shows an increase in HDs with an increase in glass thickness.

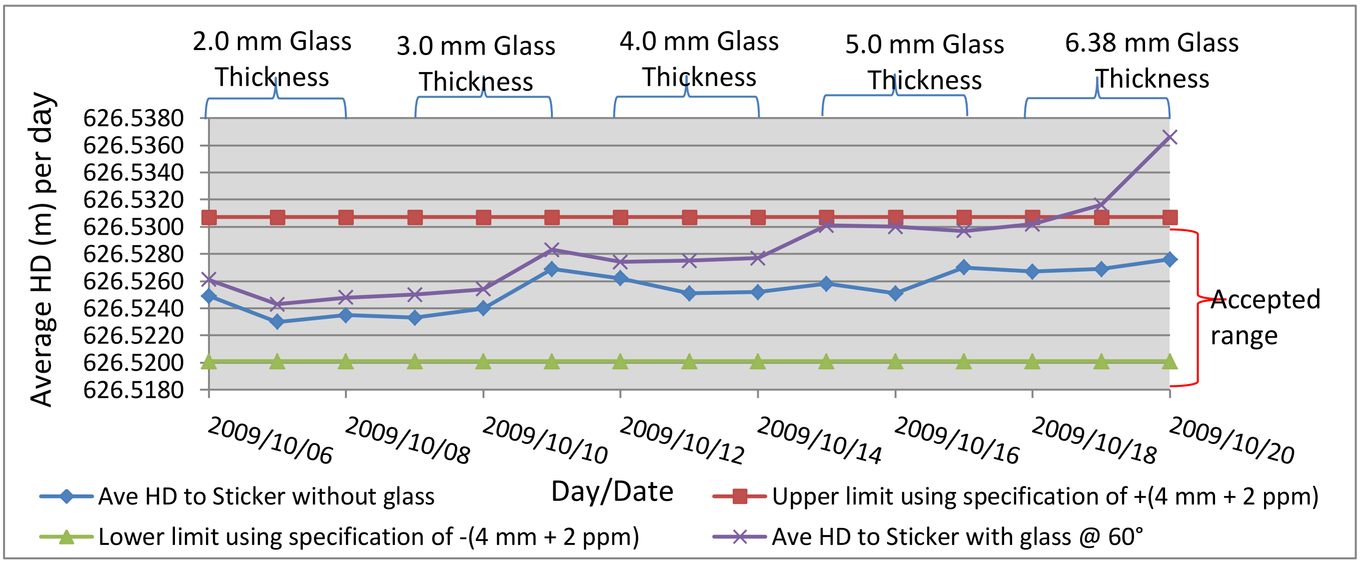

Figure 5.13: Average daily HD before atmospheric corrections using sticker as target (long-distance)

Figure 5.13 shows the graph of the average daily HD measurements to the sticker before atmospheric corrections during long distance monitoring. Distance readings to the sticker could only be achieved without glass and when glass was at angle 60° without any error alert or complaint by the total station. All other angular position resulted in different complaints (i.e. Error 254: EDM measurement not achieved, signal too weak, break in beam or air turbulence; Error 256: Measurement not achieved due to detection of moving targets, target moving, break in beam or air turbulence and Error 275: EDM measurement not achieved, ambient light too strong or distance to target exceeds supported distance range). The HD measurements without glass and the HD measurements with glass at 60° is shown in Figure 5.13. The graph shows a wide range of conformity with accuracy when 2.0 mm to 5.0 mm glass thickness were used.

5.3.4. Glass Impact on HD after Atmospheric Corrections during Long-Distance Monitoring

The result of average daily HD measurements to the Leica mini prism after atmospheric corrections during long-distance monitoring is presented in Figure 5.14. The corresponding results when monitoring to the circular prism and the sticker are presented in Figures 5.15 and 5.16.

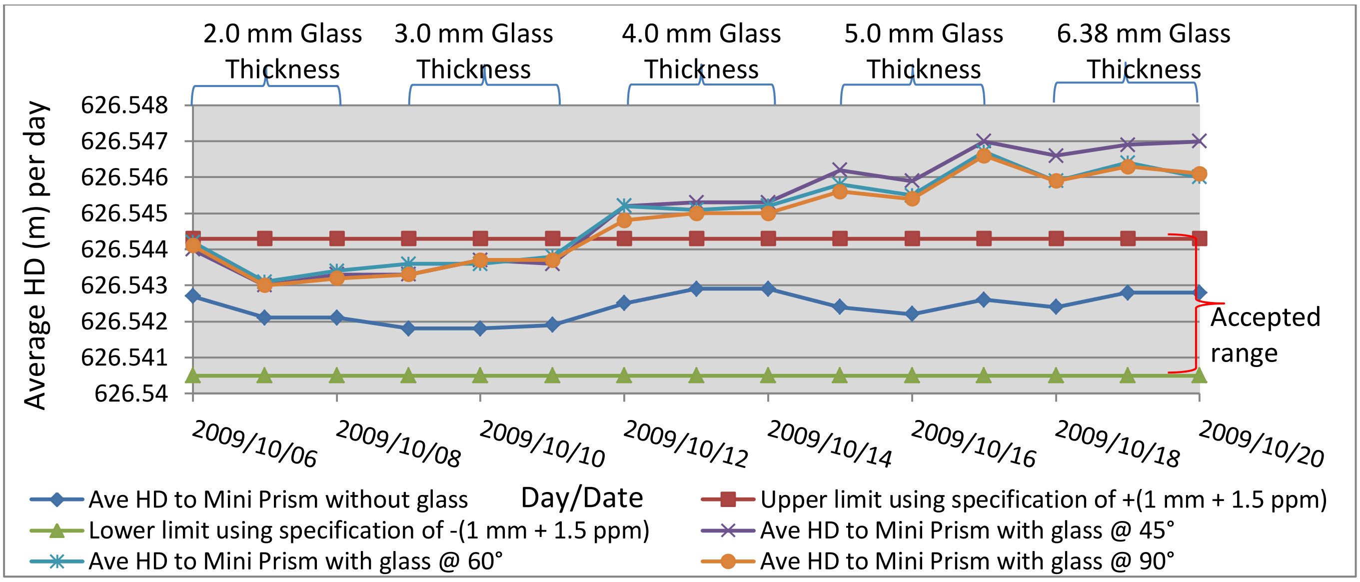

Figure 5.14: Average daily HD after corrections using mini prism as target (long-distance)

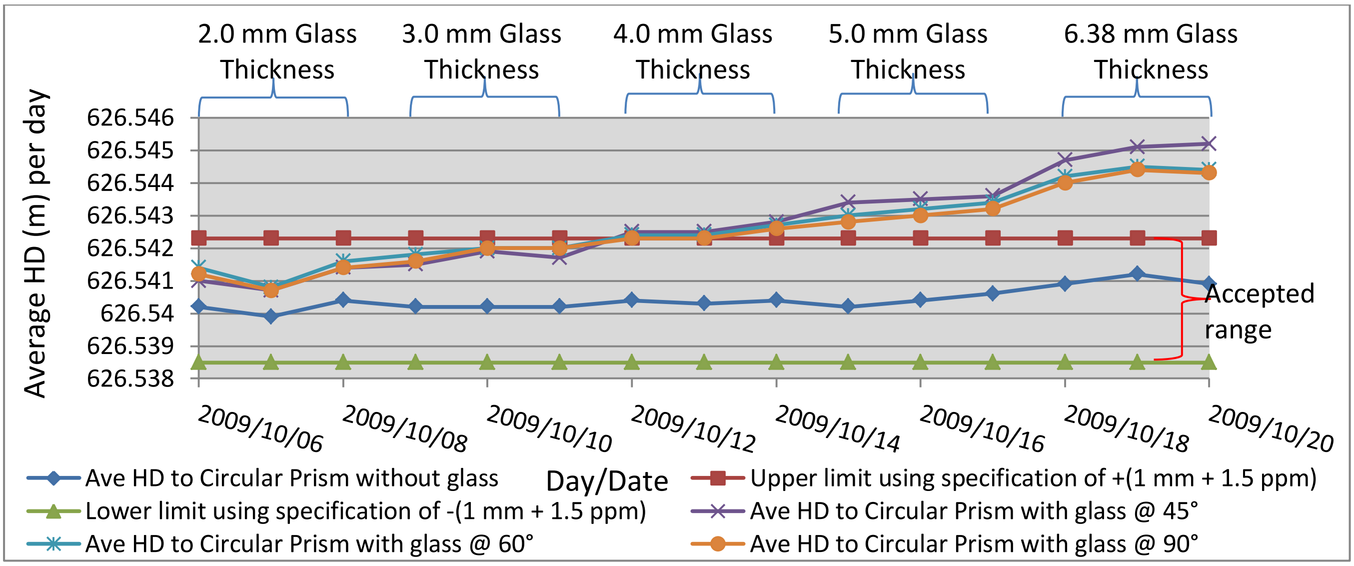

Figure 5.15: Average daily HD after atmospheric corrections using circular prism as target (long-distance)

Figures 5.14 and 5.15 show a little difference when compared with graphs of monitoring to the mini and circular prisms before atmospheric corrections. The atmospheric corrections have changed the outlook of the graphs. The alteration in the values of average HDs per day corresponded to the atmospheric corrections. Also the atmospheric corrections clearly revealed the impact of the glass thickness on the accuracy limits. The impact range (and variations range in HDs) caused by the glass medium remained the same after atmospheric corrections. In figure 5.14, the impact on HD readings when 2.0 mm glass thickness was used ranged between 0.0009 m and 0.0013 m; 3.0 mm glass impact ranged between 0.0015 m and

0.0019 m; 4.0 mm glass impact ranged between 0.0021 m and 0.0027 m; 5.0 mm glass caused impact range between 0.0031 m and 0.0045 m; while the impact of 6.38 mm glass ranged between 0.0032 m and 0.0042 m. The same is applicable to figure 5.15, where the glass impact remained the same as impact before atmospheric corrections. This is a clear indication that atmospheric corrections did not remove glass impact. The two Figures 5.14 and 5.15 also show that glass thickness 2.0 mm and 3.0 mm have no impact on accuracy. Beyond 3.0 mm glass thickness, the impact on accuracy increased with an increase in glass thickness.

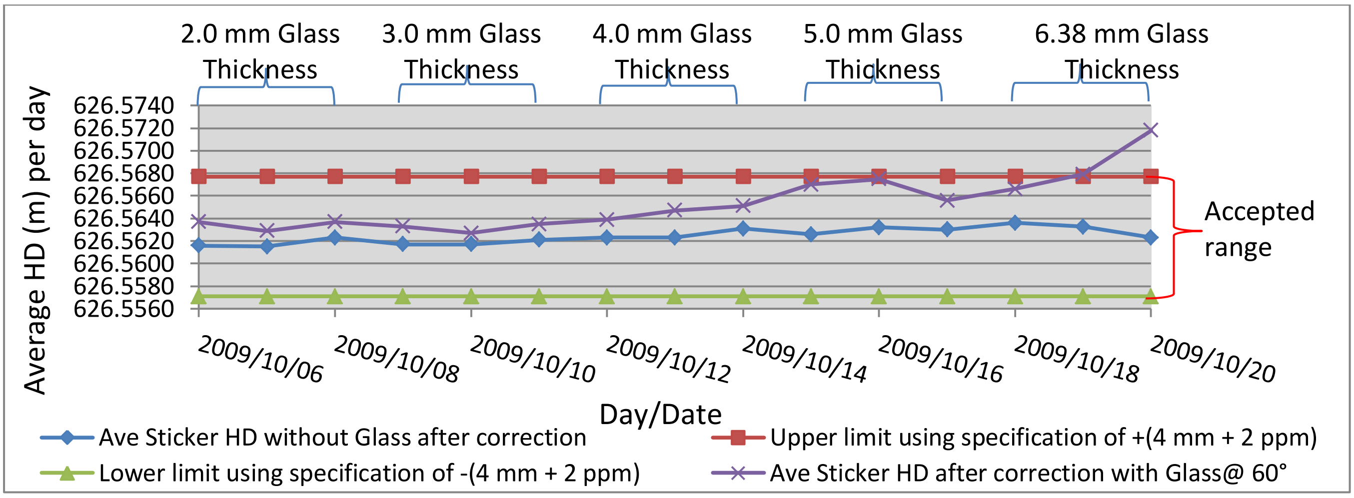

Figure 5.16: Average daily HD after atmospheric corrections using sticker as target (long-distance)

The graph of average daily HDs to the sticker after atmospheric corrections is shown in figure 5.16. The wide range in the accuracy limits shown by the graph might account for the good response to the accuracy limits even when 6.38 mm glass was used. Although, the accuracy appears to be acceptable, the range caused by the instrument capability when taking measurement to the sticker (4 mm + 2 ppm) did not provide for accurate monitoring. The main reason must be as a result of reflection of some of the red laser rays by the glass medium as earlier stated.

5.4 Vertical Distance (VD) Analysis

Figures 5.17 and 5.18 show the VD measurements to the three targets without glass during short- and long-distances monitoring. The readings were corrected for prism constant and scale factor but not corrected for atmospheric corrections. It must be noted that the same VD was not expected because the three (3) points (targets) were at different heights. The points were at 0.5 m apart in height as earlier shown in figure 4.8 in chapter four. This is also reflected in the two graphs presented in figures 5.17 and 5.18.

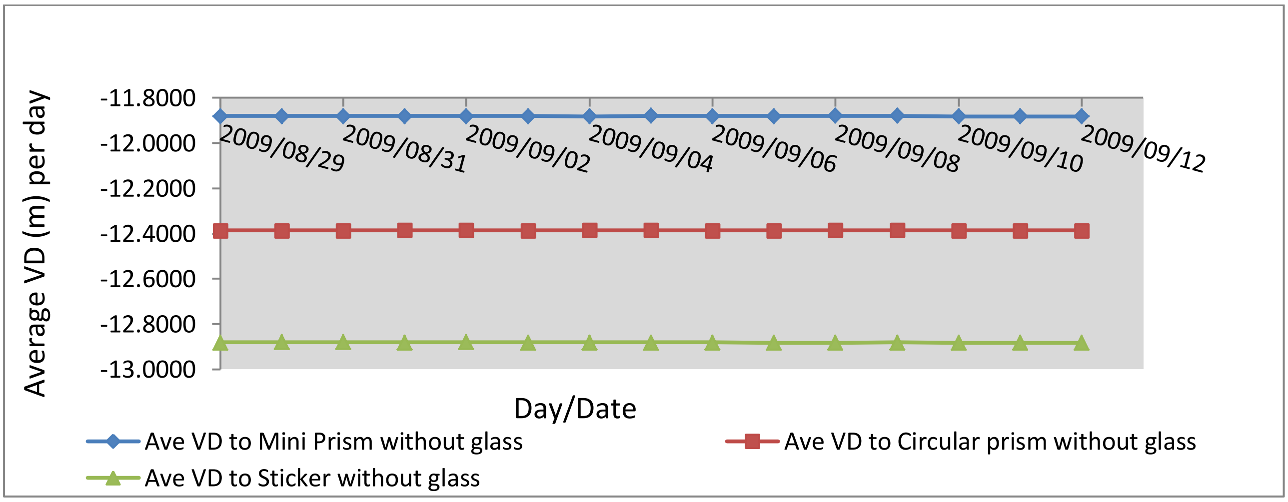

Figure 5.17: Average daily VD before atmospheric corrections (short-distance)

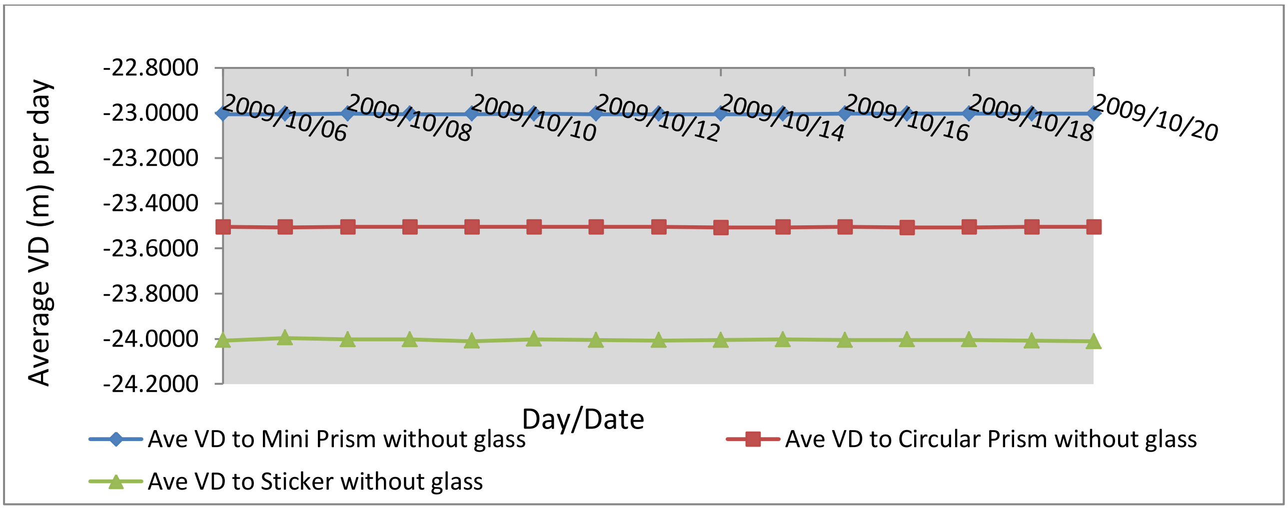

Figure 5.18: Average daily VD before atmospheric corrections (long-distance)

The trend in the two graphs follow the arrangement of the targets, with the mini prism on the top, the circular prism in the middle and the sticker at the base of the wooden structure that housed the three targets (as shown in figure 4.7 of chapter four in this report). The average daily VD readings to the mini prism ranged between -11.8788 and -11.8822; that of the circular prism ranged between -12.3850 and -12.3869; while that of sticker ranged between -12.8803 and -12.8827 during short-distance monitoring. During long-distance monitoring, the average daily VD readings to the mini prism ranged between -23.0042 and -23.0058, the circular prism VD ranged between -23.5047 and -23.50078; while the sticker ranged between -23.9962 and -24.0117.

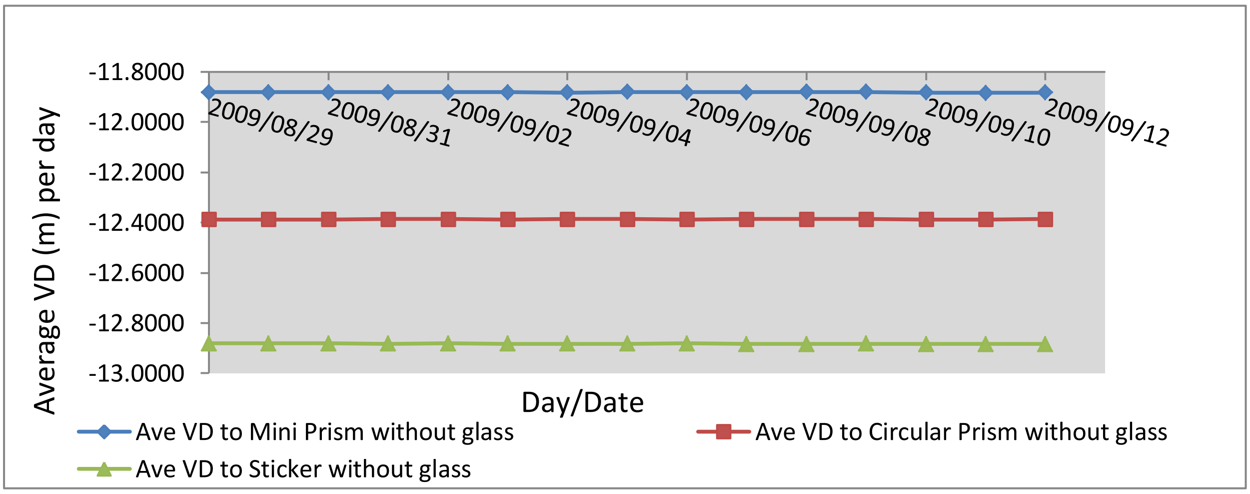

Figure 5.19: Average daily VD after atmospheric corrections (short-distance)

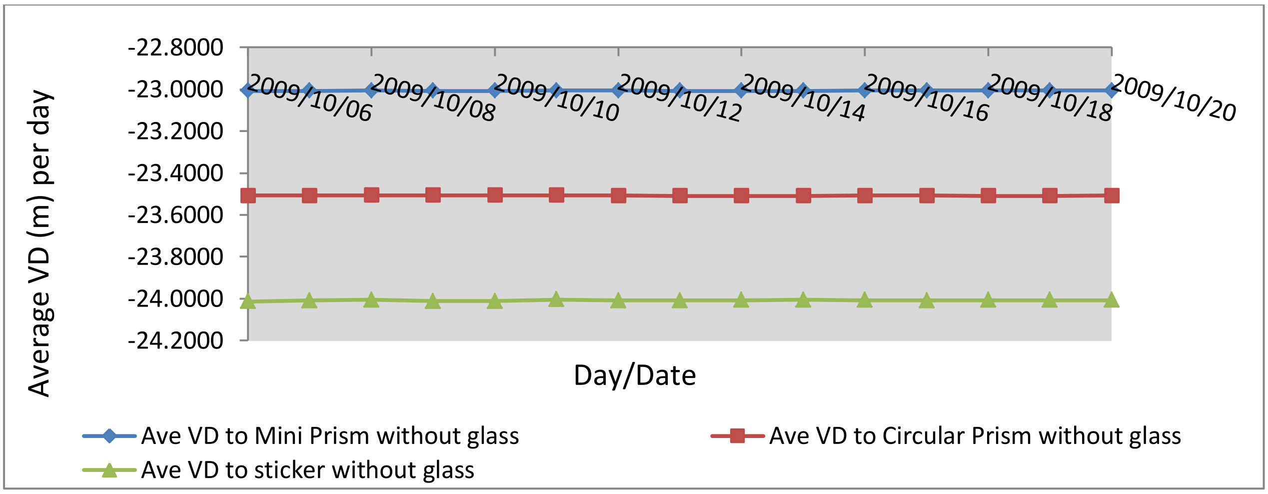

Figure 5.20: Average daily VD after atmospheric corrections (long-distance)

Figures 5.19 and 5.20 show the graphs of average daily VD measurements to the mini prism after atmospheric corrections during short- and long-distance monitoring. The graphs are similar to graphs generated before atmospheric corrections shown in Figures 5.17 and 5.18 above. The average daily VD measurements to the mini prism ranged between -11.8795 and -11.8829, the circular prism ranged between -12.3858 and -12.3876; while that of the sticker ranged between -12.8811 and -12.8833 during short-distance monitoring. During long-distance monitoring, the average daily VD measurements to the mini prism ranged between -23.0055 and -23.0071; the circular prism VD ranged between -23.5060 and -23.5092; while that of sticker ranged between -24.0043 and -24.0140. The only difference in graphs of average daily VD measurements before atmospheric corrections and graphs of average daily

VD measurements after atmospheric corrections is the change (increase) in the vertical axis of the graphs that correspond to atmospheric compensation.

In order to examine the likely impacts of the glass medium on the VD measurement to the three targets, VD measurements to each target were analyzed separately (VD before and after corrections).

5.4.1 Glass Impact on VD measurements before Atmospheric Correction during Short-Distance Monitoring

The result of average daily VD measurements to the Leica mini prism before atmospheric corrections during short-distance monitoring is presented in Figure 5.21. The corresponding results when monitoring to the Leica circular (circ) prism and the sticker are presented in Figures 5.22 and 5.23.

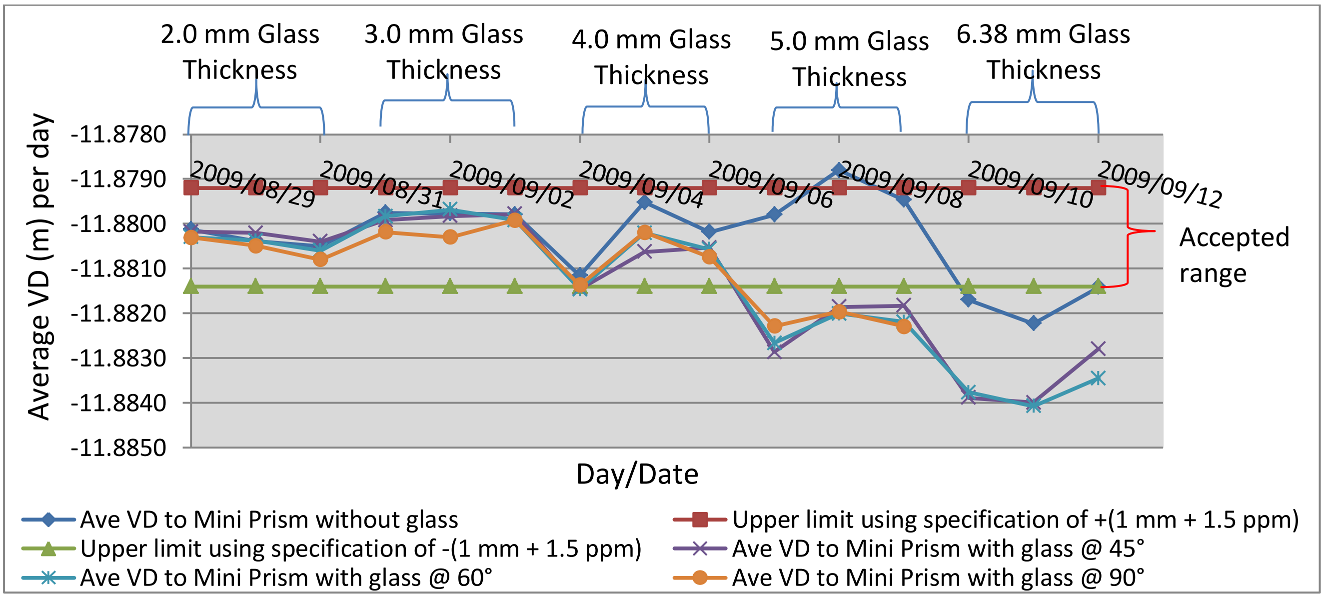

Figure 5.21: Average daily VD before atmospheric corrections using mini prism as target (short-distance)

Figure 5.21 shows the graph of average daily VD measurements to the mini prism before atmospheric corrections. The graph shows little or no difference in VD without glass and VD with glass at different angles when 2.0 mm to 3.0 mm glass thickness were used. A noticeable difference is observed when 4.0 mm glass was used, this difference increased as the glass thickness increased.

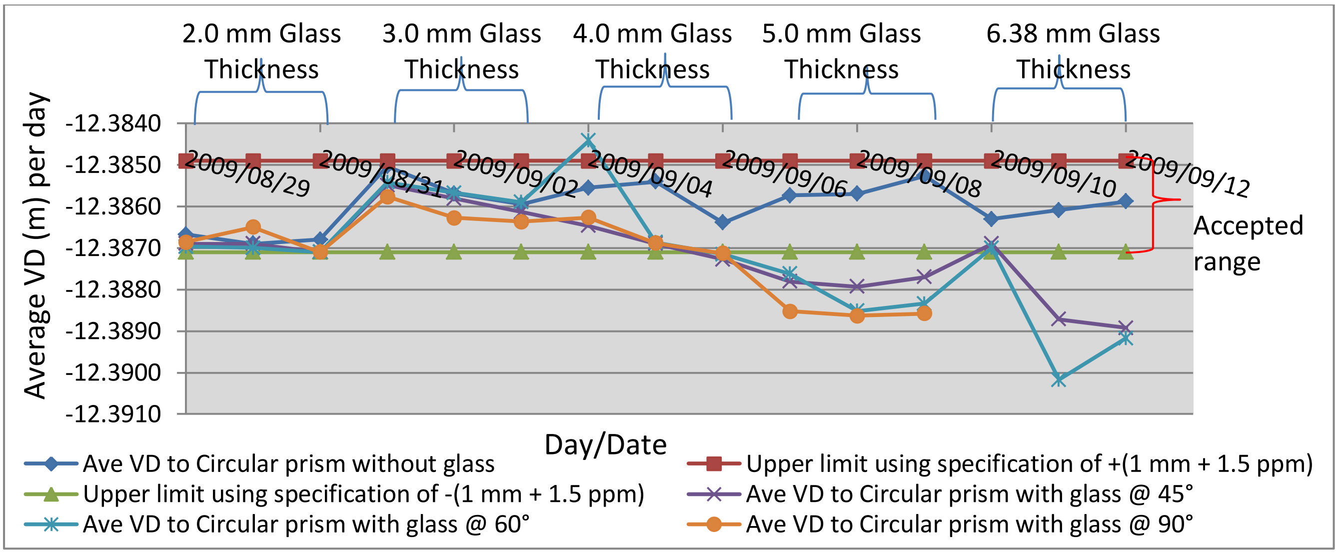

Figure 5.22: Average daily VD before atmospheric corrections using circular prism as target (short-distance)

The graph of the average daily VD measurements to the circular prism displayed in figure 5.22 shows a similar trend as the graph of average daily VD measurements to the mini prism showed in Figure 5.21 above. The graph also shows little or no difference in VD measurements without glass and VD measurements with glass at different angles up to when 3.0 mm glass thickness was used. However, beyond this, a noticeable difference began to occur.

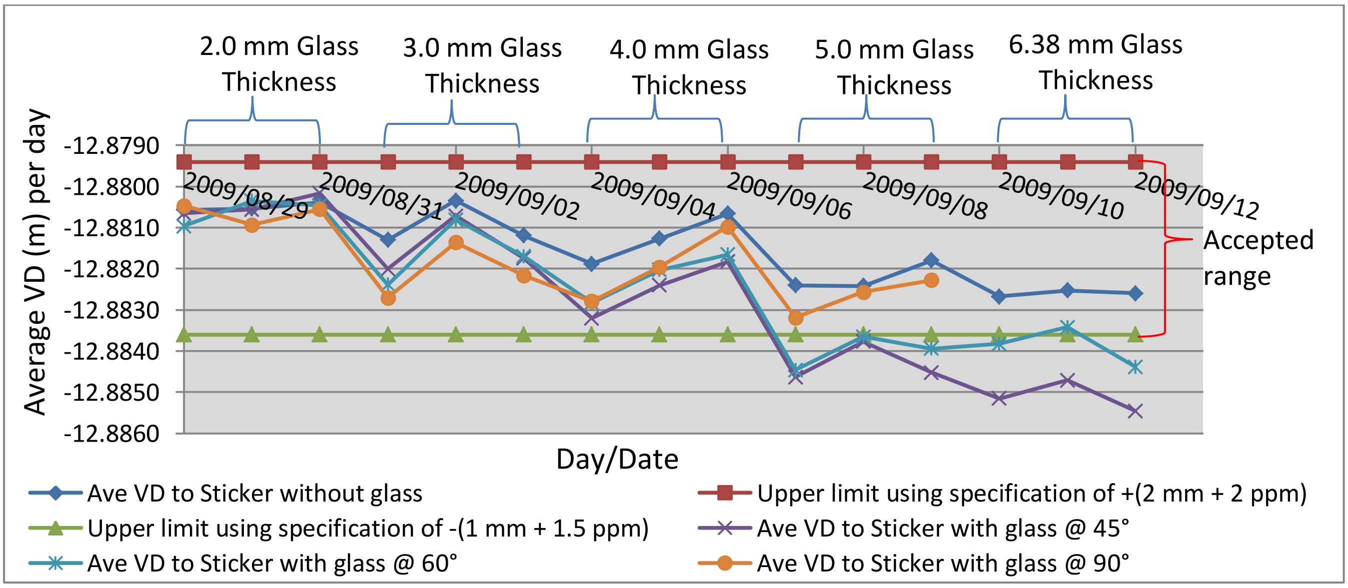

Figure 5.23: Average daily VD before atmospheric corrections using sticker as target (short-distance)

Figure 5.23 shows the graph of average daily VD measurements to the sticker before atmospheric corrections. The graph shows little or no difference in VD without glass and VD with glass at different angles only when 2.0 mm glass thickness was used. However, 3.0 mm glass and above resulted in large differences in VD without glass and VD with glass at different angles. These differences increased as the glass thickness increased. However, accuracy limits were not exceeded throughout when there was no glass in place and when there was glass in place up to 4.0 mm glass thickness. This may be due to wide accuracy limit specification of ±2 mm + 2 ppm when using reflectorless mode recommended Leica Geosystems.

5.4.2 Glass Impact on VD after Atmospheric Correction during Short-Distance Monitoring

The result of average daily VD measurements to Leica mini prism after atmospheric corrections is presented in Figure 5.24. The corresponding results when monitoring to the circular prism and the sticker are presented in Figures 5.25 and 5.26.

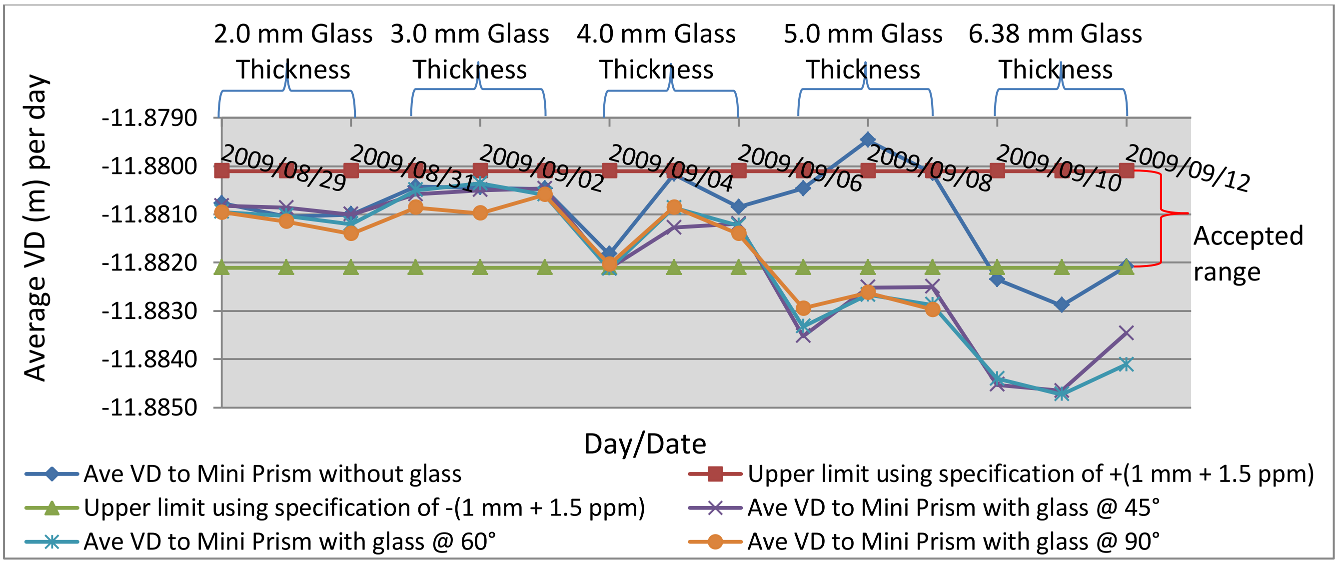

Figure 5.24: Average daily VD after atmospheric corrections using mini prism as target (short-distance)

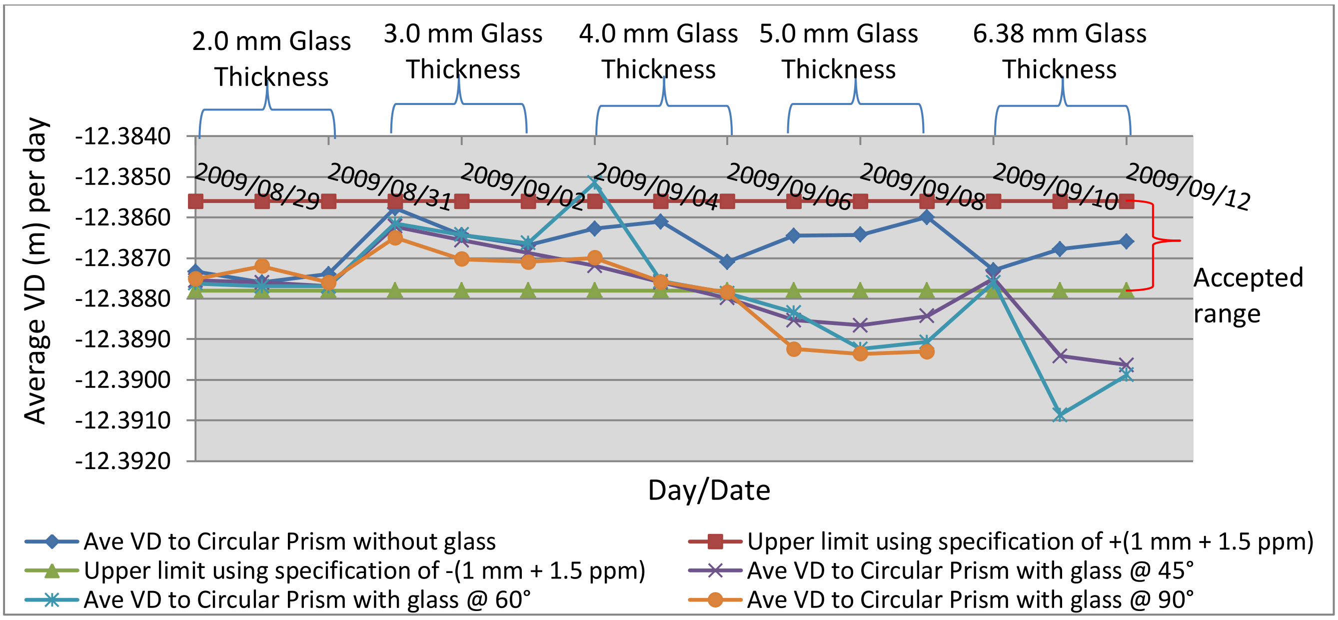

Figure 5.25: Average daily VD after atmospheric corrections using circular prism as target (short-distance)

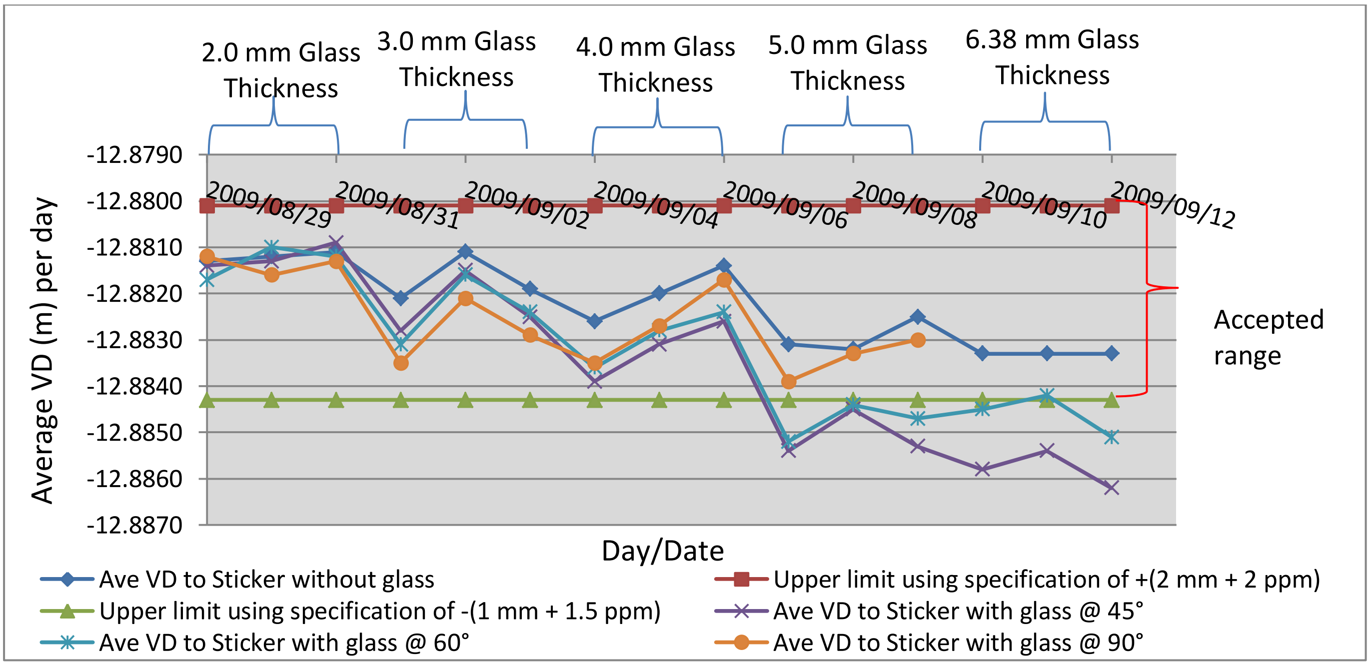

Figure 5.26: Graph of average daily VD against day after correction using sticker as target (short-distance)

All the graphs are similar to graphs generated before atmospheric corrections. This reveals that atmospheric corrections did not remove the impact of the glass.

5.4.3 Glass Impact on VD before Atmospheric Corrections during Long-Distance Monitoring

The result of the average daily VD measurements to the Leica mini prism before atmospheric corrections is presented in Figure 5.27. The corresponding results when monitoring to the Leica circular prism and the sticker are presented in Figure 5.28 and 5.29.

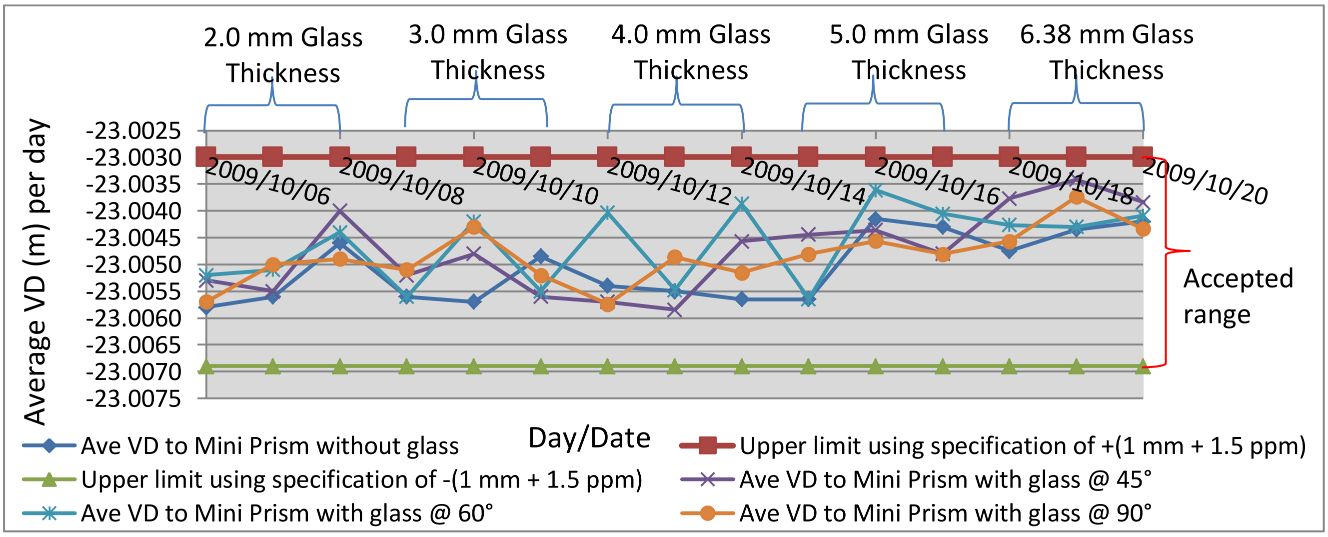

Figure 5.27: Average daily VD before atmospheric corrections using mini prism as target (long-distance)

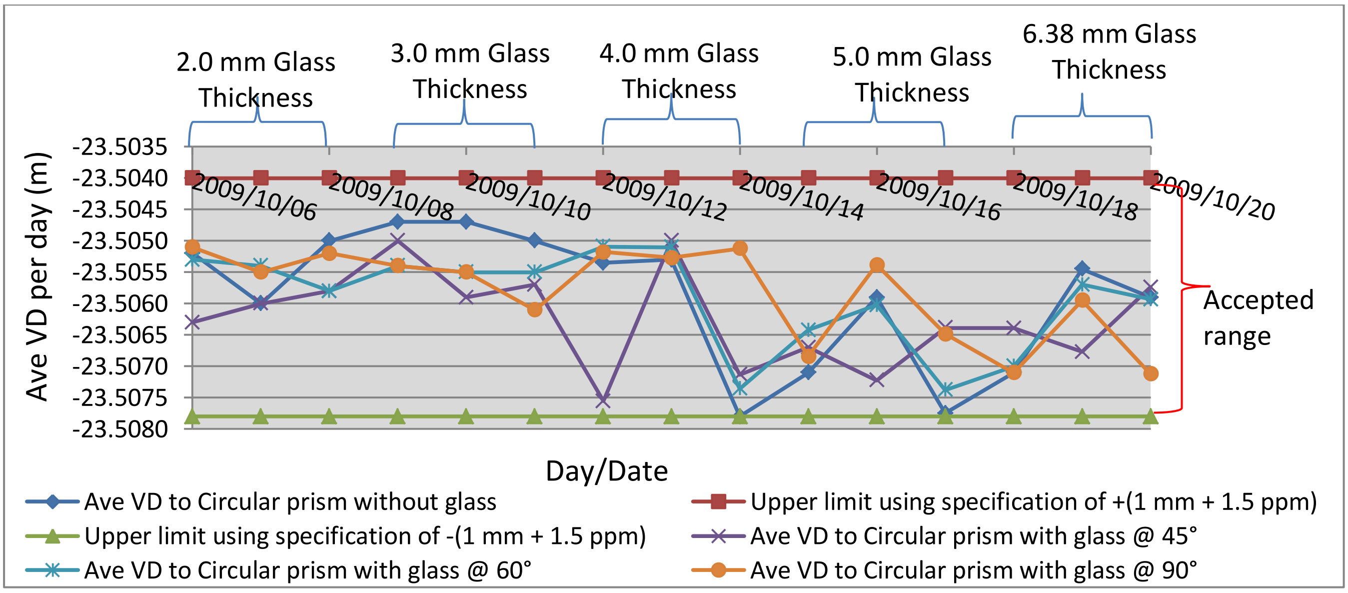

Figure 5.28: Average daily VD before atmospheric corrections using circular prism as target (long-distance)

Figures 5.27 and 5.28 show no definite impact since the VD measurements with and without glass fall within the confidence limits specification of the instrument.

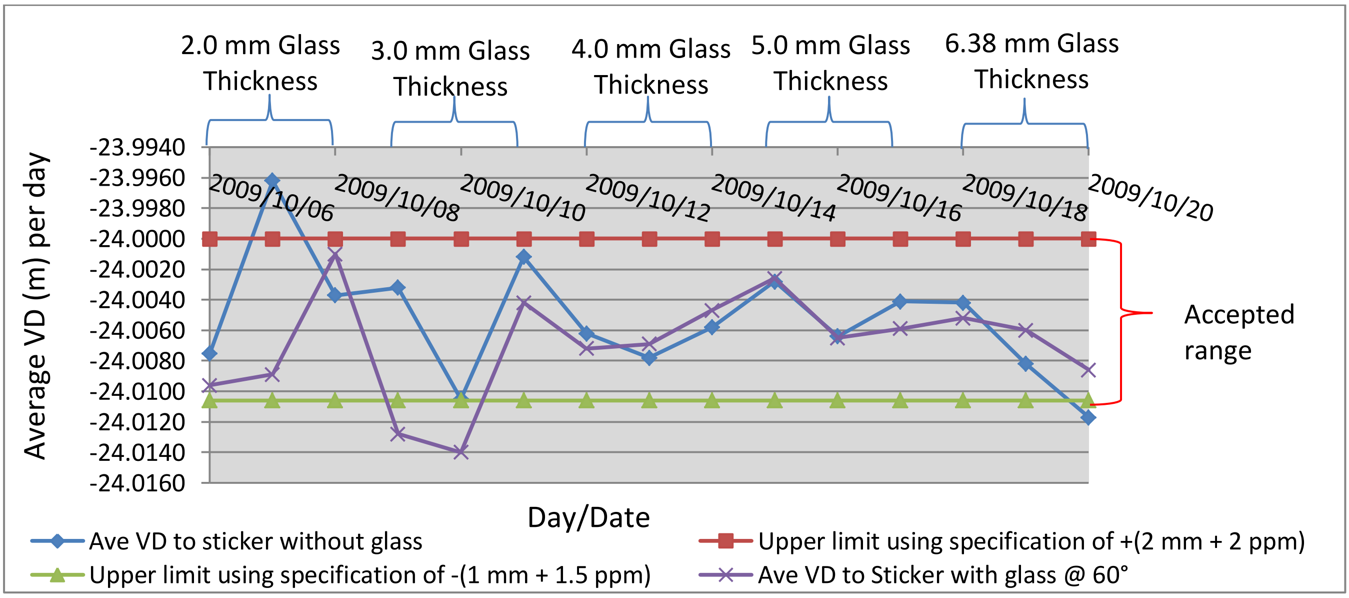

Figure 5.29: Average daily VD before atmospheric corrections using sticker as target (long-distance)

Figure 5.29 shows the graph of average daily VD measurement to the sticker. As stated earlier during analysis of HD measurements to the sticker (long distance), only data without glass and with glass at angle 60° could be acquired. The graphs show no definite impact. The problem with reflectorless measurements may be due to the distance that exceeded 500 m maximum distance specified in the instrument manual.

5.4.4 Glass Impact on VD after Atmospheric Correction during Long-Distance Monitoring

The result of average daily VD measurements to the Leica mini prism after atmospheric corrections is presented in Figure 5.30. The corresponding results when monitoring to the circular prism and the sticker are presented in Figures 5.31 and 5.32.

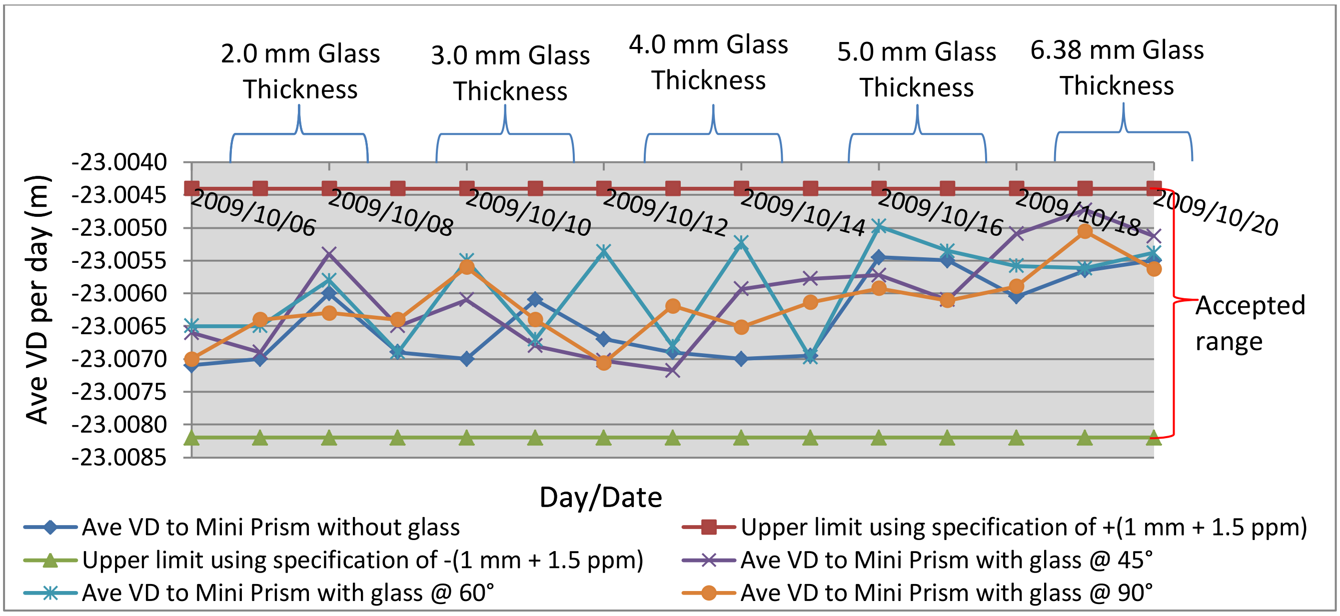

Figure 5.30: Average daily VD after atmospheric corrections using mini prism as target (long-distance)

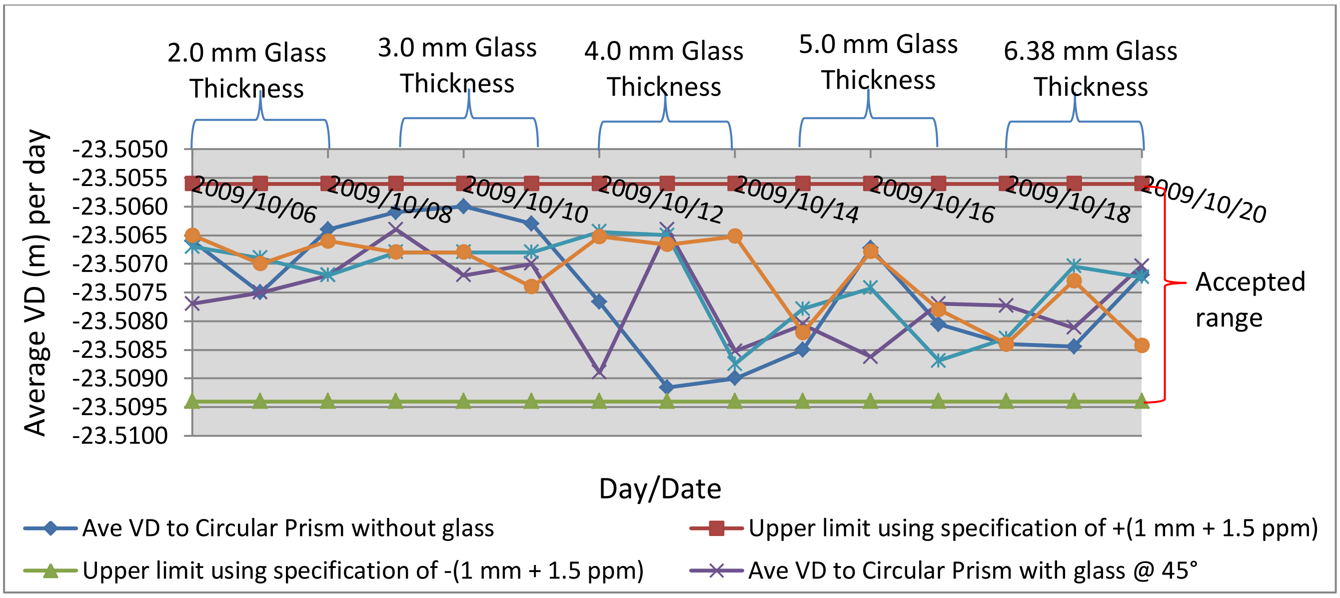

Figure 5.31: Average daily VD after atmospheric corrections using circular prism as target (long-distance)

The graphs of the average daily VD measurements to the mini prism and the circular prism after atmospheric corrections show no impact on the accuracy specification. This clearly reveals that the impact of the glass was more on the HD measurements than the VD measurements.

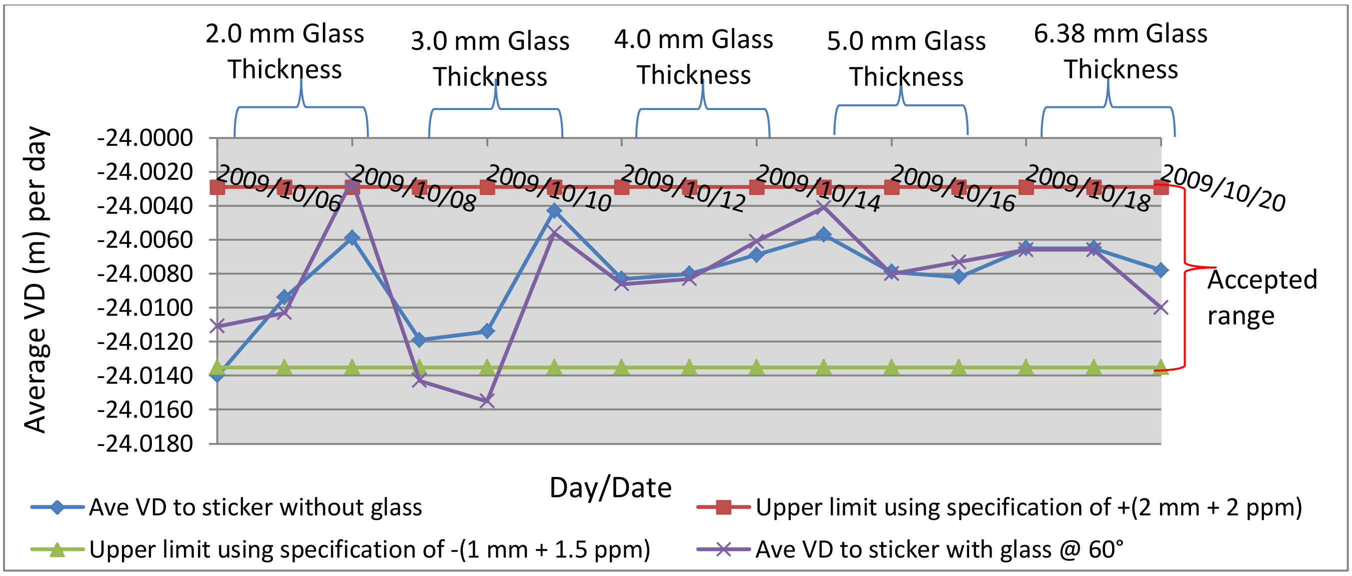

Figure 5.32: Average daily VD after atmospheric corrections using sticker as target (long-distance)

The graph of average VD measurements to the sticker shows no definite impact after the atmospheric corrections.

The noticeable impact of glass thickness on VD measurements to the prisms during short-distance monitoring analysis could be due to construction work (that involved drilling and other maintenance work which resulted in slight vibration of the building) that was being carried out on Chamber of Mine building (the building where the instrument/observation station was located) during the period when the data were acquired. The summary of all the analyzed distance results during short- and long-distances monitoring is presented in table C.3 in the appendix C. Also the summary of all angular variations during short- and long-distances monitoring is presented in table C.4 in the appendix C.

5.5. CONCLUSION

In summary, this chapter demonstrated convincingly that:

- The atmospheric corrections formulae given by the manufacturer of the total station that was used for this research are effective for atmospheric variations compensation since all HD and VD measurements without glass fell within the accuracy limits in all the plotted graphs. However, the formulae could not remove the impact of the glass on the measured distances.

- It does not matter at which angle the reading (instrument infrared ray) intersects the glass; the impact of glass angle is minimal on the final distance shown on the screen of the instrument. The chapter clearly revealed that impact of glass angles (or position to the instrument rays) on distance measurements is negligible when compare with the glass thickness impact on accuracy specification limits of the instrument.
- Glass thickness of more than 3.0 mm has impact on the accuracy specification of the instrument and need to be corrected or compensated for. Alternatively, the glass thickness may not exceed 3.0 mm.
- Glass impact was more severe on the HD measurements than on the VD measurements. The glass impact on the VD measurements was negligible as revealed by the graphs of average daily VD measurements to the prisms during long-distance monitoring as shown in figures 5.27, 5.28, 5.30 and 5.31.
- Distance measurements using the laser (reflectorless) option were not suitable for precision monitoring.

The chapter discussed the impacts of clear float glass thickness on distance (HD and VD) measurements. The chapter revealed that there is a need for a systematic error correction to cater for the effect of the glass thickness on HD measurements (when glass thickness is more than 3.0 mm). The next chapter investigates the effects of glass colour on the distance measurements and optimal distance (away from the total station) with which the glass (window glass) can be installed in an observation station (house) before proposing the equation(s) or model to cater for the glass impact.

CHAPTER SIX

6.0 DATA ACQUISITION AND PROCESSING TO INVESTIGATE THE IMPACT OF GLASS COLOUR AND SHAPE ON DISTANCE MEASUREMENTS AND TEST FOR OPTIMAL DISTANCE WHICH THE TOTAL STATION MUST BE AWAY FROM THE OBSERVATION WINDOW

Chapter five discussed how the glass thickness impacted on distance measurements. The chapter clearly revealed that glass thickness of more than 3.0 mm would cause errors in horizontal distances observed through the glass regardless of different angles of intersecting the glass. As a result of these revelations, 3.0 mm thickness was selected for the test of likely effect(s) of glass colour on distance (HD and VD) measurements and determination of the optimal distance which the total station must be away from the observation window glass during mine slope monitoring.

6.1 WHY TEST FOR GLASS COLOUR IMPACT ON DISTANCE MEASUREMENT?

The idea of colour (tinted glass) impact tests arose from the news of the frequent theft of total stations or their accessories at the mine sites. The ultimate aim of the mine surveying department at the mines is to protect the machine from harsh weather and from thieves. One of the possible ways of keeping the total station out of sight at mine sites is by tinting the observation window glass to reduce visibility from the outside of the observation window. To examine this plan, two tinted (light- and dark-tinted) 3.0 mm glass thickness were procured in addition to the 3.0 mm clear float (non-tinted) glass used in the previous tests. Each type of glass was used for a period of three days. Distances were measured to each of the three targets (Leica mini prism, circular prism and sticker) when there was no glass in place and when there was glass at different angles (30^o, 45^o, 60^o and 90^o). HD and VD readings were recorded and analyzed.

6.2 DISCUSSION ON DATA COLLECTED

The collection of data for colour analysis started on 6 May, 2010 and ended on 14 May 2010. In the first 3 days, 3.0 mm transparent glass was used after which light tinted 3.0 mm and dark tinted 3.0 mm were used each for 3 days. During each of these days, the distance readings recorded followed the same pattern. The distance readings captured were high in the morning (6 am – 10 am) when the air temperature was low and the humidity was high. These temperatures dropped as air temperature increased/decreased in humidity, then increased as air temperature reduced/increased in humidity in the evening period (3 pm – 6 pm). The variations in outside average daily temperature ranged from 1°C to 7.0°C, while the average daily pressure variation ranged from 2 mb to 7.9 mb. The average daily humidity variation ranged from 3% to 45% during the test period. On 7 and 8 May 2010 during distance measurement through transparent 3.0 mm glass, there were misty weather conditions in the morning. The total station could not achieve any distance measurement (either with or without a glass barrier) until the visibility improved later on during the day. Apart from this, the distance readings showed a positive response to the glass barrier. The distance readings when there was no glass in place were low compared to distance readings when there was glass in place. The effect of the angle position of the glass on distance readings was negligible. However, the distance readings with glass increased with an increase in the glass colour. The distance measurement during the glass colour test was about 626.6 m. The horizontal distance readings to the two prisms (mini and circular) were closer when compared the horizontal distance readings to the sticker. However, the vertical distance readings to each of the targets were different because the targets were not at the same height. They were 0.5 m apart. As a result of this, discrepancies in vertical distance readings to each of the target were expected. The 0.5 m gap between the targets manifested in the vertical readings recorded. During the data collection, distance measurements to the sticker when there was glass in place became unrealisable with increase in glass colour because the total station always gave an error/complaint notification.

Observation to test for the likely impact of distance between the total station and its shelter window glass was carried on 26 June, 2010. Twenty (20) observations (distance readings) were taken when there was no glass between the total station and the target, and when there was 3.0 mm transparent glass at 0.3 m away from the total station. The distance between the total station and the glass barrier increases by 0.1 m, at each position of the glass. Twenty observations were made to the target until when the distance reached 3.0 m. The readings showed only variation in the distance measurements with and without glass which corresponded to the impact of the glass thickness. There were no variations in distance measurement with glass at varying glass distance. Fairly constant atmospheric variation was encountered during the test because the test was carried out indoors. A constant atmospheric temperature, 1 mb variation in atmospheric pressure and 1% variation in the humidity were encountered during the test.

The test on glass shape was carried out using 2.0 mm plain, convex and concave glass. Distances were measured (six observations) to the circular prism hung at a short-distance monitoring position used for glass thickness analysis test in chapter five when there was no glass in place and when there was 2.0 mm plain glass followed by convex and concave 2.0 mm glass. The distance readings changed with shape of the glass. The plain glass had least variation, followed by convex and concave glass. The concave glass has impact on both the distance and the angle.

All the data acquired during the glass colour and shape impact tests are presented in the raw observation data book (i.e. appendix D.1 and D.2 of appendix D). The readings during the impact of distance between the total station and its shelter window glass on distance measurements are also presented in the raw observation data book (see appendix D.3 of appendix D).

6.2.1 Analysis of Glass Colour Impact on Horizontal Distance (HD)

Chapter five had established that the atmospheric corrections could remove the effects of atmospheric variations and not of glass thickness impact. An attempt has been made in this chapter to see if the atmospheric corrections could remove or reduce the colour impacts. Also whether the end results of glass colour impact tests established that the atmospheric correction formulae could only remove atmospheric impact and not glass impact altogether. An attempt was made to isolate atmospheric correction from the glass issue and to establish the glass colour impact to generate separate correction formula for the glass effects. Therefore, this report examined the analysis before and after atmospheric corrections. The result of average daily HD measurements to the Leica mini prism before atmospheric corrections during glass colour impact test is presented in Figure 6.1. The average daily change in HD measurements when monitoring to the same target is presented in Figure 6.2. The corresponding results after atmospheric corrections are presented in Figures 6.3 and 6.4.

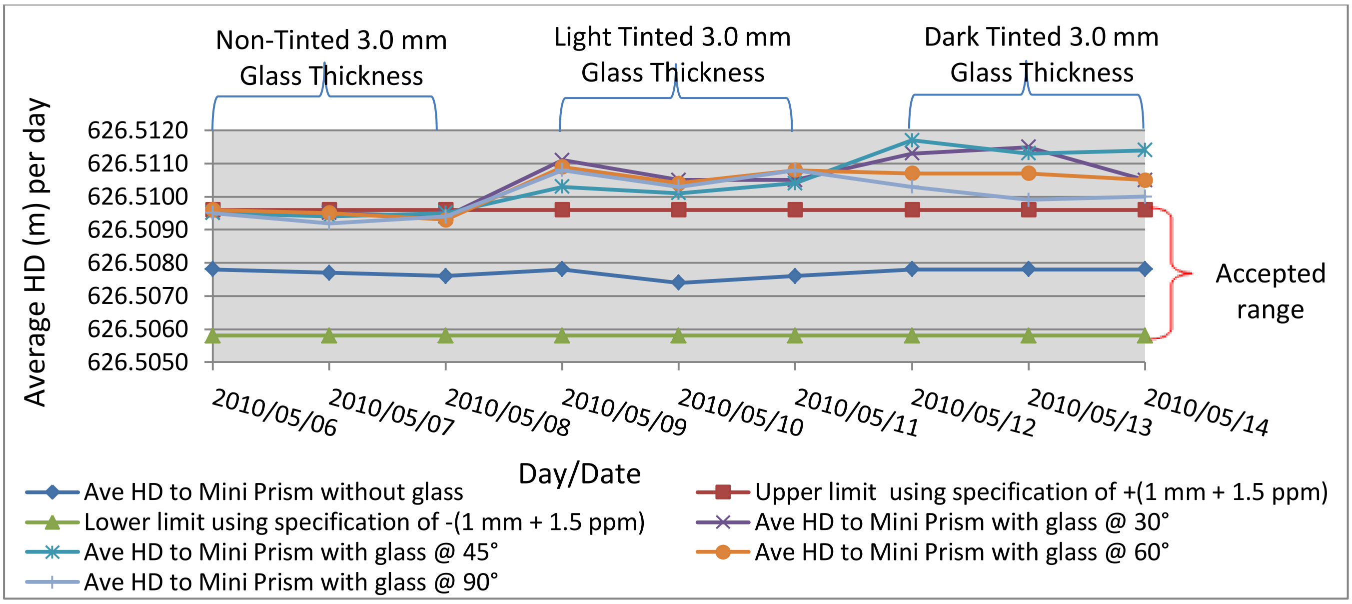

Figure 6.1: Average daily HD to mini prism before atmospheric corrections

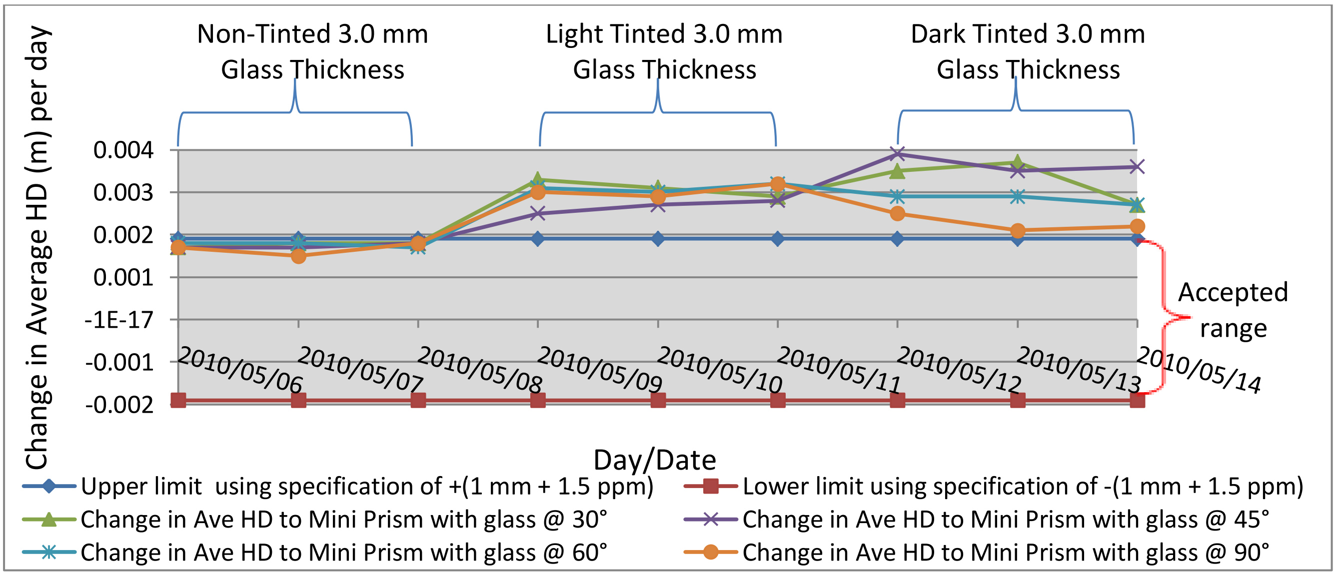

Figure 6.2: Average daily change in HD to mini prism before atmospheric corrections

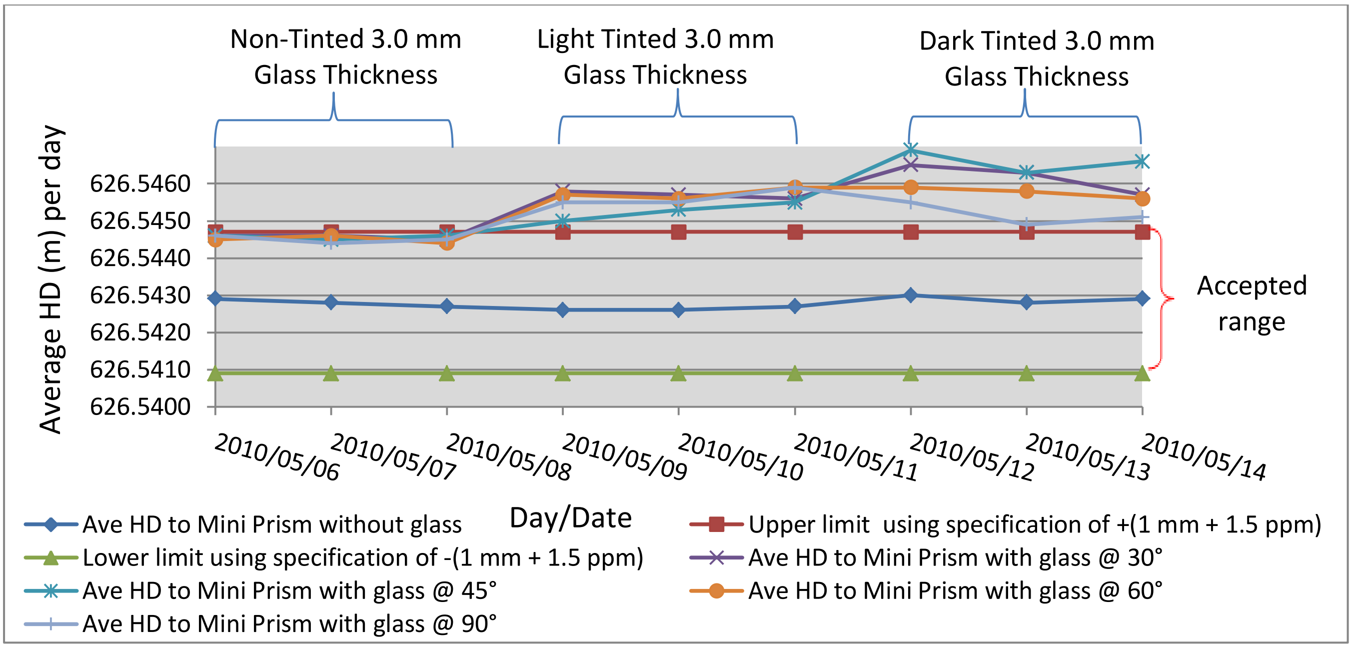

Figure 6.3: Average daily HD to mini prism after atmospheric corrections

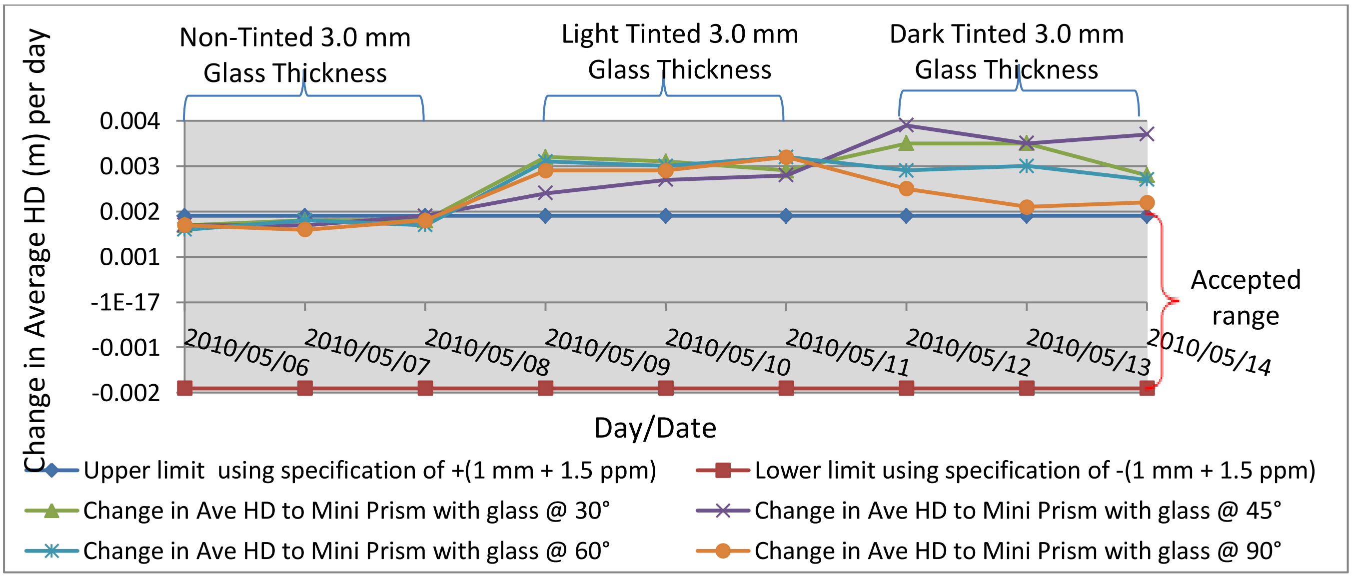

Figure 6.4: Average daily change in HD to mini prism after atmospheric corrections

In Figure 6.1, the graph of average daily HD measurements to the Leica mini prism reveals that the darker the colour of the glass, the more the impact the colour has on HD measurements. In the graph, only HDs without glass and with non-tinted glass have no impact on accuracy limits. The impact increased with an increase in tint level of the glass (light to dark tinted). This increase is revealed in Figure 6.2. The impact ranged between 1.5 mm and 1.8 mm (0.3 mm variation) when non-tinted 3.0 mm glass was used; 2.5 mm and 3.3

mm (i.e. 0.8 mm variation) when light tinted glass was used; while the impact of dark tinted 3.0 mm glass ranged between 2.1 mm and 3.9 mm (1.8 mm variation).

Figure 6.3 is similar to Figure 6.1.The only difference is that atmospheric error has been removed. The graph of average daily change in HD measurements after atmospheric corrections presented in Figure 6.4 is the same as the graph of average daily change in HDs before atmospheric corrections presented earlier in Figure 6.2. Both graphs show variations in HDs measured with glass at varying angles which increased with an increase in the glass colour (or tint level).

The result of average daily HD measurements to the Leica circular prism before atmospheric corrections is presented in Figure 6.5. The average daily change in HD measurements when monitoring to the same target is presented in Figure 6.6. The corresponding results after atmospheric corrections are presented in Figures 6.7 and 6.8.

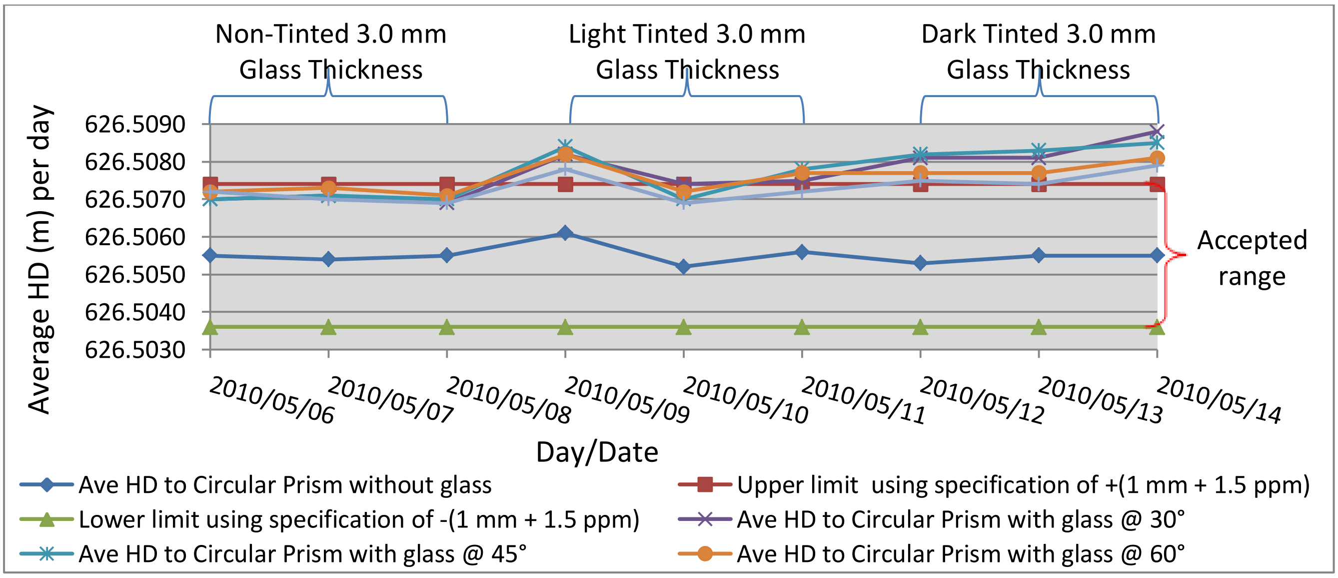

Figure 6.5: Average daily HD to circular prism before atmospheric corrections

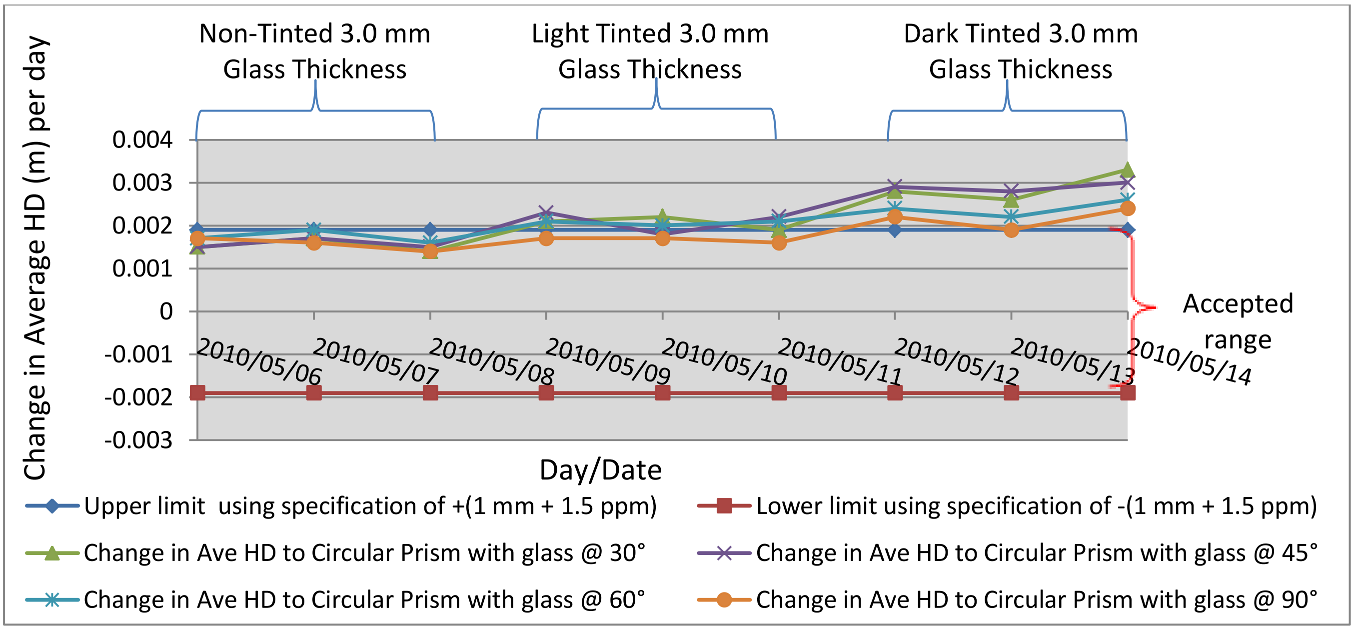

Figure 6.6: Average daily change in HD to circular prism before atmospheric corrections

Figures 6.5 and 6.6 exhibit the same trend as Figures 6.1 and 6.2. Only HDs without glass and with non-tinted glass conformed with accuracy requirement. The impact ranged between 1.4 mm and 1.9 mm (0.5 mm variation) when non-tinted glass was used; 1.6 mm and 2.3 mm (i.e. 0.7 mm variation) when light-tinted glass was used; while the impact ranged between 1.9 mm and 3.3 mm (i.e. 1.4 mm variation) when dark-tinted glass was used.

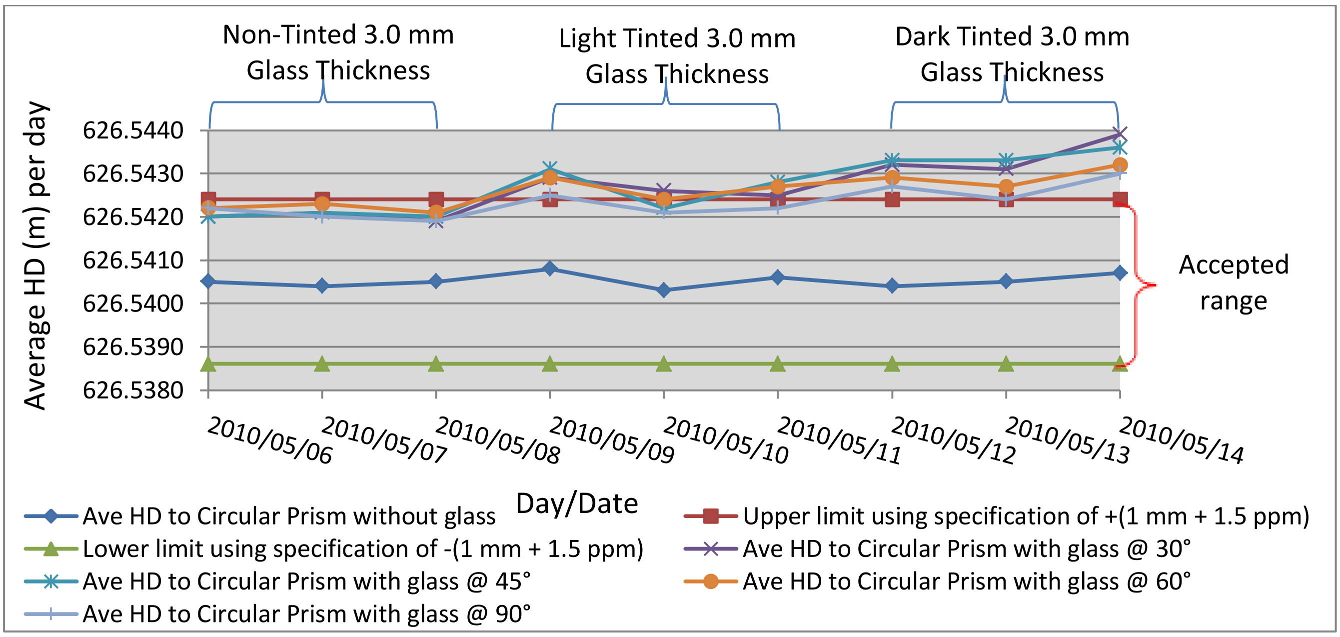

Figure 6.7: Average daily HD to circular prism after atmospheric corrections

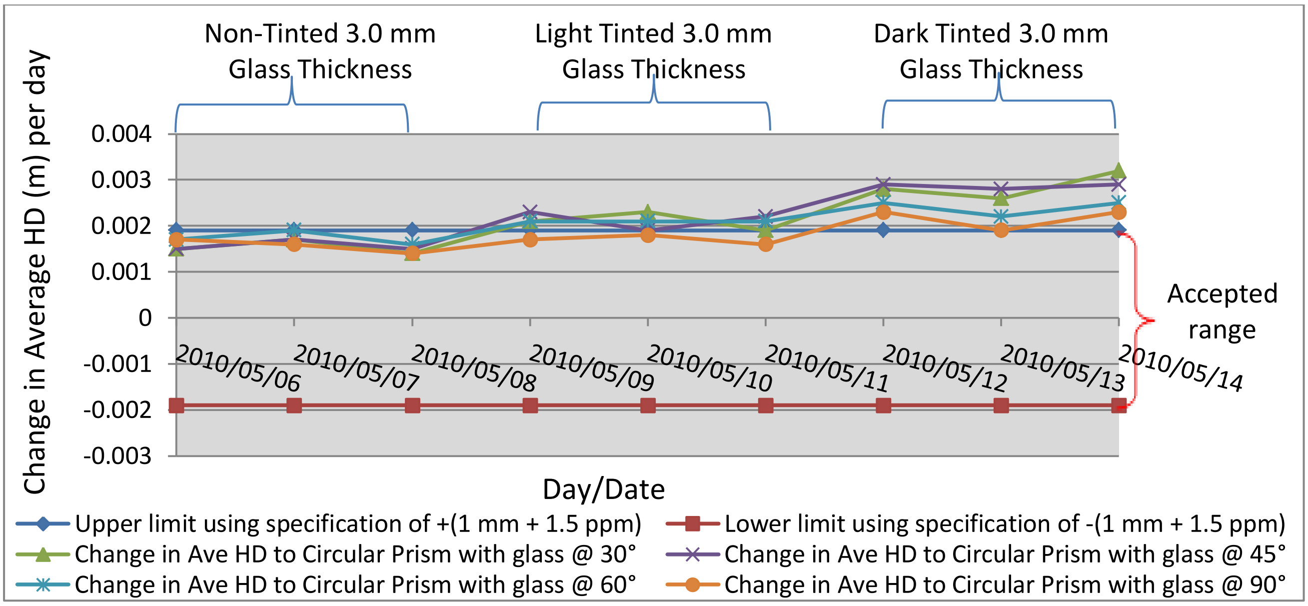

Figure 6.8: Average daily change in HD to circular prism after atmospheric corrections

Figure 6.7 is similar to Figure 6.5; the only difference is that the atmospheric error has been removed. The graph of average daily change in HD measurements after atmospheric corrections presented in Figure 6.8 is almost the same as the graph of average daily change in HDs before atmospheric corrections presented in Figure 6.6. The only difference was in dark-tinted glass impact. The dark-tinted glass impact after atmospheric correction ranged between 1.9 mm and 3.2 mm (1.3 mm variation) as against 1.9 mm and 3.3 mm recorded before atmospheric correction. Both graphs also show variations in HD measurements with glass at varying angles which increased with an increase in the glass colour.

The result of average daily HD measurements to the sticker before atmospheric corrections during glass colour impact test is presented in Figure 6.9. The average daily change in HDs when monitoring to the same target is presented in Figure 6.10. The corresponding results after atmospheric corrections are presented in Figures 6.11 and 6.12.

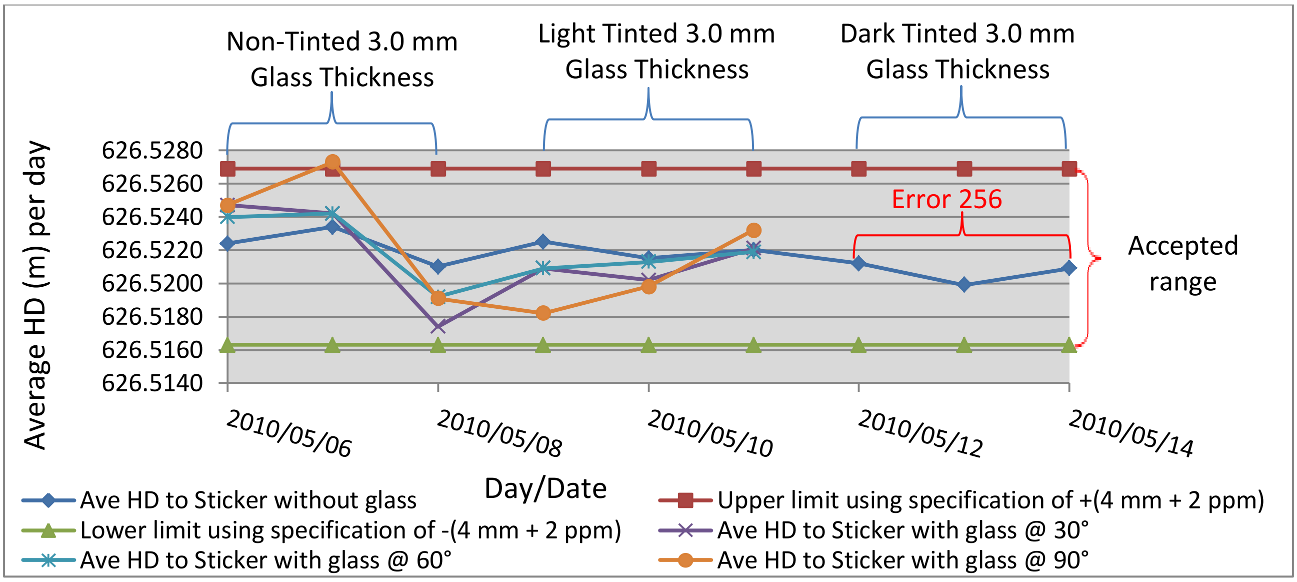

Figure 6.9: Average daily HD to sticker before atmospheric corrections

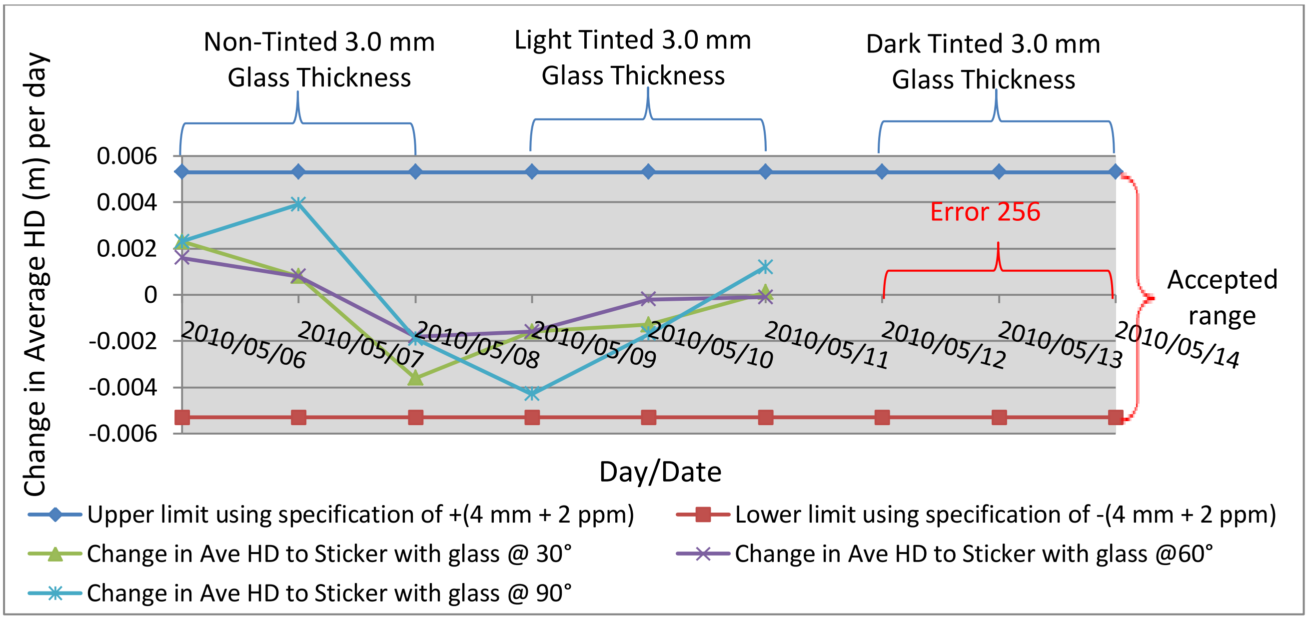

Figure 6.10: Average daily change in HD to sticker before atmospheric corrections

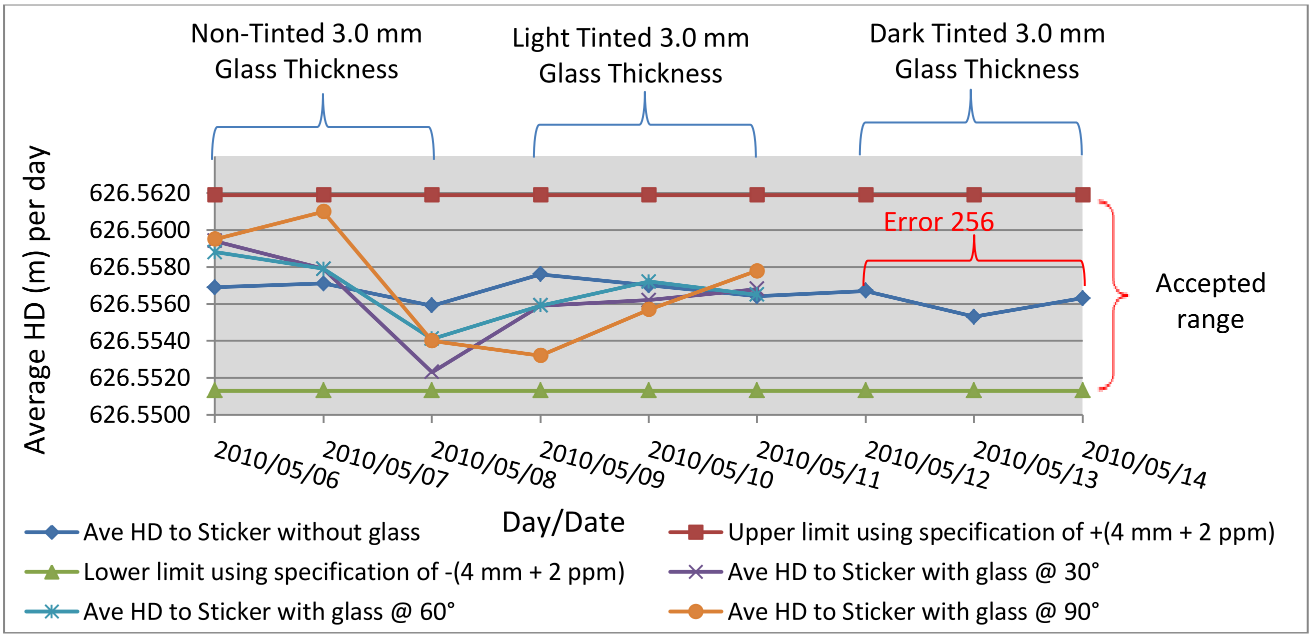

Figure 6.11: Average daily HD to sticker after atmospheric corrections

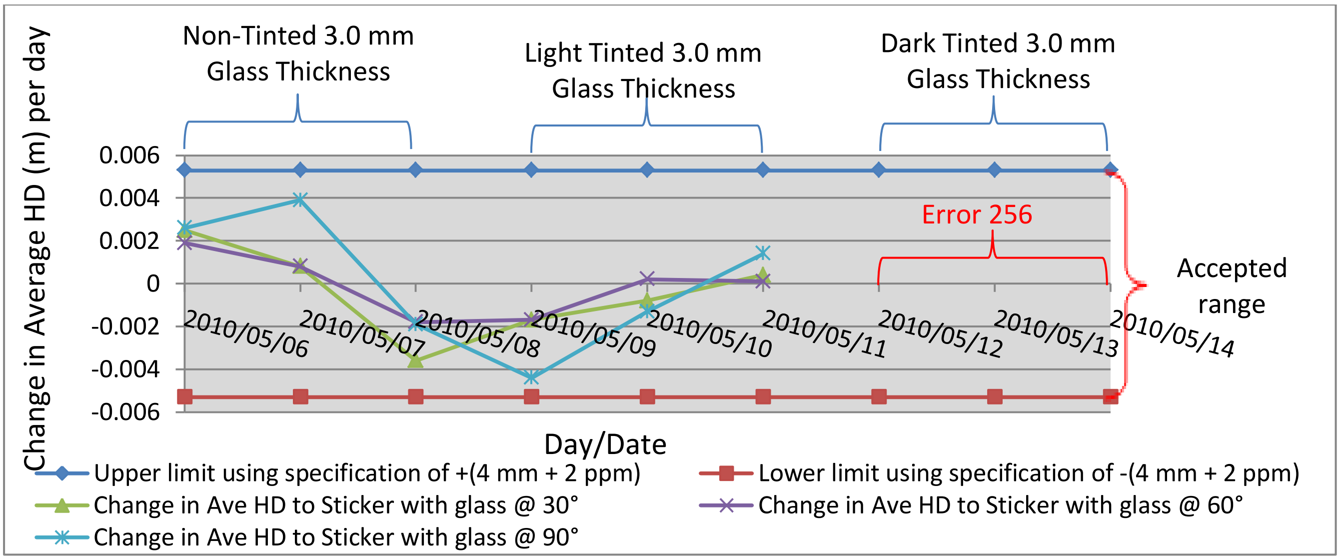

Figure 6.12: Average daily change in HD to sticker after atmospheric corrections

In Figure 6.9, HD measurements to the sticker target could not be achieved when dark-tinted glass was used because the red laser that supposed to actualize the measurement was reflected back by the glass. The total station always showed error 256 or lesser readings corresponding to the distance between the total station and the window glass. In addition, in all other glass tested during monitoring to the sticker, the total station always gave error 256 when the glass was at angle 45^{o}. Because of this, the readings at angle 45^{o} were removed from the sticker HD analysis. The graph reveals that there is no difference in HD measurements to the sticker without glass and with glass at different angles. The graphs show irrational variation in the HD readings as reflected in the graph of average daily change in HDs before atmospheric correction. The impact of the non-tinted glass ranged between -3.6 mm and 3.9 mm (7.5 mm variation); and the impact of light-tinted glass ranged between - 4.3 mm and 1.2 mm (i.e. 5.5 mm variation). However, the conformity with accuracy seemed fine with only one point exceeding the limit. This could be due to the wide range of accuracy limit specification (i.e. ±4 mm + 2 ppm) given by the manufacturer of the instrument. The graph of average daily HD measurements to the sticker improved after atmospheric corrections as shown in figure 6.11. The non-tinted glass impact ranged between -3.6 mm and 3.9 mm (7.5 mm variation), while the impact of light-tinted glass ranged between -4.4 mm and 1.4 mm (5.8 mm variation) as shown in figure 6.12.

6.2.2 Analysis of Glass Colour Impact on Vertical Distance (VD)

Chapter five revealed that the impact of glass thickness on VD measurements is negligible since all the VDs analyzed were within the accuracy specification of the instrument. Therefore, the researchers decided to analyze the impact of glass colour on the VD measurements as the glass colour could perhaps negate the result of glass thickness impact on VD measurements.

The results of the average daily VD measurements to the Leica mini prism before atmospheric corrections during glass colour impact tests is presented in Figure 6.13. The average daily change in VD measurements when monitoring to the same target is presented in Figure 6.14. The corresponding results after atmospheric corrections are presented in figures 6.15 and 6.16

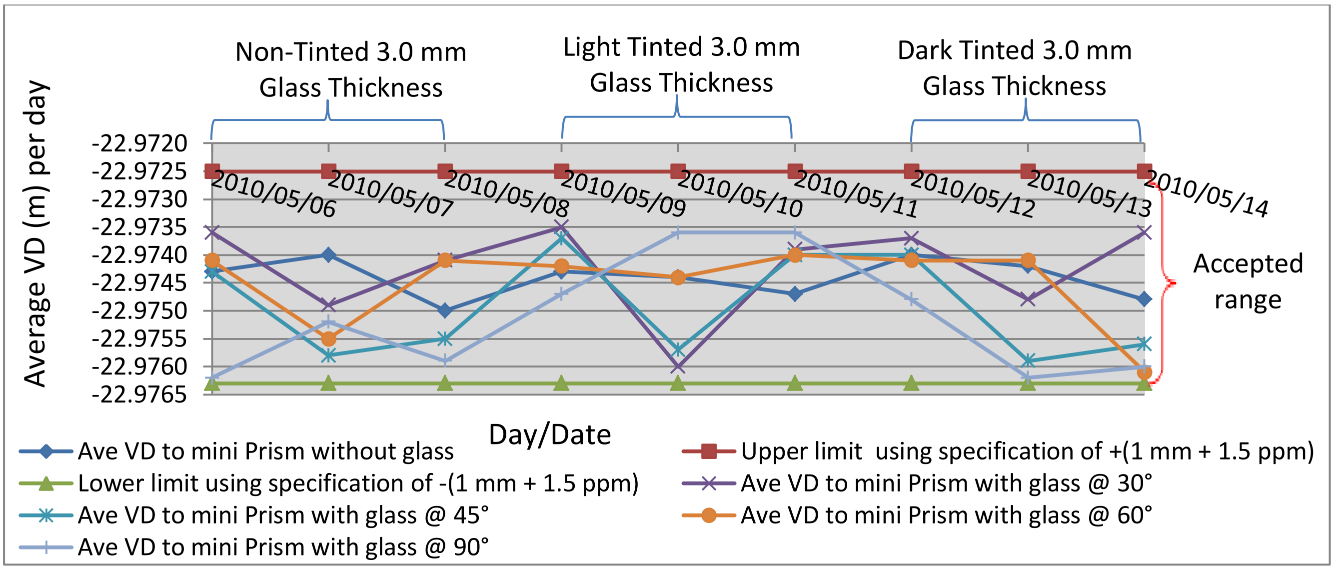

Figure 6.13: Average daily VD to mini prism before atmospheric corrections

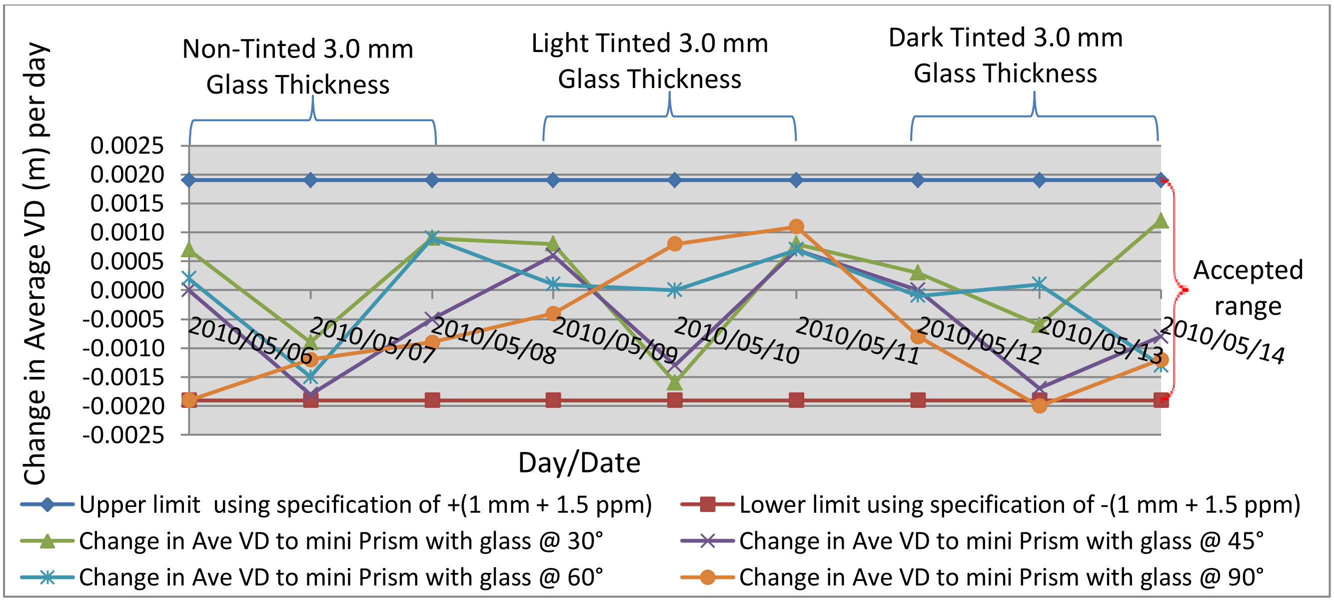

Figure 6.14: Average daily change in VD to the mini prism before atmospheric corrections

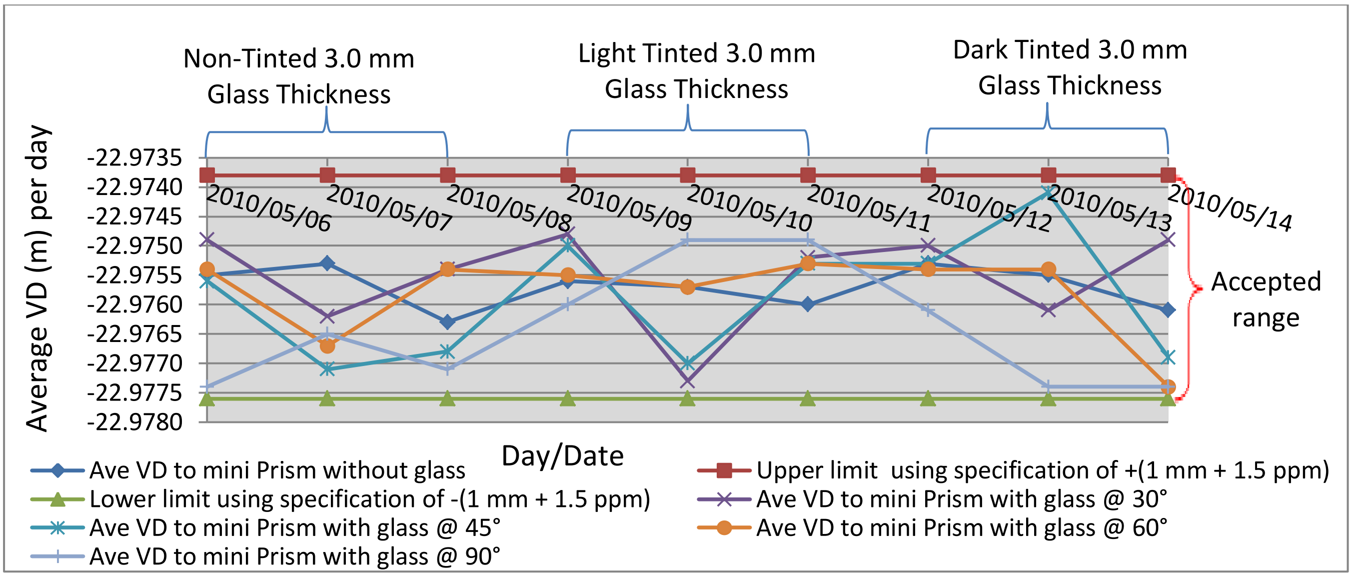

Figure 6.15: Average daily VD to mini prism after atmospheric corrections

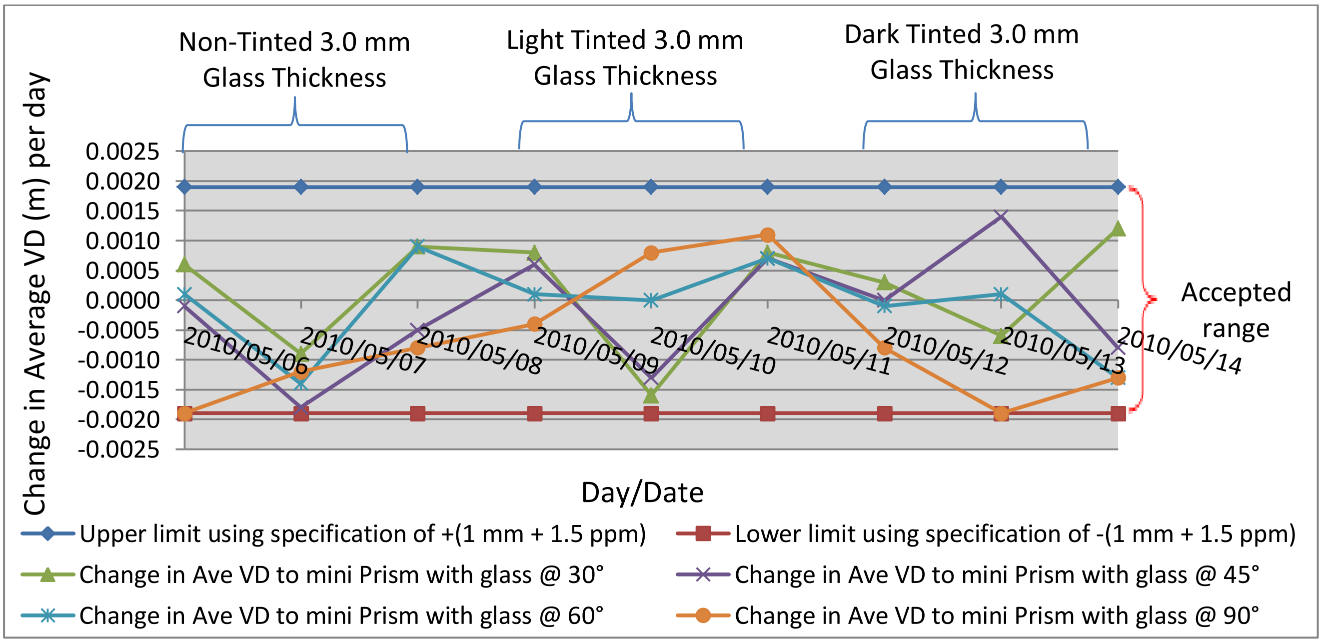

Figure 6.16: Average daily change in VD to the mini prism after atmospheric corrections

Figure 6.13 shows the graph of average daily VD measurements to the Leica Mini prism before atmospheric corrections. The graph reveals that the impact of glass colour on VD measurements is within the accuracy limits. However, the trend exhibited by VDs measured without glass were more stable than the trends exhibited by VDs measured with glass at varying angles. This is clearly shown in figure 6.14. The impact caused by non-tinted 3.0 mm glass ranged between -1.8 mm and 0.9 mm; light tinted 3.0 mm glass impact ranged between

– 1.6 mm and 1.1 mm; while the impact of dark-tinted 3.0 mm glass ranged between – 2.0 mm and 1.2 mm.

The graph of average daily VD measurements to the Leica Mini prism after atmospheric corrections shown in figure 6.15 is virtually the same as the graph generated before atmospheric corrections shown in figure 6.13. The graph of average daily change in VDs to the mini prism after atmospheric corrections is the same with graph of average daily change in VDs before atmospheric corrections. Therefore, only graphs generated after atmospheric corrections were analyzed for the remaining two targets (Leica circular prism and sticker).
The results of average daily VD measurements to the Leica Circular prism after atmospheric corrections during glass colour impact tests is presented in Figure 6.17. Its average daily change in VDs when monitoring to the same target is presented in Figure 6.18. The corresponding results when monitoring to sticker are presented in Figures 6.19 and 6.20.

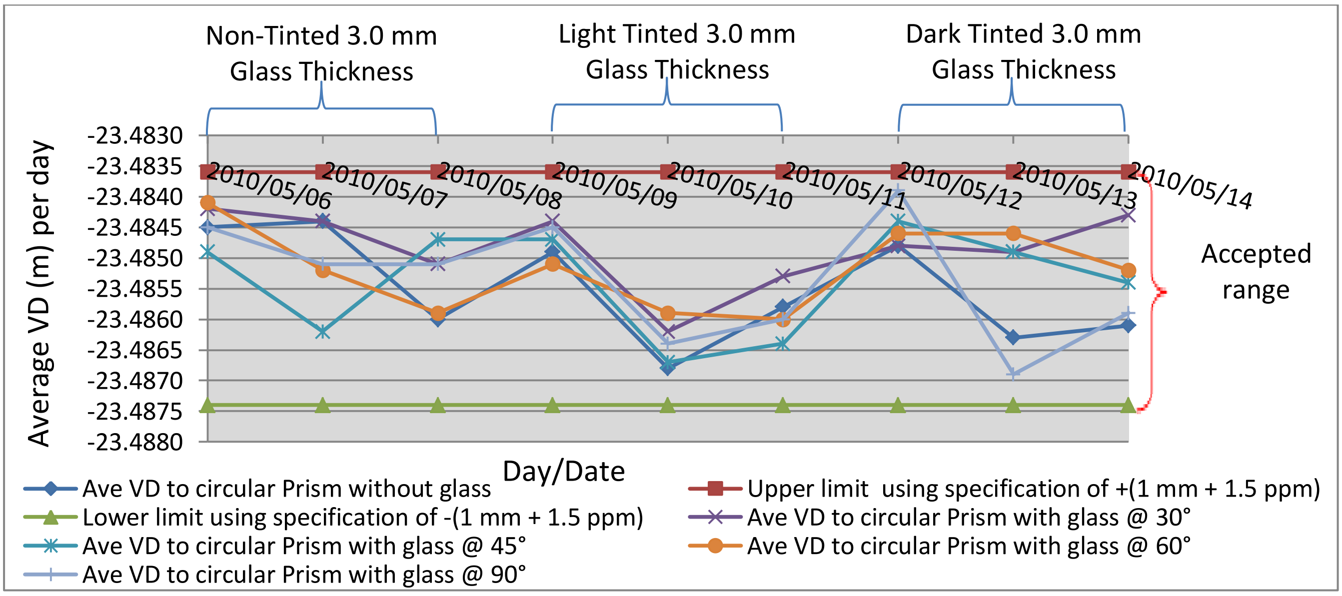

Figure 6.17: Average daily VD to circular prism after atmospheric corrections

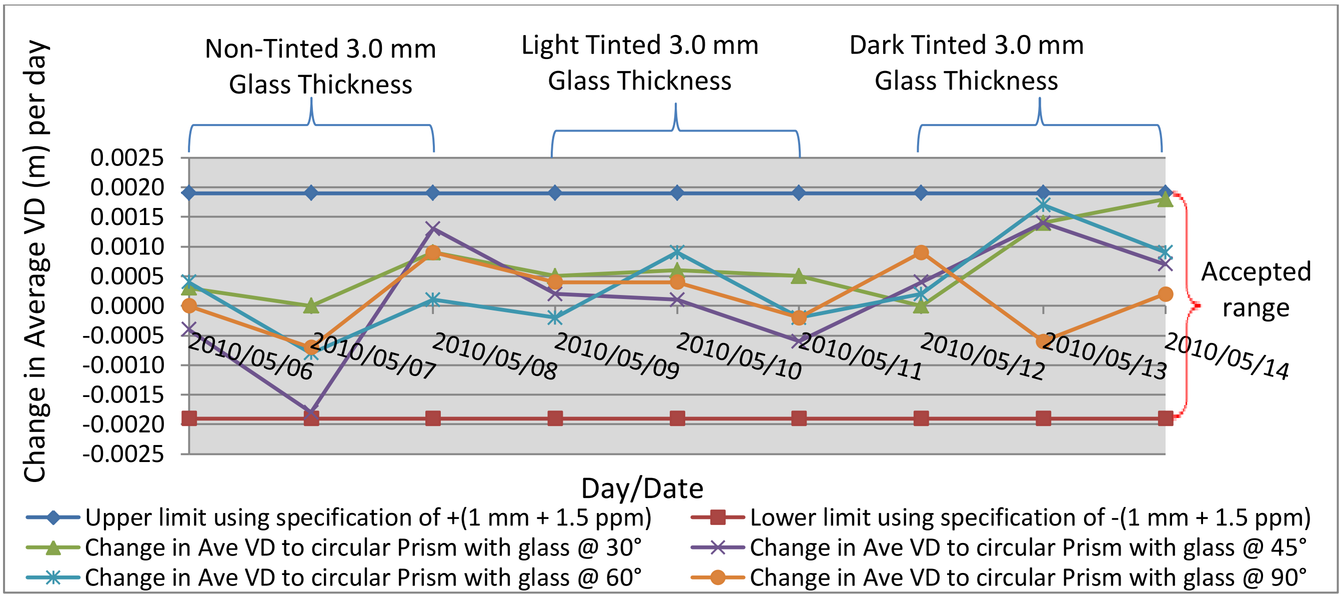

Figure 6.18: Average daily change in VD to circular prism after atmospheric corrections

Figure 6.17 reveals that the impact of glass colour on VD measurements when monitoring to the Leica circular prism is within the accuracy limits. This is clearly revealed in the graph of average daily change in VDs readings shown in Figure 6.18.

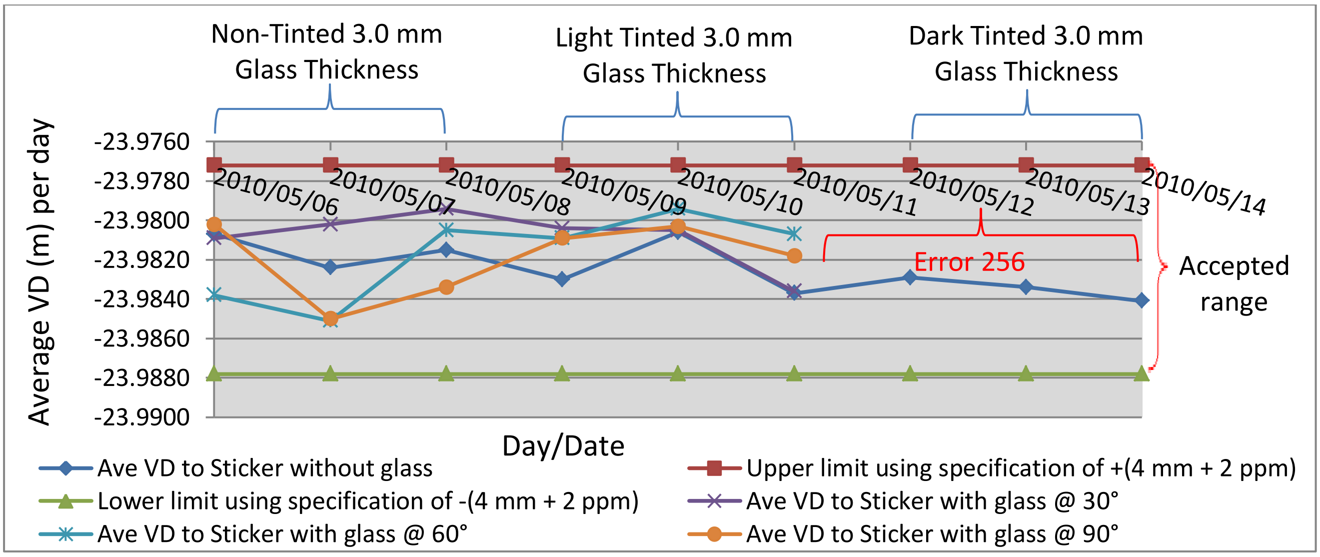

Figure 6.19: Average daily VD to sticker after atmospheric corrections

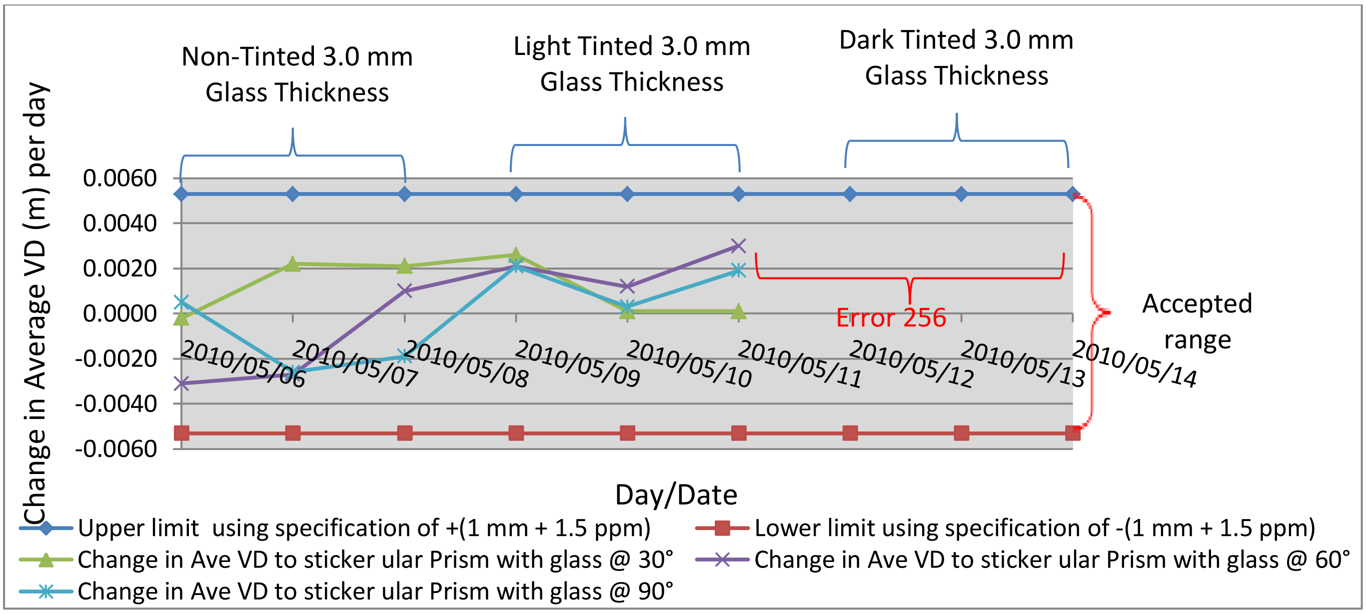

Figure 6.20: Average daily change in VD to sticker after atmospheric corrections

In Figure 6.19, the VD measurements to the sticker target could not be achieved when dark tinted glass was used because the red laser that was supposed to actualize the measurement was reflected back by the tinted glass as earlier stated in HD analysis. The graph also reveals that the impact is negligible. This is revealed in figure 6.20.

The variations in distance measurement during glass colour impact test is summarized in Table 6.1 below

The table clearly shows the glass colour impact on the measured distances. If accuracy specifications of ±1mm + 1.5 ppm for IR mode and ±4 mm + 2 ppm for RL mode (as given by the manufacturer of the Leica Total station TCR +1201 that was used for the data collection) are applied, the limit is ± 0.0019 mm for IR mode and ± 0.0053 mm for RL. Therefore, going through the table, only HDs measured with non-tinted 3.0 mm and all the VD measurements to the three targets satisfy the requirement. These are typed in blue in table 6.1.

Table 6.1: Summary of distance variations during glass colour impact test

Glass Thickness (mm)	Target	Distances	Impact range after atmospheric correction (mm)	Difference (mm)	Glass colour
3.0	Mini prism	HD	1.60 and 1.90	0.30	Non-tinted
3.0	Circular prism	HD	1.40 and 1.90	0.50	Non-tinted
3.0	Sticker	HD	-3.60 and 3.90	7.50	Non-tinted
3.0	Mini prism	HD	2.40 and 3.20	0.80	Light tinted
3.0	Circular prism	HD	1.60 and 2.30	0.70	Light tinted
3.0	Sticker	HD	-4.40 and 1.40	5.60	Light tinted
3.0	Mini prism	HD	2.10 and 3.90	1.80	Dark tinted
3.0	Circular prism	HD	1.90 and 3.20	1.30	Dark tinted
3.0	Sticker	HD	Error 256	-	Dark tinted
3.0	Mini prism	VD	-1.90 and 0.90	2.80	Non-tinted
3.0	Circular prism	VD	-1.80 and 0.90	2.70	Non-tinted
3.0	Sticker	VD	-3.60 and 3.90	7.50	Non-tinted
3.0	Mini prism	VD	-1.60 and 1.10	2.70	Light tinted
3.0	Circular prism	VD	-0.60 and 0.90	1.50	Light tinted
3.0	Sticker	VD	-4.40 and 1.40	5.80	Light tinted
3.0	Mini prism	VD	-1.90 and 1.20	3.10	Dark tinted
3.0	Circular prism	VD	-0.60 and 1.80	2.40	Dark tinted
3.0	Sticker	VD	Error 256	-	Dark tinted

6.3. TEST FOR THE IMPACT OF GLASS SHAPE ON DISTANCE MEASUREMENTS

In order to test for the impact of glass shape on distance measurements, a Leica circular prism was mounted on the short-distance position used during the thickness test in chapter five. Two 2.0 mm thick glasses were procured (2.0 mm concave glass and 2.0 mm convex glass) in addition to the 2.0 mm plane glass used during impact of glass thickness test in chapter five. Distances, both horizontal distance (HD) and vertical distance (VD) were then measured to the target for 20 minutes, meaning that 20 readings, a reading per minute, were recorded. After the 20 readings, a 2.0 mm plane glass was placed in-between the total station and the target. The glass was placed close to the total station telescope. 20 readings were also taken through the glass to the target. Later, the 2.0 mm plane glass was replaced with concave glass, followed by convex glass, and the HD and VD readings during each measurement were recorded. The experimental setups are shown in figure 6.21 below:

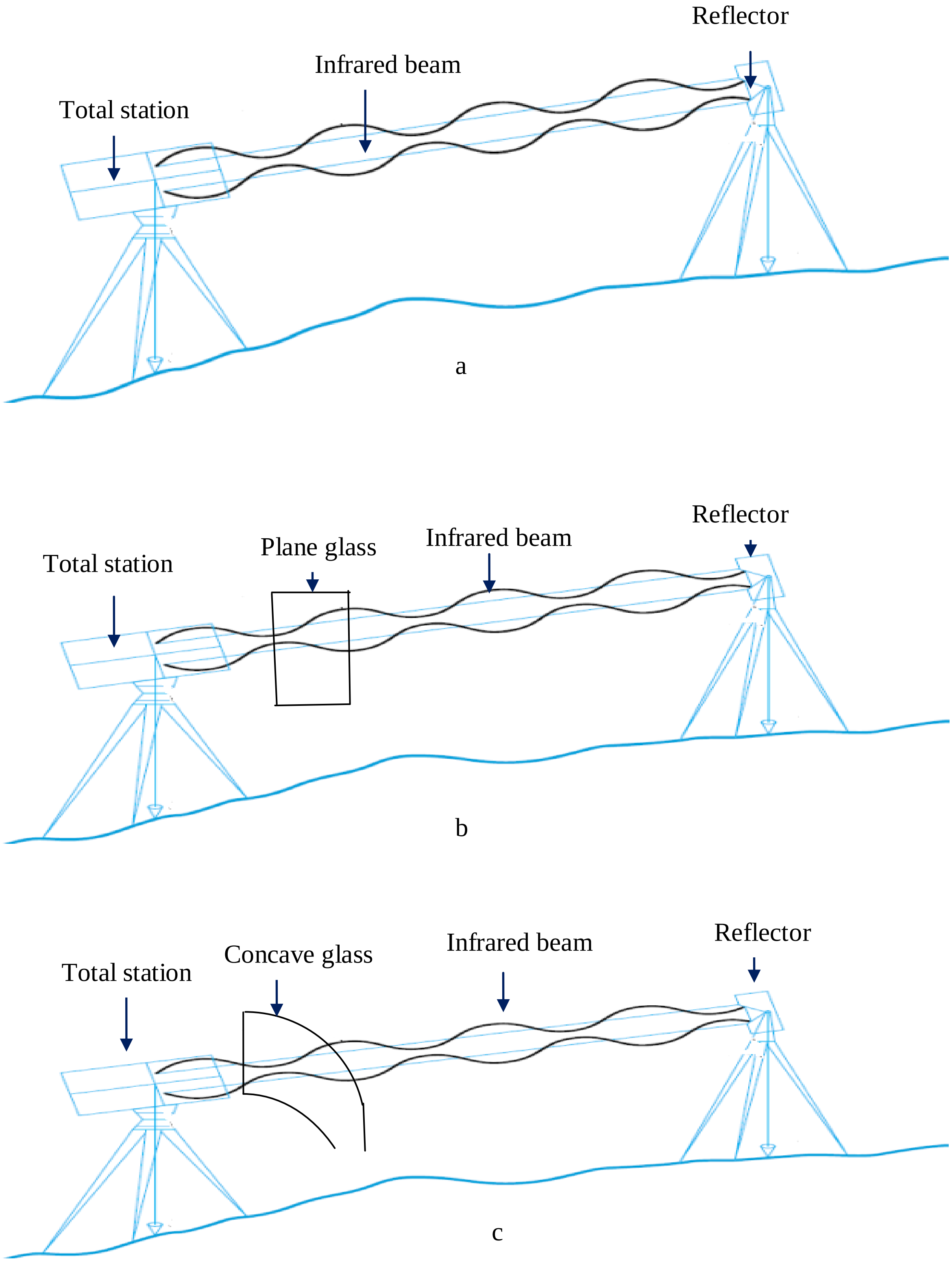
Reflector
Infrared beam
Total station
a
Reflector
Total station
Plane glass
Infrared beam
b
Reflector
Concave glass
Infrared beam
Total station
c

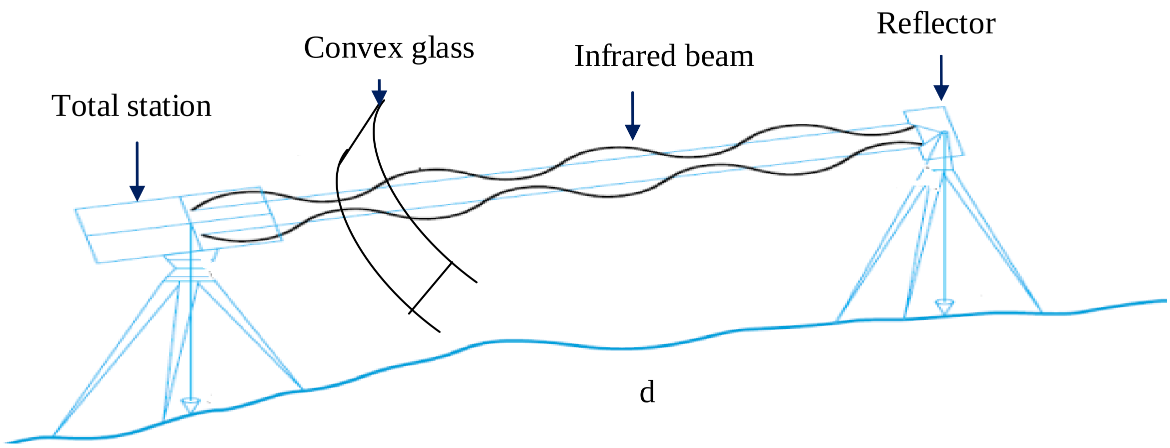

Figure 6.21: Experimental setup for the determination of impact of glass shapes on distance measurements with total station through shelter glass (a – without glass, b – with plane glass; c – concave glass and d – convex glass).

Throughout the exercise, a temperature variation of 0.5°C, a pressure variation of 0.1 mb and a humidity variation of 1 % were observed. It must be noted that the total station was programmed to correct all the readings for prism constant and scale factor before embarking on any distance measurement (see appendix D.2 of Appendix D). The recorded HD and VD readings per measurement were corrected for atmospheric variations using the formula given by Leica Geo-systems for atmospheric corrections in the instrument manual (see equation 4.1 in chapter four).

The acquired distance readings were subjected to statistical analysis before and after atmospheric corrections. The accuracy specification limit [(i.e. ± (1mm + 1.5 ppm)] stated in the TCR 1201 total station manual was also used as an indicator to detect the impact of the glass shapes on the measured distances.

6.3.1 Result and discussion on glass shape test

The results of the analysis of the distance measurements before atmospheric corrections are presented in figures 6.22 and 6.23. The corresponding results after atmospheric correction are presented in figures 6.24 and 6.25.

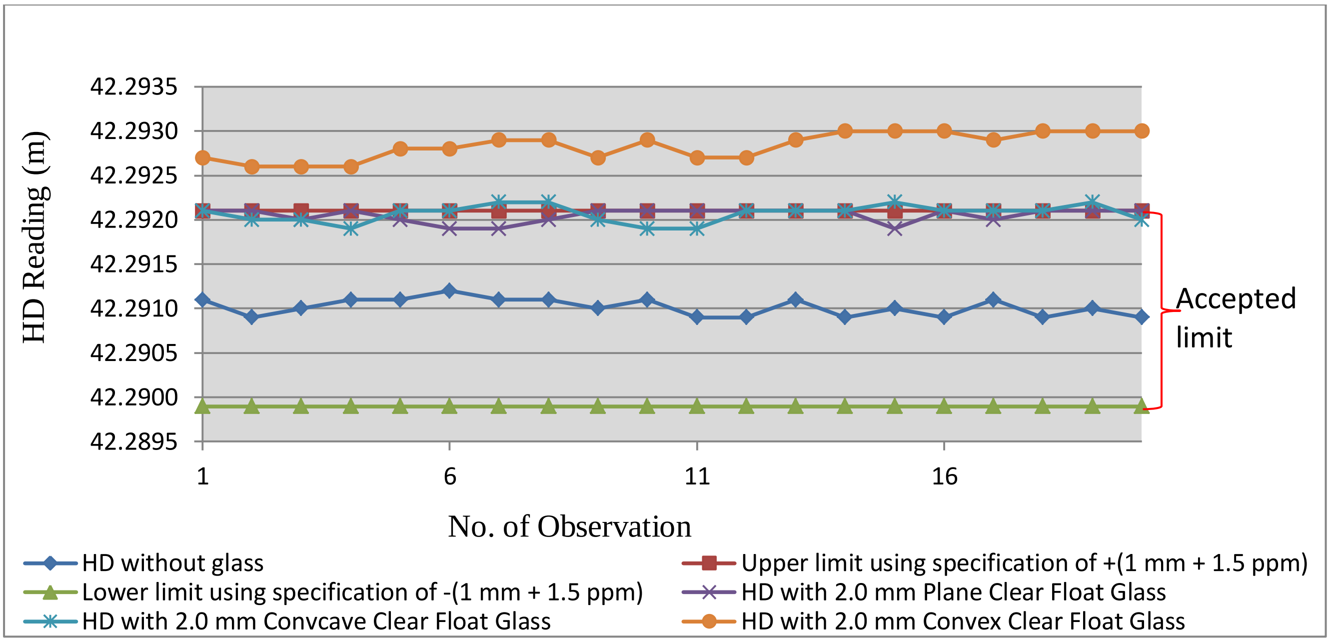

Figure 6.22: HD readings before atmospheric corrections during glass shape test.

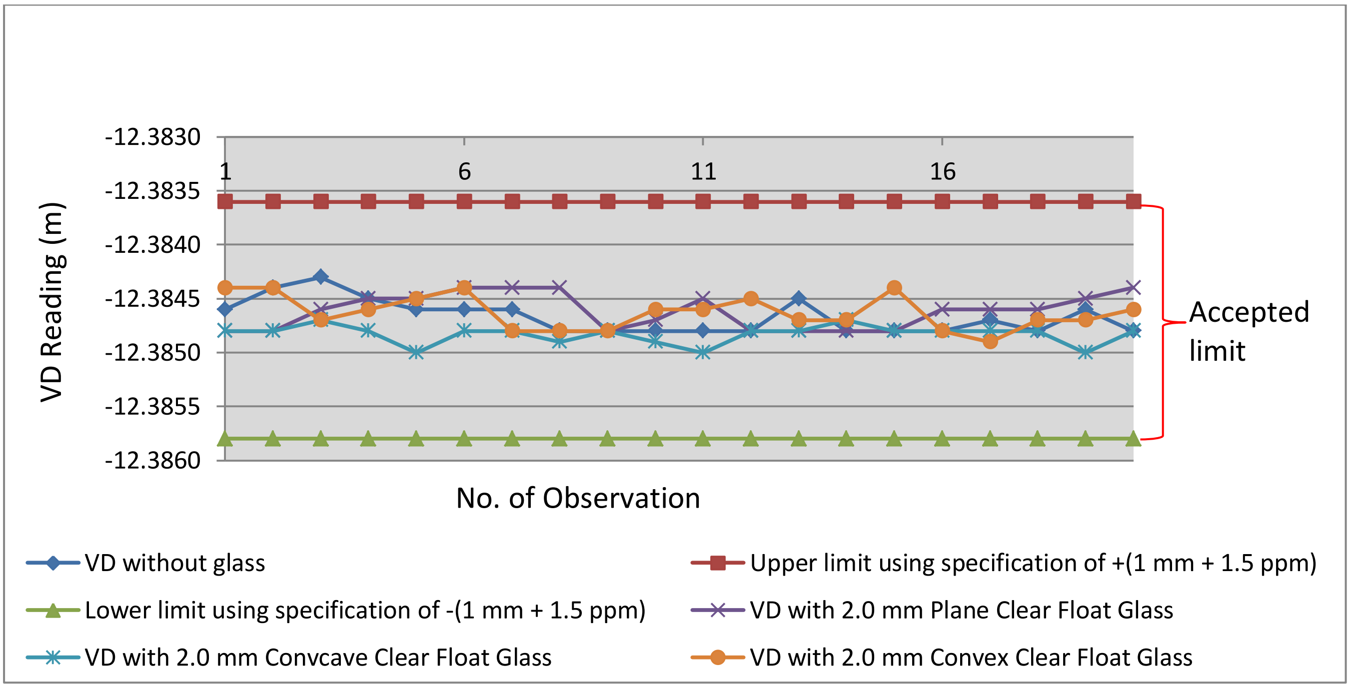

Figure 6.23 VD readings before atmospheric corrections during glass shape test.

Figure 6.22 shows the results of HD measurements before atmospheric corrections. The graph revealed that the entire glass barriers had an impact on the HD readings when compared to HD readings without glass. However, the impact of plane glass was within the accuracy specification of the instrument and this is in agreement with Afeni & Cawood

(2010). All other glass shapes were outside the limit. The impact of the concave glass was not much when compare to the impact of convex glass.

In the result of VD analysis before atmospheric corrections, as shown in figure 6.23, all the readings were within the accuracy limit. In fact, there were no differences between the VD readings without glass and VD readings with glass. This is in agreement with findings in chapters five and six of this report.

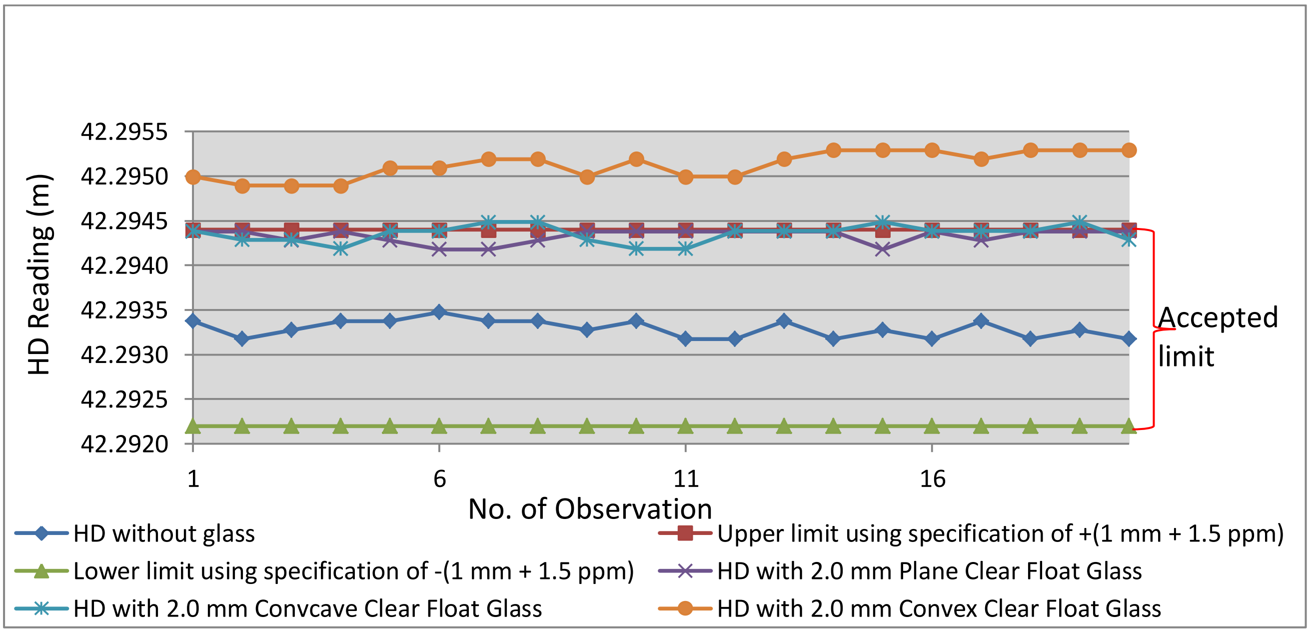

Figure 6.24: HD readings after atmospheric corrections during glass shape test.

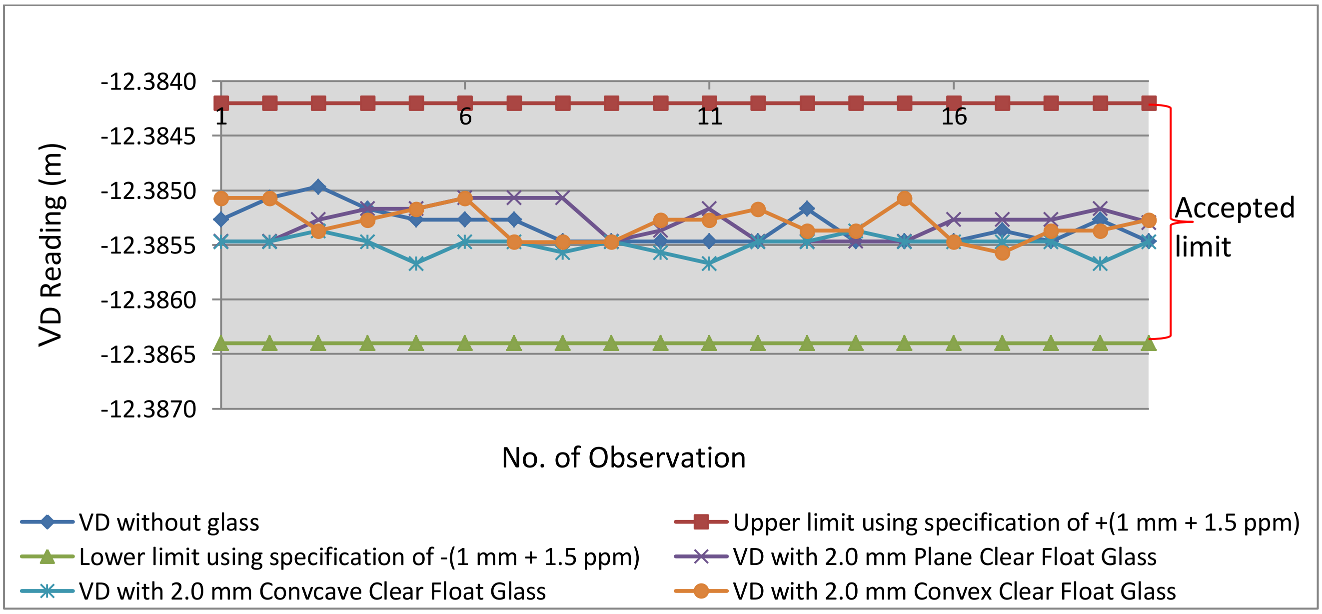

Figure 6.25: VD readings after atmospheric corrections during glass shape test.

Figure 6.24 shows the result of HD readings after atmospheric corrections. The graph is similar to the graph on HD readings before atmospheric corrections, as shown in figure 6.22. The only difference is that the atmospheric impact has been removed.
Figure 6.25 shows the result of VD readings after atmospheric corrections. It is also similar to the result of VD readings before atmospheric corrections, as shown in figure 6.23. The glass barrier has no impact on VD readings.

The findings revealed that the shape of the glass matters when carrying out observations with total station through a shelter window glass. The plane glass has the least impact on HD measurements, followed by the concave glass, while the convex glass has the highest impact. However, the impact of the plane glass was within the accuracy specification limit of the total station. The findings also showed that the glass shapes has no effect on the VD measurements.

6.4. TEST FOR THE EFFECT OF DISTANCE BETWEEN TOTAL STATION AND THE OBSERVATION WINDOW ON THE HD READINGS

Cawood and Stacey (2006) emphasized that data processing through software cannot correct a poorly designed survey system. This test will help during the construction of the monitoring survey observation station. In order to examine the likely impact of the distance between the monitoring survey total station and its shelter window glass cover, a total station (Leica total station TCR 1201+ model) was set up on a tripod at one end and the target (Leica circular prism) was set up on another tripod at the other end.
Distance measurements (HDs) were taken to the target for 20 minutes (20 readings - a reading per minute) and recorded. After the 20 readings, a 3.0 mm clear float glass (housed in a wooden frame) was mounted on a tripod and placed in-between the two (total station and the target). The glass was placed close to the total station, first at 0.30 m to the telescope of the total station and later increased by 0.1m (i.e. 0.30, 0.40, 0.50, ……. 3.00). At each position of the glass frame, 20 readings were taken through the glass to the target and the HD reading during each measurement was recorded. The experimental setup is show in Figure 6.21. The entire operation was carried out indoors to minimize the effects of atmospheric parameter variations. Throughout the exercise, constant temperature, pressure variation of 1 mb and humidity variation of 1 % were observed. The recorded HD measurement per each reading was corrected for atmospheric variations using the atmospheric correction formula stated in equation 4.1 of chapter four.

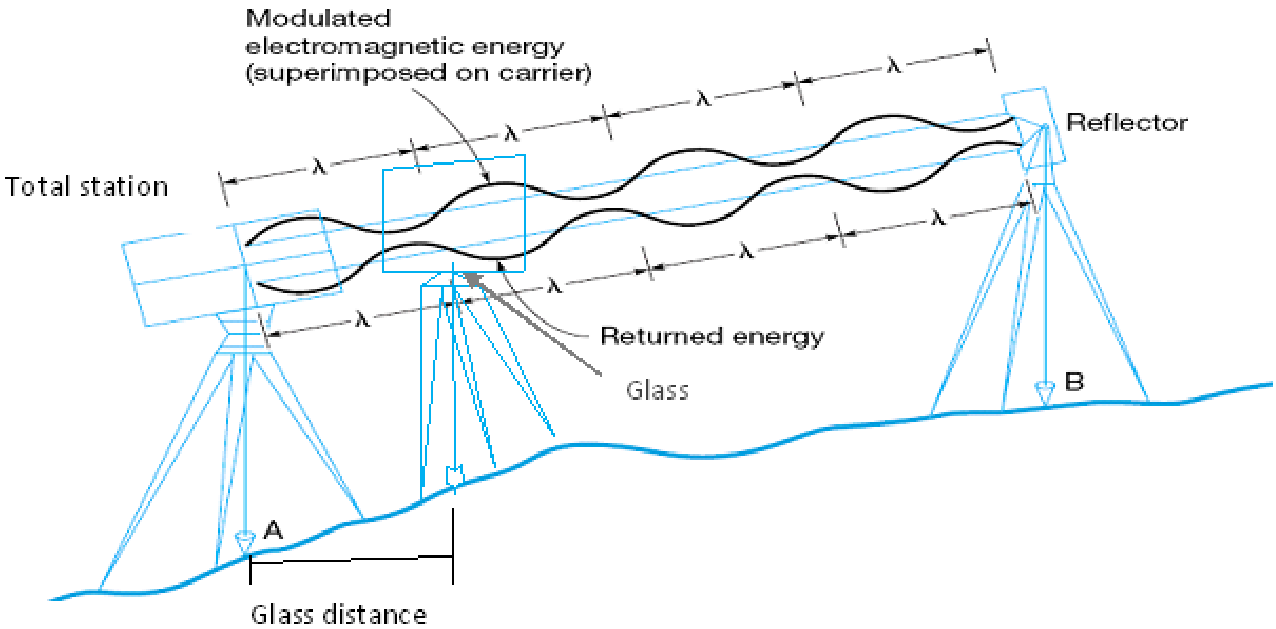

Figure 6.26: Experimental setup for the determination of optimal distance which the total station must be away from the observation window.

6.4.1 Result and discussion

The recorded HDs per 20 readings before atmospheric corrections are presented in appendix D.3; while HDs per 20 readings after atmospheric corrections are presented in table 6.2 below.

Table 6. 2: HD Readings to test for optimal distance which the total station must be away from the observation window after correction.

Reading number	HD Reading without glass	HD Reading with total station at 0.30 m away from glass	HD Reading with total station at 0.40 m away from glass	HD Reading with total station at 0.50 m away from glass	HD Reading with total station at 0.60 m away from glass	HD Reading with total station at 0.70 m away from glass	HD Reading with total station at 0.80 m away from glass	HD Reading with total station at 0.90 m away from glass
1	18.7875	18.7889	18.7888	18.7889	18.7889	18.7888	18.7889	18.7888
2	18.7876	18.7890	18.7888	18.7889	18.7889	18.7888	18.7888	18.7888
3	18.7876	18.7888	18.7888	18.7889	18.7888	18.7890	18.7889	18.7889
4	18.7876	18.7888	18.7888	18.7889	18.7888	18.7889	18.7889	18.7889
5	18.7876	18.7890	18.7889	18.7890	18.7888	18.7889	18.7889	18.7890
6	18.7875	18.7889	18.7890	18.7890	18.7888	18.7889	18.7889	18.7888
7	18.7876	18.7889	18.7890	18.7889	18.7889	18.7889	18.7889	18.7888
8	18.7875	18.7889	18.7889	18.7889	18.7889	18.7889	18.7889	18.7888
9	18.7877	18.7889	18.7889	18.7888	18.7890	18.7889	18.7890	18.7889
10	18.7875	18.7889	18.7889	18.7888	18.7888	18.7888	18.7890	18.7889
11	18.7875	18.7889	18.7889	18.7888	18.7890	18.7890	18.7889	18.7889
12	18.7876	18.7890	18.7889	18.7888	18.7889	18.7890	18.7888	18.7889
13	18.7875	18.7888	18.7890	18.7889	18.7889	18.7890	18.7888	18.7889
14	18.7875	18.7888	18.7888	18.7890	18.7889	18.7889	18.7888	18.7889
15	18.7875	18.7889	18.7888	18.7889	18.7889	18.7889	18.7888	18.7889
16	18.7876	18.7889	18.7890	18.7889	18.7890	18.7889	18.7888	18.7889
17	18.7877	18.7889	18.7888	18.7888	18.7888	18.7889	18.7888	18.7889
18	18.7876	18.7889	18.7888	18.7888	18.7888	18.7888	18.7889	18.7889
19	18.7877	18.7888	18.7889	18.7889	18.7888	18.7888	18.7889	18.7889
20	18.7877	18.7890	18.7888	18.7890	18.7890	18.7887	18.7889	18.7890
Average	18.7876	18.7889	18.7889	18.7889	18.7889	18.7889	18.7889	18.7889
Std Dev	7.7E-05	6.9E-05	7.9E-05	7.2E-05	7.7E-05	8.1E-05	6.4E-05	5.9E-05

Table 6.2: HD Readings to test for optimal distance which the total station must be away from the observation window after correction cont....

Reading number	HD Reading with total station at 1.00 m away from glass	HD Reading with total station at 1.10 m away from glass	HD Reading with total station at 1.20 m away from glass	HD Reading with total station at 1.30 m away from glass	HD Reading with total station at 1.40 m away from glass	HD Reading with total station at 1.50 m away from glass	HD Reading with total station at 1.60 m away from glass
1	18.7889	18.7890	18.7889	18.7888	18.7889	18.7888	18.7889
2	18.7890	18.7890	18.7890	18.7888	18.7890	18.7888	18.7888
3	18.7890	18.7889	18.7889	18.7888	18.7889	18.7889	18.7889
4	18.7890	18.7889	18.7889	18.7889	18.7889	18.7889	18.7889
5	18.7889	18.7889	18.7889	18.7888	18.7890	18.7889	18.7889
6	18.7889	18.7888	18.7889	18.7889	18.7889	18.7890	18.7889
7	18.7889	18.7889	18.7889	18.7889	18.7888	18.7890	18.7889
8	18.7888	18.7889	18.7889	18.7890	18.7888	18.7889	18.7890
9	18.7888	18.7888	18.7889	18.7889	18.7888	18.7889	18.7890
10	18.7889	18.7888	18.7890	18.7889	18.7888	18.7889	18.7889
11	18.7889	18.7890	18.7889	18.7890	18.7888	18.7889	18.7888
12	18.7889	18.7889	18.7888	18.7888	18.7889	18.7889	18.7888
13	18.7889	18.7889	18.7888	18.7889	18.7889	18.7889	18.7889
14	18.7889	18.7889	18.7889	18.7889	18.7889	18.7889	18.7889
15	18.7889	18.7889	18.7889	18.7889	18.7889	18.7889	18.7889
16	18.7889	18.7889	18.7888	18.7888	18.7888	18.7889	18.7889
17	18.7889	18.7889	18.7887	18.7889	18.7890	18.7888	18.7889
18	18.7889	18.7889	18.7889	18.7889	18.7890	18.7888	18.7890
19	18.7889	18.7888	18.7889	18.7890	18.7889	18.7889	18.7890
20	18.7888	18.7888	18.7889	18.7889	18.7889	18.7889	18.7889
Average	18.7889	18.7889	18.7889	18.7889	18.7889	18.7889	18.7889
Std Dev	5.6E-05	6.4E-05	6.7E-05	6.7E-05	7.2E-05	5.5E-05	6.0E-05

Table 6.2: HD Readings to test for optimal distance which the total station must be away from the observation window after correction cont.

Reading number	HD Reading with total station at 1.70 m away from glass	HD Reading with total station at 1.80 m away from glass	HD Reading with total station at 1.90 m away from glass	HD Reading with total station at 2.00 m away from glass	HD Reading with total station at 2.10 m away from glass	HD Reading with total station at 2.20 m away from glass	HD Reading with total station at 2.30 m away from glass
1	18.7888	18.7889	18.7887	18.7889	18.7889	18.7888	18.7889
2	18.7888	18.7887	18.7889	18.7889	18.7889	18.7888	18.7889
3	18.7888	18.7889	18.7889	18.7890	18.7889	18.7888	18.7889
4	18.7889	18.7889	18.7889	18.7890	18.7890	18.7889	18.7889
5	18.7889	18.7890	18.7889	18.7887	18.7890	18.7889	18.7888
6	18.7890	18.7888	18.7889	18.7887	18.7888	18.7890	18.7888
7	18.7889	18.7889	18.7889	18.7889	18.7887	18.7888	18.7889
8	18.7890	18.7889	18.7889	18.7889	18.7889	18.7890	18.7889
9	18.7890	18.7889	18.7888	18.7889	18.7889	18.7889	18.7888
10	18.7889	18.7888	18.7888	18.7890	18.7889	18.7889	18.7889
11	18.7889	18.7889	18.7889	18.7890	18.7889	18.7889	18.7890
12	18.7889	18.7889	18.7889	18.7888	18.7889	18.7889	18.7890
13	18.7888	18.7889	18.7890	18.7890	18.7888	18.7887	18.7890
14	18.7889	18.7890	18.7890	18.7889	18.7889	18.7890	18.7889
15	18.7889	18.7890	18.7889	18.7889	18.7889	18.7890	18.7889
16	18.7889	18.7888	18.7889	18.7889	18.7890	18.7888	18.7889
17	18.7889	18.7889	18.7888	18.7889	18.7890	18.7889	18.7889
18	18.7888	18.7889	18.7889	18.7889	18.7889	18.7889	18.7888
19	18.7888	18.7889	18.7889	18.7888	18.7889	18.7889	18.7889
20	18.7887	18.7889	18.7890	18.7889	18.7889	18.7890	18.7888
Average	18.7889	18.7889	18.7889	18.7889	18.7889	18.7889	18.7889
Std Dev	7.9E-05	7.2E-05	7.2E-05	8.9E-05	7.3E-05	8.5E-05	6.4E-05

Table 6.2: HD Readings to test for optimal distance which the total station must be away from the observation window after correction cont....

Reading number	HD Reading with total station at 2.40 m away from glass	HD Reading with total station at 2.50 m away from glass	HD Reading with total station at 2.60 m away from glass	HD Reading with total station at 2.70 m away from glass	HD Reading with total station at 2.80 m away from glass	HD Reading with total station at 2.90 m away from glass	HD Reading with total station at 3.00 m away from glass
1	18.7890	18.7889	18.7889	18.7887	18.7889	18.7888	18.7889
2	18.7890	18.7889	18.7889	18.7889	18.7889	18.7888	18.7889
3	18.7889	18.7890	18.7889	18.7889	18.7890	18.7888	18.7888
4	18.7889	18.7889	18.7890	18.7889	18.7890	18.7889	18.7889
5	18.7888	18.7890	18.7887	18.7889	18.7888	18.7890	18.7889
6	18.7889	18.7889	18.7888	18.7889	18.7889	18.7889	18.7888
7	18.7888	18.7889	18.7889	18.7888	18.7889	18.7889	18.7888
8	18.7889	18.7889	18.7889	18.7888	18.7888	18.7890	18.7887
9	18.7889	18.7890	18.7889	18.7888	18.7889	18.7890	18.7889
10	18.7888	18.7887	18.7888	18.7889	18.7888	18.7890	18.7889
11	18.7889	18.7889	18.7889	18.7889	18.7889	18.7887	18.7889
12	18.7890	18.7889	18.7890	18.7890	18.7889	18.7889	18.7889
13	18.7889	18.7888	18.7889	18.7889	18.7889	18.7889	18.7890
14	18.7889	18.7888	18.7890	18.7890	18.7890	18.7889	18.7890
15	18.7889	18.7888	18.7889	18.7890	18.7890	18.7890	18.7889
16	18.7890	18.7889	18.7889	18.7889	18.7889	18.7889	18.7889
17	18.7889	18.7889	18.7889	18.7889	18.7889	18.7888	18.7889
18	18.7888	18.7888	18.7890	18.7888	18.7889	18.7889	18.7890
19	18.7888	18.7889	18.7889	18.7889	18.7888	18.7889	18.7889
20	18.7889	18.7889	18.7888	18.7889	18.7887	18.7888	18.7889
Average	18.7889	18.7889	18.7889	18.7889	18.7889	18.7889	18.7889
Std Dev	6.9E-05	7.5E-05	7.6E-05	7.5E-05	7.9E-05	8.5E-05	7.2E-05

Table 6.2 shows the HD readings after atmospheric corrections. The table reveals that the HD readings without glass ranged between 18.7875 m and 18.7877 m. The average of HD readings without glass is 18.7876 m and its standard deviation was $7.7x10^{-5}$. The HD readings to the target with glass at varying distances range from 18.7887m and 18.7890 m. The average readings were the same for all the glass position (i.e. position away from the total station) tested. The average is 18.7889 m and the standard deviation of all the HD readings were within 10^{-5}. By isolating the properties of the glass from the distance the instrument was away from the glass, the observation revealed that only the glass properties mattered while the distance from the glass had no impact.

The table revealed that the distance between the total station and the observation window had no impact on accuracy of the HD measurements. The situation could change when there are severe atmospheric variations between the conditions inside and outside the observation house. In order to avoid such variations, it is advisable to keep the distance between the total station and the observation window to a practical minimum.

6.5 CONCLUSION

The chapter examined the impact of glass colour and shape on distance measurements. It also examined the likely effect of distance between the total station and its shelter window on the distance measurements with the total station. The three tests could be summarized as follows:

- It was possible to measure through glass, but it caused a systematic error in the measured distance.
- The glass colour impact test revealed that the more tinted the glass, the more the impact on distance measurement. The glass colour impact was more on HD readings than VD readings. Therefore, the use of tinted glass should be avoided or else a model must be developed to cater for the impact of the glass colour.
- The glass shape impact test revealed that the shape of the glass mattered when monitoring through glass medium. Plane glass should be used at the mines during monitoring with total station or else more research must be carried out on glass shape to compensate for the error caused by the glass shape on distance measurements.
- The analysis of the likely impact of total station distance away from the observation window on distance measurements revealed that the distance between the total station and the observation window had no impact on the total station distance measurements. However, it is advisable to keep the distance between the total station

and the observation window at practical minimum. The reason is that the test was carried out indoors where the atmospheric variations were negligible or nearly constant, unlike in the mines where the observation house atmospheric parameters could vary widely from the outside atmospheric parameters. These variations may have adverse effects on the total station distance measurements if there is wide distance between the total station and the observation window.

Based on the outcome of the above glass colour impact test, there is need for systematic error correction when total station for distance measurements through a colour glass. The next chapter proposes two equations to cater separately for the glass thickness and glass colour impact.

CHAPTER SEVEN

7.0 DEVELOPMENT OF SYSTEMATIC ERROR CORRECTION MODELS TO CORRECT THE GLASS IMPACTS

In chapters five and six, it was established after the analysis of experimental data on the impacts of glass properties (thickness, colour and shape) on HD measurements that the glass introduced a systematic error over and above the atmospheric correction formulae. Therefore, it is necessary to develop a new correction that can remove or reduce the impact when total stations are used to do precise monitoring from the inside of an observation house. Alternatively, the existing atmospheric correction formulae can also be modified to enable them accommodate the effects caused by the glass medium. This chapter discusses the steps taken to develop such corrections.

After careful analysis of the graphs in chapters five and six, one can suggest that a regression model will be suitable for removing the effects of the glass impacts especially the thickness (i.e. glass thickness ranges of 4.0 mm, 5.0 mm and 6.38 mm) in addition to colour that has an impact on accuracy. For purposes of this research, regression analysis is further explored.

7.1. REGRESSION ANALYSIS

Regression analysis is a statistical tool that identifies the relationship between two or more quantitative variables: a dependent variable whose value is to be predicted (horizontal distance readings - in the case of this research) and an independent or explanatory variable(s) about which knowledge is available (glass thickness and colour - in the case of this research). Regression technique is used to find the equation that represents the relationship between the variables.

Al-Nasser and Radaideh (2008) described regression analysis as a conceptually simple method for exploring functional relationships among variables. The relationship is expressed in the form of an equation or model connecting the response variable *(y)* and one (*x*) or more explanatory variables. The simple true relationship can be approximated by the regression model. Regression analysis can either be simple linear model or multiple.

Linear regression is a fundamental and frequently used statistical tool in all branches of observational science and management. In a simple linear regression model, the relationship between variables is established by a straight line, mathematically expressed as:

$$y = b_0 + b_1 x \text{ ....7.1}$$

The above equation 7.1 defines a line in a two dimensional or two-variable space which implies that the *y* variable can be expressed in terms of a constant (b_0) and a slope (b_1) times the *x* variable in a full text. *y* is the dependent variable (measured with error), *x* is the independent variable (known without error), b_0 is the *Y*-intercept of the regression equation and b_1 is the slope of the regression equation (b_1 is also refer to as regression coefficient).
The above equation 7.1 can also be written as:

$$y = b_0 + b_1 x + \varepsilon \text{ ....7.2}$$

where ε is assumed to be random error or random variable possessing a specified probability distribution with mean equals to zero (0). b_0 and b_1 are unknown regression parameters to be estimated from the data. A simple linear model represents variable y_i, as a linear function of one independent variable, x_i subject to a random 'disturbance' or 'error' ε_i. Thus the above equation can be rewritten as follows:

$$y_i = b_0 + b_1 x_i + \varepsilon_i \text{ ....7.3}$$

The error term ε_i is assumed to have a mean value of zero, a constant variance, and to be uncorrelated with itself across observations ($\sum \varepsilon_i \varepsilon_j$) = 0, i $\neq$ j).

The aim of linear regression is to adjust the values of slope and intercept by finding the line that best predicts y from x. More precisely, the goal of linear regression is to minimize the sum of the squares of vertical distances of the points from the line.
A "simple" regression model has a single independent variable instead of multiple independent variables. Because simple is in the name, mistakes are often made by having the assumption that they are simple to use. One mistake is to first apply them to someone's data, without checking to see whether the basic requirements are met. The complexity in linear regression analysis arises from a variety of reasons (Feigleson & Babu, 1992):

a. attributes of the data are not always the same (i.e. the scatter may or may not have a normal distribution, the data may be heteroscedastic where the degree of scatter depends on the data value in one or both variables);
b. scientists' knowledge of the problem under investigation is not always the same (i.e. they may or may not know how much of the scatter in each variable is due to the measurement steps rather than the objects under study); and
c. the aim of the analysis is always the same (i.e. one situation might need an optimized estimate of the intercept, and another problem may seek to apply the regression to new data points).

To overcome these problems, it is imperative to first list the types of simple linear regressions, and to stress not applying them blindly or mechanically to a new data. An initial graphical exploration of the data to determine the qualitative properties of the variables can be carried out to answer the following:

a. Are variables stationary or nonstationary? Do they show linear or compound growth?
b. Do they have a constant variance or increasing variance (heteroscedasticity)?

It's essential to carry out rigorous statistical tests to ascertain the character of data at hand. After ascertaining the character of the data to the required degree of rigor, the next step is to choose transformations, if any, that would be suitable to apply before attempting to fit a linear model.

In a multivariate case, when there is more than one independent variable, the regression line cannot be visualized in the two dimensional space as expressed in equation 7.1. Generally, a multiple regression procedures will estimate a linear equation of the form:

$$y = b_0 + b_1 x_1 + b_2 x_2 + \ldots\ldots\ldots\ldots b_n x_n \ldots\ldots\ldots\ldots\ldots\ldots\ldots\ldots\ldots\ldots 7.4$$

Abu-Bakar and Tahir (2009) described a multiple regression as the mostly used statistical technique for modelling linear relationship between two or more variables. The general multiple linear regressions with normal error terms, simple in terms of x variables is shown in equation 7.5:

$$y = b_0 + b_1 x_1 + b_2 x_2 + \ldots\ldots\ldots\ldots b_n x_n + \varepsilon \ldots\ldots\ldots\ldots\ldots\ldots\ldots\ldots\ldots\ldots 7.5$$

where:

y is the dependent variable; b's are the regression weight (also call regression coefficients); and x_1……x_n are the independent variables (n stands for number of independent variables).

In this study two variables are involved i.e. the distance measurement (which is dependent variable) and the glass thickness (which is the independent variable). The relationship between the glass colour impact on HD readings is modeled separately since only 3.0 mm glass thickness were used. Before finally accepting the idea of using linear regression for the analysis of these data, the following questions in the table below are used as confirmation test:

Table 7.1: Check lists for linear regression analysis for glass thickness model

Test question	Test answer and discussion
Can the relationship between x and y be graphed as a straight line?	Yes. All the graphs in Figures 5.5 to 5.16 in chapter five of this report, clearly show that the relationship between x and y is linear. Therefore, linear regression will be appropriate for the analysis
Is the scatter of data around the line Gaussian or at least approximately to the line Gaussian?	Yes. There is no outlier in any of the data used as shown in the Figures 5.5 to 5.16 of chapter five of this report.
Is the variability the same everywhere?	Yes, the data has nearly the same standard deviation and the scatter of point around the best-fit line has the same standard deviation
Do we know the precise values of x?	Yes, x values are the various glass thickness, 4.0 mm, 5.0 mm and 6.38 mm.

Based on the above check list, simple linear regression model will be a suitable correction for glass thickness model aspect of this research. The steps taken to arrive at the model equation are explained below:

7.2 GLASS THICKNESS IMPACT EQUATION MODEL

The average daily HD readings to the Leica mini and circular prisms during short- and long-HD monitoring were subjected to further analysis to generate a regression equation that can relate the glass thickness and the HD readings. The average daily HD readings to mini and circular prisms during short-distance monitoring are presented in Tables 7.2 and 7.3, while Tables 7.4 and 7.5 show the average daily HD readings to mini and circular prisms during long-distance monitoring. It should be noted that all the HD readings presented in the above tables had been corrected for atmospheric influence.

Table 7.2: Average daily HD readings to Mini Prism

Date	Glass Thickness (mm)	Ave HD to Mini Prism without glass	Ave HD to Mini Prism with glass @ 45°	Ave HD to Mini Prism with glass @ 60°	Ave HD to Mini Prism with glass @ 90°
2009/08/29	2.00	42.2881	42.2892	42.2891	42.2890
2009/08/30	2.00	42.2881	42.2893	42.2893	42.2892
2009/08/31	2.00	42.2882	42.2894	42.2893	42.2893
2009/09/01	3.00	42.2875	42.2892	42.2891	42.2889
2009/09/02	3.00	42.2874	42.2891	42.2890	42.2889
2009/09/03	3.00	42.2875	42.2892	42.2891	42.2891
2009/09/04	4.00	42.2873	42.2896	42.2896	42.2894
2009/09/05	4.00	42.2878	42.2899	42.2898	42.2898
2009/09/06	4.00	42.2874	42.2898	42.2897	42.2895
2009/09/07	5.00	42.2887	42.2908	42.2907	42.2907
2009/09/08	5.00	42.2888	42.2910	42.2908	42.2907
2009/09/09	5.00	42.2880	42.2903	42.2902	42.2900
2009/09/10	6.38	42.2894	42.2927	42.2925	NM
2009/09/11	6.38	42.2887	42.2923	42.2919	NM
2009/09/12	6.38	42.2885	42.2915	42.2915	NM

NM means Not Measured

Table 7.3: Average daily HD readings to Circular Prism

Date	Glass Thickness (mm)	Ave HD (m) to Circular Prism without glass	Ave HD (m) to Circular Prism with glass @ 45°	Ave HD (m) to Circular Prism with glass @ 60°	Ave HD (m) to Circular Prism with glass @ 90°
2009/08/29	2.00	42.2888	42.2900	42.2899	42.2899
2009/08/30	2.00	42.2888	42.2900	42.2899	42.2898
2009/08/31	2.00	42.2888	42.2899	42.2899	42.2899
2009/09/01	3.00	42.2890	42.2906	42.2906	42.2904
2009/09/02	3.00	42.2887	42.2904	42.2904	42.2901
2009/09/03	3.00	42.2886	42.2904	42.2904	42.2902
2009/09/04	4.00	42.2892	42.2912	42.2912	42.2910
2009/09/05	4.00	42.2887	42.2910	42.2908	42.2908
2009/09/06	4.00	42.2886	42.2908	42.2908	42.2906
2009/09/07	5.00	42.2898	42.2923	42.2923	42.2918
2009/09/08	5.00	42.2897	42.2921	42.2919	42.2916
2009/09/09	5.00	42.2895	42.2916	42.2914	42.2911
2009/09/10	6.38	42.2907	42.2937	42.2937	NM
2009/09/11	6.38	42.2904	42.2935	42.2928	NM
2009/09/12	6.38	42.2900	42.2929	42.2927	NM

NM means Not Measured

Table 7.4: Average daily HD readings to Mini Prism

Date	Glass Thickness (mm)	Ave HD to Mini Prism without glass	Ave HD to Mini Prism with glass @ 45°	Ave HD to Mini Prism with glass @ 60°	Ave HD to Mini Prism with glass @ 90°
2009/10/06	2.00	626.5427	626.5440	626.5442	626.5441
2009/10/07	2.00	626.5421	626.5430	626.5431	626.5430
2009/10/08	2.00	626.5421	626.5433	626.5434	626.5432
2009/10/09	3.00	626.5418	626.5433	626.5436	626.5433
2009/10/10	3.00	626.5418	626.5437	626.5436	626.5437
2009/10/11	3.00	626.5419	626.5436	626.5438	626.5437
2009/10/12	4.00	626.5425	626.5452	626.5452	626.5448
2009/10/13	4.00	626.5429	626.5453	626.5451	626.5450
2009/10/14	4.00	626.5429	626.5453	626.5452	626.5450
2009/10/15	5.00	626.5424	626.5462	626.5458	626.5456
2009/10/16	5.00	626.5422	626.5459	626.5455	626.5454
2009/10/17	5.00	626.5426	626.5470	626.5467	626.5466
2009/10/18	6.38	626.5424	626.5466	626.5459	626.5459
2009/10/19	6.38	626.5428	626.5469	626.5464	626.5463
2009/10/20	6.38	626.5428	626.5470	626.5460	626.5461

Table 7.5: Average daily HD readings to Circular Prism

Date	Glass Thickness (mm)	Ave HD (m) to Circular Prism without glass	Ave HD (m) to Circular Prism with glass @ 45°	Ave HD (m) to Circular Prism with glass @ 60°	Ave HD (m) to Circular Prism with glass @ 90°
2009/10/06	2.00	626.5402	626.5410	626.5414	626.5412
2009/10/07	2.00	626.5399	626.5407	626.5408	626.5407
2009/10/08	2.00	626.5404	626.5414	626.5416	626.5414
2009/10/09	3.00	626.5402	626.5415	626.5418	626.5416
2009/10/10	3.00	626.5402	626.5419	626.5420	626.5420
2009/10/11	3.00	626.5402	626.5417	626.5420	626.5420
2009/10/12	4.00	626.5404	626.5425	626.5424	626.5423
2009/10/13	4.00	626.5403	626.5425	626.5424	626.5423
2009/10/14	4.00	626.5404	626.5428	626.5427	626.5426
2009/10/15	5.00	626.5402	626.5434	626.5430	626.5428
2009/10/16	5.00	626.5404	626.5435	626.5432	626.5430
2009/10/17	5.00	626.5406	626.5436	626.5434	626.5432
2009/10/18	6.38	626.5409	626.5447	626.5442	626.5440
2009/10/19	6.38	626.5412	626.5451	626.5445	626.5444
2009/10/20	6.38	626.5409	626.5452	626.5444	626.5443

To generate the regression equation, the above data was plotted using Microsoft Excel but the equations generated did not agree with one another. Therefore, it resulted in averaging HD readings to the mini and circular prisms together during each monitoring operation (e.g.

short-distance monitoring operation) and being called HD readings to the prism. The average daily HD readings to the prisms during short- and long-distance monitoring are presented in tables 7.6 and 7.7.

Table 7.6: Average daily HD readings to Prism (Short distance)

Date	Glass Thickness (mm)	HD to Prism without glass	HD to Prism with glass @ 45°	HD to Prism with glass @ 60°	HD to Prism with glass @ 90°
2009/08/29	2.00	42.2885	42.2896	42.2895	42.2895
2009/08/30	2.00	42.2885	42.2897	42.2896	42.2895
2009/08/31	2.00	42.2885	42.2897	42.2896	42.2896
2009/09/01	3.00	42.2883	42.2899	42.2899	42.2897
2009/09/02	3.00	42.2881	42.2898	42.2897	42.2895
2009/09/03	3.00	42.2881	42.2898	42.2898	42.2897
2009/09/04	4.00	42.2883	42.2904	42.2904	42.2902
2009/09/05	4.00	42.2883	42.2905	42.2903	42.2903
2009/09/06	4.00	42.2880	42.2903	42.2903	42.2901
2009/09/07	5.00	42.2893	42.2916	42.2915	42.2913
2009/09/08	5.00	42.2893	42.2916	42.2914	42.2912
2009/09/09	5.00	42.2888	42.2910	42.2908	42.2906
2009/09/10	6.38	42.2901	42.2932	42.2931	NM
2009/09/11	6.38	42.2896	42.2929	42.2924	NM
2009/09/12	6.38	42.2893	42.2922	42.2921	NM

NM means Not Measured

Table 7.7: Average daily HD readings to prism (Long distance)

Date	Glass Thickness (mm)	HD to Prism without glass	HD to Prism with glass @ 45°	HD to Prism with glass @ 60°	HD to Prism with glass @ 90°
2009/10/06	2.00	626.5415	626.5425	626.5428	626.5427
2009/10/07	2.00	626.5410	626.5419	626.5420	626.5419
2009/10/08	2.00	626.5413	626.5424	626.5425	626.5423
2009/10/09	3.00	626.5410	626.5424	626.5427	626.5425
2009/10/10	3.00	626.5410	626.5428	626.5428	626.5429
2009/10/11	3.00	626.5411	626.5427	626.5429	626.5429
2009/10/12	4.00	626.5415	626.5439	626.5438	626.5436
2009/10/13	4.00	626.5416	626.5439	626.5438	626.5437
2009/10/14	4.00	626.5417	626.5441	626.5440	626.5438
2009/10/15	5.00	626.5413	626.5448	626.5444	626.5442
2009/10/16	5.00	626.5413	626.5447	626.5444	626.5442
2009/10/17	5.00	626.5416	626.5453	626.5451	626.5449
2009/10/18	6.38	626.5417	626.5457	626.5451	626.5450
2009/10/19	6.38	626.5420	626.5460	626.5455	626.5454
2009/10/20	6.38	626.5419	626.5461	626.5452	626.5452

The above tables 7.6 and 7.7 are reduced to average of three days HD readings per glass thickness. The impact of the angular variations on the HD readings are still within the accuracy limits in all the glass thickness and angles tested; therefore the researcher average all HD readings without minding the glass angles. Table 7.8 shows the average HD readings per 3days without and with glass.

Table 7. 8: Average HD per glass thickness (a - short distance, b - long distance)

a Glass thickness	Average HD without glass	Average HD with glass	Difference (Glass impact)
2	42.2887	42.2896	0.0009
3	42.2887	42.2903	0.0016
4	42.2887	42.2909	0.0022
5	42.2887	42.2912	0.0029
6.38	42.2887	42.2927	0.0040

b Glass thickness	Average HD without glass	Average HD with glass	Difference (Glass impact)
2	626.5414	626.5424	0.0010
3	626.5414	626.5431	0.0017
4	626.5414	626.5438	0.0024
5	626.5414	626.5447	0.0033
6.38	626.5414	626.5455	0.0041

Chapter five of this report established that impacts of 2.0 mm and 3.0 mm glass thickness on measured HDs were within the accuracy specification of the TCR 1201 total station used to measure the distances. Also based on the accuracy specification of 1 mm + 1.5 ppm stated in the manual of the instrument, the researcher decided to reduce the data to three decimal places as shown in the table 7.9. Apart from this, the researcher used the difference column and kept the column without glass constant.

Table 7.9: Average change in HD per glass thickness (a - short distance, b - long distance)

a	Glass thickness	Without glass	With Glass (glass impact)
	4	0	0.002
	5	0	0.003
	6.38	0	0.004

b	Glass thickness	Without glass	With Glass (glass impact)
	4	0	0.002
	5	0	0.003
	6.38	0	0.004

The method of least squares estimators for linear regression model is applied to tables 7.9. The glass thickness is tag x, while the glass impact is tag y.

7.2.1. Least Squares Estimator method for Glass Thickness.

Least squares estimators are the most commonly used form of linear regression. They provide the specific way of measuring "accuracy" and hence give a rule for how precisely to choose "best" constant in a group of data set. If the researcher postulates equation 7.2 above:

$$y = b_0 + b_1 x + \varepsilon \qquad \text{7.2}$$

where ε possesses some probability distribution with E(ε) = 0.

If $\hat{b}_0$ and $\hat{b}_1$ are estimators of parameters b_0 and b_1, then $\hat{y} = \hat{b}_0 + \hat{b}_1 x$ is a clear estimator of E(y).

The least squares procedure for fitting a line through a set of n data points is to ensure that the differences between the observed values and corresponding points on the fitted line is "small" in overall sense. According to Wackerly *et al* (2008), a convenient way to accomplish this and one that yields estimators with good properties is to minimize the sum of squares of the vertical deviations from fitted line as shown in figure 7.1:

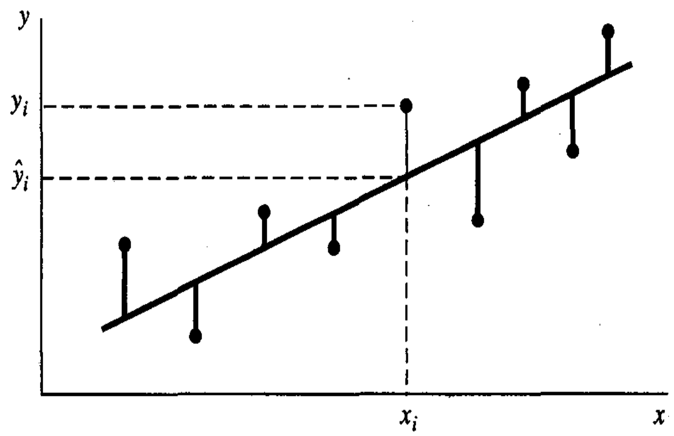

Figure 7.1: Fitting a straight line through a set data points (source: Wackerly *et al.*, 2008)

Thus, if

$$\hat{y}_i = b_0 + b_1 \hat{x}_i \qquad \text{7.6}$$

where $\hat{y}$ is the predicted value of the *i*th y value (when $x = x_i$), then the deviation (also known as error) of the observed value y_i from $\hat{y}_i = b_0 + b_1 \hat{x}_i$ is the difference $y_i - \hat{y}_i$ and the sum of squares of deviation (also called sum of squares for error) to be minimized is:

$$SSD = \sum_{i=1}^{n} (y_i - \hat{y}_i)^2 = \sum_{i=1}^{n} \left[y_i - \left(\hat{b}_0 + \hat{b}_1 x_i \right) \right]^2 \qquad \text{7.7}$$

To find the values of $\hat{b}_0$ and $\hat{b}_1$ that minimize SSD in equation 7.7, we differentiate with respect to $\hat{b}_0$ and $\hat{b}_1$ and set the results equal to 0:

$$\frac{\partial SSD}{\partial b_0} = \frac{\left\{\sum_{i=1}^{n}\left[y_i - \left(\hat{b}_0 + \hat{b}_1 x_i\right)\right]^2\right\}}{\partial b_0} = -\sum_{i=1}^{n} 2\left[y_i - \left(\hat{b}_0 + \hat{b}_1 x_i\right)\right] = -2\sum_{i=1}^{n}\left(y_1 - \hat{b}_0 - \hat{b}_1 x_i\right) = 0 \text{ .....7.8}$$

$$\frac{\partial SSD}{\partial b_1} = \frac{\left\{\sum_{i=1}^{n}\left[y_i - \left(\hat{b}_0 + \hat{b}_1 x_i\right)\right]^2\right\}}{\partial b_1} = -\sum_{i=1}^{n} 2\left[y_i - \left(\hat{b}_0 + \hat{b}_1 x_i\right)\right]x_i = -2\sum_{i=1}^{n}\left(y_1 - \hat{b}_0 - \hat{b}_1 x_i\right)x_i = 0 \text{ ..7.9}$$

Equations 7.8 and 7.9 above are called the least squares equations for estimating the parameters of a line. The least squares equations are linear in $\hat{b}_0$ and $\hat{b}_1$, hence they can be solved simultaneously. By solving equations 7.8 and 7.9 simultaneously (Rencher & Schaalje, 2007), we have:

$$\hat{b}_1 = \frac{\sum_{i=1}^{n} x_i y_i - n\bar{y}\bar{x}}{\sum_{i=1}^{n} x_i^2 - n\bar{x}^2} = \frac{\sum_{i=1}^{n}(x_i - \bar{x})(y_i - \bar{y})}{\sum_{i=1}^{n}(x_i - \bar{x})^2} = \frac{\sum_{i=1}^{n} x_i y_i - n\bar{y}\bar{x}}{\sum_{i=1}^{n} x_i^2 - n\bar{x}^2} \text{ ....7.10}$$

$$\hat{b}_0 = \bar{y} - \hat{b}_1\bar{x} \text{ ....7.11}$$

Where:

x_i is glass thickness (mm) or glass colour (% tint)

y_i is glass impact (m)

n is number of observation

$\bar{x}$ is mean of x_i

$\bar{y}$ is mean of y_i

Equations 7.10 and 7.11 are used to work out the regression model that best suit data set in table 7.9 as shown below:

Table 7.10: Average change in HD per glass thickness for least squares regression model

S/No	x_i (glass thickness, mm)	y_i (glass impact, m)	$x_i y_i$	x_i^2
1	4	0.002	0.008	16.000
2	5	0.003	0.015	25.000
3	6.38	0.004	0.026	40.704
Sum	15.38000	0.00900	0.04852	81.70440
Mean	5.12667	0.00300		

By substitute for these values in equations 7.10 and 7.11, we have:

$$\hat{b}_1 = \frac{\sum_{i=1}^{n} x_i y_i - n\bar{y}\bar{x}}{\sum_{i=1}^{n} x_i^2 - n\bar{x}^2} = \frac{0.04852 - 3(5.12667\,X\,0.00300)}{81.70440 - 3(5.12667)^2} = 0.00083$$

$$\hat{b}_0 = \bar{y} - \hat{b}_1\bar{x} = 0.00300 - 0.00083(5.12667) = -0.00126$$

$$\hat{y} = -0.00126 + 0.00083x$$

If we approximate to 4 decimal places, we have:

$$\hat{y} = 0.0008x - 0.0013 \quad \text{......} 7.12$$

The above tables 7.9a and 7.9b were used to plot graph with Microsoft Excel to generate linear equation as shown in figures 7.2 and 7.3.

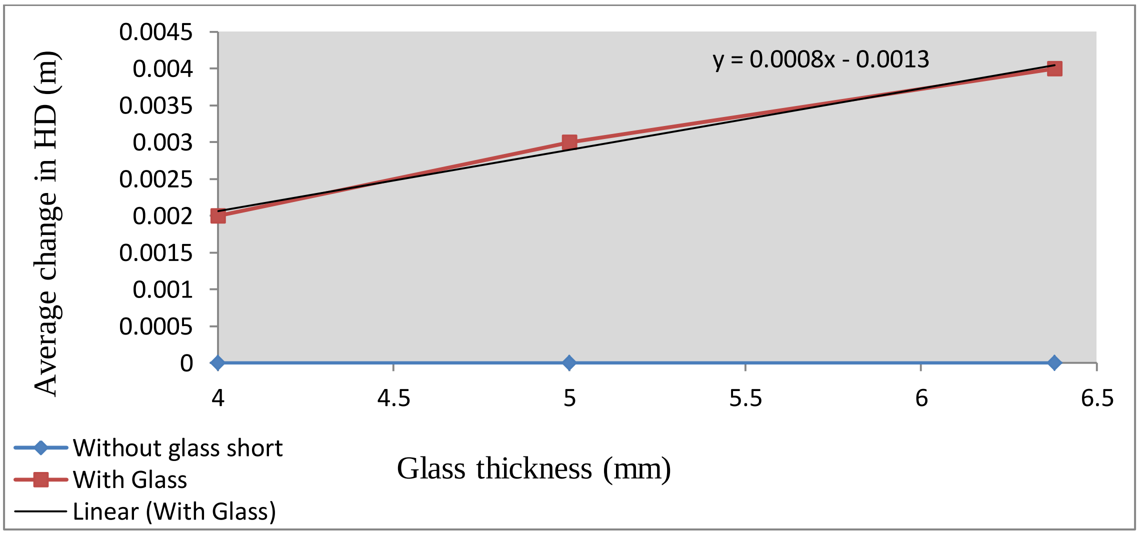

Figure 7.2: Graph of average change in HD against glass thickness (short-distance)

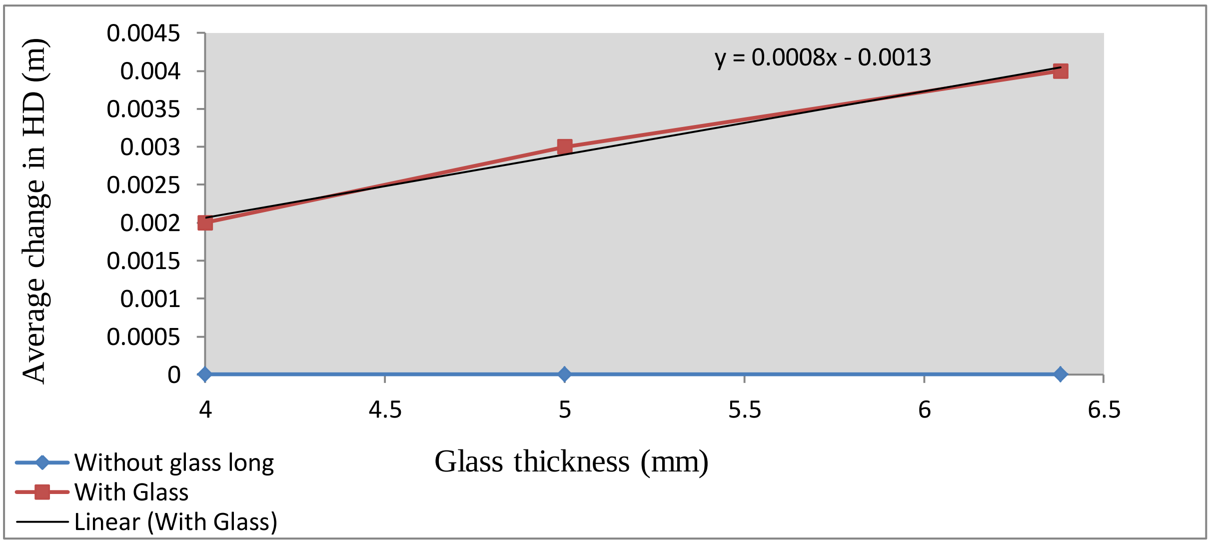

Figure 7.3: Graph of average change in HD against glass thickness (Long-distance)

Figure 7.2 and 7.3 clearly yield the same linear regression equations with equation 7.12 above. Therefore, the linear regression equation for correction of error generated as a result of glass thickness is:

$$\hat{y} = 0.0008x - 0.0013 \ldots\ldots\ldots\ldots\ldots\ldots\ldots\ldots\ldots\ldots\ldots\ldots\ldots\ldots 7.12$$

where:

$\hat{y}$ is the error caused by the glass thickness (m); and

x is the thickness of the glass (mm).

The implication of equation 8.1 above is that, when a glass of 4.0 mm thick is used, 0.0019 m must be subtracted from the HD measured through such glass to make such HD reading conform to the HD reading without glass. So also when 5.0 mm and 6.38 mm glass thicknesses are used, 0.0027 m and 0.0038 m must be subtracted from each of the HD readings measured through such glass to make the readings conform to the HD readings measured without glass.

The above equation 7.12 can be merged with formula for atmospheric variations correction equation (also known as first velocity correction in chapter two equation 2.34) when using infra-red EDM presented in equation 4.1 (the equation can be rewrite as shown below for clarity purpose):

$$C_1 = \left[283.05 - \frac{79.7489P}{(273.15 + t)} + \frac{11.27e}{(273.15 + t)} \right] .10^{-6} d' \ldots\ldots\ldots\ldots\ldots\ldots\ldots\ldots\ldots\ldots 4.1$$

Where:

C_1 is the first velocity correction (shown in equation 2.34 of chapter two) also known as atmospheric correction.

Thus the new combined formula for atmospheric variations correction and glass thickness (when using 4.0 mm thickness and above) impact correction is:

For infra-red EDM (IR):

$$k' = \left[283.05 - \frac{79.7489P}{(273.15 + t)} + \frac{11.27e}{(273.15 + t)} \right] .10^{-6} d' - [0.0008x - 0.0013] \ldots\ldots\ldots 7.13$$

The above equation 7.13 can be expressed as follows

$$k' = a.10^{-6} d' - \hat{y} \ldots\ldots\ldots\ldots\ldots\ldots\ldots\ldots\ldots\ldots\ldots\ldots\ldots\ldots\ldots\ldots 7.14$$

where:

k’ is the correction factor for atmospheric variation and glass thickness effect;

$a.10^{-6}$ is the atmospheric variation correction formula;

d' is the measured distance as it appears on the total station digital screen; and

$\hat{y}$ is the glass thickness impact formula.

7.3 GLASS COLOUR IMPACT EQUATION MODEL

To select the suitable model for the glass colour impact on distance measurement, the graphs of colour impact analysis plotted in chapter six were subjected to the check list questions in table 7.11:

Table 7.11: Check list for linear regression analysis for glass colour model

Test question	**Test answer and discussion**
Can the relationship between x and y be graphed as a straight line?	Yes. All the glass colour impact analysis graphs (Figures 6.1 to 6.8) plotted in chapter six of this report, clearly show that the relationship between x and y is linear. Therefore, linear regression will be appropriate for the analysis.
Is the scatter of data around the line Gaussian or at least approximately to the line Gaussian?	Yes. There is no outlier in any of the data used as shown in the Figures 6.1 to 6.8 of chapter six of this report.
Is the variability the same everywhere?	Yes, the data has nearly the same standard deviation and the scatter of point around the best-fit line has the same standard deviation.
Do we know the precise values of x?	Yes, x values are the various glass colour, light tinted (5% tint) and dark tinted (50% tint)
Are the x and y values intertwined?	No, the values of x that are known cannot be used to calculate the values of y

As established in the table 7.11 above, linear regression would be appropriate for glass colour impact model equation generation.

Therefore, the average daily HD readings to the Leica mini and circular prisms during long HD monitoring when light tinted (5%) and dark tinted (50%) glasses were used as a monitoring window cover were subjected to further analyses to generate regression equations that can relate the glass colour and the HD readings. The average daily HD readings to the mini and the circular prisms during long distance monitoring when tinted glass was used are presented in tables 7.12 and 7.13. The HD readings to the mini and the circular prisms were averaged together as carried out in section 7.2 during glass thickness modeling. Table 7.14

shows the average daily HD readings to the prisms during long distance monitoring when tinted glass medium was used.

Table 7.12: Average daily HD readings to Mini Prism

Date	Glass Colour (Tinted)	Ave HD to Mini Prism without glass	Ave HD to Mini Prism with glass @ 30°	Ave HD to Mini Prism with glass @ 45°	Ave HD to Mini Prism with glass @ 60°	Ave HD to Mini Prism with glass @ 90°
2010/05/06	Dark	626.5430	626.5465	626.5469	626.5459	626.5455
2010/05/07	Dark	626.5428	626.5463	626.5463	626.5458	626.5449
2010/05/08	Dark	626.5429	626.5457	626.5466	626.5456	626.5451
2010/05/09	Light	626.5426	626.5458	626.5450	626.5457	626.5455
2010/05/10	Light	626.5426	626.5457	626.5453	626.5456	626.5455
2010/05/11	Light	626.5427	626.5456	626.5455	626.5459	626.5459
2010/05/12	Non	626.5429	626.5447	626.5446	626.5447	626.5446
2010/05/13	Non	626.5428	626.5446	626.5445	626.5446	626.5444
2010/05/14	Non	626.5427	626.5445	626.5446	626.5444	626.5445

Table 7.13: Average daily HD readings to Circular Prism

Date	Glass Colour (Tinted)	Ave HD to Circular Prism without glass	Ave HD to Circular Prism with glass @ 30°	Ave HD to Circular Prism with glass @ 45°	Ave HD to Circular Prism with glass @ 60°	Ave HD to Circular Prism with glass @ 90°
2010/05/06	Dark	626.5404	626.5432	626.5433	626.5429	626.5427
2010/05/07	Dark	626.5405	626.5431	626.5433	626.5427	626.5424
2010/05/08	Dark	626.5407	626.5439	626.5436	626.5432	626.5430
2010/05/09	Light	626.5408	626.5429	626.5431	626.5429	626.5425
2010/05/10	Light	626.5403	626.5426	626.5422	626.5424	626.5421
2010/05/11	Light	626.5406	626.5425	626.5428	626.5427	626.5422
2010/05/12	Non	626.5405	626.5420	626.5420	626.5422	626.5422
2010/05/13	Non	626.5404	626.5421	626.5421	626.5423	626.5420
2010/05/14	Non	626.5405	626.5419	626.5420	626.5421	626.5419

Table 7.14: Average daily HD readings to Prism

Date	Glass Colour (Tinted)	Ave HD to Prism without glass	Ave HD to Prism with glass @ 30°	Ave HD to Prism with glass @ 45°	Ave HD to Prism with glass @ 60°	Ave HD to Prism with glass @ 90°
2010/05/06	Dark	626.5417	626.5449	626.5451	626.5444	626.5441
2010/05/07	Dark	626.5417	626.5447	626.5448	626.5443	626.5437
2010/05/08	Dark	626.5418	626.5448	626.5451	626.5444	626.5441
2010/05/09	Light	626.5417	626.5444	626.5441	626.5443	626.544
2010/05/10	Light	626.5415	626.5442	626.5438	626.544	626.5438
2010/05/11	Light	626.5416	626.5441	626.5442	626.5443	626.5441
2010/05/12	Non	626.5417	626.5434	626.5433	626.5435	626.5434
2010/05/13	Non	626.5416	626.5434	626.5433	626.5435	626.5432
2010/05/14	Non	626.5416	626.5432	626.5433	626.5433	626.5432

The above table 7.14 is reduced to an average of three days HD readings per glass colour. The impact of the angular variations on the HD readings is still within the accuracy limits in all the glass colour and angles tested. Therefore the researcher averaged all HD readings without minding the angles. Table 7.15 shows the average HD readings per 3days without and with glass.

Table 7.15: Average HD per glass colour

Glass Colour	Glass Thickness (mm)	Average HD without glass	Average HD with glass	Difference (Glass colour impact)
None tinted (0%)	3.00	626.5416	626.5433	0.0017
Light Tinted (5%)	3.00	626.5416	626.5441	0.0025
Dark Tinted (50%)	3.00	626.5416	626.5445	0.0029

Based on the established fact that 3.0 mm glass thickness (non-tinted) had not impact on the accuracy specification of the TCR 1201 total station used to measure the distances, the researcher removed non-tinted 3.0 mm glass reading from the glass colour analysis. Therefore we have:

Table 7.16: Average change in HD per glass colour

Glass colour	Without glass	With Glass (glass colour impact)
Light tinted (5% tint)	0	0.0025
Dark tinted (50% tint)	0	0.0029

The researcher applied the method of least squares estimators for simple linear regression model to analyze table 7.16, and tag glass colour (percentage tint level) as x and glass impact as y.

Table 7.17: Average change in HD per glass tint level or colour for least squares regression model

S/No	x_i (glass colour, i.e. % tint level)	y_i (glass impact, m)	$x_i y_i$	x_i^2
1	5	0.0025	0.0125	25
2	50	0.0029	0.1450	2500
Sum	55	0.0054	0.1575	2525
Mean	27.5	0.0027		

By substitute for the values in equations 7.10 and 7.11, we have:

$$\hat{b}_1 = \frac{\sum_{i=1}^{n} x_i y_i - n\bar{y}\bar{x}}{\sum_{i=1}^{n} x_i^2 - n\bar{x}^2} = \frac{0.1575 - 2(27.5X\,0.0027)}{2525 - 2(27.5)^2} = 9Exp^{-6}$$

$$\hat{b}_0 = \bar{y} - \hat{b}_1\bar{x} = 0.0027 - 9E^{-6}(27.5) = -0.0025$$

$$\hat{y}' = 9Exp^{-6}x' + 0.0025 \quad \text{.........} 7.15$$

The above table 7.16 was used to plot graph with Microsoft Excel to generate linear equation as shown in figure 7.4

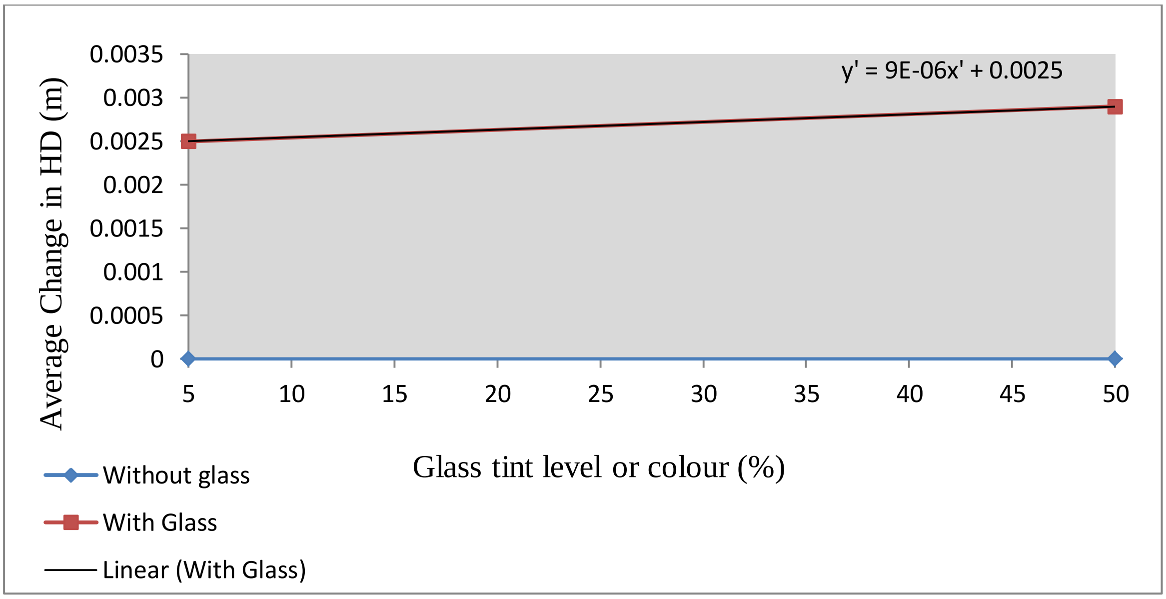

Figure 7.4: Graph of average change in HD against glass colour

Figure 7.4 yields the same linear regression equation as the equation 7.15 above. Therefore, the linear regression equation for correction of error generated as a result of glass colour is:

$$\hat{y}' = 9Exp^{-6}x' + 0.0025 \quad \text{.........} 7.15$$

where:

$\hat{y}'$ is the error caused by the glass colour (m); and

x' is the tint level or colour of the glass (%).

The implication of equation 7.15 above is that, when a 3.0 mm glass with light tinted (i.e. 5% level) colour is used; 0.0025 m must be subtracted from the HD measured through such glass to make such HD reading conform to the average HD reading without glass. Furthermore, when a 3.0 mm glass with dark tinted (i.e. 50% tint level) is used, 0.0029 m must be subtracted from each of the HD readings measured through such glass to make the readings conform to the average HD readings measured without glass.

The above equation 7.15 can be merged with formula for atmospheric variations correction when using infra-red EDM presented in equation 4.1 of chapter four.

Thus the new combined formula for atmospheric variations correction and glass colour (when using 3.0 mm tinted glass) impact correction is:

For infra-red EDM (IR):

$$k^{"} = \left[283.05 - \frac{79.7489P}{(273.15+t)} + \frac{11.27e}{(273.15+t)}\right].10^{-6} d^{'} - \left[9Exp^{-6} x' + 0.0025\right] \text{..................7.16}$$

The above equation 7.16 can be expressed as follows

$$k'' = a.10^{-6} d^{'} - \hat{y}' \text{...7.17}$$

where:

k" is the correction factor for atmospheric variation and glass colour effect;

$a.10^{-6}$ is the atmospheric variation correction formula;

d' is the measured distance as it appears on the total station digital screen; and

$\hat{y}'$ is the glass colour impact formula.

7.4 REMARK

In the glass thickness and the glass colour systematic error corrections formulae derived above, only the data set from the observations that has impact on the specification limits of the total station were used in the regression analysis (i.e. Tables 7.9 and 7.16). The likely effects of the data sets removed before the regression analysis are discussed below.

The complete observation data set presented in table 7.8 would yield:

Table 7.18: Average change in HD per glass thickness

Glass thickness	Without glass	With Glass (glass impact)
2	0	0.001
3	0	0.0016
4	0	0.0024
5	0	0.0031
6.38	0	0.0040

The above table was used to plot graph with Microsoft Excel to generate regression equation:

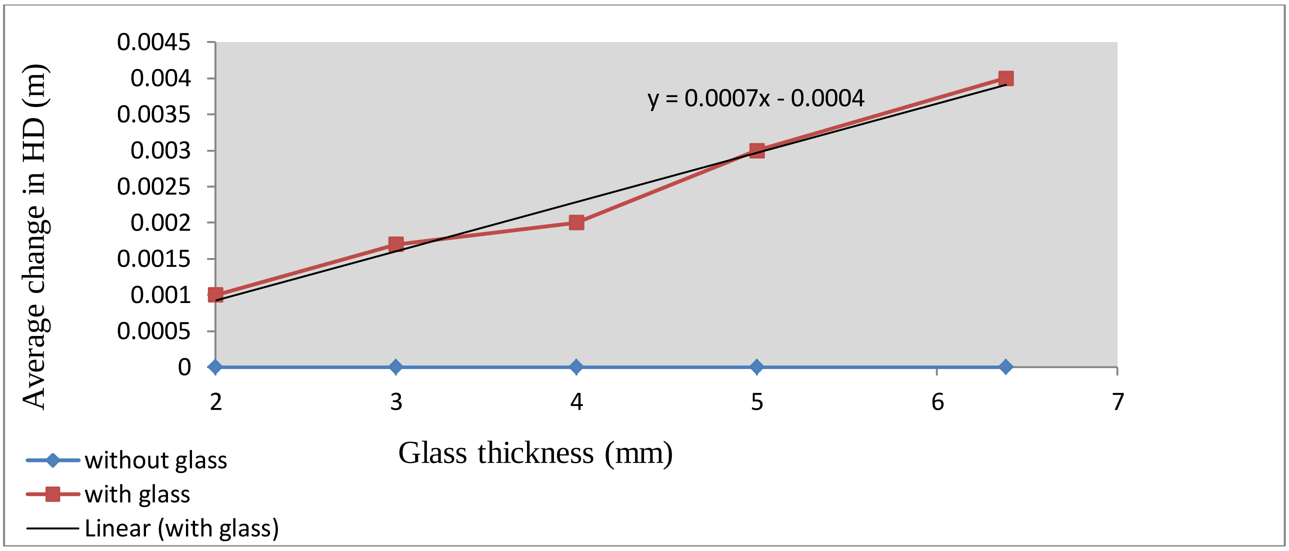

Figure 7.5: Graph of average change in HD against glass thickness when complete data set is used

Likewise, the complete data set presented in table 7.15 would yield:

Table 7.19: Average change in HD per glass colour

Glass colour	Without glass	With Glass (glass colour impact)
Non–tinted (0% tint)	0	0.0017
Light tinted (5% tint)	0	0.0025
Dark tinted (50% tint)	0	0.0029

The above table was used to plot graph with Microsoft Excel to generate regression equation:

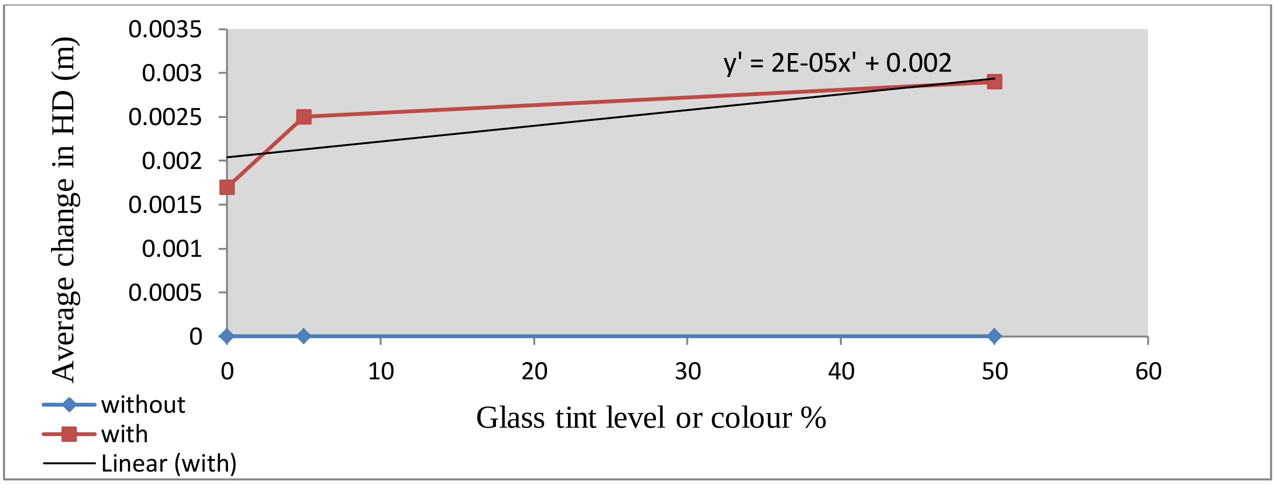

Figure 7.6: Graph of average change in HD against glass tint level when complete data set is used

The effect of not using complete observation data set (i.e. 2.0 mm and 3.0 mm) is presented in the table below:

Table 7.20: Effect on glass thickness regression analysis

Using only affected set of observation data in regression formation	Using all set of observation data in regression formation
y = 0.0008x - 0.0013	y = 0.0007x - 0.0004
when x = 4,	when x = 4,
y = 0.0008(4) – 0.0013 = 0.0019	y = 0.0007(4) – 0.0004 = 0.0024
Difference = 0.0005	
when x = 5	When x = 5
y = 0.0008(5) – 0.0013 = 0.0027	y = 0.0007(5) – 0.0004 = 0.0031
Difference = 0.0004	
when x = 6.38	when x = 6.38
y = 0.0008(6.38) – 0.0013 = 0.0038	y = 0.0007(6.38) – 0.0004 = 0.0041
Difference = 0.0003	

Table 7.21: Effect on glass colour regression analysis

Using only affected set of observation data in regression formation	Using all set of observation data in regression formation
y’ = $9E^{-6}$x’ + 0.0025	y’ = $2E^{-5}$x’ + 0.0020
when x’ = 5% i.e. light tinted glass	when x’ = 5% i.e. light tinted glass
y’ = $9E^{-6}$(5) + 0.0025 = 0.0025	y’ = $2E^{-5}$(5) + 0.002 = 0.0021
Difference = 0.0004	
when x’ = 50% i.e. dark tinted glass	when x’ = 50% i.e. dark tinted glass
y’ = $9E^{-6}$(50) + 0.0025 = 0.003	y’ = $2E^{-5}$(50) + 0.002 = 0.003
Difference = 0.0000	

The differences in results of the two formulae are small. As demonstrated in chapter five that it is not necessary to apply correction if the glass thickness is less than 3.0 mm. Therefore, it is recommended that the regression formula only be applied for thickness above 3.0 mm and tint 3.0 mm glass.

However, if deem it fit to apply corrections to glass thickness ≤ 3.0 mm in any situation at hand, especially when short observation (i.e. < 20 m) are made with total station from shelter glass, the equations 7.12, 7.13, 7.15 and 7.16 above would change to:

$$\hat{y} = 0.0007x - 0.0004 \qquad \text{7.12}a$$

$$k^{'} = \left[283.05 - \frac{79.7489P}{(273.15+t)} + \frac{11.27e}{(273.15+t)}\right].10^{-6} d^{'} - [0.0007x - 0.0004] \qquad \text{7.13}a$$

$$\hat{y}' = 2Exp^{-5}x' + 0.002 \qquad \text{7.15}a$$

$$k^{''} = \left[283.05 - \frac{79.7489P}{(273.15 + t)} + \frac{11.27e}{(273.15 + t)} \right] .10^{-6} d^{'} - \left[2Exp^{-5} x' + 0.002 \right] \text{......................} 7.16a$$

7.5 FINAL DISTANCE EQUATIONS AFTER ALL CORRECTIONS

The final distance after atmospheric and glass correction (i.e. if glass thickness 4.0 mm and above is used) will be:

$$d = d^{'} + k^{'} \text{..} 7.18$$

If 3.0 mm coloured glass is used, correct distance reading will be:

$$d = d^{'} + k^{''} \text{..} 7.19$$

7.6 COMPARISON OF REGRESSION MODEL DEVELOPED TO PHYSICAL MODEL.

The regression model developed for glass thickness correction was compared to the physical model by using information on physical effect of glass medium on light beam discussed in section 2.12 in chapter two of this report.

Computation of Refractive Effects on Distance Measurements

During distance measurement to the short monitoring target, the following were recorded:

t_g = 3.0 mm — Thickness of the glass

θ' = 60° — Angle of incidence of total station beam with shelter glass

n_{ao} = 1.00028 — Refractive index of air (see table 2.6 in chapter two)

n_g = 1.52 — Refractive index of shelter glass (see sub-section 4.2.5 in chapter four)

The angle of refraction of the total station beam

Using equation 2.50 in chapter two:

$sd_{total} = sd_i + sd_g + sd_o$ ……………………………………………2.50

(where $sd_g = \frac{t_g}{\cos(\theta_g)}$; and $\theta_g = \sin^{-1}\left[\sin(\theta)\times\frac{n_a}{n_g}\right]$)

θ_g is the angle of refraction within the glass;

sd_g is the actual distance within the glass that the beam suppose to travel

$$\theta_g = \sin^{-1}\left[\sin 60\times\frac{1.00028}{1.52}\right] = 34.7^\circ$$

$$sd_g = \frac{3}{\cos 34.7} = 3.65mm$$

The measured distance within the glass by the total station is sd_{gm} (see equation 2.53 in chapter two):

$Prism_m (Y_m) = (sd_i + sd_{gm} + sdo).\sin(\theta)$; $Prism_m (X_m) = (sd_i + sd_{gm} + sdo).\cos(\theta)$;

(where: $sd_{gm} = sd_g \times\frac{n_g}{n_{ao}}$)

$$= 3.65\times\frac{1.52}{1.00028} = 5.546mm$$

The difference between the actual distance sd_g that the RTS suppose to measure and the measured distance sd_{gm} is the refractive effect caused by the glass material.

Refractive effect of 3.0 mm glass = 5.546 – 3.65

= 1.89 mm

Using the same procedures, the sd_g for 4.0 mm, 5.0 mm and 6.38 mm would be: 4.868 mm, 6.085 mm and 7.764 mm. While the corresponding sd_{gm} would be: 7.3967 mm, 9.246 mm and 11.798 mm.

Therefore, their refractive effects would be: 2.51 mm, 3.2 mm and 4.03 mm.

These can be summarized in the table below:

Difference between the physical model and the regression model results

Glass thickness	Physical model (mm)	Regression model (mm)	Difference (mm)
3	1.89	1.70	0.19
4	2.51	2.40	0.11
5	3.20	3.10	0.10
6.38	4.03	4.07	0.04

The variation is very small (i.e. less than 0.2 mm). This is an indication that the regression model developed is effective despite being a much simpler approach.

However, the little variation may be as a result of non-attainability of the assumptions stated in section 2.12 in chapter two of this report. The assumptions are:

a. the glass is perfectly flat on both sides;
b. the inside and outside surfaces of the glass are parallel;
c. the glass molecules are pure, i.e. without bubbles in the inner structure of the glass
d. the glass refractive index is uniform;
e. the refractive index of air inside the shelter is identical to that outside of the shelter; and
f. the refractive index of the air is uniform.

7.7 CONCLUSION

This chapter has given a brief discussion of steps taken to develop systematic error correction formulae that can cater for the effect of glass properties (thickness and colour) on distance measurement. It generated the following corrections for:

- Glass thickness impact correction, $\hat{y} = 0.0008x - 0.0013$
- Glass colour impact correction, $\hat{y}' = 9Exp^{-6}x' + 0.0025$
- Combined atmospheric and glass thickness corrections,

$$k^{'} = \left[283.05 - \frac{79.7489P}{(273.15+t)} + \frac{11.27e}{(273.15+t)} \right].10^{-6}d^{'} - [0.0008x - 0.0013]$$

- Combined atmospheric and glass colour corrections,

$$k^{''} = \left[283.05 - \frac{79.7489P}{(273.15+t)} + \frac{11.27e}{(273.15+t)} \right].10^{-6}d^{'} - [9Exp^{-6}x' + 0.0025]$$

The chapter also compared the regression model developed to physical model. The outcome of the comparison revealed that the model is good with maximum deviation of less than 0.2 mm from physical model.

The next chapter tests the effectiveness of the formulae generated on new set of distance readings. The bases for validation of the new formulae on new distance readings and not on the earlier set of distance readings is to confirm the efficacy of these formulae. The chapter also discusses steps taken to write a computer programming and develop nomograms based on the result validation.

CHAPTER EIGHT

8.0 VALIDATION OF THE FORMULAE AND SOFTWARE DEVELOPMENT

The previous chapter described the steps taken to develop the systematic error correction formulae required when taking measurements through a glass medium. This chapter describes the tests performed on the new glass impact formulae to ascertain their effectiveness in reducing the glass impacts on HD readings. Also covered in this chapter is a description of the software and nomograms developed when applying the said formulae.

8.1 DATA COLLECTION FOR VALIDATION PURPOSES

In order to test for the effectiveness of the systematic correction formulae, two new target stations were chosen to resemble the surface mine environment. The line-of-sight to the two stations passed through a roofing sheets (for varying heat generation), football pitch (for dust generation) and high way (for car exhaust and dust generation). Dust, smoke and varying temperature reading are characteristics of mine environments; all these factors were experienced in these new target stations. The first sets of HD readings were taken when the target was placed between (i.e. about 468 m horizontal distance between the total station and the targets) short- and long-distance monitoring stations used for the data analyzed in chapters five and six. The target was placed far away from the total station (i.e. about 697 m length) to generate the second set of HD readings for the validation purposes. This second target position was beyond the long-distance monitoring position used in chapters five and six. (Figure E.1 of appendix E shows the map of campus observation stations and the two new target positions used for the validation tests and their line-of-sights). During the first set of HD measurements for the model tests, each glass material (i.e. glass thickness 4.0 mm, 5.0 mm and 6.38 mm for thickness test, while light- and dark-tinted glass were used for glass colour test) was used for two days from 6.0 am to 6.0 pm daily. The data acquired were corrected for prism constant, scale factor and atmospheric corrections. The targets were later moved to the second station and each glass material was used for only one day as against two days in the first target station. The data acquired for the systematic error correction formulae validation tests are presented in the raw observation data book (i.e. appendix E.1 of appendix E). The data acquired was later corrected for prism constant, scale factor and atmospheric corrections. This data was subjected to further analysis and tests to remove the glass impacts on the acquired HD readings as shown below:

8.2 GLASS THICKNESS CORRECTION FORMULA TEST

The results of glass thickness model test are presented graphically in two ways: before applying the glass thickness correction formula and after applying the glass thickness correction formula. Each target (Leica mini and circular prisms) was analyzed separately.

8.2.1. First target station

The results of data analysis when monitoring to the Leica mini prism at the first target station are shown in figures 8.1 and 8.2. The corresponding results when monitoring to the Leica circular prism are shown in figures 8.3 and 8.4.

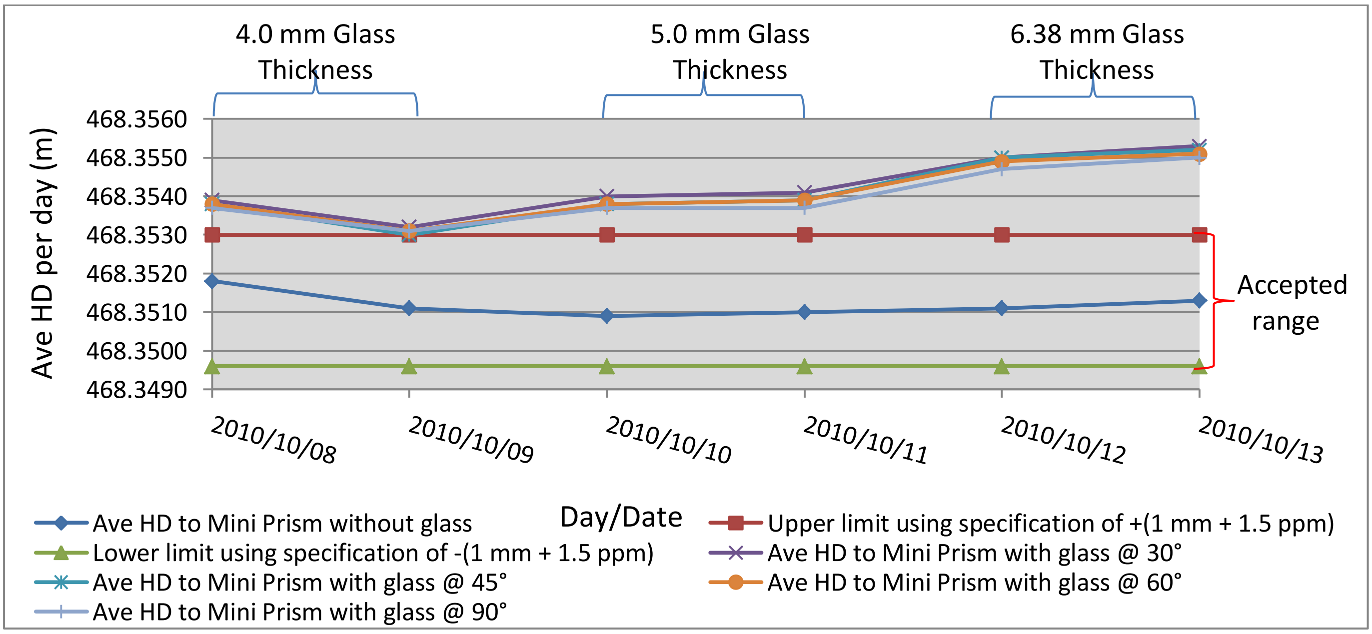

Figure 8.1: Average HDs to mini prism after prism constant, scale factor and atmospheric corrections but before glass thickness correction – first target station

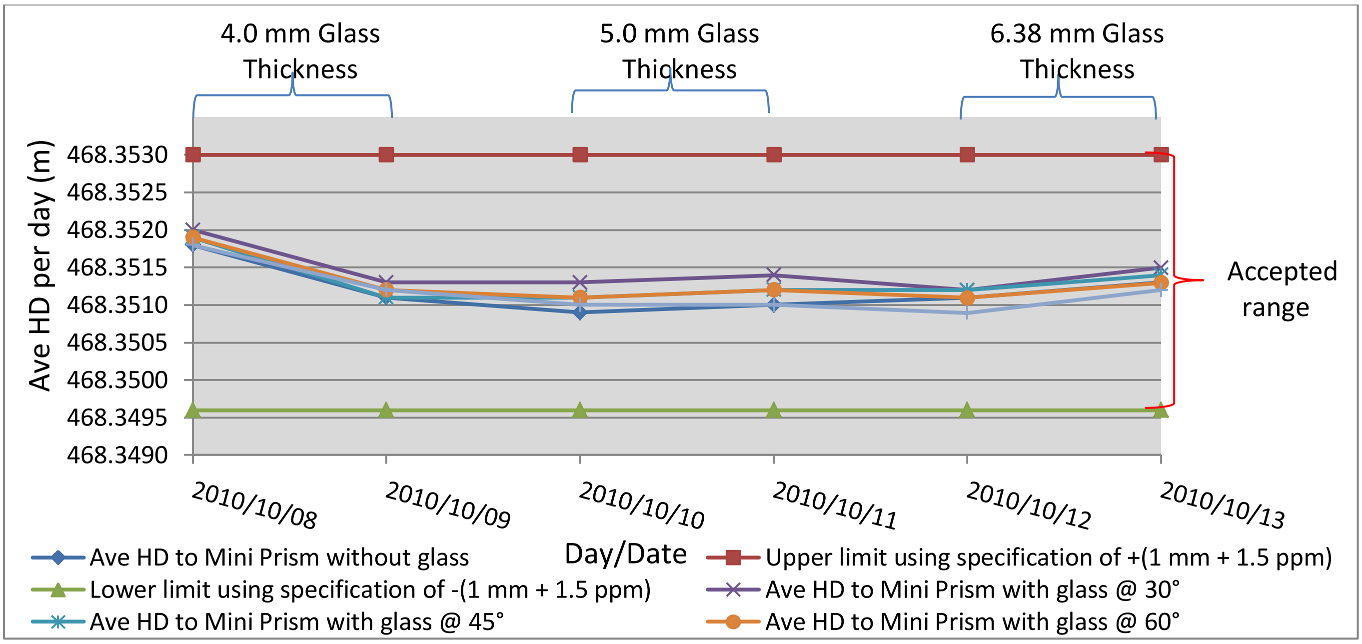

Figure 8.2: Average HDs to mini prism after all corrections (i.e. prism constant, scale factor, atmospheric and glass thickness corrections) – first target station.

Figure 8.1 shows the result of HD measurements to the mini prism when the target was placed in the first target station (i.e. between short- and long-monitoring stations). The graph clearly reveals that only HD readings taken without glass are within the accuracy limits, while all other readings taken when there was glass in place are outside the accuracy limits even after correcting for scale factor, prism constant and atmospheric corrections. The glass thickness impact on the HD measurements ranged between 1.9 mm and 2.1 mm when 4.0 mm glass was used. It ranged between 2.7 mm and 3.1 mm when 5.0 mm glass was used; while 6.38 mm glass impact ranged between 3.6 mm and 4.0 mm. The result trend changed after taking the glass thickness correction formula into account, with all the HD readings coming within the accuracy limits. The impact range caused by 4.0 mm glass thickness reduced to 0.0 mm and 0.2 mm; while 5.0 mm glass impact range changed to 0.0 mm and 0.4 mm. The 6.38 mm glass impact range reduced to -0.2 mm and 0.2 mm after correcting for glass thickness. These trends are shown in figure 8.2.

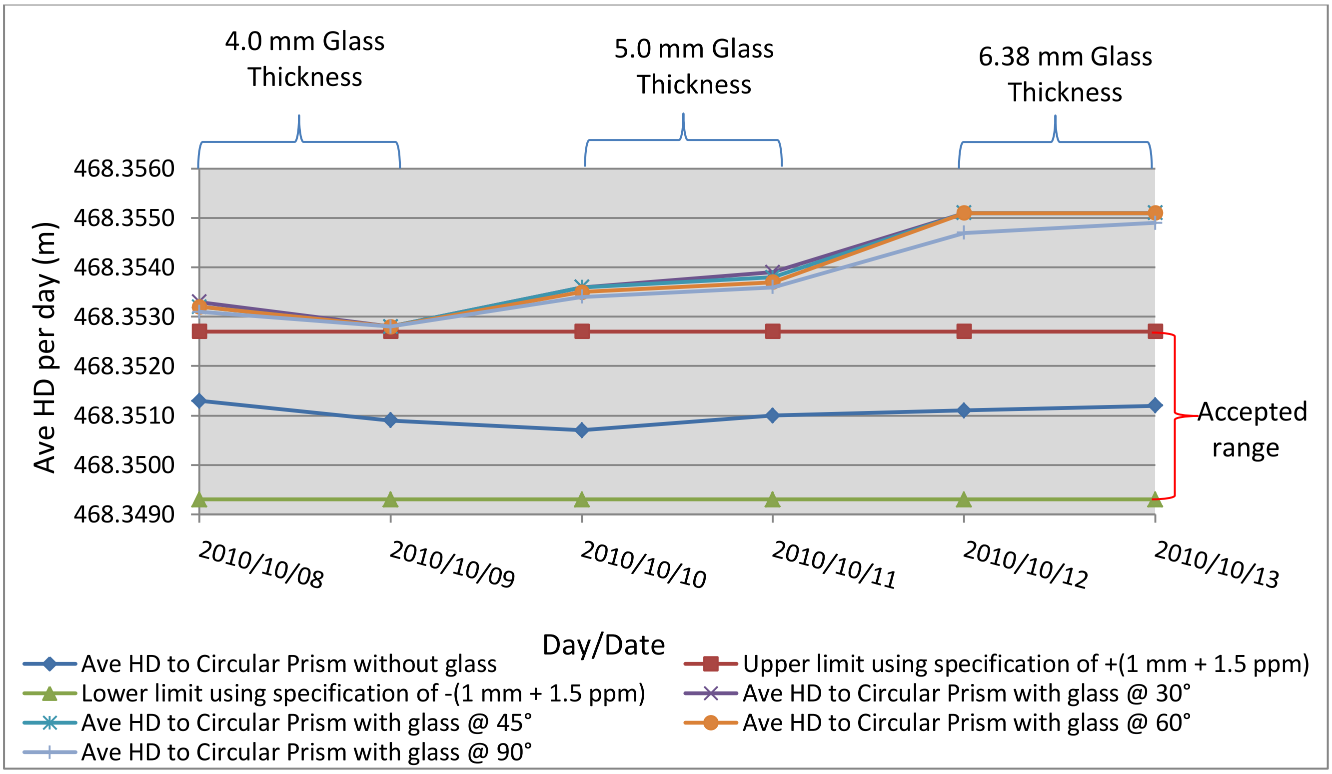

Figure 8.3: Average HDs to circular prism after prism constant, scale factor and atmospheric corrections but before glass thickness correction – first target station

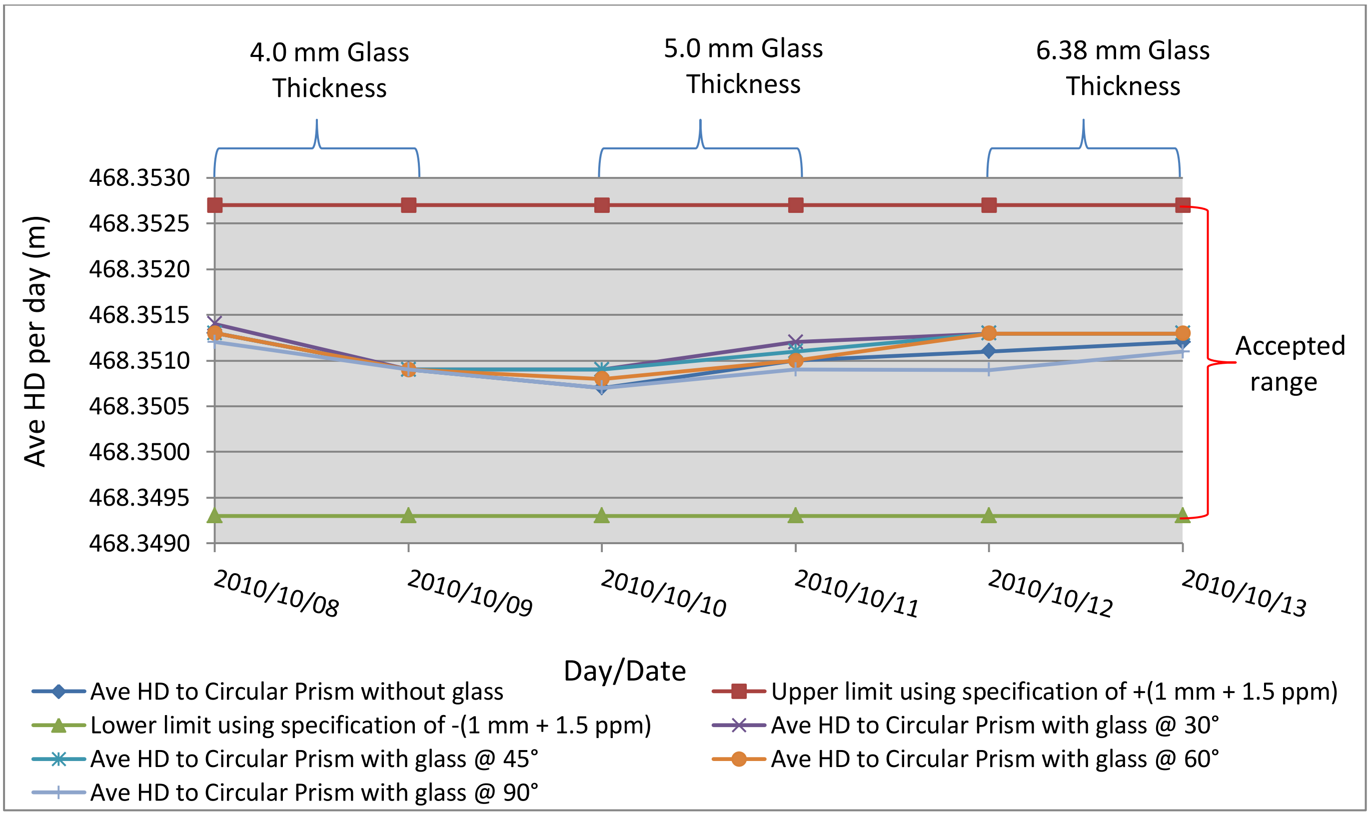

Figure 8.4: Average HDs to Circular prism after all corrections (i.e. prism constant, scale factor, atmospheric and glass thickness corrections) – first target station

Figure 8.3 shows the result of HD measurements to the circular prism at the first target station. The trend in figure 8.3 is similar to that of figure 8.1. The impact ranged between 1.8 mm and 2.0 mm when 4.0 mm glass was used. It ranged between 2.6 mm and 2.9 mm when 5.0 mm glass was used; while 6.38 mm glass caused 3.6 mm and 4.0 mm impacts. The situation also changed after applying the glass thickness correction formula as shown in figure 8.4. The impact range caused by 4.0 mm glass reduced to -0.1 mm and 0.1 mm; 5.0 mm glass impact range changed to -0.1 mm and 0.2 mm; while 6.38 mm glass impact changed to -0.1 mm and 0.2 mm after applying the glass thickness correction formula to the HD readings. The formula was deemed more effective when applying to HDs measured to the circular prism than when measured to the mini prism because of the highest impact range after applying the glass thickness factor to the circular prism is 0.2 mm as against 0.4 mm in mini prism as shown in figure 8.2. This is a clear indication that the size of the prism mattered during slope monitoring to prism targets.

8.2.2. Second target station

The results when monitoring to the Leica mini prism at the second target station during glass thickness correction formula test are shown in figures 8.5 and 8.6. The corresponding results when monitoring to the Leica circular prism are shown in figures 8.7 and 8.8.

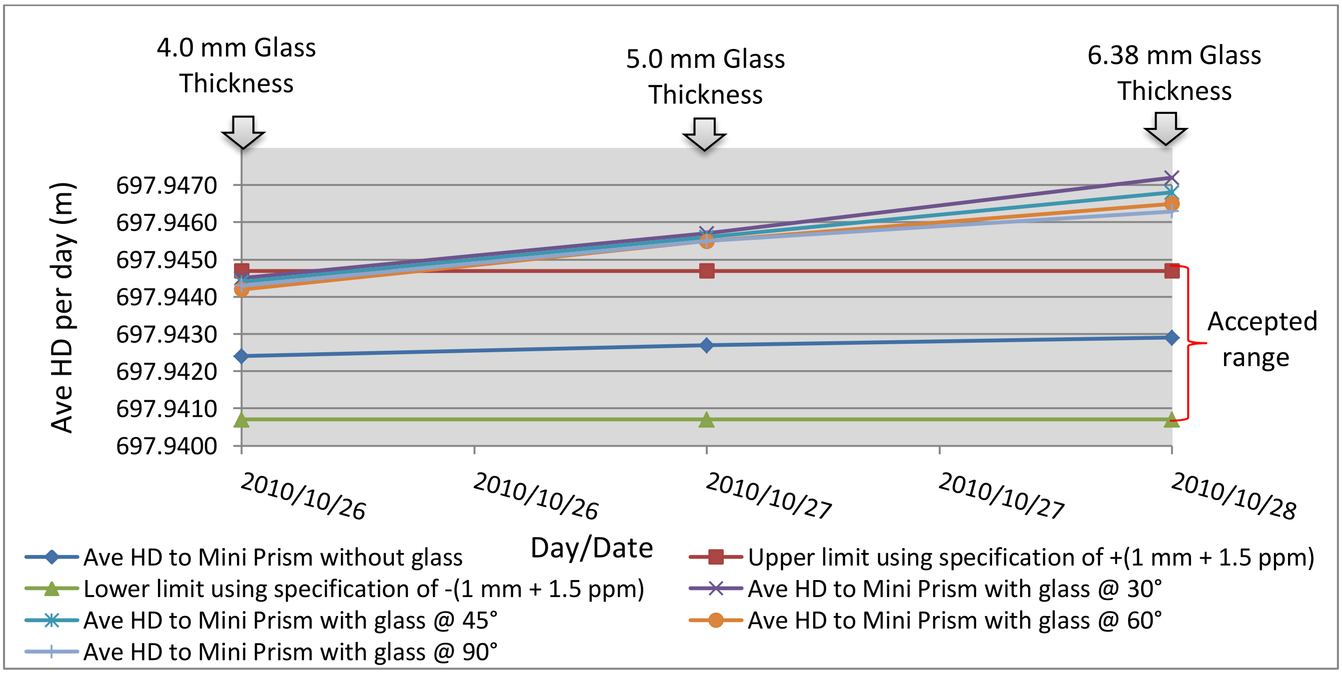

Figure 8.5: Average HDs to mini prism after prism constant, scale factor and atmospheric corrections but before glass thickness correction – second target station

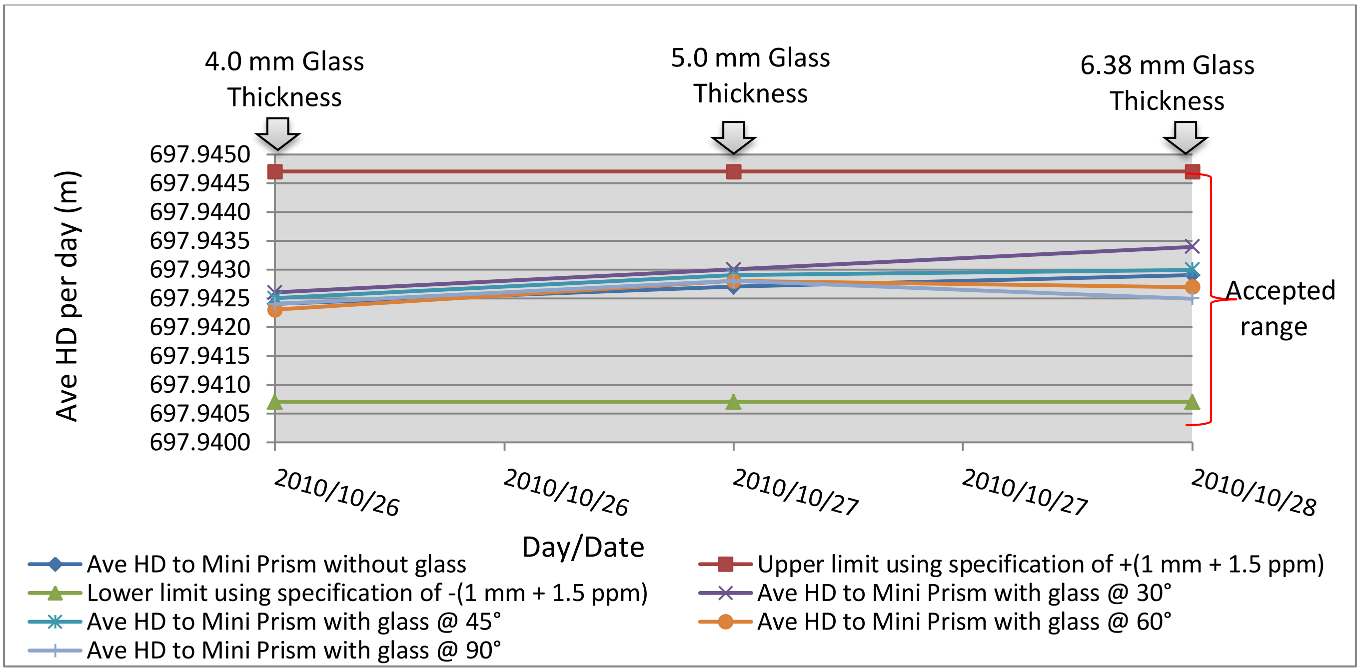

Figure 8.6: Average HDs to mini prism after all corrections (i.e. prism constant, scale factor, atmospheric and glass thickness corrections) – second target station.

Figure 8.5 is similar to Figures 8.1 and 8.3 described above. However, the impact caused by 4.0 mm glass was within the accuracy limits together with HD readings without glass; the reason for could have been attributed to the accuracy limits increase with an increase in HD measurements. All other HDs measured, when there was glass in place, were outside the accuracy limits. The impact ranged between 1.8 mm and 2.1 mm when 4.0 mm glass was used. It ranged between 2.8 mm and 3.0 mm when 5.0 mm glass was used; while 6.38 mm glass caused 3.4 mm and 4.3 mm impacts. The impacts changed after applying the glass thickness correction formula as shown in figure 8.6. The impact reduced drastically. 4.0 mm glass impact range changed to -0.1 mm and 0.2 mm; 5.0 mm glass impact range changed to 0.1 mm and 0.3 mm; while 6.38 mm glass impact range changed to -0.4 mm and 0.5 mm after applying the glass thickness correction formula to the HD readings.

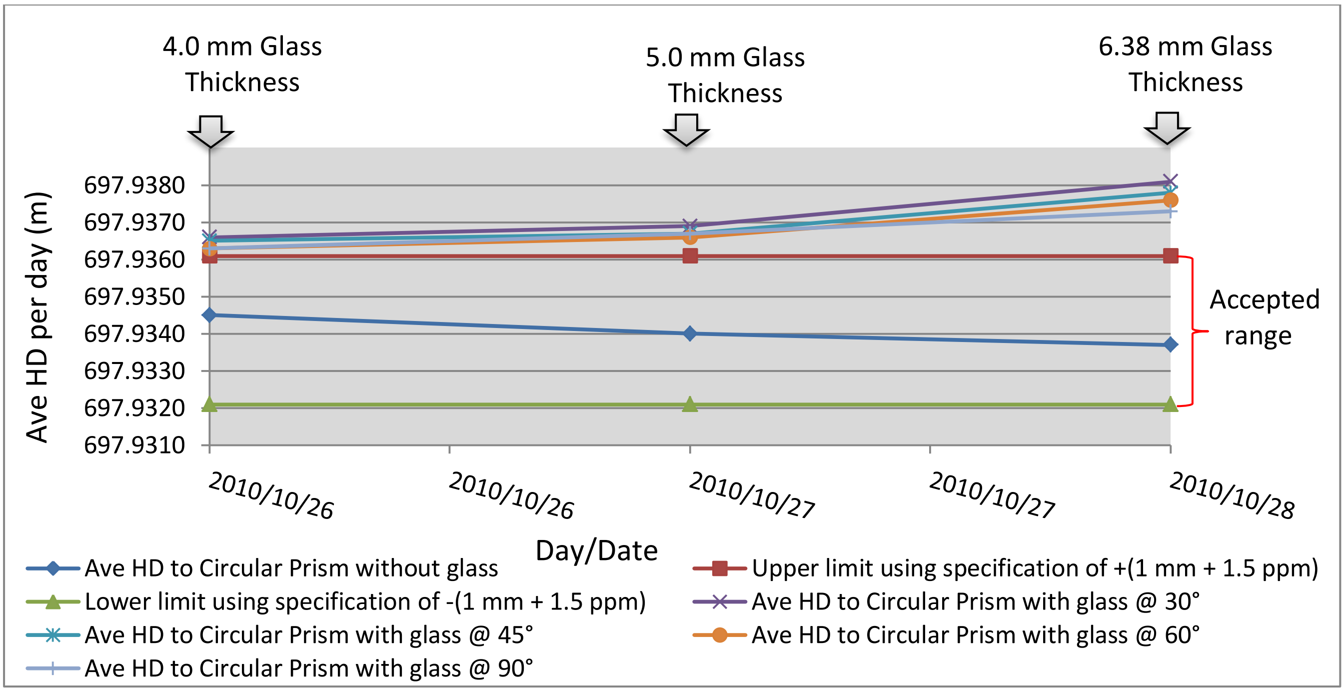

Figure 8.7: Average HDs to circular prism after prism constant, scale factor and atmospheric corrections but before glass thickness correction – second target station

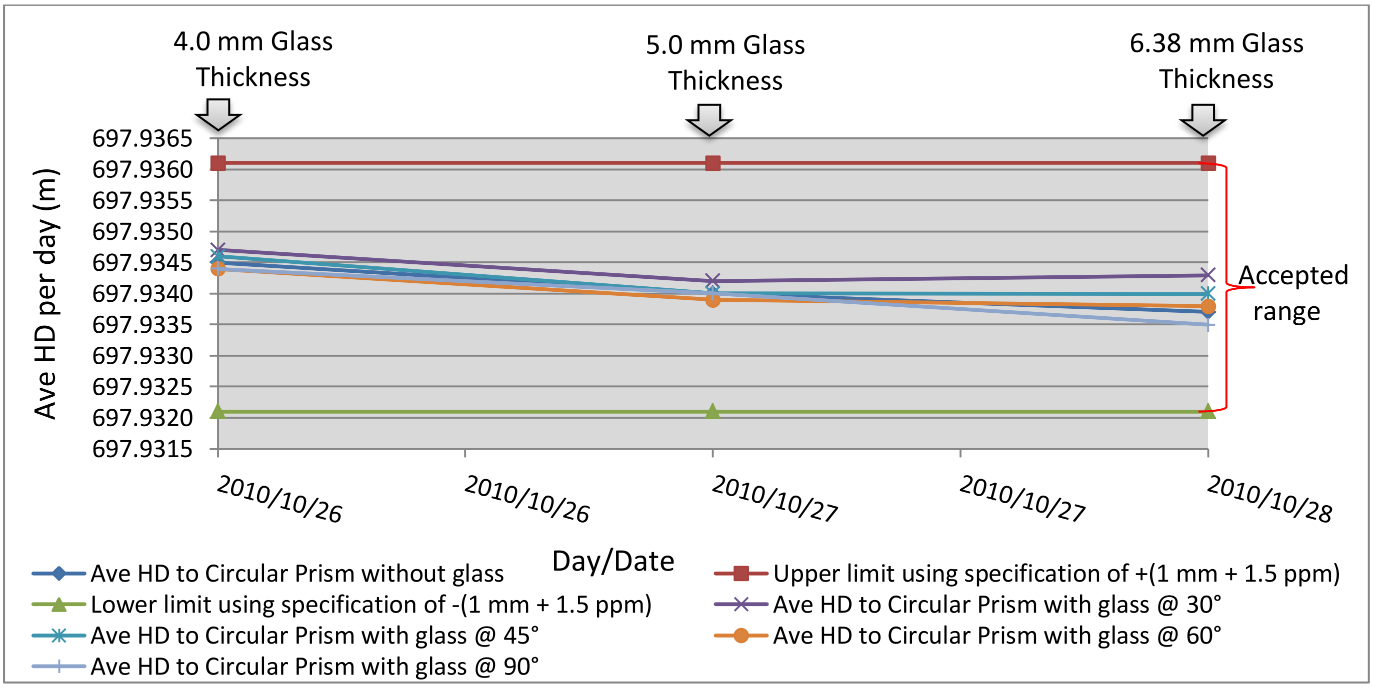

Figure 8.8: Average HDs to Circular prism after all corrections (i.e. prism constant, scale factor, atmospheric and glass thickness corrections) – second target station

Figure 8.7 is also similar to figures 8.1 and 8.3 described above. Only HDs measured without glass were within the accuracy limits. All other HDs measured when there was glass in place were outside the accuracy limits. The impact ranged between 1.8 mm and 2.1 mm when 4.0

mm glass was used. It ranged between 2.6 mm and 2.9 mm when 5.0 mm glass was used; while the impact caused by 6.38 mm glass ranged between 3.6 mm and 4.4 mm. The impact also changed after applying the glass thickness correction formula as shown in figure 8.8. The range of the impact caused by 4.0 mm glass thickness reduced to -0.1 mm and 0.2 mm; 5.0 mm glass impact changed to -0.1 mm and 0.2 mm; while 6.38 mm glass impact changed to -0.2 mm and 0.6 mm.

8.3 GLASS COLOUR CORRECTION FORMULA TEST

The results of glass colour formula test are also presented graphically in two ways: graph before applying glass colour correction formula and graph after applying glass colour correction formula. Each target (Leica mini and circular prisms) was also analyzed separately.

8.3.1 First target station

The results when monitoring to the Leica mini prism during glass colour model test when the target was placed in the first target station are shown in figures 8.9 and 8.10. The corresponding results when monitoring to the Leica circular prism are shown in figures 8.11 and 8.12.

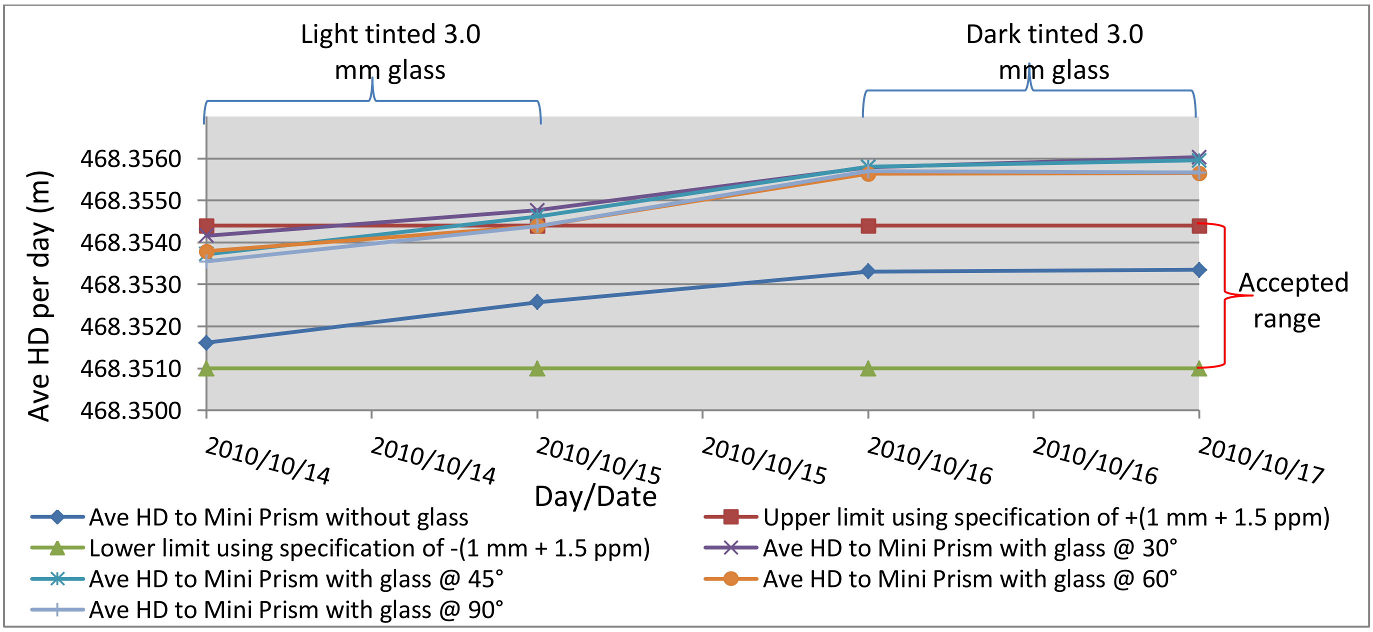

Figure 8.9: Average HDs to mini prism after prism constant, scale factor and atmospheric corrections but before glass colour correction – first target station

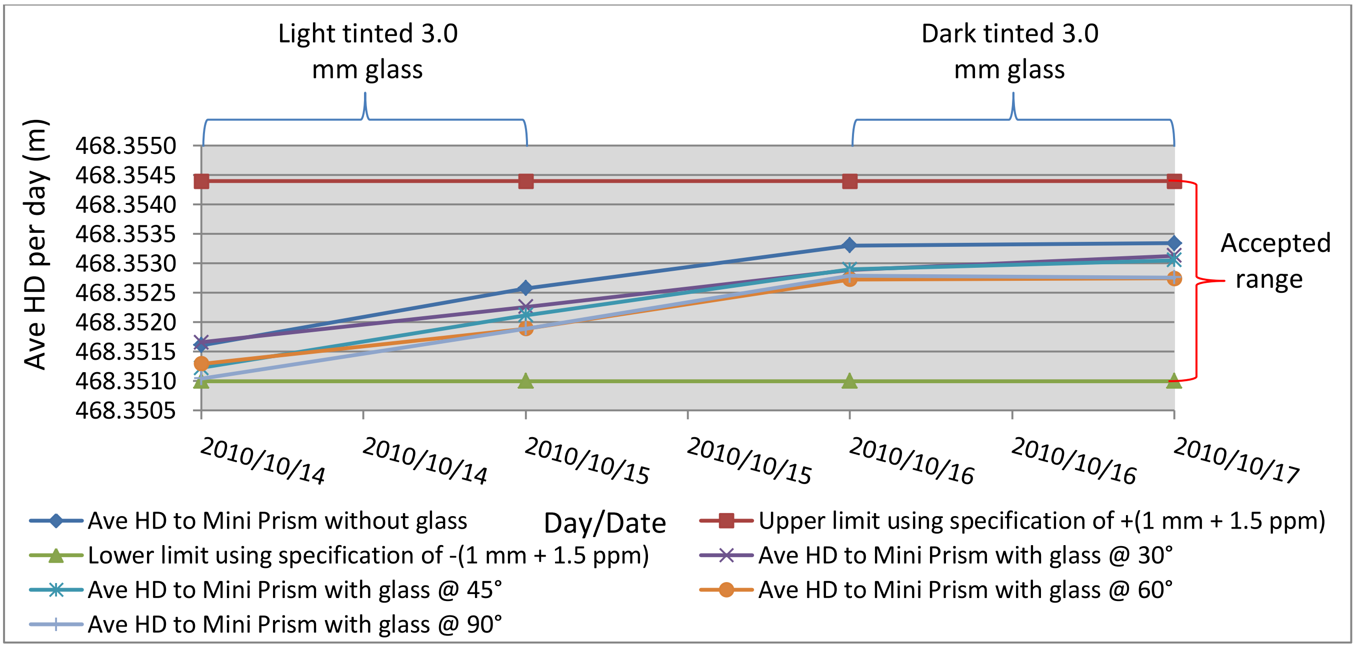

Figure 8.10: Average HDs to min prism after all corrections (i.e. prism constant scale factor, atmospheric and glass colour corrections) – first target station

Figure 8.9 shows the result of HD measurements to the mini prism when the target was placed in the first target station during glass colour model test. The graph clearly reveals that only HD readings taken without glass and with light-tinted glass on the first day of observation were within the accuracy limits. This conformity with the accuracy limits of light-tinted glass was not consistent as revealed on the second day of using light-tinted glass. All other HD readings taken when the glass was in place were outside the accuracy limits in spite of correcting the HDs for scale factor, prism constant and atmospheric corrections. The impact ranged between 1.8 mm and 2.6 mm when light-tinted glass was used. It also ranged between 2.3 mm and 2.7 mm when dark-tinted glass was used. The situation changed after applying the glass colour correction formula as shown in figure 8.10. In the graph, all the HDs are within the accuracy limits. The light-tinted glass impact changed to -0.7 mm and 0.1 mm, while dark-tinted glass impact changed to -0.6 mm and -0.2 after applying the glass colour impact correction formula to the HD readings.

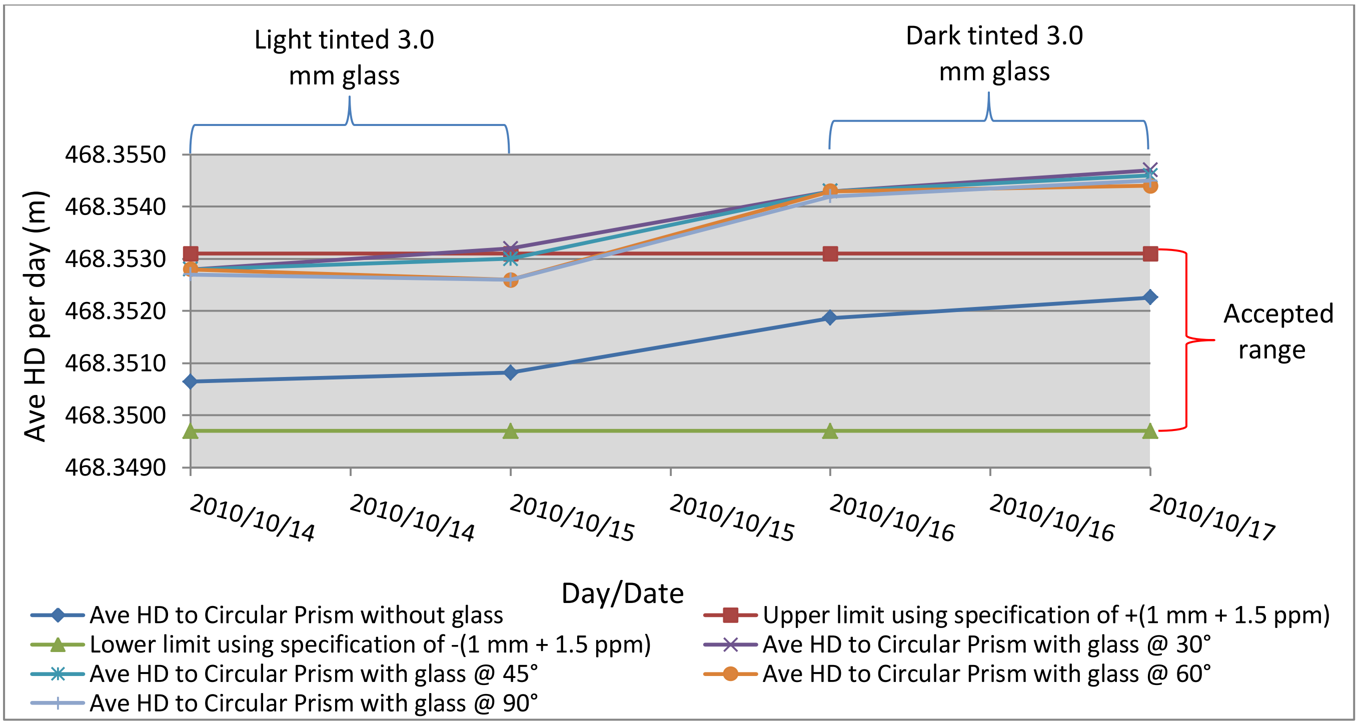

Figure 8.11: Average HDs to circular prism after prism constant, scale factor and atmospheric corrections but before glass colour correction – first target station

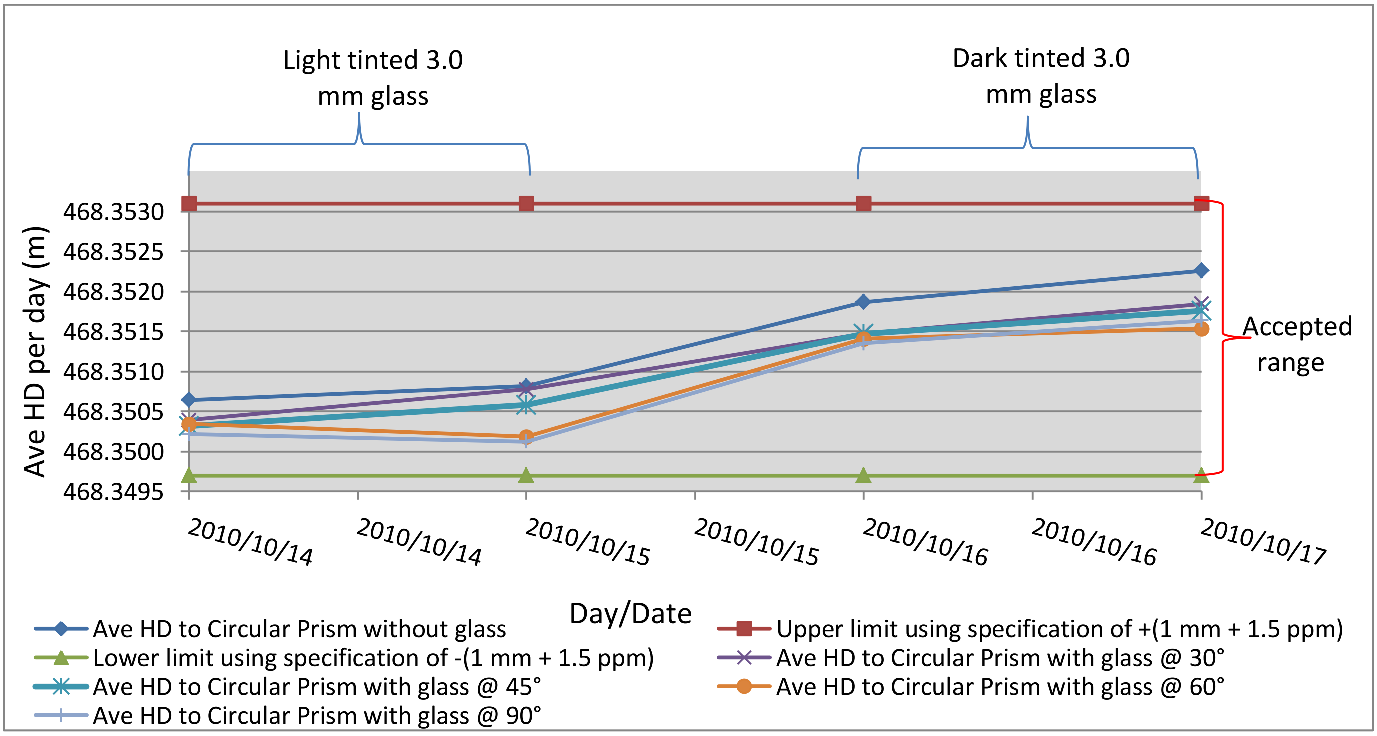

Figure 8.12: Average HDs to circular prism after all corrections (i.e. prism constant scale factor, atmospheric and glass colour corrections) – first target station

Figure 8.11 shows the result of HD measurements to the circular prism during glass colour impact model test when the target was placed in the first target station. The trend in Figure 8.11 is similar to that of figure 8.9. The impact ranged between 1.8 mm and 2.4 mm when light-tinted glass was used. It also ranged between 2.1 mm and 2.4 mm when dark-tinted glass was used. In addition, the situation changed after applying the glass colour impact correction formula as shown in figure 8.12. The impact caused by 3.0 mm light-tinted glass reduced to -0.7 mm and 0.0 mm, while dark-tinted 3.0 mm glass impact changed to -0.7 mm and -0.4 after applying the glass colour impact correction formula to the HD readings.

8.3.2 Second target station

At the second target station, only HD readings without and with light-tinted glass could be measured. The total station consistently signalled Error 256 when measurements were taken through dark-tinted glass. Therefore, only HDs without and with light-tinted glass were analysed. The results when monitoring to Leica mini prism at second target station during glass colour model test are shown in figures 8.13 and 8.14. The corresponding results when monitoring to Leica circular prism are shown in figures 8.15 and 8.16.

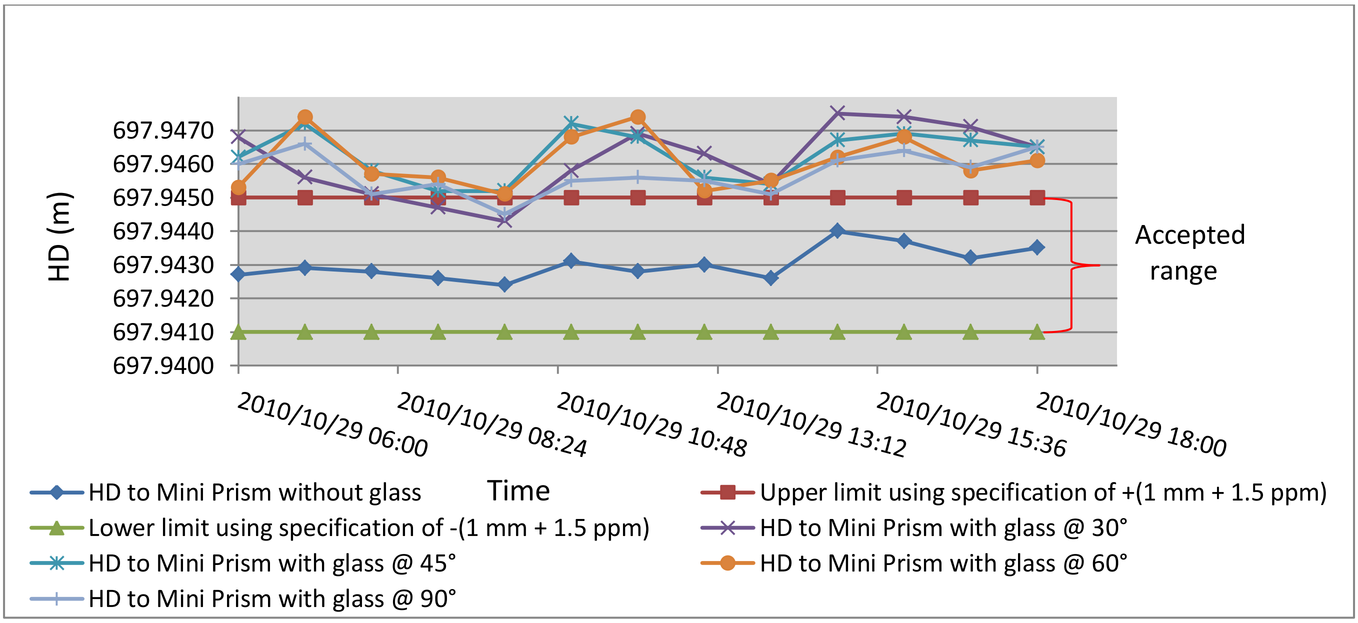

Figure 8.13: HDs to mini prism after prism constant, scale factor and atmospheric corrections but before glass colour correction using light tinted 3.0 mm glass – second target station

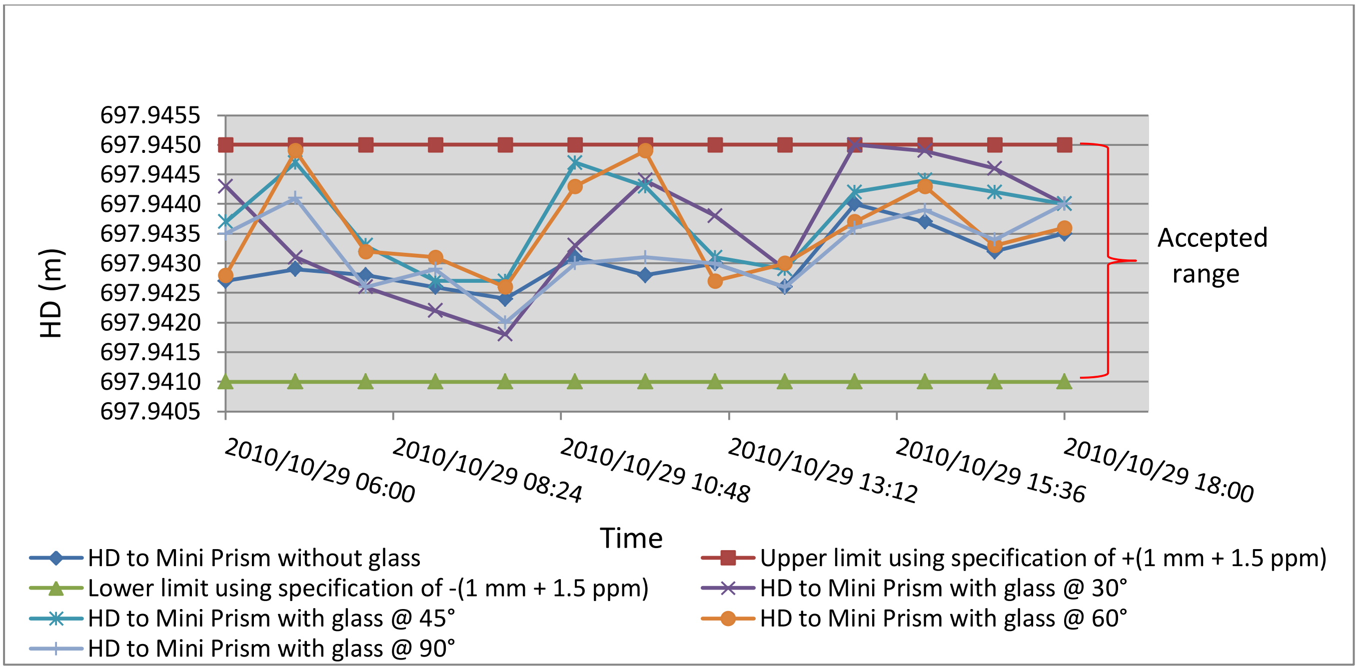

Figure 8.14: HDs to mini prism after all corrections (i.e. prism constant scale factor, atmospheric and glass colour corrections) using light tinted 3.0 mm glass – second target station

Figure 8.13 reveals that only HD readings without glass are within the accuracy limits. All other HDs measured when light-tinted glass in place was outside the accuracy limits. The impact ranged between 1.9 mm and 4.1 mm when light-tinted glass was used. The impact changed to -0.6 mm and 1.6 mm after applying the glass colour impact correction formula as shown in figure 8.14.

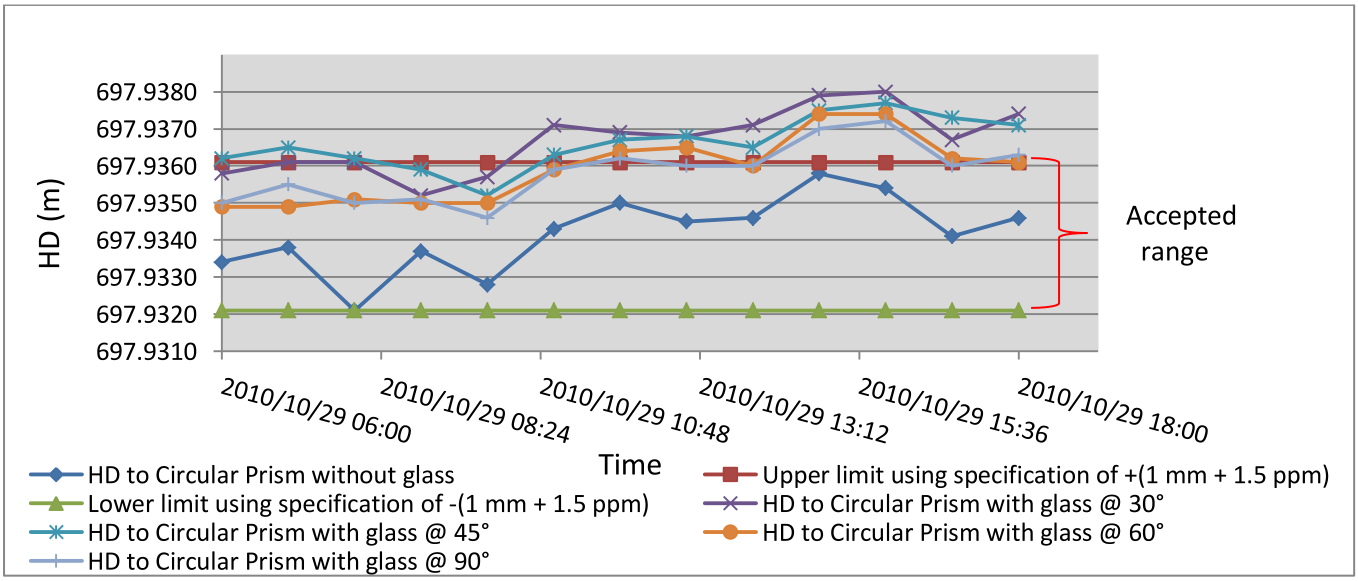

Figure 8.15: HDs to circular prism after prism constant, scale factor and atmospheric corrections but before glass colour correction using light tinted 3.0 mm glass – second target station

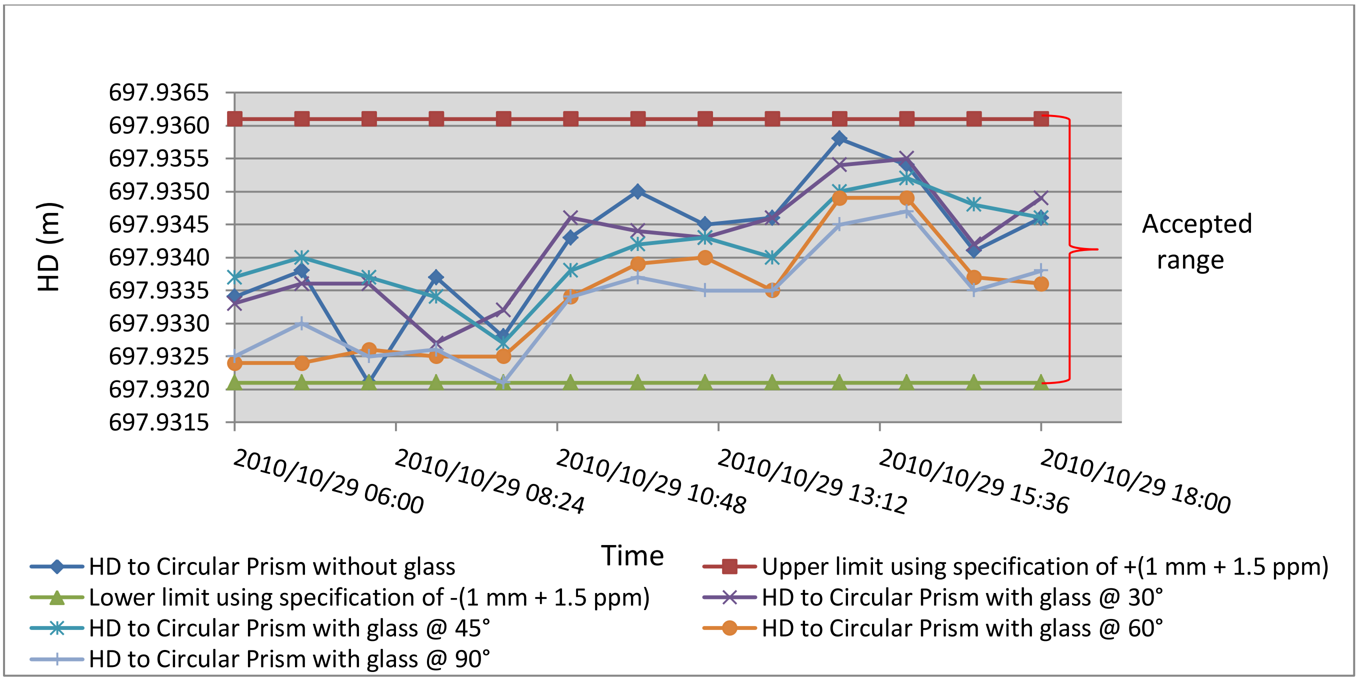

Figure 8.16: HDs to circular prism after all corrections (i.e. prism constant scale factor, atmospheric and glass colour corrections) using light tinted 3.0 mm glass – second target station.

Figure 8.15 is similar to figures 8.13 described above. Only HDs measured without glass were within the accuracy limits; all other HDs measured with light-tinted glass in place were outside the accuracy limits. The impact caused by the light-tinted glass ranged between 1.2 mm and 4.0 mm. In addition, the impact reduced to -1.1 mm and 1.6 mm after the application of the glass thickness correction formula as shown in figure 8.16.

8.4 DATA COLLECTION FOR VALIDATION PURPOSES AT OPEN PIT MINE

In order to evaluate the performance of the correction formulae in actual mine conditions, an active open pit mine was identified. The mine's existing monitoring beacons and prisms were used in the test. These beacons initially were established by the survey department using conventional survey and GPS post processing methods so that accuracy specifications could be met. The mine is 1.5 km wide by 3.0 km long and 400 m deep. To carrying out the validation test, two of the secondary beacons were used (i.e. one as monitoring beacon and the other for orientation), because the primary beacons were fully occupied by the slope stability monitoring department of the mine. A monitoring target installed on the southern side of the pit was used for distance monitoring purposes. The southern side of the pit is the most active area with activities such as drilling, blasting and hauling (i.e. ideal mine environment).

The total station (Leica TM 30) was mounted on the selected secondary beacon and orientated. Twenty distance readings were taken to a target (Leica Circular prism) and recorded in the field book. A 4.0 mm glass was place (closed to the total station telescope) in between the total station and the target, another twenty distance readings were taken and recorded. The 4.0 mm was later replaced by 5.0 mm 6.83 mm, 3.0 mm light-tinted and dark-tinted glass. Distance reading could not be achieved with 3.0 mm dark-tinted glass in place. This means that the regression formula could only be tested on the light-tinted glass. Before the commencement of each distance reading the prevailing atmospheric parameters (temperature, atmospheric pressure and humidity) were recorded. Throughout the exercise, a temperature variation of 4.5°C, pressure variation of 1 mb and humidity variation of 22 % were observed (see appendix E.2 of appendix E for raw field data). The data acquired was later corrected for prism constant, scale factor and atmospheric corrections. This data was subjected to further analysis and tests to remove the glass impacts on the acquired HD readings as shown below in paragraph 8.4.1.

8.4.1 Glass Thickness Correction Formula Test – Open Pit Mine

The results of the glass thickness model test are presented in tables 8.1 and 8.2. Table 8.1 shows the distance readings (corrected for prism constant, scale factor and atmospheric corrections) before applying the glass thickness correction formula and table 8.2 shows the distance readings after applying the glass thickness correction formula.

Table 8.1: HD readings to the target before glass thickness correction.

SNo	HD reading without glass (m)	HD reading with 4.0 mm glass (m)	HD reading with 5.0 mm glass (m)	HD reading with 6.38 mm glass (m)
1	883.563	883.566	883.567	883.567
2	883.564	883.566	883.567	883.568
3	883.564	883.566	883.567	883.569
4	883.564	883.566	883.567	883.568
5	883.564	883.566	883.566	883.567
6	883.564	883.565	883.567	883.568
7	883.564	883.565	883.567	883.568
8	883.564	883.565	883.567	883.568
9	883.563	883.565	883.567	883.568
10	883.563	883.565	883.567	883.567
11	883.564	883.565	883.567	883.568
12	883.564	883.566	883.566	883.568
13	883.563	883.566	883.567	883.567
14	883.563	883.566	883.567	883.568
15	883.563	883.566	883.567	883.567
16	883.563	883.566	883.567	883.566
17	883.564	883.566	883.567	883.567
18	883.563	883.565	883.566	883.568
19	883.563	883.565	883.567	883.568
20	883.563	883.565	883.567	883.567
Ave	883.564	883.566	883.567	883.568

In table 8.1, the variation in HD readings without or with glass is 1.0 mm. The average distance reading was 883.546 m when distances were measured to the target without glass. It was 883.566 m when distances were measured through 4.0 mm glass and 833.567 m when 5.0 mm glass was used. The average distance reading when 6.38 mm glass was used is 883.568 m.

Table 8.2: HD readings to the target after glass thickness correction.

SNo	HD reading without glass (m)	HD reading with 4.0 mm glass (m)	HD reading with 5.0 mm glass (m)	HD reading with 6.38 mm glass (m)
1	883.563	883.564	883.564	883.563
2	883.564	883.564	883.564	883.564
3	883.564	883.564	883.564	883.564
4	883.564	883.564	883.564	883.564
5	883.564	883.564	883.563	883.563
6	883.564	883.563	883.564	883.564
7	883.564	883.563	883.564	883.564
8	883.564	883.563	883.564	883.564
9	883.563	883.563	883.564	883.564
10	883.563	883.563	883.564	883.563
11	883.564	883.563	883.564	883.564
12	883.564	883.564	883.563	883.564
13	883.563	883.564	883.564	883.563
14	883.563	883.564	883.564	883.564
15	883.563	883.564	883.564	883.563
16	883.563	883.564	883.564	883.562
17	883.564	883.564	883.564	883.563
18	883.563	883.563	883.563	883.564
19	883.563	883.563	883.564	883.564
20	883.563	883.563	883.564	883.563
Ave	883.564	883.564	883.564	883.564

The table 8.2 showed the distance readings after all the corrections (scale factor, prism constant, atmospheric and glass thickness corrections). The variability in the distance readings still remain as 1.0 mm. The average distance readings were the same for distances measured without and with glass. This clearly revealed that the model perform well in actual mine environment.

8.4.2 Glass Colour Correction Formula Test – Open Pit Mine

The result of glass colour model test is presented in table 8.3. The table shows the distance readings without glass in the second column, distance readings with light-tinted glass (corrected for prism constant, scale factor and atmospheric corrections) before applying the glass colour correction formula in the third column. The forth column shows distance readings after applying the glass colour correction formula.

Table 8.3: HD readings to the target before and after glass colour correction.

SNo	HD reading without glass (m)	HD reading with3.0 mm light tinted glass before glass colour correction (m)	HD reading with3.0 mm light tinted glass after glass colour correction (m)
1	883.563	883.566	883.564
2	883.564	883.567	883.565
3	883.564	883.567	883.565
4	883.564	883.567	883.565
5	883.564	883.566	883.564
6	883.564	883.566	883.564
7	883.564	883.566	883.564
8	883.564	883.566	883.564
9	883.563	883.565	883.563
10	883.563	883.566	883.564
11	883.564	883.566	883.564
12	883.564	883.567	883.565
13	883.563	883.566	883.564
14	883.563	883.567	883.565
15	883.563	883.567	883.565
16	883.563	883.565	883.563
17	883.564	883.567	883.565
18	883.563	883.566	883.564
19	883.563	883.566	883.564
20	883.563	883.567	883.565
Ave	883.564	883.566	883.564

In the table, the variation in distance reading without and with glass was 1.0 mm. The average distance readings without glass was 883.564 m, while that of distance readings with 3.0 mm tinted glass was 883.566 m before applying glass colour correction. The average distance readings with 3.0 mm tinted glass is the same with average distance reading without glass after the glass colour formula was applied.

8.5 SOFTWARE DEVELOPMENT

The software was developed using the combined formulae generated in equations 7.13 and 7.16 of chapter seven. The total station manufacturer atmospheric correction formulae for reflectorless mode (i.e. equation 2.31 of chapter two) were also used to cater for the need of distance measurements without prism. The name of the software developed for the total station atmospheric and glass impact corrections is called *Agcomo*. *Agcomo* is an acronym for **A**tmospheric and **G**lass **Co**rrections **Mo**del. It is a software tool developed to assist mine surveyors and other total station users (especially those that engage in operations that required total station distance measurements from observation office) to eliminate the systematic error caused by atmospheric variations and glass properties on distance measurements through an observation office window glass cover. *Agcomo* is a suit of computer programs that incorporate atmospheric variations, glass thickness (i.e. 4.0 mm glass thickness and above) and colour (i.e. 3.0 mm light- and dark-tinted glass). With the application of *Agcomo* on distances measured through a window glass, the corrected distances would be nearly the same as the distances measured through open air without a glass barrier. The software requires a memory space of about 6 MB. Upon installation, the users have access to the graphic user interface (see the enclosed CD at the back of this thesis report).

The Graphic User Interface (GUI) in this *Agcomo* was developed using Java^{TM}. The user-friendly interface was designed as a point and click process to provide interactive access to an input, output and action screen. The user interface has two sections: the manual input section and the read from file and plot section.

8.5.1 Manual Input

The manual input section enables the user to enter the atmospheric parameters (and glass information when glass is used) and raw distance reading and to calculate the true distance per total station single reading. The section has the following modules: Atmospheric Parameters - temperature, pressure and humidity; Instrument – mode; Glass – no glass, glass thickness and glass colour; Distance - measured distance and calculated true distance.

A. **Atmospheric Parameters:** these are the atmospheric constituents that vary with time or the weather around the field where distance measurements were carried out. They had an impact on the velocity of light.

i. **Temperature information**: In the interface, users can enter the atmospheric temperature (the atmospheric temperature may be average of temperature readings at the instrument station and the target station or average of temperature readings taken around strategic locations at the mine) and pick the corresponding units (i.e. degree Fahrenheit, °F or degree Celsius, °C).

ii. **Pressure information**: In the interface, users can enter the atmospheric pressure (the atmospheric pressure may be the average of pressure readings at the instrument station and the target station or average of pressure readings taken around strategic locations at the mine) and can pick the corresponding units (i.e. Millibar, mba; HectoPascals hPa or Millimeter of Mecury, mmHg).

iii. **Humidity information**: Although it had been proved (see error analysis in chapter two) that the impact of humidity on new electro-optical instrument (total stations) was minimal and negligible, during slope monitoring with total station at the mines, there was a need to measure the humidity and to apply it during atmospheric corrections. In the interface, users can enter the atmospheric humidity (the atmospheric humidity may be average of humidity readings at the instrument station and the target station or average of humidity readings taken around strategic locations at the mine) and can pick the corresponding unit (percentage, %).

B. **Instrument:** This term refers to the total station surveying instrument. The operator or the surveyor must select or enter the right prism constant and scale factor into the memory of the machine.

i. **Mode:** The interface allows the software users to pick the instrument mode in use during distance measurement since this will help the software to use appropriate formula during correction process. There are two modes from which the user can pick: the Infra-red mode, IR (when taking distance measurement to prism target) and the reflectorless mode, RL (when taking distance measurement without using any prism or when taking distance measurement to object surface)

C. **Glass:** This term refers to the barrier through which light beams usually pass through during slope monitoring at the mines. The aspect deals with the properties of the glass medium.

i. **No glass:** Users can pick no-glass when distance measurements are taken without a glass barrier. It means the software will perform only atmospheric corrections on the measured distances like other available atmospheric corrections software in the market. In addition, when using reflectorless mode, no glass must be selected because reflectorless mode uses visible red light during distance measurement. It is advisable not to use the mode when there is glass barrier because the glass will reflect part of the red light and may lead to error as established in chapter five of this report.

ii. **Glass thickness:** The software can perform glass thickness and atmospheric corrections on measured distances. The users enter the thickness of the glass barrier and pick the corresponding unit (i.e. Millimetre, mm or Metre, m). The software was designed to perform glass correction on 4.0 mm glass and above. If the user enters any thickness below 4.0 mm, the software will only implement atmospheric corrections on the measured distance because it will assume that there is no need for glass correction. This factor was established in the chapter five of this report when it was found that the impact of 3.0 mm glass thickness and below on distance readings were within the accuracy specification limits of the instrument.

iii. **Glass colour:** This aspect deals with the glass tint level. In the user interface, the users can pick either transparent - when clear float or plain glass (i.e. user must click this when dealing with atmospheric and glass thickness corrections), or light- or dark-tinted is used. It must be noted that the glass thickness when using colour (tint glass) glass must be 3.0 mm.

D. Distance: This aspect can be twofold: the measured distance and the calculated distance

i. **Measured distance:** The distance that appears on the screen of the total station is the measured distance. The users can type in this distance reading and pick the corresponding unit (i.e. Kilometre, km or Metre, m).

ii. **True distance:** The true distance is the distance value that will be displayed by the software when the calculate function is clicked after entering required information. This distance depends on the information (i.e. the atmospheric and the glass information) entered into the software. The unit of the true distance displayed by the software is the same as the unit of the measured distance (i.e. the unit picked by the users when entering the measured distance).

8.5.2 Read from File and Plot

The software is compatible with Microsoft Excel. The distance readings, atmospheric parameters and glass information can be imported from Microsoft Excel into the software through the user interface read from file and plot. The software will perform the necessary corrections (either atmospheric corrections – when no glass; or both atmospheric and glass corrections, when glass is used) and generate the graph of distances against time.

The read from file and plot section includes the following modules: Choose file – open file; Instrument – mode; Glass colour; and Plot results. The instrument mode and glass colour is the same as that explained in the manual section. Therefore, the researcher did not repeat them under this section.

A. **Choose file:** This choice enables the user to select files that contain distance readings, atmospheric parameters and glass information for the software to perform required corrections.

   i. **Open file:** This option enables the user to open a Microsoft Excel file that contains the data to be uploaded for corrections (atmospheric corrections or combined atmospheric and glass corrections) and plot the graph of distance against time. The imported file should always be an "xls" file not an "xlsx" file. This means that the file should always be in "***Compatibility Mode***" (i.e. Excel 97-2003).

B. Plot result: after opening the file operation, the plot result helps with the corrections and plots the graph of corrected distance against time. Figure 8.17 shows the user interface of the *Agcomo* (see the enclosed CD at the back of this thesis report).

Figure 8.17: ***Agcomo*** **user interface**

Note that the software assumes that the prism constant and the scale factor corrections have been performed mechanically by the total station (or manually by the operator) on measured distance readings before subjecting it to *Agcomo* software. The flowchart that summarizes the all the steps to be taken when using the Agcomo software is presented in figure 8.18.

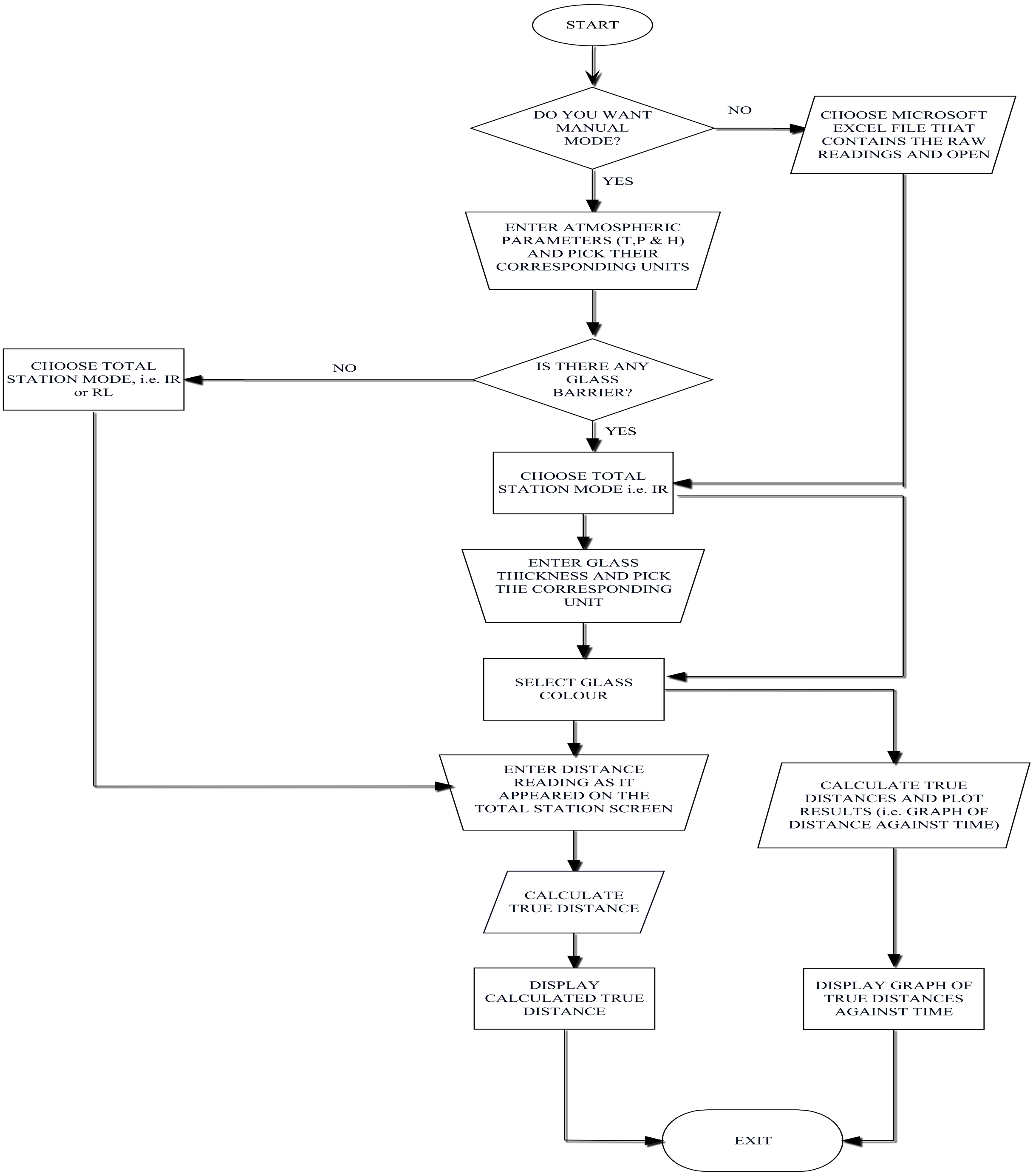

Figure 8.18: Flowchart showing *Agcomo* users' steps

Other instructions to follow when using the *Agcomo* software is presented in appendix E.2, while the sample format of the Microsoft Excel is presented in appendix E.2.1 of appendix E. Table E.1 of appendix E shows raw HD readings and the atmospheric parameters captured during distance measurements using total station on 12 October, 2010. The readings in table E.1 were subjected to the manual option of the *Agcomo* and the results (true HD readings as calculated by *Agcomo*) are presented in table E.2 of appendix E. In addition, the sample graphs plotted when using read from file and plot option of the *Agcomo* are presented in figures E.2, E.3, E.4 and E.5 of appendix E. However a new version 1.2 of the Agcomo was written (using equations 7.13a and 7.16a) to create option for users that intend to correct the impact of ≤ 3.0 mm glass especially when carrying out observation from shelter glass to a distance less than 20 m. Although, if the original Agcomo is used, the variation is less than 1.0 mm on the display calculated true distance.

8.6 DEVELOPMENT OF NOMOGRAM

A nomogram was developed as an alternative to equation 4.1 in chapter four of this thesis for atmospheric corrections in parts per million (ppm). A second nomogram was developed using the regression formulae generated for glass thickness and colour corrections (i.e. equations 7.13a and 7.16a) in chapter seven. The nomograms will assist in the absence of computing facilities where quick corrections are needed in the field. Two steps must be followed when using the nomograms: one – when observations are made without considering glass properties and two – when observations are made through glass.

Step 1

When observations are made without considering glass properties:

- The Slope distance must be used to multiply atmospheric correction value that corresponds to the prevailing atmospheric parameters (temperature and atmospheric pressure) at the time when the observation is made. The result is the atmospheric correction.
- Add the result to the slope distance reading display on the total station screen again to the result of multiplication above to get true distance reading.

Figure 8.19 shows the atmospheric corrections in ppm with temperature (°C), air pressure (mb) and height (m) at 60% humidity as recommended in the Leica TCR 1201 manual.

Example on how to use the atmospheric corrections nomogram:

d' is the distance reading displayed on the total station screen = 468.4197 m

t is the ambient temperature when the observation is made = +16.3°C

p is the atmospheric pressure = 826 mb

h is the humidity = 64%

Solution

Reading the atmospheric parameters on the nomogram in figure 8.19, the closest atmospheric correction for the above parameters is 55 ppm.

Therefore, the atmospheric correction would be:

$= d' \times (55 \times 10^{-6})$

= 468.4197 x 0.000055 = **+ 0.025763 m**

True distance d = d' + atmospheric correction

= 468.4197 + 0.0258 = **468.4455 m**

Step 2

When observations are made through glass:

- The slope distance reading displayed on the total station screen must be used to multiply atmospheric correction value that corresponds to the prevailing atmospheric parameters (temperature and atmospheric pressure) at the time when the observation is made as discussed in step 1 to get atmospheric correction.
- Subtract the glass impact correction from the result of atmospheric correction.
- Add the end result to the distance reading display on total station screen to get true distance reading.

Figure 8.20 shows the nomogram for glass correction (m) on the vertical axis, the glass thickness (mm) and glass percentage tint (%) on the horizontal axis.

For example, a 5.0 mm glass was placed immediately after the observation in step 1 above was made (i.e. observation was made through 5.0 mm glass). The prevailing atmospheric situations were the same.

d' shown on the total station is 468.4228 m (as measured through the glass)

t is the ambient temperature when the observation is made = +16.3°C

p is the atmospheric pressure = 826 mb

h is the humidity = 64%

Solution

Reading the atmospheric parameters on the nomogram in figure 8.19, the closest atmospheric correction for the above parameters is 55 ppm.

Therefore, the atmospheric correction would be:

$= d' \times (55 \times 10^{-6})$

= 468.4228 x 0.000055 = **+ 0.025763 m**

Glass thickness correction for 5.0 mm glass = 0.0031 m (see nomogram in figure 8.20)

Subtract the glass thickness correction from atmospheric correction i.e.

= 0.025763 – 0.0031

= **0.0227**

True distance d = d' + (atmospheric correction – glass impact correction)

= 468.4228 + 0.0227 = **468.4455 m**

Remark

The two observations were made to the same target from the same instrument station. Only the conditions changed. After subjecting both observations to the nomograms, the corrected (or true) distances should be the same, which is illustrated above.

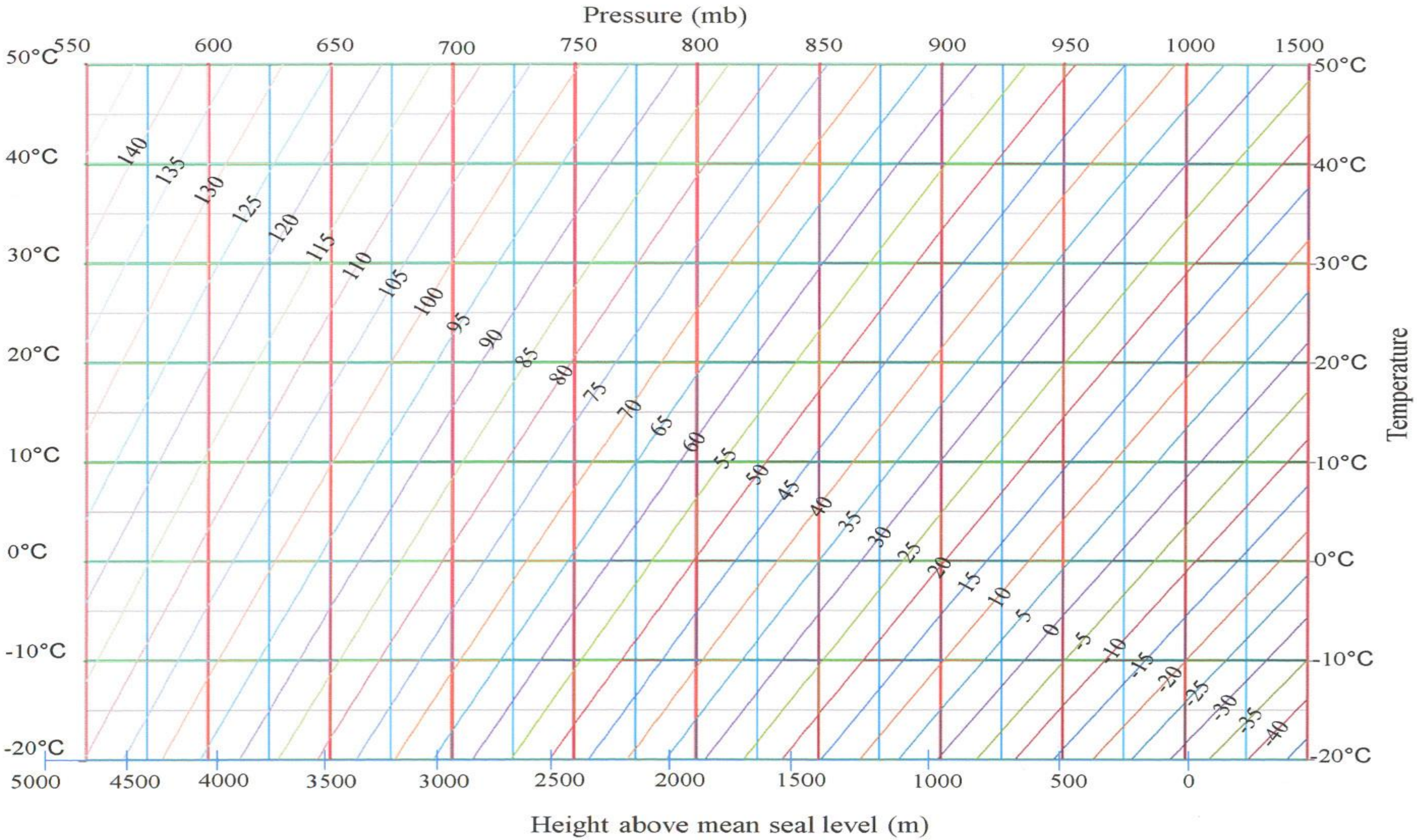

Figure 8.19: Atmospheric corrections nomogram

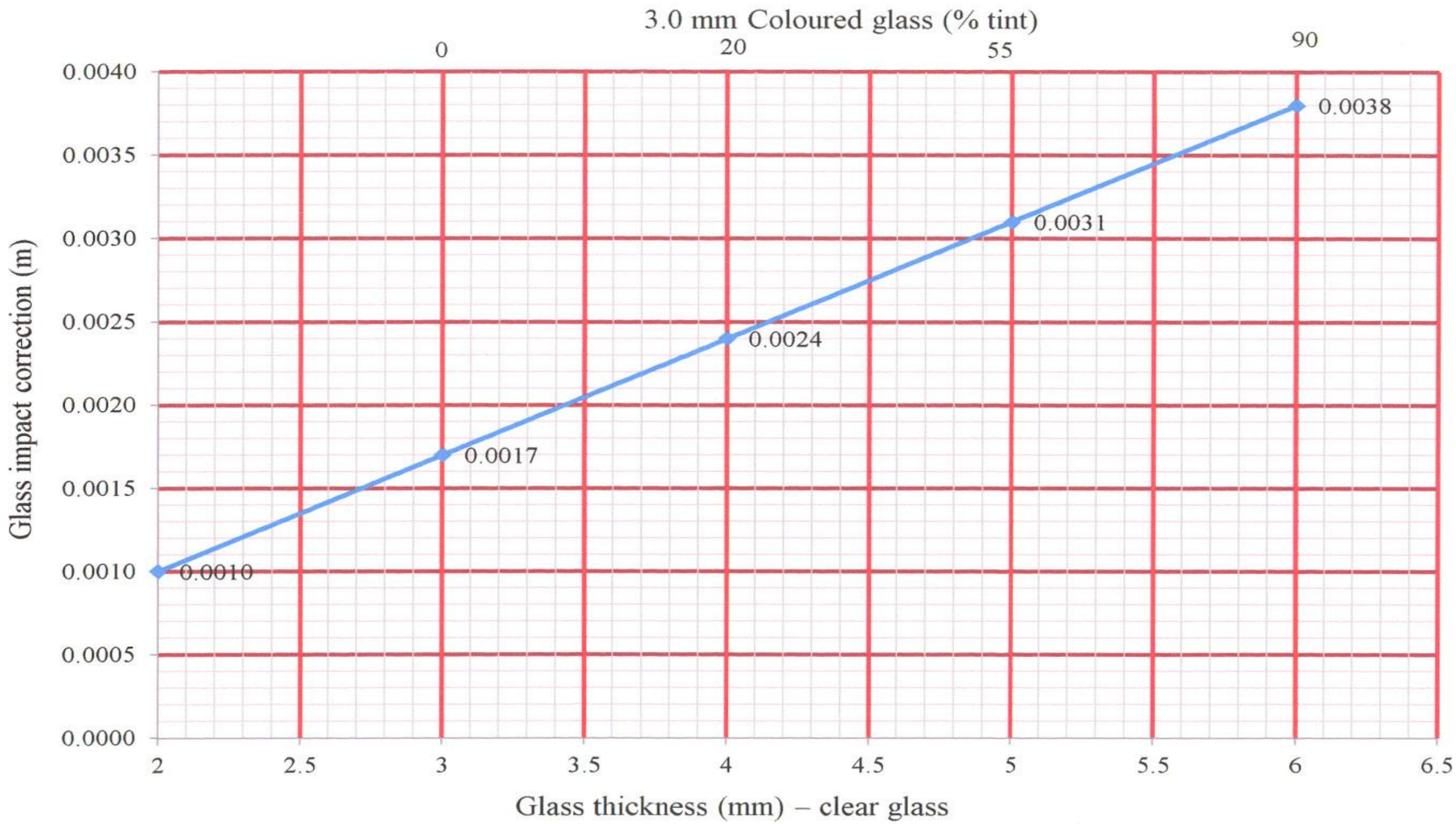

Figure 8.20: Glass impact correction nomogram

8.7 CONCLUSION

The chapter showed the effectiveness of the model developed in removing systematic error in distance readings. It revealed that the models performed well in correcting the glass impact on distance measurements. However, the glass-thickness correction formula seemed to perform better than the glass-colour correction formula as shown in the graphs generated after the two models were applied to measured distances. It also revealed that the use of dark tinted glass at a distance above 400 m is not possible. In light of these findings, the use of tinted glass for observation needs to be further tested with a wide range of coloured glass of varying thickness and tint level.

The *Agcomo* software performed well in removing both the atmospheric variations impact and the glass properties impact on distance measurements. It has the advantage of performing atmospheric corrections alone or combined atmospheric and glass corrections when the need arose. The software is user friendly and easy to use. Users can use the manual or import file from Microsoft Excel option depending on the job at hand. The chapter also showed steps to follow when using nomograms developed as a handy alternative to the software.

CHAPTER NINE

9.0 CONCLUSION AND RECOMMENDATION

In this chapter the conclusions of this research are discussed. Recommendations are based on the outcome of the findings and areas of further studies are also suggested.

9.1 CONCLUSION

Technological advancements in the field of surveying have meant that the mine surveyor must guard against merely becoming an operator of survey equipment, relying on technology and computer software to deliver survey results. The mine surveyor should not become accustomed to accepting survey results generated by sophisticated instruments and computer software without questioning the accuracy. Mine surveyors should have a better understanding of survey accuracies required and survey accuracies achieved as these will better equip them for other survey tasks that require high precision surveys (Thomas, 2011).

Distance measurement requires high accuracy and precision, especially during slope monitoring surveys at mines. When slopes fail unexpectedly, human and financial losses are encountered. The research examined three major things:

- the efficiency of the total station manufacturer recommended atmospheric corrections formulae;
- the impact of glass properties (thickness, colour and shape) on distance measurements; and
- design parameters when positioning a total station to observe through a glass window.

The research established that the atmospheric corrections formulae stated in the total station manual (i.e. a modified version of existing Barrel and Sears (1939) and IAG (1999) recommended formulae for EDM atmospheric corrections) accurately compensate for variations in atmospheric parameters during distance measurements. These findings were explained in chapters five and six of this thesis.

The research affirmed the possibility of carrying out total station distance measurements through a glass medium. It also established that the properties of the glass matter when total station distance measurements were taken through a window glass. The glass had little or no impact on the instrument accuracy specification during vertical distance measurements, but it did affect accuracy during horizontal distance measurements. This impact increased with an increase in glass thickness and tint or shades. The probability that the impact could be reduced or removed by total station manufacturer atmospheric correction formulae was zero. However, the research revealed that the impact of 3.0 mm (plain and transparent) glass thickness and less on distance measurements was minimal and still within the accuracy specification limits of the instrument regardless of angles at which the line of sight intersected the glass.

The research revealed that glass thicknesses of more than 3.0 mm caused a systematic error in horizontal distances observed through the glass. In addition, 3.0 mm coloured (3.0 mm – light- and dark-tinted) glass would affect the accuracy limits specification regardless of different angles of intersecting the glass. Therefore, there was a need for additional formulae to compensate for the glass impact and to make the distances measured through such glass the same (or nearly the same) with distances measured without window glass barrier as well as to make such measured distances conform to the instrument accuracy specification limits.

In the South African context, equipment theft, damage by wildlife and harsh weather conditions necessitate housing the total station and required observation through a window.

Systematic error correction formula was developed to remove the impact caused by 4.0 mm glass thickness and above on distance measurements. A separate formula was developed to cater for the effect of 3.0 mm tinted glass on horizontal distance measurements. The comparison of the regression model developed to physical model revealed that the model is good with less than 0.2 mm difference from physical model results (as shown below):

Glass thickness	Physical model (mm)	Regression model (mm)	Difference (mm)
3	1.89	1.70	0.19
4	2.51	2.40	0.11
5	3.20	3.10	0.10
6.38	4.03	4.07	0.04

The formulae were tested on a new set of distance readings (acquired on the University campus and in an open pit mine) to examine their effectiveness in removing the effect of a glass barrier on total station distance measurements taken through a glass medium. The results indicated that all the horizontal distances measured through window glass conformed to the accuracy limits specification of the total station after applying the developed glass impact correction formulae. These distances were the same or very close to horizontal distances measured through open atmosphere without the window glass barrier.

The computer software program, *Agcomo,* was written using the manufacturer-generated atmospheric corrections formulae and the systematic error correction formulae developed in this research for glass impact (thickness and colour) corrections. The software proved accurate when tested using horizontal distances measured with or without glass. The software also performed well in removing both the atmospheric variations impact and the glass properties impact on distance measurements. The program has the advantage of performing atmospheric corrections alone or with combined atmospheric and glass corrections when the need arises. Nomograms were developed as alternative to software for distances corrections in the mine field.

Tests on the likely impact of the glass shape on the distance measurements revealed that the shape of the glass mattered during monitoring through a glass medium. Plain glass had the least impact, followed by convex glass, while the concave glass had the highest impact.

The tests on the likely impact of the distance between the total station and window glass on distance measurements revealed that the distance between the total station and the observation window had no impact on the total station distance measurements. However, it is advised to keep the distance between the total station and the observation window to barest minimum. The test was carried out indoors where the atmospheric variations were negligible or nearly constant unlike in the mines, where the observation house atmospheric parameters could vary considerably because of the atmospheric parameters. These differences could have adverse effect on the total station distance measurements, if there is a wide distance between the total station and the observation window in a surface mine environment.

9.2 RECOMMENDATION

The changes in distance and angular measurements are the key parameters usually used to determine the stability of a slope in open-pit mines. Any default in the processes used in acquiring data on these two parameters could lead to major errors in the end result during data analysis and usage. Such errors would automatically mar the objectives of the slope monitoring program implemented in the mines. Therefore, all the processes must be tested to ascertain the likelihood of the error source in them and mitigate such error.

The method of distance measurements through glass medium must be avoided. If distance must be measured through glass medium, the properties of the glass material must be considered when selecting glass material for total station observation house window construction at the surface mine environments. Such consideration would enable the surveyors and geotechnical analysts to cater for the impact of the glass on acquired data when the need arises. The glass thickness must not exceed 3.0 mm, it must be transparent (i.e. not tinted) and must be plain (i.e. neither convex nor concave). If glass thickness above 3.0 mm and tinted glass must be used, their effect on measured distances must be quantified and catered for during data processing. In addition, when using tinted glass for total station observation window, dark-tinted (50% tint and above) glass must be avoided if the distance to be monitored is more than 500.0 m; alternately, light-tinted glass must be used. Plain glass must be used at the mine during slope monitoring, otherwise more research must be conducted to quantify the impact of glass shape on distance measurement and develop a model to compensate for it.

Furthermore, the surveyors must ensure that they supervise the construction of the observation house (house constructed at the mine sites to shelter the total station from direct sunlight, rain, flying rocks and other unfavourable conditions at mine site) and make sure that the distance between the observation station (where the total station will be mounted inside the house) and the observation house window glass cover does not exceed 0.5 m. Alternatively during distance measurement from observation house, the total station must be put on for about 30 minutes before the actual distance measurements to enable the total station acclimatize to the observation room temperature. The GeoMos meteo sensor must be installed outside the observation house at mines not outside surveyors' offices located at the administrative block.

The above recommendations can be summarized as follows:

- Total station shelter must be left without any cover on its side to create a direct (no barrier) line-of-sight between the total station and the target.
- If glass materials must be used, the thickness of the glass should be 3.0 mm or less.
- The glass material must not be coloured or tinted.
- When the thickness exceeds 3.0 mm and when the glass is tinted, a systematic error is introduced.
- The formula for glass thickness correction when using Leica total station to measure distances through glass medium generated in this research must be used:

$$\hat{y} = 0.0008x - 0.0013$$

- Its glass colour impact correction when tinted 3.0 mm glass medium is used is:

$$\hat{y}' = 9Exp^{-6}x' + 0.0025$$

- The combined atmospheric and glass thickness corrections is:

$$k^{'} = \left[283.05 - \frac{79.7489P}{(273.15+t)} + \frac{11.27e}{(273.15+t)} \right].10^{-6}d^{'} - [0.0008x - 0.0013]$$

- The combined atmospheric and glass colour corrections is:

$$k^{''} = \left[283.05 - \frac{79.7489P}{(273.15+t)} + \frac{11.27e}{(273.15+t)} \right].10^{-6}d^{'} - [9Exp^{-6}x' + 0.0025]$$

- The glass must be plain and not concave or convex. If other glass shapes (concave and convex) must be used, further research must be carried out to quantify their impact on distance measurements and develop a model to cater for the glass shape.
- The distance between the total station and the observation window must be kept at a practical minimum during total station sheltering construction at the mines. In addition, the total station should be switched on for about 30 minutes before embarking on distance measurements.

If the above recommendations are put into practice, the systematic error caused by the atmospheric variation and glass barrier will be minimal.

9.3 AREAS OF FURTHER RESEARCH

Further research must be carried out using other brands of total station. The systematic error correction formulae generated in this research were developed and tested using Leica total station. Total stations of other makers of similar accuracy must be tested.

Further research must also be carried out to ascertain the impact of coloured glass of different thickness on distance measurements. This research will create room for a combined formula that can remove the impact of coloured glass of different thickness as against only 3.0 mm coloured glass used in this research. Also, more research must be carried out on the impact of glass shape on distance measurements.

REFERENCES

Abahamid, A., Jabiri, A., Vernin, J., Benkhaldooun, Z., Azouit, M. And Agabi, A. (2004). Optical turbulence modelling in the boundary layer and free atmosphere using instrumented meteorological balloons. *Journal of Astronomy and astrophysics, 416(3):1193 – 1200.*

Abu-Bakar, N.M. and Tahir, I.M. (2009). Applying multiple linear regression and neural network to predict bank performance. *International Business Research, 2(4):176 – 183.*

Afeni, T.B. and Cawood, F.T. (2010). Pre-delivery calibration on a new total station – Geosystems African Laboratory experience. Journal of the Institute of Mine surveyors of South Africa, 34(1): 8 – 16.

Ahrens, C.D. (1993). Essentials of Meteorology – An invitation to the atmosphere. St. Paul, New York: West Publishing Company.

Albanis, A. (1993). A simple accurate empirical model for short-range EDM distances during daytime measurement. Unpublished doctoral thesis, Johannesburg, South Africa: University of the Witwatersrand.

Al-Nasseri, A.D. and Radaideh, A. (2008). Estimation of simple linear regression model using l ranked set sampling. *International Journal of Open Problems Computational Mathematics, 1(1):18 – 33.*

Amiri-Simkooei, A. (2003). Least-squares formula for zero Error (Z_o) of electromagnetic distance measuring instrument. *Journal of Surveying Engineering, 129(4):136 – 140.*

Anderson, J. M. and E. M. Mikhail. (1998). Surveying, theory and practice - 7th Ed. New York: McGraw-Hill Companies, Inc.

Angus-Leppan, P.V. (1962). Atmospheric refraction and temperature gradient. *The Canadian Surveyor, 16(1):24 – 31.*

Angus-Leppan, P.V. (1972). Meteorological physics applied to the calculation of refractive corrections. Conference Proceedings of the Commonwealth Survey Officer; Cambridge paper B5 HMSO: 153 – 165.

Angus-Leppan, P.V. (1972). Adjustment of trilateration using length ratios. *Survey Review, 21(166): 355 – 368.*

Angus-Leppan, P.V. (1979). Use of meteorological measurements for computing refractional effects – a review. Proceedings from IAU (International Astronomical Union) Symposium on Refractional Influences in Astrometry and Geodesy, 89:165 – 174.

Angus-Leppan, P.V. and Brunner, F.K. (1980). Atmospheric temperature models for short-range EDM. *The Canadian Surveyor, 34(2):153 – 165.*

Angus-Leppan, P.V. and Webb, E.K. (1971). Turbulent heat transfer and atmospheric refraction. Proceedings of IAG General Assembly (section 1), Moscow 1971.

Arumala, J.O. (2000). The impact of new surveying instruments on the construction surveying course of study. *Journal of Construction Education, 5(3):227 – 243.*

Arya, S.P. (2001). Introduction to micrometeorology. New York: Academic Press.

ASCE –American Society of Civil Engineers (1999). Topographic surveying. Technology and Engineering Series.

Astronomy 161 online Lecture notes on the earth's atmosphere. Available at: http://csep10.phys.utk.edu/astr161/lect/index.html (Accessed 26 June 2008).

Atkinson, B.W. (1981). Dynamic Meteorology – An introductory selection. New York: Methuen and Co Ltd.

Bahuguna, P.P. (2003). Correlation survey for shaft deepening in Digwadih Underground Coal Mine. *Journal of Surveying Engineering, 129(1):33 – 36.*

Balletti, C., Guerra, F., Mander, S. and Manzin, M. (2005). Survey of modern architecture. XXth International Symposium of CIPA (The International Committee for Documentation of Cultural Heritage) held in Torino, Italy.

Bannister, A., Raymond, S. and Baker, R. (1998). Surveying. Edinburgh Gate, England: Pearson Education Ltd.

Barrell, H. and Sears, J.E. (1939). The refraction and dispersion of air for the visible spectrum. *Philosophical Transaction of the Royal Society, Series A, 238: 1 – 64.*

Becker, J.M. (2002). Recommendations concerning instruments maintenance and quality specification. Proceeding of FIG (Federation Internationale Des Geometres – International Federation of Surveyors) XXII International Congress on Standard Quality Assurance and Calibration, held in Washington, DC USA, 19 – 26 April 2006.

Becker, J. M. (2001). Field procedures for determining achievable precision of surveying instruments: levels. Proceedings of FIG Working Week 2001, held in Seoul Korea, 6–11 May 2001.

Becker, J. M., Heister, H. and Slaboch V. (2000). New technical standards improving the quality in positioning and measurement. Proceedings of FIG Working Week 2000, held in Prague, 21-26 May 2000.

Bergmann, L., Schaefer, C. And Neindrig, H. (1999). Optics of waves and particles. New York: Walter de Gruyter and Co.

Birch, K.P. and Downs, M.J. (1993). An updated Edlen equation for the refractive index of air. *Metrologia, 30(3):155 – 162.*

Birch, K.P. and Downs, M.J. (1994). Correction to the updated Edlen equation for the refractive index of air. *Metrologia, 31(4):316 – 316.*

Bonsh, G. And Potulski, E. (1998). Measurement of the refractive index of air and comparison with modified Edlen's formulae. *Metrologia, 35(2):133 – 139.*

Bossler, J.D. (1984). Standards and specifications for geodetic control networks. Federal Geodetic Control Committee, Rockville, Maryland. Available at: http://www.ngs.noaa.gov/FGCS/tech_pub/1984-stds-specs-geodetic-controlnetworks.htm (Accessed 12 May 2009).

Brincker, R.C. and Wolf, P.R. (1984). Elementary surveying. New York: Harper and Row, Publishers.

Brincker, R.C. and Minnick, R. (1995). Surveying handbook. New York: Springer Publishers.

Brunner, F.K. (1977). The refractive coefficient of microwaves. *Bulletin Geodesique, 51(4):257-264.*

Brunner, F.K. and Fraser, C.S. (1977). An atmospheric turbulent transfer model for EDM reduction. Proceedings of the International Symposium on Electromagnetic Distance Measurement and the Influence of Atmospheric Refraction, Wageningen.

Buckner, B. (1998). The nature of measurement*: Part 10* - Achieving accuracy in distances. *Professional Surveyor, 18(6).* Available at: http://www.profsurv.com/archive.php?issue=25&article=332. (Accessed 15 June 2008).

Bulut, F. and Tude, S. (1996). Determination of discontinuity traces on inaccessible rock slopes using electronic Tacheometer: An example from the Ikizdere (Rize) Region, Turkey. *Engineering Geology, 44(1-4):229 – 233.*

Burnside, C.D. (1991). Electromagnetic distance measurement. 3rd Edition, Great Britain: BSP Professional Books.

Cacuci, D.G. (2003). Sensitivity and uncertainty analysis theory. LLC Boca Raton, Florida: Chapman and Hall CRC Press.

Cawood, F.T. and Stacey, T.R. (2007). Survey and geotechnical slope monitoring considerations. *The South African Institute of Mining and Metallurgy (SAIMM), 106(7):495 – 501.*

Ciddor, P.E. (1996). Refractive index of air: New equations for the visible and near infrared. *Applied Optic, 35(9):1566-1573.*

Coggan, J., Stead, D. and Howe, J. (2001). Application of surveying techniques for monitoring and appraisal of excavated China clay slopes. 10th FIG International Symposium on Deformation Measurements, held in Orange, Califonia, USA.

Cosser, E., Roberts, G.W., Meng. X. and Dodson, A.H. (2003). Measuring the dynamic deformation of bridges using a total station. Proceedings, 11th FIG Symposium on Deformation Measurements, Santorini, Greece. Available at: http://www.fig.net/commission6/santorini/IMonitoring%20Static%20and%20Dyn/I9.pdf**.** (Accessed 6 March 2008).

Cruden, D.M. and Masoumzadeh, S. (1987). Accelerating creep of the slopes of a coal mine. *Rock Mechanics and Rock Engineering, 20(2):123-135.*

Cruikshank, K. (1999). Use of the electronic total station – Introduction and basic techniques. *Journal of Geosciences Education.* Available at: htt://geomechanics.geol.pdx.edu/courses/G485/totalstation/JGE%20paper%201%introduction .pdf. (Accessed 3 April 2008).

Danielson, E.W., Levin, J. and Abram, E. (2003). Meteorology. 2nd edition, Dubuque, Iowa: Mcgraw-Hill College.

Davis Weather Shop: Stevenson Screen Kit: How to build your own. Available at: http://shop.davisnet.com.au/index.php?main_page=page&id=1 (Accessed 12 August 2009)

Deulich, F. (1982). Surveying Instruments. Berlin, New York: Walter de Gruyter.

Direct Industry. Total Station-All the manufacturer industries. Available at: http:// www.directindustry.com/industrial.manufacturer/total station.73859.html. (Accessed 16 May 2008).

Ding, X., Montgomery, S.B. and Tsakiri, M. (1998). Integrated monitoring systems for open pit wall deformation. Australian Centre for Geo-mechanics, MERIWA Project Report No. 186.

Dodson, A. H. And Zaher, M. (1985). Refraction effects on vertical angle measurements. *Survey Review, 28(217):169 – 183.*

Duggal, S.K. (2004). Surveying. 2nd Edition, New Delhi: Tata McGraw – Hill.

Dzierzega, A. and Scherrer, R. (2002). Testing total station. *GIM International, 16(6): 31-33.*

Edlen, B. (1966). The refractive index of air. *Metrologia, 2(2):71 – 80.*

Eiteljorg, H. (1994). Using a total station. CSA (Centre for Studying Architecture) Newsletter August Edition, 7(2). Available at: http://www.csanet.org/newsletter/aug94/nl089407.html**.** (Accessed 13 July 2008).

El-Rabbany, A. (2002). Introduction to GPS: The Global Positioning System. Boston, London: Artech House Publishers.

Esser, D. (1998). Atmospheric stability. *Continental Airlines' In-Flight Magazine, October, 1998 issue.* Available at: http://www.erau.edu/er/newsmedia/articles/cont18.html**.** (Accessed 31 September 2009).

Feigleson, E.D. and Babu, G.J. (1992). Linear regression in Astronomy II. *The Astrophysical Journal 397(1):55-67.*

Feng, Q., Sjogren, p. and Jing, S.L. (2001). Measuring fracture orientation at exposed rock face by using a non-reflector total station. *Engineering Geology, 59: 133 – 146.*

Font Jiménez, C.O. (2006). Understanding the atmospheric turbulence structure parameter, C_n^2, in the littoral regime**.** Unpublished M.Sc thesis, Department of Physics, University of Puerto Rico, M AYAGÜEZ Campus.
Fosburgh, B. and Paiva, J.V.R. (2001). Surveying with GPS. American Congress on Surveying & Mapping (A.C.S.M.) Conference paper.

Fraser, C.F. (1979). Identification of optimum meteorological conditions for EDM via potential refractivity. *The Canadian Surveyor, 33(1):27 – 38.*

Fraser, C.F. (1981). A simple atmospheric model for Electro-Optical EDM reduction. *The Australian Surveyor, 30(6):352 – 362.*

Ganic, E.N. and Hicks, T.G. (2002). McGraw-Hill's Engineering Companion: Technology and Engineering. New York: McGraw-Hill.

Gaudreault, F., Gassner, G., Gaydosh, M and Rogers, M. (2004). The Leica TCRA 1105 reflectorless total station. SLAC (Stanford Linear Accelerator Center) International Workshop on Accelerator Alignment. Available at: http://www.slac.stanford.edu/econf/c04100411/papers/022.pdf. (Accessed 15 June 2008).

Geosystems: Structural monitoring equipment list manual. Available at: http://www.servco1.com/Site/Instrument%20PDF's/Software%20&%20Data%20Collectors/Leica%20GeoMoS/GeoMoS_Equipmentlist_en.pdf**.** (Accessed 24 July 2008).

Ghilani, C.D. and Wolf, P.R. (2008). Elementary Surveying: An introduction to Geomatics. Upper Saddle River, New Jersey: Prentice Hall.

Gili, J.A., Corominas, J. and Rius, J. (2000). Using global positioning system techniques in landslide monitoring. *Journal of Engineering Geology, 55(3):167 – 192.*

Greenway, I. (2000). Surveyors and standardisation. Proceedings of FIG Working Week 2000, held in Prague, 21-26 May 2000.

Haddad, N and Ishakat, F. (2007). 3D laser scanner and reflectorless total station: A comparative study of the slots of El-Khazneh at Petra in Jordan. XXI International CIPA Symposium, held in Athens, Greece.

Haentjens, H. (1992). Monitoring a landslip - Saint-Etienne-de-Tinee (France). Switzerland: Leica Heerburgg AG.

Hartman, H.L., Britton S.G., Mutmansky, J.N., Gentry, D.W., Schlitt, W.J., Karmis M. and Singh, M.M. (1992). SME Mining Engineering Handbook. Published by Society for Mining Metallurgy & Exploration.

Hartman, H.L., Britton S.G., Mutmansky, J.N., Gentry, D.W., Schlitt, W.J., Karmis M. and Singh, M.M. (1992). SME Mining Engineering Handbook. 2nd Edition, Published by Society for Mining Metallurgy & Exploration.(Mine surveying and aerial mapping section written by Solomon, B.W., Morgan, J., Britton, S.G. and Frush, C.O.).

Heister, H. (2001). A new concept for stating accuracy in standards - exemplified by ISO / Dis 17123-6 Rotating Lasers. Proceedings of FIG Working Week 2001 held in Seoul, Korea, 6–11 May 2001.

Hill, C.D. (2005). Leica smart station – The combination of GPS and total station technologyies. Leica Geosystem publications.

Hill, C. D. and Sippel, K. D. (2002). Modern Deformation Monitoring: A Multi Sensor Approach. FIG XXII International Congress, held in Washington DC, USA. Available at: http://www.fig.net/pub/fig_2002/Ts6-3/TS6_3_hill_sippel.pdf**.** (Accessed 6 March 2008).

Hirst, K.K. (2006). A mapping device. Available at: http://archaeology.about.com/od/fieldlabgear/ig/Archaeology-Tools-of-the-Trade/Total-Station-Transit.htm (Accessed 11 June 2008).

Hoffman, E. (2005). Specifying Laser Scanning Services. *Chemical Engineering Progress (CEP),* May 2005: 34-39.

Huang, P.H. (1998). New equations for water vapour pressure in the temperature range -100°C to 100°C for use with the 1997 NIST/ASME steam table. 3rd International Symposium on Humidity and Moisture, 1: 68 – 76.

IAG, (1999). Resolutions adopted at XXII General Assembly of International Association of Geodesy, held between 19 - 30 July at Birmingham, U.K.

Iliffe, J.C. and Dodson, A.H. (1987). Refraction effects on precise EDM observations. *Survey Review, 29(226):181 – 190.*

Jacobson, M.Z. (2005). Fundamentals of atmospheric modeling. New York: Cambridge University Press.

Jenkins, F.A. and White, H.E. (1981). Fundamentals of optics. 4th edition, New York: McGraw-Hill, Inc.

Jobling-Purser, J. (2006). A robotic surveying vehicle for hazardous mining conditions. *BCRA Cave Radio and Electronics Group Journal, 64:9 – 11.*

Jones, A.Z. (2009). What is a photon? Free Physics Newsletter. Available at: http://physics.about.com/od/lightoptics/f/photon.htm (Accessed 24 March 2009).

Kaimal, J.C. and Finnigan, J.J. (1994). Atmospheric boundary layer flows- Their structure and measurement. UK: Oxford University Press.

Kavanagh, B.F. and Glenn Bird, S.J. (1995). Surveying principle and applications. 3rd Edition, Englewood Cliffs, NJ: Prentice Hall.

Keim, R.F., Skaugset, A.E. and Bateman, D.S. (1999). Digital terrain modeling of small channels with a total station theodolite. *Advances in Water Resources, 23(1): 41 – 48.*

Key, H. And Lemmens, M. (2008). Robotic Total Station. *GIM International, vol. 22 issue 6*. Available at: http://www.gim-international.com/issues/articles/id1128 Robotic_Total_Stations.html (Accessed 14 May 2008).

Khalil, R., (2005). New compact method for laboratory testing EDM instruments. FIG Working Week 2005 and GSDI-8, Cairo, Egypt; 8pages. Available at: http://www.gsdidocs.org/gsdiconf/GSDI-8/papers/ts_22/ts22_06_khalil.pdf (Accessed 22 March 2009).

Khurmi, R.S. and Gupta, J.K. (2003). Civil Engineering (Conventional and Objective types). Ram Nagar, New Delhi: Eurasia Publishing House PVT ltd.

Kuhlmann, H. and Glaser, A. (2002). Investigation of new measurement techniques for bridge monitoring. 2nd Symposium on Geodesy for Geotechnical and Structural Engineering, Berlin, Germany, 10p. Available at: http://www.unistuttgart.de/iagb/forschung/messtechnik/projekte/download/brueckenueberw.pdf**.** (Accessed 11 June 2008).

Lavine, A., Gardner, J.N. and Reneau, S.L. (2003). Total station geologic mapping: an innovative approach to analysing surface – faulting hazard. *Journal of Engineering Geology, 70(1-2):71 – 91.*

Lehtonen, H. (2005). Virtual Archaeology – what is it? Mirator theme issue. Proceedings from the Symposium "Virtually Medieval?" Available at: http://www.glossa.fi/mirator/themeissue2005/vmlehtonen.pdf (Accessed 11 June 2008).

Leica Geosystems. (2002). Bridge surveys. Available at: http://www.leicageosystems. com/civil/application/bridge.htm. (Accessed 11 June 2008).

Leica Geosystems: Leica TPS800 series. Available at: http://www.leica-geosystems.com/corporate/en/products/total_stations/lgs_5520.htm (Accessed 11 June 2008).

Leica Geosystems technical specifications and system features of TPS400. Available at: http://www.visualstatement.com/pdf/brochures/leica-comp.pdf (Accessed 11 June 2008).

Leica TPS 1200+ Applications field manual. Version 6.0: 245.

Lutes, J.A. (2002). "Automated dam displacement monitoring using a robotic total station". Master of Science dissertation, University of New Brunswick, Fredericton, Canada.

MacDonald, M. (2001) Total station – more jobs in sight. The Carpenter Magazine, pp.33 - 37. Available at: http://www.carpenters.org/carpentermag/TotalStation78_01.pdf (Accessed 23 April 2008).

Manual of Survey Practice. Verification of survey equipment, 2(10). Government of South Australia, Land Services Group. Available at: http://www.landservices.sa.gov.au/1Professional_Access/Manual_of_Survey_Practice/Volume_2/2010v2sec10.asp. (Accessed 16 April, 2009).

Martin, D. (2007). Calibrating surveying instruments: A modern calibration bench. *GIM International, The Global Magazine for Geomatics, 21(8):1- 3.*

McCormac, J.C. (1983). Surveying Fundamentals. Englewood Cliffs, New Jersey: Prentice-Hall, Inc..

McLaren, J.N. (1990). Global monitoring of unstable slope in the North East of Portland Dorset. Proceedings of the Conference Geotechnical Instrumentation in Civil Engineering Projects, held in Nottingham 1989: 145 – 164.

Mclntyre, D.H. (2000). Using great circle to understand motion on a rotating sphere. *American Journal of Physics, 68(12):1097 – 1105.*

Merkle, W and Myers, J.J. (2004). Use of the total station for serviceability monitoring of bridges with limited access in Missouri, USA. Proceedings of 16TH World Conference on Non-destructive Testing (WCNDT) held in Montreal, Canada.

Moffitt, F.H., and Bouchard, H., (1992). Surveying. New York: Harper Collins.

Moss, J.L., McGuire, W.J. and Page D. (1999). Ground deformation monitoring of a potential landslide at La Palma, Canary Island. *Journal of Volcanology and Geothermal Research, 94: 251 – 265.*

Newcomen, Warren H., C. Murray and L. Shwydiuk (2003). Monitoring pit wall deformations in real time at Highland Valley Copper. Proceedings of the Fourth International Conference on Computer Applications in the Minerals Industry held in Calgary, Alberta - Canada, 8-10 September 2003.

Oregon Scientific Manual. Wireless weather station with world time clock model: BAR916HG.

Ostdiek, V.J. and Bord, D.J. (2008): Inquiry into Physics. 6th edition, Thomson Learning Academic Resources Center, 10, Drive, Belmont, CA, USA.

Owens, J.C. (1968). The use of atmospheric dispersion in optical distance measurement. *Journal of Geodesy, 42(3):277 – 291.*

Panofsky, H.A. and Dutton, J.A. (1984). Atmospheric turbulence. New York, USA: Wiley and Sons Inc.

Paiva, J.V.R. (2006). Technology transitions: a review of surveying field technology from 1950 to today. *American Journal Point of Beginning (POB). April 2006 online edition.* Available at: http://www.pobonline.com/Article/Cover_Story/49343dc. (Accessed 11 June 2008).

Peck, E.R. and Reeder, K. (1972). Dispersion of air. *Journal of Optical Society of America, 62(8):958 – 962.*

Persson, A. (1998). How do we understand the Coriolis force? *Bulletin of the American Meteorological Society, March Edition, 79(7):1373 – 1385.*

Philpotts, A.R., Gray, N.H., Carroll, M. Steinen, R.P. and Reid, J.B. (1997). The electronic total station – a versatile, revolutionary new geologic mapping tool. *Journal of Geoscience Education, 45: 38 – 45.*

Price, W. F., and Uren, J. (1989). Laser surveying. London: Van Nostrand Reinhold (International Edition).

Rabinovich, S. (2005). Measurement errors and uncertainties: theory and practice. New York, USA: Springer Science Media Inc.

Rencher, A.C. and Schaalje, G.B. (2007). Linear models in statistics. Hoboken, New Jersey: John Wiley & Sons Inc.

Rick, J.W. (1996). Total station in archaeology. *Society for American Archaeology (SAA) Bulletin 14(4): 24 – 27*. Available at**:** http://www.saa.org/publications/SAAbulletin/14-4/SAA16.html (Accessed 11 June 2008).

Ritchiewiki: Drift mining. Available online at: http://www.ritchiewiki.com/wiki/index.php/Drift_mining#_note-0 (Accessed 11 June 2008).

Roberts, Jack. (1995). Construction surveying, layout and dimension control. Clifton Park, New York: Delmar Publishers Inc.

Roy, S.K. (2004). Fundamentals of surveying. India: Prentice-Hall.

Rueger, J.M. (1980): Introduction to electronic distance measurement. Monograph No.7, Second Edition, University of New South Wales.

Rueger, J.M. (1980a). Recent development in electronic distance measurement. *The Australian Surveyor, 30(3):170 – 177.*

Rueger, J.M. (1984). A test of atmospheric temperature models in EDM, using a Wild Distomat DI 20. *Australian Journal of Geod Photogram Survey, 41: 61 – 96.*

Rueger, J.M. (1994). Practical use of surveying robots with EDM beam point. Proceeding of 20th FIG Congress held in Melbourne, Australia.

Rueger, J.M. (1994a). Monitoring with surveying robots. *Geodetical Info Magazine (GIM) and International Journal for Surveying, Mapping and Applied GIS, 8(2):58 – 63.*

Rueger, J.M. (1996). Electronic distance measurement – an introduction. New York: Springer – Verlag Berlin Heidelberg.

Rueger, J.M. (1998). Refractive index formulae for electr-optical distance measurement. Proceeding of International Federation of Surveyors (FIG'98), Paper TS28/1: 191 – 208.

Rueger, J.M. (2003). Electronic surveying instruments. a review of principles, problems and procedures. The University of New South Wales, Monograph 18.

Rueger, J.M., Alanko, G. and Snow, T.J. (1994). Monitoring of an open cut mine with a surveying robot. *The Australian Surveyor, 39(4):252 – 266.*

Safari Now. Johannesburg and Gauteng weather and climate. Available at: www.safarinow.com/cms/johannesburg-gauteng/irie.aspx**.** (Accessed 21 March 2009).

Schlische, R.W. and Ackermann, R.V. (1998). Integrating computers into the field geology curriculum. *Journal of Geoscience Education,46(1):30– 40.*

Schlische, R.W., Reilly, T.J., Ackermann, R.V. and Ashley, G.M. (1997). Field investigations of structural and stratigraphic expressions of Mesozoic Rifting on the New Brunswick Campuses of Rutgers University. *Geological Society of America Abstracts with Programs 29(6):24.*

Schofield, W. (1993). Engineering Surveying: theory and examination problems for students. Oxford England: Boston Butterworth-Heinemann.

Schofield, W. and Breach, M. (2007). Engineering Surveying. UK: Butterworth-Heinemann Elsevies Publisher.

Science Free Encyclopaedia. Optics – wavelength, frequency, and the speed of light. Available at:http://science.jrank.org/pages/4870/Optics-Wavelength-frequency-speed-light.html (Accessed 29 June 2008).

Signoret, P. and Borelli, N. (1992). Deformation monitoring of a hydroelectric reservoir's surroundings – Italy. Switzerland: Leica Heerbrugg AG.

Skyttner, L. (2002). Minitoring and early warning system – a design for human survival. *Kybernetes, 31(2):220 -245.*

Slatyer, R. O. and Mcilroy, I. C. (1961). Practical Microclimatology. CSIRO, Melbourne (for UNESCO).

SÖNMEZ S. (2005). Elementary Surveying. Lecture note on Engineering Surveying, Ankara University, Turkey.

Steve, W.W. (2009). Atmospheric stability. Los Angeles Pierce College weather station. Available at: http://data-piercecollege.edu/weather/stability.html (Accessed 12 March 2009).

Stiros, S.C., Vichas, V. and Skourtis, C. (2004). Landslide monitoring based on geodetically derived distance changes. *Journal of Surveying Engineering (ASCE), 130(4):156 – 162.*

Talbot, N.C. and McCusker, M.V, (2003). Calibrating electronic distance measurement instrument. Available at: http://www.freepatentsonline.com/6,670.913.html (Accessed 12 May 2009).

Thomas, H.G. (2003). Slope stability monitoring project. University of the Witwatersrand, Johannesburg, South Africa.

Thomas, H.G. (2011). Slope stability prism monitoring: A guide for practising mine surveyors. Unpublished M.Sc dissertation, University of the Witwatersrand, Johannesburg, South Africa.

Tokovinin, A., Vernin, J.,Ziad, A. And Chun, M.R. (2005). Optical turbulence profiles of Mauna Kea measured by MASS and SCIDAR. PASP (Publication of the Astronomical Society of the Pacific), 117(830):395 – 400.

US Army Corps of Engineers (2002). Sources of measurement error and instrument calibrations. Engineering manual 1110-2-1009, Chapter 4, June 2002. Available at: http://www.usace.army.mil/inet/usace-docs/eng-manuals/ em1110-2-1009/c-4.pdf. (Accessed 21 June 2008).

Wackerly, D.D., Mendenhall, W. And Scheaffer, R.L. (2008). Mathematical statistics with applications. Belmont, USA: Thomson Learning Inc.

Wallance, R.G., Dinaso, S.M. and Gutowski, V.P. (1996). Use of total stations and computers in geologic field camp. *Geological Society of America Abstracts with Programs, 28(7): 329.*

Webb, E.K. (1964). Daytime thermal fluctuations in the lower atmosphere. *Applied Optic, 3: 1329 – 1336.*

Weber, J.P. and Lazowick, A.D. (1984). Total station capability. American Society of Photogrammetry – American Congress on Surveying and Mapping (ASP-ACSM), Fall Convention, pp. 166 – 171.

Whyte, W and Paul, R.E. (1997). Basic Surveying. Oxford, Burlington, UK: Elsevier Butterworth-Heinemann.

Wilkins, R. (2004). Mining with robots. Available at: http://www.leicageosystems.com/media/new/product_solution/Oct2004_pob_mining.pdf. (Accessed 23 September 2008).

Williams, E.D. (2003). Atmospheric stability, a primer for pilots. SMXGIG (Santa Maria, CA, Airport gig) May 2003. Available at: http://williams.best.vwh.net/ (Accessed 21 March 2009).

Wirshing, R., Wirshing, J.R. and Wirshing R.H. (1985). Introductory Surveying. McGraw-Hill Companies.

Wolf, P.R. (2002). Surveying and mapping: history, current status and future projections. *Journal of Surveying Engineering, 128(3):79 – 107.*

Wolf, P.R. and Ghilani, C.D. (1997). Adjustment computations: statistics and least squares in surveying and GIS. New York: John Wiley and Sons, Inc.

Wright, A.F. and Sturman, B. (2008). The history of Tellurometer. Integrating the generations. FIG Working Week, Stockholm, Sweden, 14 – 19, June 2008.

Wyngaard, J.C. (1992). Atmospheric Turbulence. *Annual Review of Fluid Mechanics, 24: 205 – 234.*

Yildiz, F., Karabork, H., Yakar, M., Altuntas, C., Karasaka, L. and Goktepe, A. (2007). 3D modeling by advance total station. XXI International CIPA Symposium, held in Athens, Greece.

Young A. T. (2007). Refractivity of air. San Diego State University, California, USA. Available at**:** http://mintaka.sdsu.edu/GF/explain/atmos_refr/air_refr.html. (Accessed 11 August 2008).

Zeiske, K. (2001). Current status of the ISO standardization of accuracy determination procedures for surveying instruments. Proceedings of FIG Working Week 2001, Seoul, Korea 6–11 May 2001.

Zeng, X., Zhang, Q., Johnson, D. and Tao, W.K. (2002). Parameterization of Wind Gustiness for the Computation of Ocean Surface fluxes at different Spatial Scale. *American Meteorological Society, 130(8):2125 – 2133.*

APPENDIX A

Table A.1: Surface roughness parameter scale

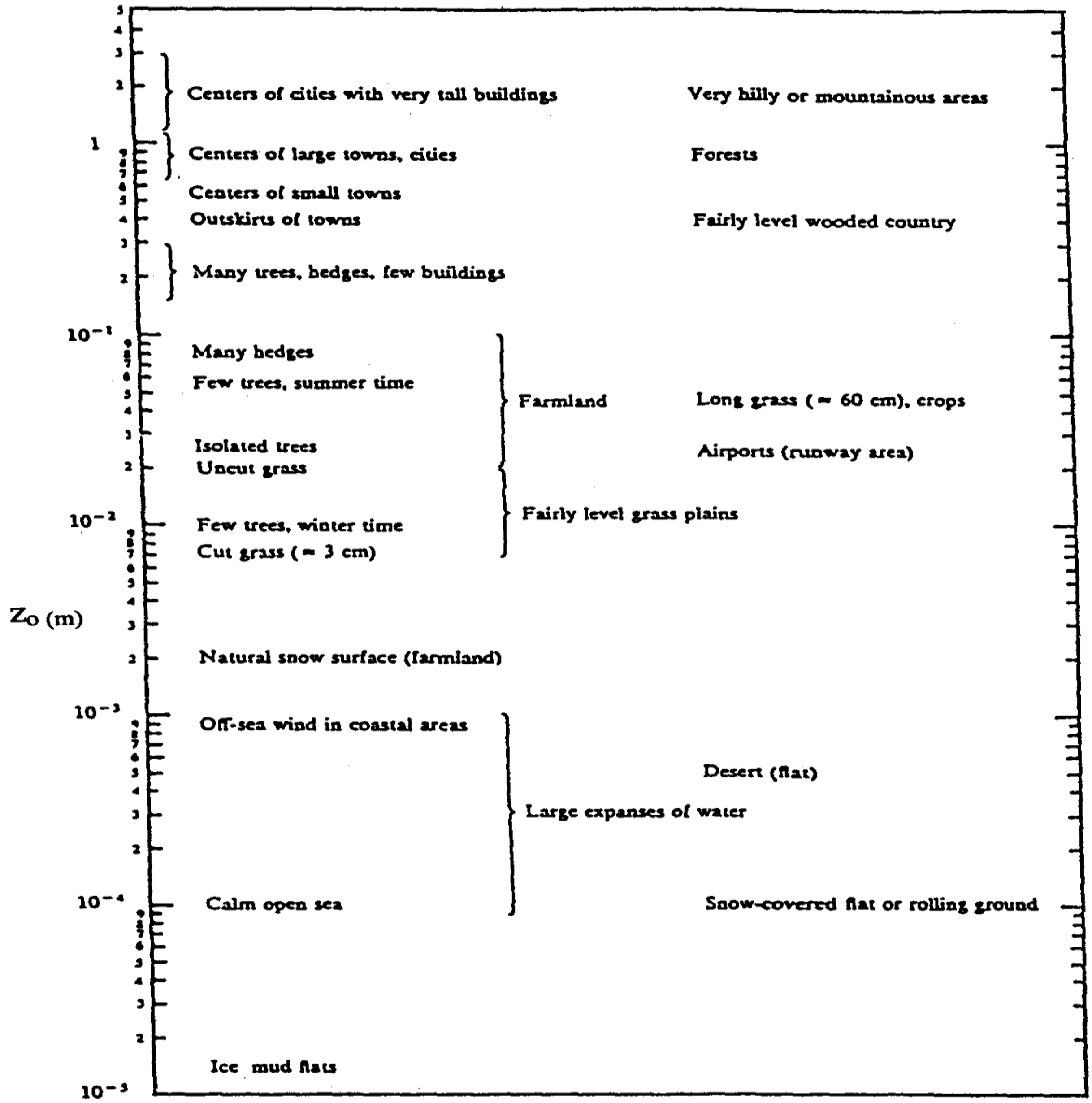

Ground Cover	Roughness Length (m)
Water or ice (smooth) (over water z_0 increases with wind speed)	10^{-4}
Mown grass	10^{-2}
Long grass, rocky ground	0.05
Pasture land	0.20
Suburban housing	0.6
Forests, cities	1–5

(Source: Rueger 1984)

Table A.2: Parameter (A) values

Temperature (^oC)	Parameter (A)
-10	0.74
0	0.60
10	0.44
20	0.31
30	0.21
40	0.14

(Source: Angus-Leppan, 1971)

Table A.3: Auxiliary scale shows the Bulk Aerodynamical coefficient as a function of surface roughness (Source: Augus-Leppan, 1971)

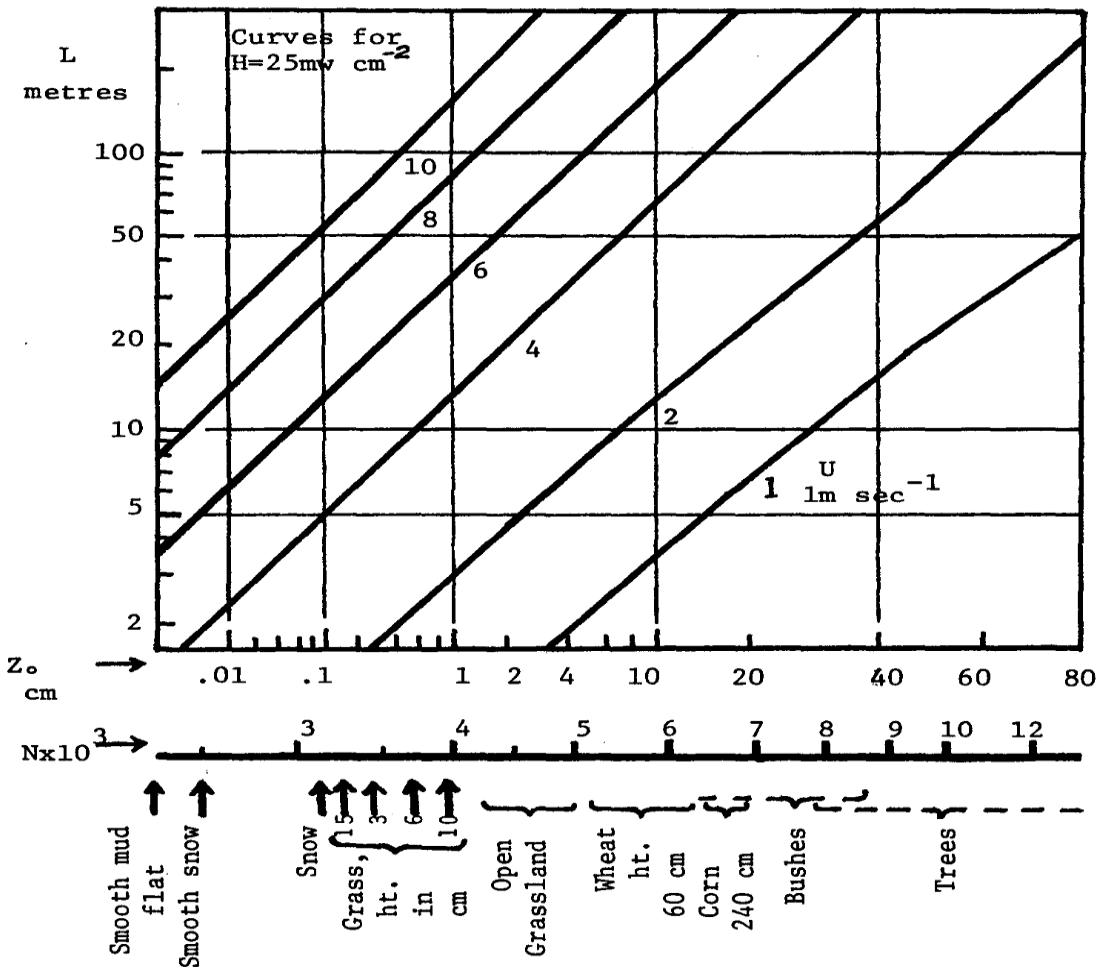

APPENDIX B

Appendix B.1

Pre-delivery Test Results

********** TCR1201+ R1000 / V2008.07 / 17.11.2008 / 61062 / Tol: V1.0*****
Date: 2008-11-17 10:42
Instrument No.: 871187
Technician: SHV Visagie
Customer: University of Witwatersrand
Notes: Outgoing test
Test Result: PASS
000000000000000000000000000000000000000000000000000000000000000
********** TCR1201+ R1000 Outgoing Test **********
1. Reading out instrument data

------ General ------		------- NLQ -------	
Instrument type	: TCR1201+ R1000	Accuracy	: 000.00020
Instrument number	: 871187	L Factor (E)	: 227454
Equipment number	: 3343804	T Factor (F)	: -116737
Mainboard number	: 757782230708148	Default L Factor	: 0.00022783
Firmware version	: 6.02	Default Q Factor	:-0.00011753
Boot Version	: 2.02	L Index	: 000.00000
EDM Version	: 4.17	Q Index	: 000.00000
ATR Version	: 0.00	L Coarse index	: -002.54598
PS Version	: 0.00	T Coarse index	: -000.78512
KDM Version	: 4.06 / ---	TK L Index (C)	: -54
EFI Version	: 2.00	TK Q Index (D)	: -4
Intern temperature	: 26.7 / 24.6	T factor L	: 0.00077958
Gear version	: None	T factor Q	: 0.00077958
------- TIM -------		Factor L to T (G)	: 19696
MOT-Adjustment Flag	: ---	Factor T to L (H)	: -24293
Operating hours MOT	: 0.000	NLQ Swamp (S)	: 389
Operating hours GUS	: 0.000	Exposure time	: 339
------- ANG -------		------- EDM -------	
Adjustment flag	: O.K.	EDM Temperature	: 36.0/36.0
Accuracy	: 000.00030	Quartz Reference F0	: 99997516
Diametric	: 1	Quarz Poly F1	: 5107
H1 Eccen. phase (O)	: 000.0	Quarz Poly F2	: -8435
H1 Eccen. ampl. (Q)	: 0.0	Quarz Poly F3	: 9449
V1 Eccen. phase (P)	: 0.0	Add. constant IR (I)	: -427
V1 Eccen. ampl. (R)	: 0.0	Add. constant SR (J)	: -423
H2 Eccen. phase	: 000.0	EDM Board number	: 20009344
H2 Eccen. ampl.	: 0	Identification / SW	: 70 / 4.17
V2 Eccen. phase	: 000.0	APD Voltage V25	: 143.2
V2 Eccen. ampl.	: 0	Temp. value t25	: 250
H1 Exposure time	: 298	Temp. cof. TK1	: 66
V1 Exposure time	: 303	Temp. cof. TK2	: 0

H2 Exposure time	: 282	Boomerang	: 8
V2 Exposure time	: 268	Filter offset	: 4 / 13
H1 Array table	: OK	Laser IR PWM	: 192
V1 Array table	: OK	Laser IR TK	: 0
H2 Array table	: OK	Laser SR PWM	: 204
V2 Array table	: OK	Laser SR TK	: 0
H1 Circle table	: Corr. No	EGL number	: 0
V1 Circle table	: Corr. No	---- End of the initial read-out ----	
H2 Circle table	: Corr. No		
V2 Circle table	: Corr. No		

------- TMC -------

Adjustment flag	: O.K.
V Coarse index	: 004.22209
V Coarse index	: 000.00000
TK V Index (B)	: 157
Collimation error	: -000.00051
TK Collimation (A)	: 10
Tilting axis error	: -000.00078

2. Tribrach screws	Manual test : O.K.
3. Locking mechanism	Manual test : O.K.
4. Spherical level for tribrach	Manual test : O.K.
5. Laser / Optical plummet	Manual test : O.K.
6. Spherical level	Manual test : O.K.
7. Standing axis	Manual test : O.K.
8. Horizontal friction clamp	Manual test : O.K.
9. Horizontal drive	Manual test : O.K.
10. Tilting axis	Manual test : O.K.
11. Vertical friction clamp	Manual test : O.K.
12. Vertical Drive	Manual test : O.K.
13. Carrying handle	Manual test : O.K.
14. Battery cover	Manual test : O.K.
15. Optical sight	Manual test : O.K.
16. Telescope eyepiece	Manual test : O.K.
17. Bayonet lock	Manual test : O.K.
18. Telescope reticle	Manual test : O.K.
19 Focusing	Manual test : O.K.
20. Image quality	Manual test : O.K.

21. True running of standing axis

M0 : -000.0008

M1 : 000.0034

M2 : 000.0008

M3 : -000.0033

X1 : -000.0000 X2 : 000.0001

Diff : 2 cc

22. Stability of V collimation

M1 : 100.0016

M2 : 100.0026

Diff : 11 cc

23. Horizontal collimation

Collimator Face I : 020.9060

Collimator Face II : 220.9054
Collimation4.6m : 000.0002
Collimator Face I : 020.6835
Collimator Face II : 220.6845
Collim. infinity : -000.0006

24. Tilting axis error with SW
Collimator Face I : 060.4385
Collimator Face II : 260.4391
Tilting axis error : 000.0004

25. V coarse index, L coarse index, T coarse index
Collimator Face I : 104.2262
Collimator Face II : 304.2226
V Coarse index : 004.2233
L Coarse index : -002.5458
T Coarse index : -000.7854

26. L factor, T factor
V1 : 100.0722 L1 : -000.0711
Q1 : 000.0711
V2 : 099.9312 L2 : 000.0702
Q2 : -000.0703
FL : 455 FQ : 465

27. Factor T on L
L1 : -000.0003 Q1 : -000.0717
L2 : -000.0006 Q2 : 000.0720
FQL : 654

28. Factor L on T
L1 : 000.0737 Q1 : 000.0007
L2 : 000.0013 Q2 : -000.0734
L3 : -000.0733 Q3 : -000.0005
L4 : -000.0008 Q4 : 000.0731
FLQ : 167

29. Inspecting tilt sensor
Peak Distance mean : 11.52 11-12 Pixel
Max. Peak Difference : 0.46 <1.00/1.00 Pixel
Pixel Amplitude diff. : 79.5 >70 %
P to P Amplitude diff. : 93.3 >70 %
Pixel sharpness : 85.5 >50 %
Swamp maximum : 174 <100 ADC
Cleanliness : OK

30. Socket and contacts Manual test : O.K.

31. Current consumption
Off : 00 mA WNG : 272 mA
EDM : 425 mA

32. Monitoring voltage Manual test : O.K.
33. Display test , display illumination Manual test : O.K.
34. Keyboard test Manual test : O.K.
35. Plug-in battery Manual test : O.K.
36. Memory card
Inserted : Yes
37. IR Transmitter power

Las.Dark	: 133	
Las.D-RL	: 103	
IR	: 275.1 uW	

38. SR Transmitter power

SR	: 4155.4 uW	

39. Frequency difference

Fcalc	: 100382740 Hz	
Fmeas	: 100382703 Hz	
Fdiff	: 37 Hz	

40. Sensitivity IR

SigMax	: 415 ADC	

41. Sensitivity SR

SigMax	: 2.0799m / 486 ADC	
SigMax	: 7.0426m / 549 ADC	

42. Cal Signal

Cal IR	: 1704	
Cal SR	: 1781 ADC	

43.Crosstalk

IR	: 45 uV	
SR	: 146 uV	

44. Dynamic test

DIST 01	: 7.1575 m	F/C : ---
DIST 02	: 7.1578 m	F/C : ---
DIST 03	: 7.1577 m	F/C : ---
DIST 04	: 7.1579 m	F/C : ---
DIST 05	: 7.1581 m	F/C : ---
DIST 06	: 7.1578 m	F/C : ---
DIST 07	: 7.1579 m	F/C : ---
DIST 08	: 7.1581 m	F/C : ---
DIST 09	: 7.1583 m	F/C : ---
DIST 10	: 7.1584 m	F/C : ---
DIST 11	: 7.1585 m	F/C : ---
DIST 12	: 7.1592 m	F/C : ---

45. Distance SR

DIST	: 7.1582 m	F/C : ---
DIST	: 7.1581 m	F/C : ---
DIST	: 7.1581 m	F/C : ---
DIST	: 7.1581 m	F/C : ---
DIST	: 7.1581 m	F/C : ---
Max Sig.	: 975 ADC	

46.Dist after power On

ON	: 7.2869 m	F/C : ---
ON	: 7.2869 m	F/C : ---
ON	: 7.2869 m	F/C : ---
ON	: 7.2869 m	F/C : ---
ON	: 7.2867 m	F/C : ---
Standby	: 7.2867 m	F/C : ---
Standby	: 7.2867 m	F/C : ---
Standby	: 7.2869 m	F/C : ---
Standby	: 7.2868 m	F/C : ---

Standby : 7.2867 m F/C : ---
Standby : 7.2868 m F/C : ---

47. EDM - Optical axis — Manual test : O.K.
48. Inspecting automatic targeting — No test necessary for this type of instrument.
49. Hz positioning — No test necessary for this type of instrument.
50. V positioning — No test necessary for this type of instrument.
51. Gear Test — No test necessary for this type of instrument.
52. Measure the output of the ATR transmitter diode — No test necessary for this type of instrument.
53. ATR Center the transmitter diode — No test necessary for this type of instrument.
54. ATR CCD camera, zero position — No test necessary for this type of instrument.
55. ATR Light volume test — No test necessary for this type of instrument.
56. ATR function test — No test necessary for this type of instrument.
57. PS Measure power output — No test necessary for this type of instrument.
58. PS function test — No test necessary for this type of instrument.
59. PS Distance difference over reference — No test necessary for this type of instrument.
60. EGL Measuring the diode output — No test necessary for this type of instrument.
61. EGL Aligning the line of sight — No test necessary for this type of instrument.
62. GUSMeasure the laser pointer output — No test necessary for this type of instrument.
63. GUS Aligning the laser line of sight — No test necessary for this type of instrument.
64. Reading out Bluetooth — No test necessary for this type of instrument.
65. Bluetooth Test — No test necessary for this type of instrument.
66. Enter TPS condition
    O.K.
    Problems in

67. Labelling — Manual test : O.K.
68. Reading out instrument data

------ General ------		------- NLQ -------	
Instrument type	: TCR1201+ R1000	Accuracy	: 000.00020
Instrument number	: 871187	L Factor (E)	: 227454
Equipment number	: 3343804	T Factor (F)	: -116737
Mainboard number	: 757782230708148	Default L Factor	: 0.00022783
Firmware version	: 6.02	Default Q Factor	: -0.00011753
Boot Version	: 2.02	L Index	: 000.00000
EDM Version	: 4.17	Q Index	: 000.00000
ATR Version	: 0.00	L Coarse index	: -002.54576
PS Version	: 0.00	T Coarse index	: -000.78543
KDM			
Version	: 4.06 / ---	TK L Index (C)	: -54
EFI Version	: 2.00	TK Q Index (D)	: -4
Intern temperature	: 27.9 / 26.3	T factor L	: 0.00077958
Gear version	: None	T factor Q	: 0.00077958
------- TIM -------		Factor L to T (G)	: 19696
MOT-Adjustment Flag	: ---	Factor T to L (H)	: -24293
Operating hours MOT	: 0.000	NLQ Swamp (S)	: 389
Operating hours GUS	: 0.000	Exposure time	: 343
------- ANG -------		------- EDM -------	
Adjustment flag	: O.K.	EDM Temperature	: O.K./ 4.17
Accuracy	: 000.00030	Quartz Reference F0	: 99997516
Diametric	: 1	Quarz Poly F1	: 5107

H1 Eccen. phase (O)	: 000.0
H1 Eccen. ampl. (Q)	: 0.0
V1 Eccen. phase (P)	: 0.0
V1 Eccen. ampl. (R)	: 0.0
H2 Eccen. phase	: 000.0
H2 Eccen. ampl.	: 0
V2 Eccen. phase	: 000.0
V2 Eccen. ampl.	: 0
H1 Exposure time	: 288
V1 Exposure time	: 305
H2 Exposure time	: 282
V2 Exposure time	: 272
H1 Array table	: OK
V1 Array table	: OK
H2 Array table	: OK
V2 Array table	: OK
H1 Circle table	: Corr. No
V1 Circle table	: Corr. No
H2 Circle table	: Corr. No
V2 Circle table	: Corr. No
------- TMC -------	
Adjustment flag	: O.K.
V Coarse index	: 004.22328
V Coarse index	: 000.00000
TK V Index (B)	: 157
Collimation error	: -000.00056
TK Collimation (A)	: 10
Tilting axis error	: 000.00042

Quarz Poly F2	: -8435
Quarz Poly F3	: 9449
Add. constant IR (I)	: -427
Add. constant SR (J)	: -423
EDM Board number	: 20009344
Identification / SW	: 70 / 4.17
APD Voltage V25	: 143.2
Temp. value t25	: 250
Temp. cof. TK1	: 66
Temp. cof. TK2	: 0
Boomerang	: 8
Filter offset	: 4 / 13
Laser IR PWM	: 192
Laser IR TK	: 0
Laser SR PWM	: 204
Laser SR TK	: 0
EGL number	: 0

---- End of the initial read-out ----

APPENDIX B.2

Pre-Delivery Calibration on a New Total Station – Geosystems Africa Laboratory Experience

T.B. Afeni and F.T. Cawood

Abstract

This report centred on the pre-delivery test on a new total station carried out at Geosystem Africa Laboratory in Johannesburg, South Africa. The report describes total station areas of applications, errors and sheds more light on pre-delivery calibration procedures.

Keywords: *Total station, areas of application, errors, and pre-delivery calibration*

Introduction

Pre-delivery calibration is the tests carried out by the manufacturer (or designated person/authority) on some major components of a new instrument or good to ascertain if such components meet the manufacturer specifications as submitted to either the International Organization for Standardization (ISO) or equipment manufacturer specification before delivering such instrument or good to end-users.

The ethics of the surveying profession requires surveyors to comply with certain legal, regulatory and/or accuracy requirements. They will typically strive to do so in an optimally cost-effective way and with the most appropriate equipment for the job at hand. This in most cases requires good understanding of and confidence in the instrumentation employed. Clients want value for money and assurance that the products of survey services deliver quality. Legislative authorities and public companies require assurance that the services rendered conform to globally accepted rules of best practice. Today, however, ease and speed of modern survey instruments result in a tendency to assume measurements are free from errors. This is, of course, simply not true. Instrument verification, testing and calibration are just as important today as what they were in the past (Martin, 2007). As a matter of fact, the high technological level of such equipment requires high-level skills for understanding the operation and on-board processing of survey results.

Geomatics practitioners, engineers, developers, owners and even regulatory authorities use various parts of the surveying process in contributing to the conceptualization, design, actualization and maintenance of engineering and land development projects. With respect to surveying, their requirements in the field and office with respect to the tools they use are for:

1. Accuracy;
2. Functionality;
3. Integration;
4. Productivity; and
5. Ease of use.

These requirements are to ensure that the activities required by surveying processes that contribute to the project are done properly and in a timely manner. Today, a wide variety of tools are available to the surveyor to accomplish these activities. It is no longer a matter of just having a transit, tape and dumpy level at hand. The tools themselves overlap the required functionality in some respects. It is incumbent on the surveyor to do the analysis, synthesis and integration to most effectively use the resources at hand. When the surveyor's toolbox is integrated properly, it is possible to optimize the tool to the application. The primary concept in tool integration in the field is to provide the ability to work independently of the sensor. By sensor is meant surveying instruments that are used to sense position in one, two or three dimensions. The predominant sensors in use are optical total stations and real time kinematic global positioning system (GPS) (Fosburgh and Paiva, 2001).

Total Station

Recent developments in photogrammetric and surveying equipment have been closely associated with advances in electronic and computer technologies. Electronic distance measuring instruments for ground surveying now are capable of output data in machine-readable language for computer input and/or combining distance and angle measurements for direct readout of horizontal and vertical distances to decimals of millimetre length and second of arc (Roy, 2004). The incorporation of data collectors and electronic field books with interfaces to computer, printer, and plotter devices has resulted in the era of **total station** surveying.

According to Eiteljorg (1994), 'a total station is a combination electric transit (theodolite) and electronic distance measuring device (EDM)'. This device would enable the user to determine angles and distances from the instrument to the point to be surveyed just like the old transit and tape. Total stations are therefore electronic tachometers, i.e. a geodetic instrument for measuring slope distance, horizontal and vertical angles to a target point (Kavanagh and Glenn Bird, 1992).

Types of total station

A typical Total Station EDM can measure distances accurate to about 3 millimeters or 1/100th of a foot. The ability to measure to a reflector or even without reflector is one of the criteria used to group the instruments into two types (reflector and reflectorless types). Also the tasks that can be performed on the instruments can be used to separate them into three types:

1. Manual Total Station: Both distance measuring and angle measuring make use of the same telescope optics (coaxial). Slope reduction of distances is done by optically reading the vertical angle (or Zenith angle) and keying it into an on-board calculator or any pocket calculator. Horizontal angles are also read optically.
2. Semi-Automatic Total Station: Contains a vertical angle sensor for automatic reduction of distances (without keying in a slope angle). Horizontal angles are read optically.
3. Automatic Total Station: Both horizontal and vertical are read electronically for use with slope distances in a data collector or internal computer.

Some modern total stations are 'robotic' allowing the operator to control the instrument from a distance via remote control. This eliminates the need for an assistant to hold the reflector prism over the point to be measured. The operator holds the reflector him/herself and controls the total station instrument from the observed point. An automated monitoring survey system using a robotic total station removes the manual repetition factor from the survey. The robotic system is "taught" the sequence of measuring to each of the monitoring points and continues measuring at pre-set intervals. Thus the human (error) element is removed from the task (Thomas, 2003).

In the teaching environment, a total station fulfils several purposes. Learning how to properly use a total station involves the physics of making measurements, the geometry of calculations and statistics for analyzing the result of a traverse (Cruikshank, 1999).

Areas of Application

The areas of application of total station instruments continue to expand. An overview of the electronic total station and some of its uses were given by Philpotts *et al* (1997), Schlische and Ackermann (1998). This section describes some of the applications, namely: application in mining, geology, engineering surveying, road and safety surveys and archaeology surveys.

Mining Surveys

The total station is the primary survey instrument used in many mining applications at both surface and underground mines. In underground surveys as the development drifts are driven, a total station is used to record the absolute location of the tunnel walls, ceilings, and floors. This data is then downloaded into a CADD environment, and compared to the designed layout of the tunnel. At regular intervals, the survey party will install stations made of small steel plugs that are drilled into the walls or the roof. The plugs are installed in sets. For wall stations, two plugs are installed in opposite walls, forming a line perpendicular to the drift. When the survey crew wants to set up the total station in a drift, they use a set of stations to locate the total station. The use of total station for correlation survey for shaft deepening in underground mine was discussed by Bahuguna (2003).

The recent development in total stations made them reliable for remote monitoring of rock slope movements; as was discussed by Cruden and Masoumdazadeh (1987). Observation of slope movements in surface mines can now be extrapolated to assist with prediction of slope failure.

The use of total stations to generate essential spatial data to produce production plans, undertake initial hazard appraisal of excavated slopes, perform slope face geometry profiling and provide spatial data for blast design purposes and monitor slope stability of identified critical excavations was explained by Coggan *et al* (2001).

The increasing use of servo-driven electronic total stations in the mining industry due to their high survey efficiency and accuracy was discussed by Ding *et al* (1998). Fully automatic total stations (also referred to as survey robots) have been developed to automate field deformation surveys. When the instrument is properly set up, it is automatically capable of find prisms and takes the observation and stores the readings (angles, distances and coordinates readings). Therefore, much less human involvement is required in the field. This is a great advantage as manual observations are usually repetitive, labour-intensive, time consuming and more prone to error.

The use of a remote surveying vehicle (RSV) fitted with reflectorless or robotic total stations (RTS) to carry out surveying work in hazardous mining areas was explained by Jobling-Purser (2006). The RSV fitted with reflectorless or RTS would help to conduct a non contact survey thereby eliminate the risk of exposing personnel to any hazardous area in a mine.

Geology Surveys

The use of total station surveying instruments as a basic tool for various geological surveys including monitoring and analysing surface - faulting and hazards, was recorded by Lavine *et al* (2003) in confirmation with various publications of other authors (Philpotts *et al*, 1997; Schlische *et al*, 1997; Bulut and Tude, 1996) who had in one time or the other used a total station for geologic mapping work.

Total station surveys have replaced compass directions for measuring fracture orientation at exposed rock faces (Feng *et al*, 2001). Ground deformation monitoring at potential landslide sites using total station surveying instruments have been discussed by Moss *et al* (1999) and Haentjens (1992).

Total stations made the use of plane table surveying and alidades for mapping obsolete. Its usage in topographic surveys and for measuring the directions/velocities of steams flow was discussed by Keim *et al* (1999) and Philpotts *et al* (1997). Digital terrain modelling of small stream channels with a total station was also described by Keim *et al* (1999).

Engineering Surveys

EDM devices are extensively used in the construction industry nowadays. The early instruments, which were capable of very precise measurement over very long distances, were large, heavy, complicated and expensive. Technological advancement has provided lighter, smaller, simpler and less expensive models (Roberts, 1995). The new instruments offer many advantages including accuracy, productivity and interconnectivity. Owing to the advantages offered by the instruments, many construction companies are now readily adopting the use of these instruments in their businesses (Arumala, 2000). The total station instrument has shown itself to be very useful for planning new construction areas and providing quick measurements to inaccessible surfaces (Gaudreault, 2004). Engineering applications of the total station have been reported for monitoring of high rise buildings (Rueger, 1994) and stability of water storage dams (Signoret and Borelli, 1992; Rueger, 1994a). The use of total station instruments during highways and bridges construction work and other construction sites due to the rugged nature of these instruments was recorded by MacDonald (2001).

Geodetic techniques have been used over the last decades for structures monitoring. Recent developments allow total stations to track, make measurements of distances and angles to a moving target (target in motion) and to store data automatically. It has been demonstrated that RTS can be used for dynamic deformation monitoring of structures in certain circumstances with good results (Cosser *et al*, 2003).

Slow–deforming structures such as dams require sub-millimetre accuracy to monitor wall displacement. Although such precision may be achieved with GPS under certain conditions, from an accuracy perspective, it is not always the preferred method. To effectively monitor such structures, GPS should be supplemented with geotechnical sensors and high-accuracy total stations (El -Rabbany, 2002).

The uses of total station for monitoring bridges and structural deformations have been explained by many authors (Merkle and Myers, 2004; Hill and Sippel, 2002; Kuhlmann and Glaser, 2002; Leica Geosystem, 2002). Also landslide monitoring based on geodetically derived distance changes was discussed by Stiros *et al* (2004).

Road Safety Surveys

Total stations are also used for police crime scene investigations, private accident re-constructionists and insurance companies for the measurement of accident scenes. Such accurate measurements are downloaded into modelling software in order to recreate the accident in a 3D environment and have better interpretation of what happened at the time of the accident (Philpotts *et al*, 1997; Schlische and Ackermann, 1998).

Archaeology Surveys

Cultural heritages should be preserved for future generations, therefore it is important to keep records of such sites. The main reasons for use of total station in archaeology were stated by Rick (1996):

> *'Because of reducing prices, increasing reliability and numbers of features, and decreasing weight, total stations are increasingly likely to enter the archaeologist's toolkit. For mapping of all kinds, the additional speed and accuracy offered by total stations demand archaeologists attention. The greater annotation potential, reduced error rate and higher efficiency of electronic data transfer contribute to timely, successful data processing. Total stations could be quite useful in place of or in conjunction with GPS instruments for local area surveys'.*

The use of total stations to collect data on cultural heritage and using 3D modelling to generate computer graphics were discussed in many publications (Yildiz *et al*, 2007; Hirst, 2006; Lehtonen, 2005).

A comparative measurement study using a 3D laser scanner and reflectorless total station of the slots of El-khazneh at Petra in Jordan was carried out by Haddad and Ishakat (2007). The results indicated that the difference in the measurement was within the range of 0.2 to 2 cm. The author concluded that the accuracy of laser scanning cannot beat that of geodetic instruments (such as reflectorless total stations).

Modern architecture or contemporary architecture can be difficult to survey. Most of the time, a survey is done as support to an analytical view that is constructed as support for a conservation or restoration project. Due to the fact that by and large, contemporary or modern architecture does not call for these types of interventions, the case history of surveys of modern buildings is extremely limited. The survey of the modern architecture of Giardino delle Scultire in Biennale Italian Pavillon was carried out using Total Station – Leica TCA 2003 (Balletti *et al*, 2005).

Total Station errors

The error affecting a total station measurement can be divided into two - internal and external components. For electro-optical instruments with their reflectors, the internal errors have been identified as zero error, scale error, cyclic error, and phase measurement error (Amiri-Simkooei, 2003). These may arise from imperfections of the instruments and/or reflectors. Zero error, scale error, and cyclic error are grouped as systematic errors while phase measurement error is a random error. Zero error is a constant systematic error (i.e. additive constant), scale error is an incremental systematic error (i.e. linearly proportional), and cyclic error is a periodic systematic error (i.e. short periodic error). External errors are mainly due to atmospheric refraction and human mistakes.

The Zero or Index error is a near-constant systematic error that can arise from a number of sources. In essence, such an error will be present if the geometric path length, as defined by the mechanical centring marks of the instrument and reflectors, is not identical to the electro-optical path measured by the instrument. It might have an obvious source, as when reflectors with a different prism constant are interchanged. Errors of this nature can also arise if an instrument has been repaired or adjusted such that the internal electro-optic path within the instrument has been tampered with (Burnside, 1991). This means that the zero error includes both the position of the electrical centre of the EDM and any un-modelled prism offset. The causes of zero/index error can be grouped into three factors as follows:

1. Electrical delays, geometric detours and eccentricities in EDM;
2. Differences between the electronic centre and mechanical centre of the EDM; and
3. Differences between the optical and mechanical centre of the reflector.

An additive constant is added to the measured distances to correct for these differences. This type of error may vary with changes of reflector, to avoid or curb this; only one reflector should be used for total station calibration.

A Scale error is an incremental systematic error and it's linearly proportional to the distance being measured. This error can arise from both internal and external sources. If the oscillator does not generate the required measurement frequency value within the design tolerance a scale error will be introduced, arising from an internal source. Inaccurate information concerning the average group refractive index along the measured line which is external may also produce the same effect on the other hand. Instruments working on longer ranges, such as microwave equipment, are more at risk than short-range infrared (IR) instruments. This error can be summarized as follows:

1. Internal frequency error, including those caused by external temperature and instrument warm-up effects;
2. Un-modelled variations in atmospheric conditions which affect the velocity of propagation; and
3. Non-homogeneous emission/reception patterns from the emitting and receiving diodes i.e. phase inhomogeneities.

The Cyclic error is also known as short periodic error. It is usually sinusoidal in nature with a wave length equal to the unit length of the EDM. Cyclic error is inversely proportional to the strength of the returning signal since measured distance is a function of the fine measuring frequency and wavelength of the machine; its effects will increase with increasing distance i.e. low signal return strength (Khalil, 2005). The procedure for its correction requires specialized calibration baseline designed to detect the presences of cyclic error from the spacing of the measurement interval (US Army, 2002).

Accurate measurements with total stations assume that all instrument axes are perfectly perpendicular to each other. The reflectorless (RL) EDM reference laser beam, the automatic target recognition (ATR) zero point, and the line of sight must also coincide precisely. Unfortunately these requirements are never perfectly fulfilled. Even with great care when manufacturing the instrument, small deviations from the target position of the different components occur. Also during the normal working life of the instrument, small movements inside the instrument can occur. There are different possible reasons for this (Geosystem, 2003):

1. Result of temperature changes, as every material expands and contracts with temperature;
2. Shocks (e.g. during transportation);
3. Long storage periods; and
4. Stress during normal use.

Even small deviations can lead to measurement errors which are greater than the specified accuracy of the instrument. These deviations can happen with every instrument, regardless of whether it is mechanical or electronic, and are independent of the manufacturer. For most electronic instruments the main deviations can be determined by the user. This procedure is called **calibration**.

Temperature variations: Most equipment is manufactured in Europe and the equipment are standardised based on the prevailing atmospheric conditions. To make the equipment work effectively in Africa (a region with predominant harsh weather), it has to be calibrated to make the equipment acclimatise to typical African atmospheric conditions.

Shocks: In the course of transporting the equipment through various means of transportation (air, water and land) shocks are likely to occur. The shock or vibration in the course of transportation might alter the internal assemblage of the equipment hence there is a need for pre-delivery and frequent calibration.

Long storage: Most equipment is not immediately purchased after manufactured. Therefore, whenever new survey equipment is bought, they need to be calibrated to make sure that the equipment meets the manufacturer specification.

Stress during normal use: During field usage at engineering projects that require high precision and accuracy, the instrument should be calibrated at least twice a year, or before and after each important project (Skyttner, 2002).

Pre-delivery calibration of a new total station

This case study describes the pre-delivery calibration of a new total station – Leica TCR 1201 model (this type of total station belongs to TPS 1200+ series). The machine was procured by the School of Mining Engineering, University of the Witwatersrand purposely for a PhD research project on likely impacts of atmospheric parameters variation and norms of taking observations through a window glass at the mines on the quality of data generated during slope monitoring using total station surveying instrument.

The School decided to buy TCR 1201 type of total station due to the nature of the research at hand that requires high precision and accuracy equipment. The TCR 1201 has the following attributes: high accuracy angle measurements (Hz, V; 1" or 0.3 mgon) and precise long-range distance measurements backed by automatic fine pointing and fast reliable reflector location (i.e. 3 km to a single prism and accuracy superb of 1 mm + 1.5 ppm). It has intuitive interface, power data management, on-board routines and programs, easy viewing of entire surveyed area and immediate access to all measured data.

The pre-delivery calibration was carried out at the Geosystems African laboratory, located at Midrand in Johannesburg, South Africa. The laboratory is appropriately equipped for calibration testing with reflectors mounted on the sides and corners of the laboratory (see pictures 1 to 4).

The pre-delivery calibration of the new TCR 1201 was carried out using computer software purposely designed for calibration exercise. Although, the software has sixty eight (68) steps or operations to be followed when carrying out full calibration on total station survey instruments; because the TCR 1201 was new, only some of these steps were carried out during the pre-delivery calibration. The selected operations are steps 23 to 28, 29 to 30, 31 to 37, 44 to 47 and 66 (see Appendix A for details).

The collimation and tilting axis error test

The steps 23 to 28 catered for collimation and tilting axis error; the steps were carried out using collimation testing equipment. The total station was mounted in such a way that its optical lens is of the same height with that of the collimation calibrator as shown in pictures 5 to 6. Both the collimation testing equipment and the total station were connected to the computer laptop for data exchange between the three. The collimation testing equipment senses the tilting axis reading of the total station with the help of the software and displays it on the screen of the laptop. Adjustment could be made if the error exceeds the manufacturer specification. This adjusted data is communicated back to the total station under test with the help of cables from the computer laptop to the total station.

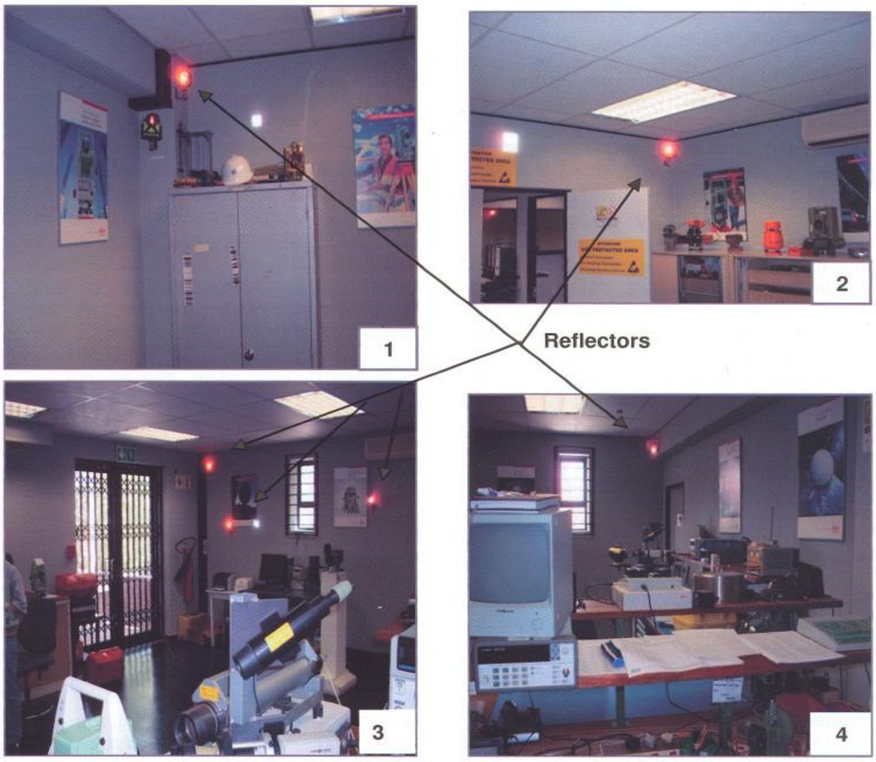

Pictures 1 to 4: Reflectors on the Laboratory Corners and Walls

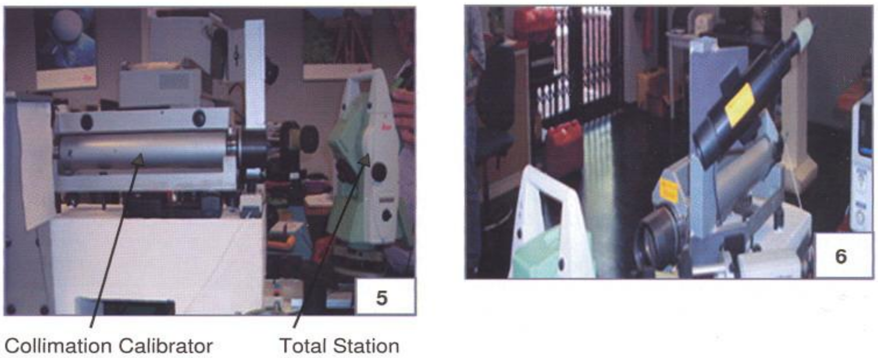

Pictures 5 to 6: Collimation Calibrator (5 - shows side view, 6 – shows front view)

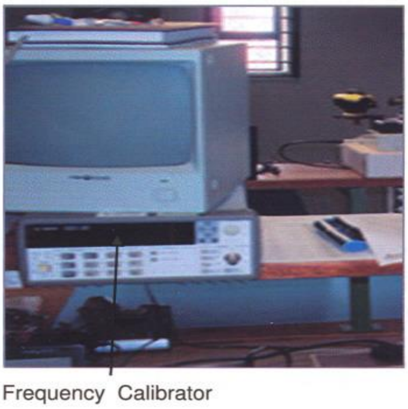

Picture 7: Frequency Calibrator Instrument

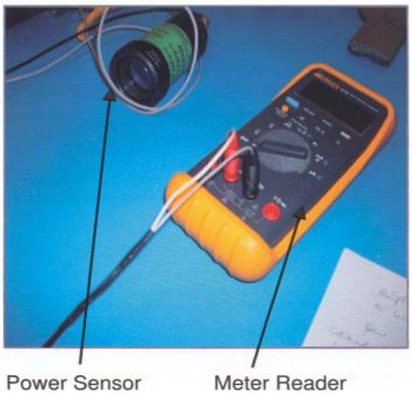

Picture 8: Power Sensor and Meter

Frequency and power consumption verification test

Step 29 to 30 deal with sensing the frequency and power consumption of the new total station. The frequency sensor connected to a frequency calibrator as shown in picture 7 is placed on the optical lens of the new total station and the frequency is displaced digitally on the frequency calibrator equipment. Adjustment could be made via the connection between the frequency calibrator and the software. Also to examine the power consumption rate of the new total station, a power sensor is connected to a meter reader (picture 8 shows the digital electric signal level meter), the current consumption of the total station is displayed on the meter. The displayed power consumption reading is then compared with the specification given by the manufacturer to see if there is much deviation. If there is a discrepancy between the two, adjustments could be made to make the reading conform to the manufacturer specification.

Dynamic and distance test

According to Zeiske (2001), "the first stage in system evaluation is to determining the level of consistency that can be achieved by the total station over a course of measuring circle. This will give a good indication of the instrument performance in real-world conditions as opposed the factory – certified instrument ratings that does not reflect the changing atmospheric effects encountered in practice". The steps 44 to 46 entail dynamic testing, short-range (SR) distance and distance after power on. To achieve these, shots were taken to a know distance, in the case of this exercise – distance was measured to one of the reflectors hanged on the wall of the laboratory several times. The distance readings displayed on the total station screen. These readings were compared after each shot to check consistency in the displaced readings when observations were made to the same target at different time intervals.

Finally any alteration or upgrade made during any of the above steps can be uploaded to the machine (total station) via the calibration software. Picture 9 shows a laptop connected to various calibration tools.

Picture 9: Computer laptop with connection cables to other calibration instruments

Result and Discussion

The results of the pre-delivery test carried on the new total station in most cases were within the limits specified by the manufacturer and developer of the calibration software. All the steps required for full calibration exercise and the selected once out of these steps (reason for selection and not carrying out all the steps being that the total station under consideration is new) is presented in **Appendix A**. The result of the pre-delivery calibration carried out on the new total station TCR 1201 using the 68 steps calibration software clearly shows that the instrument collimation error is -000.00056, this is within the limit stated under step 23 (collimation infinity -000.0006). Also tilting axis error of the new total station is 000.00042 which is in conformity with tilting axis error of 000.0004 as required under step 24 of the software. The V coarse index and L coarse index of the instrument are 004.22328 and -002.54576, which are also within the limit of 004.2233 and -002.5458 stated under step 25. The T coarse index of the new total station is -000.75843, this also conform to -000.7854 as stated under step 25. Lastly, the distance measurements readings shown in 45 and 46 of the appendix indicated consistency in the distance measured with the new total station under test.

Conclusion

This paper gave a brief overview of total station surveying instruments, areas of application, and types of errors that are common to newly procured equipments. Also the reasons for pre-delivery calibration were discussed. The key parameters examined during the pre-delivery mini-calibration of new total station TCR 1201 are in most cases conform to the manufacturer standard specification. In a rare occasion when there is a little deviation, adjustment are made to make such parameter(s) agree with the given manufacturer specifications.

Appreciation: The authors would like to thank the management of Geosystem Africa for their cooperation in the course of this study and Mr. SHV Visagie for taken his time to explain many technical terms during the pre-delivery calibration exercise. Also the authors would like to thank Coaltech Research Association, South Africa for their financial support in the course of this research work.

References

*[1]*Amiri-Simkooei, A. 2003. "Least-Squares Formula for Zero Error (Z_o) of Electromagnetic Distance Measuring Instrument*". Journal of Surveying Engineering, vol.129, Issue 4, pp. 136 – 140.*

[2]Arumala, J.O., 2000. The Impact of New Surveying Instruments on the Construction Surveying Course of Study. *Journal of Construction Education, 5(3): 227 – 243.*

[3] Bahuguna, P.P., 2003. Correlation Survey for Shaft Deepening in Digwadih Underground Coal Mine. *Journal of Surveying Engineering*, 129(1): 33 – 36.

[4]Balletti, C., Guerra, F., Mander, S. and Manzin, M., 2005. Survey of Modern Architecture. *XXth International Symposium of CIPA (The International Committee for Documentation of Cultural Heritage) held in Torino, Italy. 6 pages.*

[5]Bulut, F. and Tude, S., 1996. Determination of Discontinuity Traces on Inaccessible Rock Slopes using Electronic Tacheometer: An Example from the Ikizdere (Rize) Region, Turkey. *Engineering Geology, 44(1): 229 – 233.*

*[6]*Burnside, C.D., 1991. "*Electromagnetic Distance Measurement*". BSP Professional Books, Great Britain; 3rd Edition, 278pages.

[7]Coggan, J., Stead, D. and Howe, J., 2001. Application of Surveying Techniques for Monitoring and Appraisal of Excavated China Clay Slopes. *10th FIG International Symposium on Deformation Measurements. Held in Orange, Califonia, USA. 240 – 249.*

[8]Cosser, E., Roberts, G.W., Meng. X. and Dodson, A.H. (2003**)**: Measuring the Dynamic Deformation of Bridges using a Total Station. Proceedings, 11th FIG Symposium on Deformation Measurements, Santorini, Greece, 8p. Available on line at:http://www.fig.net/commission6/santorini/IMonitoring%20Static%20and%20Dyn/I9.pdf.

[9]Cruden, D.M. and Masoumzadeh, S., 1987. Accelerating Creep of the Slopes of a Coal Mine. *Rock Mechanics and Rock Engineering*, 20(2): 123-135.

*[10]*Cruikshank, K., 1999. Use of the Electronic Total Station – Introduction and Basic Techniques. *Journal of Geosciences Education.* Available online at: http://geomechanics.geol.pdx.edu/courses/G485/totalstation/JGE%20paper%201%introduction.pdf

[11] Ding, X., Montgomery, S.B. and Tsakiri, M., 1998. Integrated Monitoring Systems for Open Pit Wall Deformation. *Australian Centre for Geomechanics, MERIWA Project Report. 4 – 5.*

[12] Eiteljorg, H., 1994. Using a Total Station. *CSA (Centre for Studying Architecture) Newsletter, 7 (2).* Available online at: http://csanet.org/newsletter/aug94/nl089407.html

[13] El-Rabbany, A., 2002. *Introduction to GPS: The Global Positioning System.* Artech House Publishers, Boston, Lon-

don. 176pp.

[14] Feng, Q., Sjogren, p. and Jing, S.L., 2001. Measuring Fracture Orientation at Exposed Rock Face by using a Non-reflector Total Station. *Engineering Geology, 59(1-2):133 – 146.*

[15] Fosburgh, B. and Paiva, J.V.R., 2001. Surveying with GPS. *A.C.S.M. (American Congress on Surveying & Mapping) Conference paper.* 7 pages

[16] Gaudreault, F., Gassner, G., Gaydosh, M and Rogers, M., 2004. The Leica TCRA1105 Reflectorless Total Station. Stanford Linear Accelerator Center (SLAC), *International Workshop on Accelerator Alignment.* Available online at: http://www.slac.stanford.edu/econf/c04100411/papers/022.pdf.

*[17]*Geosystem Publication on TPS Info 01/2003 – Calibration, 6pages. Available online at: http://www.mainetechnicalsource.com/downloadfiles/Calibration.pdf

[18] Haddad, N and Ishakat, F., 2007. 3D Laser Scanner and Reflectorless Total Station: A comparative Study of the Slots of El-Khazneh at Petra in Jordan. *XXI International CIPA Symposium, Athens, Greece. 6pages.*

[19] Haentjens, H., 1992. Monitoring a landslip-Saint-Etienne-de-Tinee (France). Leica Heerburgg AG, Switzerland, 4pp.

*[20]*Hill, C. D. and Sippel, K. D., 2002. Modern Deformation Monitoring: A Multi Sensor Approach." *FIG XXII International Congress, Washington DC, USA.* 12pp. Available at: http://www.fig.net/pub/fig 2002/Ts6 3/TS6 3 hill sippel.pdf.

[21] Hirst, K.K., 2006. A Mapping Device. Available at: http://archaeology.about.com/od/fieldlabgear/ig/Archaeology-Tools-of-the-Trade/Total-Station-Transit.htm

[22] Jobling-Purser, J., 2006. A Robotic Surveying Vehicle for Hazardous Mining Conditions. *BCRA Cave Radio and Electronics Group Journal, 64: 9 – 11.* Available online at: http://www.rsv.eu.com/about/BCRA%2006.pdf

[23] Kavanagh, B.F. and Glenn Bird, S.J., 1992. Surveying Principle and Applications. 3rd Edition, Prentice Hall, Englewood Cliffs, NJ.

[24] Keim, R.F., Skaugset, A.E. and Bateman, D.S., 1999. Digital Terrain Modeling of Small Channels with a Total Station Theodolite. *Advances in Water Resources, 23(1): 41 – 48.*

[25] Khalil, R., 2005. "New Compact Method for laboratory Testing EDM Instruments". FIG Working Week 2005 and GSDI-8, Cairo, Egypt; 8pages. Available online at: http://www.gsdidocs.org/gsdiconf/GSDI-8/papers/ts 22/ts22 06 khalil.pdf

[26] Kuhlmann, H. and Glaser, A., 2002: "Investigation of New Measurement Techniques for Bridge Monitoring." *2nd Symposium on Geodesy for Geotechnical and Structural Engineering, Berlin, Germany, 10pp.* Available at: http://www.unistuttgart.de/iagb/forschung/messtechnik/projekte/download/brueckenueberw.pdf.

[27]Lavine, A., Gardner, J.N. and Reneau, S.L., 2003. Total Station Geologic Mapping: An Innovative Approach to Analysing Surface – faulting Hazard. *Journal of Engineering Geology, 70(1-2): 71 – 91.*

[28] Lehtonen, H., 2005. Virtual Archaeology – What Is It? Mirator Theme Issue. Proceedings from the Symposium "Virtually Medieval?"8pages. Available online at: http://www.glossa.fi/mirator/themeissue2005/vmlehtonen.pdf

[29] Leica Geosystems., 2002. "Bridge Surveys". Available at: http://www.leicageosystems. com/civil/application/bridge.htm.

[30] MacDonald, M., 2001. Total Station – More Jobs in Sight. The Carpenter Magazine, pp.33 -37. Available online at: http://www.carpenters.org/carpentermag/TotalStation78 01.pdf

[31] Martin, D., 2007. Calibrating Surveying Instruments: A Modern Calibration Bench. GIM International, *The Global Magazine for Geomatics, 21(8): 1-3.*

[32] Merkle, W and Myers, J.J., 2004. Use of the Total Station for Serviceability Monitoring of Bridges with Limited Access in Missouri, USA. *16TH World Conference on Non-destructive Testing (WCNDT) Proceedings, pp 570 – 578.*

[33] Moss, J.L., McGuire, W.J. and Page D., 1999. Ground Deformation Monitoring of a Potential Landslide at La Palma, Canary Island. *Journal of Volcanology and Geothermal Research, 94(1-4): 251 – 265.*

[34] Philpotts, A.R., Gray, N.H., Carroll, M. Steinen, R.P. and Reid, J.B., 1997. The Electronic Total Station – a Versatile, Revolutionary New Geologic Mapping Tool. *Journal of Geoscience Education, 45(1): 38 – 45.*

[35] Rick, J.W., 1996. Total Station in Archaeology. *Society for American Archaeology (SAA) Bulletin 14(4): 24 – 27. Available online at:* http://www.saa.org/publications/SAAbulletin/14-4/SAA16.html

[36] Roberts, Jack., 1995. *Construction Surveying, Layout, and Dimension Control.* Delmar Publishers Inc. 372pages

[37] Roy, S.K., 2004. *Fundamentals of Surveying.* Prentice-Hall of India Pvt. Ltd. 620 pages.

[38] Rueger, J.M., 1994. Practical Use of Surveying Robots with EDM Beam Point. *Proceeding of 20th FIG Congress, Melbourne, Australia, pp 1-13.*

[39] Rueger, J.M., 1994a. Monitoring with Surveying Robots. *Geodetical Info Magazine (GIM) and International Journal for Surveying, Mapping and Applied GIS, 8(2): 58 – 63.*

[40] Schlische, R.W. and Ackermann, R.V., 1998. Integrating Computers into the Field Geology Curriculum. *Journal of Geoscience Education, 46(1): 30– 40.*

[41] Schlische, R.W., Reilly, T.J., Ackermann, R.V. and Ashley, G.M., 1997. Field Investigations of Structural and Stratigraphic Expressions of Mesozoic Rifting on the New Brunswick Campuses of Rutgers University. *Geological Society of America Abstracts with Programs, 29(6): 24.*

[42] Signoret, P. and Borelli, N., 1992. *Deformation Monitoring of a Hydroelectric Reservoir's Surroundings – Italy.* Leica Heerbrugg AG, Switzerland. 6pp.

[43] Skyttner, L. 2002. "Minitoring and early Warning System – A design for human Survival". Kybernetes, vol.31 no.2, pp.220 -245.

[44] Stiros, S.C., Vichas, V. and Skourtis, C., 2004. Landslide Monitoring Based on Geodetically Derived Distance Changes. *Journal of Surveying Engineering (ASCE), 130(4): 156 – 162.*

[45] Thomas, H., 2003. Slope Stability Monitoring Project. University of the Witwatersrand, Johannesburg, South Africa. pp. 14 – 15.

[46]US Army Corps of Engineers, 2002. "Sources of Measurement Error and Instrument Calibrations", Engineering Manual 1110-2-1009. Available online at: http://www.usace.army.mil/inet/usace-docs/eng-manuals/em1110-2-1009/c-4.pdf

*[47]*Wallance, R.G., Dinaso, S.M. and Gutowski, V.P., 1996. Use of Total Stations and Computers in Geologic Field Camp. *Geological Society of America Abstracts with Programs, 28(7): 329.*

[48]Yildiz, F., Karabork, H., Yakar, M., Altuntas, C., Karasaka, L. and Goktepe, A., 2007. 3D Modelling by Advance Total Station. *XXI International CIPA Symposium, held in Athens, Greece. 3pages.*

[49]Zeiske, K. 2001. "Current Status of the ISO Standardization of Accuracy Determination Procedures for Survey Instruments". Paper presented at FIG Working Week, Seoul, Korea, 6-11 May.

Appendix A

```
********** TCR1201+ R1000 / V2008.07 / 17.11.2008 / 61062 / Tol: V1.0*****
Date:  2008-11-17 10:42
Instrument No.:  871187
Technician:  SHV Visagie
Customer:  University of Witwatersrand
Notes:  Outgoing test
Test Result:  PASS
0000000000000000000000000000000000000000000000000000000000000000000
********** TCR1201+ R1000 Outgoing Test **********
1.  Reading out instrument data
    ------ General ------                          ------- NLQ -------
 Instrument type        :  TCR1201+ R1000  Accuracy              :  000.00020
 Instrument number      :  871187          L Factor (E)          :  227454
 Equipment number       :  3343804         T Factor (F)          :  -116737
 Mainboard number       :  757782230708148 Default L Factor      : 0.00022783
 Firmware version       :  6.02            Default Q Factor      :-0.00011753
 Boot Version           :  2.02            L Index               :  000.00000
 EDM Version            :  4.17            Q Index               :  000.00000
 ATR Version            :  0.00            L Coarse index        : -002.54598
 PS Version             :  0.00            T Coarse index        : -000.78512
 KDM Version            :  4.06 / ---      TK L Index (C)        :  -54
 EFI Version            :  2.00            TK Q Index (D)        :  -4
 Intern temperature     :  26.7 / 24.6     T factor L            : 0.00077958
 Gear version           :  None            T factor Q            : 0.00077958
 ------- TIM -------                         Factor L to T (G)   :  19696
 MOT-Adjustment Flag    :  ---             Factor T to L (H)     :  -24293
 Operating hours MOT    :  0.000           NLQ Swamp (S)         :  389
 Operating hours GUS    :  0.000           Exposure time         :  339
 ------- ANG -------                       ------- EDM -------
 Adjustment flag        :  O.K.            EDM Temperature       :  36.0/36.0
 Accuracy               :  000.00030       Quartz Reference F0   :  99997516
 Diametric              :  1               Quarz Poly F1         :  5107
 H1 Eccen. phase (O)    :  000.0           Quarz Poly F2         : -8435
 H1 Eccen. ampl. (Q)    :  0.0             Quarz Poly F3         :  9449
 V1 Eccen. phase (P)    :  0.0             Add. constant IR (I): -427
 V1 Eccen. ampl. (R)    :  0.0             Add. constant SR (J): -423
 H2 Eccen. phase        :  000.0           EDM Board number      :  20009344
 H2 Eccen. ampl.        :  0               Identification / SW :  70 / 4.17
 V2 Eccen. phase        :  000.0           APD Voltage V25       :  143.2
 V2 Eccen. ampl.        :  0               Temp. value t25       :  250
 H1 Exposure time       :  298             Temp. cof. TK1        :  66
 V1 Exposure time       :  303             Temp. cof. TK2        :  0
 H2 Exposure time       :  282             Boomerang             :  8
 V2 Exposure time       :  268             Filter offset         :  4 / 13
 H1 Array table         :  OK              Laser IR PWM          :  192
 V1 Array table         :  OK              Laser IR TK           :  0
 H2 Array table         :  OK              Laser SR PWM          :  204
 V2 Array table         :  OK              Laser SR TK           :  0
 H1 Circle table        :  Corr. No        EGL number            :  0
 V1 Circle table        :  Corr. No   ---- End of the initial read-out ----
 H2 Circle table        :  Corr. No
 V2 Circle table        :  Corr. No
 ------- TMC -------
 Adjustment flag        :  O.K.
 V Coarse index         :  004.22209
 V Coarse index         :  000.00000
 TK V Index (B)         :  157
 Collimation error      : -000.00051
 TK Collimation (A)     :  10
 Tilting axis error     : -000.00078
2.  Tribrach screws                        Manual test : O.K.
3.  Locking mechanism                      Manual test : O.K.
4.  Spherical level for tribrach           Manual test : O.K.
5.  Laser / Optical plummet                Manual test : O.K.
6.  Spherical level                        Manual test : O.K.
7.  Standing axis                          Manual test : O.K.
8.  Horizontal friction clamp              Manual test : O.K.
9.  Horizontal drive                       Manual test : O.K.
10. Tilting axis                           Manual test : O.K.
11. Vertical friction clamp                Manual test : O.K.
12. Vertical Drive                         Manual test : O.K.
13. Carrying handle                        Manual test : O.K.
```

```
14. Battery cover                           Manual test : O.K.
15. Optical sight                           Manual test : O.K.
16. Telescope eyepiece                      Manual test : O.K.
17. Bayonet lock                            Manual test : O.K.
18. Telescope reticle                       Manual test : O.K.
19 Focusing                                 Manual test : O.K.
20. Image quality                           Manual test : O.K.
21. True running of standing axis
    M0    : -000.0008
    M1    :  000.0034
    M2    :  000.0008
    M3    : -000.0033
    X1    : -000.0000                       X2    :  000.0001
    Diff : 2 cc
22. Stability of V collimation
    M1    :  100.0016
    M2    :  100.0026
    Diff : 11 cc
23. Horizontal collimation
    Collimator Face I  :  020.9060
    Collimator Face II :  220.9054
    Collimation4.6m    :  000.0002
    Collimator Face I  :  020.6835
    Collimator Face II :  220.6845
    Collim. infinity   : -000.0006
24. Tilting axis error with SW
    Collimator Face I  :  060.4385
    Collimator Face II :  260.4391
    Tilting axis error :  000.0004
25. V coarse index, L coarse index, T coarse index
    Collimator Face I  :  104.2262
    Collimator Face II :  304.2226
    V Coarse index     :  004.2233
    L Coarse index     : -002.5458
    T Coarse index     : -000.7854
26. L factor, T factor
    V1    :  100.0722                       L1    : -000.0711
    Q1    :  000.0711
    V2    :  099.9312                       L2    :  000.0702
    Q2    : -000.0703
    FL    : 455                             FQ    : 465
27 Factor T on L
    L1    : -000.0003                       Q1    : -000.0717
    L2    : -000.0006                       Q2    :  000.0720
    FQL   : 654
28. Factor L on T
    L1    :  000.0737                       Q1    :  000.0007
    L2    :  000.0013                       Q2    : -000.0734
    L3    : -000.0733                       Q3    : -000.0005
    L4    : -000.0008                       Q4    :  000.0731
    FLQ   : 167
29. Inspecting tilt sensor
    Peak Distance mean      : 11.52         11-12 Pixel
    Max. Peak Difference    : 0.46          <1.00/1.00 Pixel
    Pixel Amplitude diff.   : 79.5          >70 %
    P to P Amplitude diff.  : 93.3          >70 %
    Pixel sharpness         : 85.5          >50 %
    Swamp maximum           : 174           <100 ADC
    Cleanliness             : OK
30. Socket and contacts                     Manual test : O.K.
31. Current consumption
    Off   : 00 mA                           WNG   : 272 mA
    EDM   : 425 mA
32. Monitoring voltage                      Manual test : O.K.
33. Display test , display illumination     Manual test : O.K.
34. Keyboard test                           Manual test : O.K.
35. Plug-in battery                         Manual test : O.K.
36. Memory card
     Inserted             : Yes
37. IR Transmitter power
    Las.Dark : 133
    Las.D-RL : 103
    IR       : 275.1 uW
```

```
38. SR Transmitter power
    SR       : 4155.4 uW
39. Frequency difference
    Fcalc    : 100382740 Hz
    Fmeas    : 100382703 Hz
    Fdiff    : 37 Hz
40. Sensitivity IR
    SigMax   : 415 ADC
41. Sensitivity SR
    SigMax   : 2.0799m / 486 ADC
    SigMax   : 7.0426m / 549 ADC
42. Cal Signal
    Cal IR   : 1704
    Cal SR   : 1781 ADC
43. Crosstalk
    IR       : 45 uV
    SR       : 146 uV
44. Dynamic test
    DIST 01 : 7.1575 m   F/C : ---
    DIST 02 : 7.1578 m   F/C : ---
    DIST 03 : 7.1577 m   F/C : ---
    DIST 04 : 7.1579 m   F/C : ---
    DIST 05 : 7.1581 m   F/C : ---
    DIST 06 : 7.1578 m   F/C : ---
    DIST 07 : 7.1579 m   F/C : ---
    DIST 08 : 7.1581 m   F/C : ---
    DIST 09 : 7.1583 m   F/C : ---
    DIST 10 : 7.1584 m   F/C : ---
    DIST 11 : 7.1585 m   F/C : ---
    DIST 12 : 7.1592 m   F/C : ---
45. Distance SR
    DIST     : 7.1582 m   F/C : ---
    DIST     : 7.1581 m   F/C : ---
    DIST     : 7.1581 m   F/C : ---
    DIST     : 7.1581 m   F/C : ---
    DIST     : 7.1581 m   F/C : ---
    Max Sig.: 975 ADC
46. Dist after power On
    ON       : 7.2869 m   F/C : ---
    ON       : 7.2869 m   F/C : ---
    ON       : 7.2869 m   F/C : ---
    ON       : 7.2869 m   F/C : ---
    ON       : 7.2867 m   F/C : ---
    Standby : 7.2867 m   F/C : ---
    Standby : 7.2867 m   F/C : ---
    Standby : 7.2869 m   F/C : ---
    Standby : 7.2868 m   F/C : ---
    Standby : 7.2867 m   F/C : ---
    Standby : 7.2868 m   F/C : ---
47. EDM - Optical axis                    Manual test :
O.K.
48. Inspecting automatic targeting
    No test necessary for this type of instrument.
49. Hz positioning
    No test necessary for this type of instrument.
50. V positioning
    No test necessary for this type of instrument.
51. Gear Test
    No test necessary for this type of instrument.
52. Measure the output of the ATR transmitter diode
    No test necessary for this type of instrument.
53. ATR Center the transmitter diode
    No test necessary for this type of instrument.
54. ATR CCD camera, zero position
    No test necessary for this type of instrument.
55. ATR Light volume test
    No test necessary for this type of instrument.
56. ATR function test
    No test necessary for this type of instrument.
57. PS Measure power output
    No test necessary for this type of instrument.
58. PS function test
    No test necessary for this type of instrument.
59. PS Distance difference over reference
    No test necessary for this type of instrument.
60. EGL Measuring the diode output
    No test necessary for this type of instrument.
61. EGL Aligning the line of sight
    No test necessary for this type of instrument.
62. GUSMeasure the laser pointer output
    No test necessary for this type of instrument.
63. GUS Aligning the laser line of sight
    No test necessary for this type of instrument.
64. Reading out Bluetooth
    No test necessary for this type of instrument.
65. Bluetooth Test
    No test necessary for this type of instrument.
66. Enter TPS condition
    O.K.
    Problems in

67. Labelling                          Manual test : O.K.

68. Reading out instrument data
    ------ General ------
   Instrument type      :  TCR1201+ R1000
   Instrument number    :  871187
   Equipment number     :   3343804
   Mainboard number     :  757782230708148
   Firmware version     :  6.02
   Boot Version         :  2.02
   EDM Version          :  4.17
   ATR Version          :  0.00
   PS Version           :  0.00
   KDM Version          :  4.06 / ---
   EFI Version          :  2.00
   Intern temperature   :  27.9 / 26.3
   Gear version         :  None
------- TIM -------
   MOT-Adjustment Flag: ---
   Operating hours MOT: 0.000
   Operating hours GUS: 0.000
------- ANG -------
   Adjustment flag      :  O.K.
   Accuracy             :  000.00030
   Diametric            :  1
   H1 Eccen. phase (O):   000.0

   ------- NLQ -------
Accuracy             :  000.00020
L Factor (E)         :  227454
T Factor (F)         :  -116737
Default L Factor     :   0.00022783
Default Q Factor     :  -0.00011753
L Index              :  000.00000
Q Index              :  000.00000
L Coarse index       : -002.54576
T Coarse index       : -000.78543
TK L Index (C)       :  -54
TK Q Index (D)       :  -4
T factor L           :  0.00077958
T factor Q           :  0.00077958
Factor L to T (G)    :  19696
Factor T to L (H)    :  -24293
NLQ Swamp (S)        :  389
Exposure time        :  343
------- EDM -------
EDM Temperature      :  O.K./ 4.17
Quartz Reference F0:    99997516
Quarz Poly F1        :  5107
Quarz Poly F2        : -8435
```

```
  H1 Eccen. ampl. (Q):  0.0
  V1 Eccen. phase (P):  0.0
  V1 Eccen. ampl. (R):  0.0
  H2 Eccen. phase    :  000.0
  H2 Eccen. ampl.    :  0
  V2 Eccen. phase    :  000.0
  V2 Eccen. ampl.    :  0
  H1 Exposure time   :  288
  V1 Exposure time   :  305
  H2 Exposure time   :  282
  V2 Exposure time   :  272
  H1 Array table     :  OK
  V1 Array table     :  OK
  H2 Array table     :  OK
  V2 Array table     :  OK
  H1 Circle table    :  Corr. No
  V1 Circle table    :  Corr. No
  H2 Circle table    :  Corr. No
  V2 Circle table    :  Corr. No
------- TMC -------
  Adjustment flag    :  O.K.
  V Coarse index     :  004.22328
  V Coarse index     :  000.00000
  TK V Index (B)     :  157
  Collimation error  : -000.00056
  TK Collimation (A) :  10
  Tilting axis error :  000.00042

     Quarz Poly F3        :  9449
  Add. constant IR (I)    : -427
  Add. constant SR (J)    : -423
  EDM Board number        : 20009344
  Identification / SW     : 70 / 4.17
  APD Voltage V25         :  143.2
  Temp. value t25         :  250
  Temp. cof. TK1          :  66
  Temp. cof. TK2          :  0
  Boomerang               :  8
  Filter offset           :  4 / 13
  Laser IR PWM            :  192
  Laser IR TK             :  0
  Laser SR PWM            :  204
  Laser SR TK             :  0
  EGL number              :  0
---- End of the initial read-out ----
```

Appendix B.4

Stevenson Screen Kit Construction Steps (Source: Davis Weather shop)

Parts required: 4 threaded rods approx. 40 - 45 cm in length, nine 25cm Planterra Terrapot saucers, 72 nuts and 72 washers, No Gaps gap sealer. For our own Stevenson screen kit, we used eight 25 cm and one 40 cm saucers. The 40 cm saucer was used as the base as can be seen in Figure 4.11 of chapter four.

Steps to follow

a. Mark evenly around saucer, and drill the hole fractionally larger than the threaded rods as shown below. This larger hole allows for slight movement to occur during assembly.

b. Mark a circle approximately 15cm in size, and cut out the large opening. If one has the same saucers as shown above, one can use two of the cut outs to help fill the centre depressions in the bottom and top saucers as shown below.

.

c. Assemble from the base upwards on the threaded rods in these order: Nut, washer, saucer, washer, and nut. This image below shows the first few saucers assembled, with the lips partially filled so there are no gaps. The saucers are then painted.

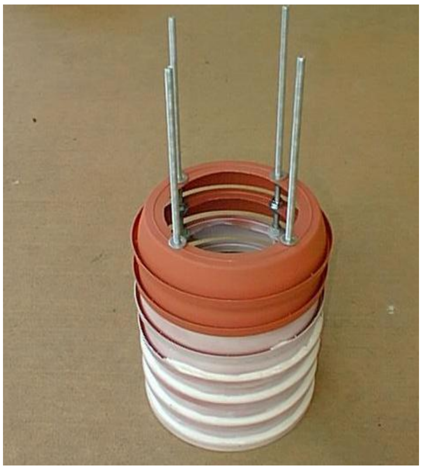

d. Observe how the nuts and washers fit in together, i.e. Nut, washer, saucer, washer, nut.

e. The gap between each layer which needs to be there will vary according to the style of saucers chosen.

f. In this image, the gaps should be around 30 to 35mm, as can be seen prior to adding the next saucer.

g. Prior to this stage, all the saucers are painted in white if the available saucers are not white plastic (in this research construction, white plastic saucers were used). Place the Sensor bracket inside and secure this one with cable ties.

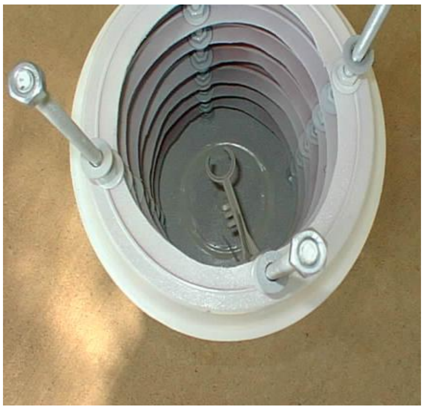

h. Clip the sensor in place, and secure cable with cable ties. Finally fit the last saucer in place on the top. Trim two of the threaded rods flush with the top. The other two rods left long enough to secure a hanging chain to, or to bolt up to a bracket.

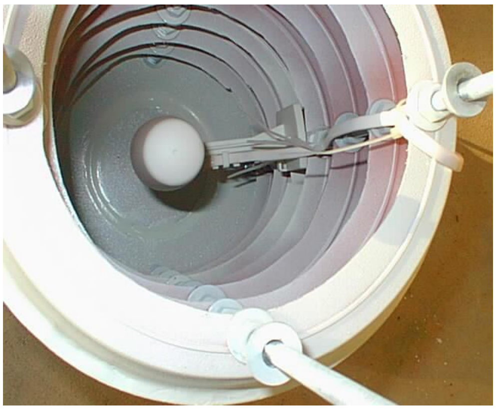

After following the above eight steps, the researcher obtained a self-built Stevenson screen kit shown in figure 4.11 of chapter four of this report.

Comment:

For the Stevenson screen kit, the researcher used eight 25 cm and one 40 cm Planterra Terrapot saucers. The 40 cm Planterra Terrapot saucer was used as the base as can be seen in Figure 4.11 of chapter four.

APPENDIX C

Appendix C.2

Analysis of Atmospheric Conditions

The weather parameters were collected using two different instruments – GeoMos (combined temperature and pressure sensor) and Oregon scientific weather sensors. The GeoMos sensor, commonly used at most mines has no humidity sensor. The GeoMos meteo sensor was placed inside a constructed Stephenson screen mounted outside the building (window) close to the instrument station at Chamber of Mines building. In the experimental data it was referred to as GeoMos. One Oregon weather sensor was placed permanently inside the observation office to measure the office (i.e. room) temperature, pressure and humidity. In the data analysis it was referred to as Oregon inside. The second Oregon sensor was placed outside beside the Stephenson screen mounted by the window side at the instrument station and a third Oregon sensor was placed close to the monitoring target (at the target station). The second and the third Oregon were referred to as Oregon outside 1 and Oregon outside 2. The average of the two was referred to as Oregon average outside. The results of the weather analysis are presented in three headlines: temperature, pressure and humidity, as illustrated in the figures below.

Temperature

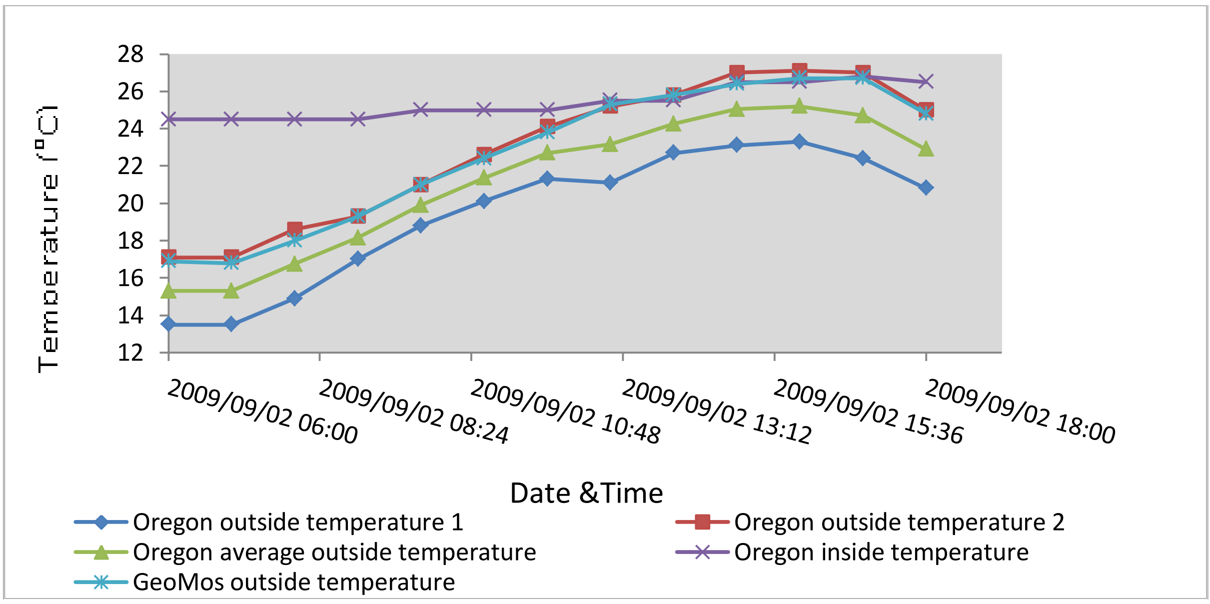

Figure C.1: A day temperature readings (short distance)

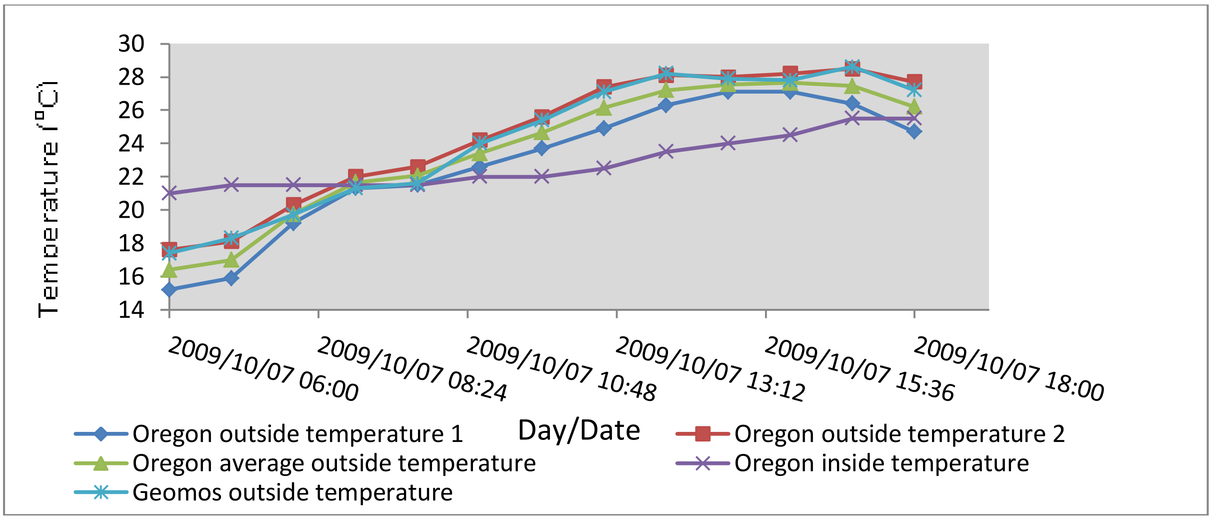

Figure C.2: A day temperature readings (long distance)

Figures C.1 and C.2 show the sample graphs for a typical day's temperature readings during short- and long-distances monitoring. From the graphs, the early morning (6:00 am) temperature readings for both the Oregon and the GeoMos outside readings were low. These trends continued to increase with time up until 15:00 pm before decreasing gradually. The Oregon inside temperature readings (Oregon in) remained fairly constant on both days. The graphs also reveal that an equilibrium exists between the three readings (Oregon average outside, Oregon inside and the GeoMos) around 13:00 pm in figure C.1 and around 9:00 am in figure C.2. The graphs also show that the readings in both Oregon average outside and the Geomos readings are close to each other.

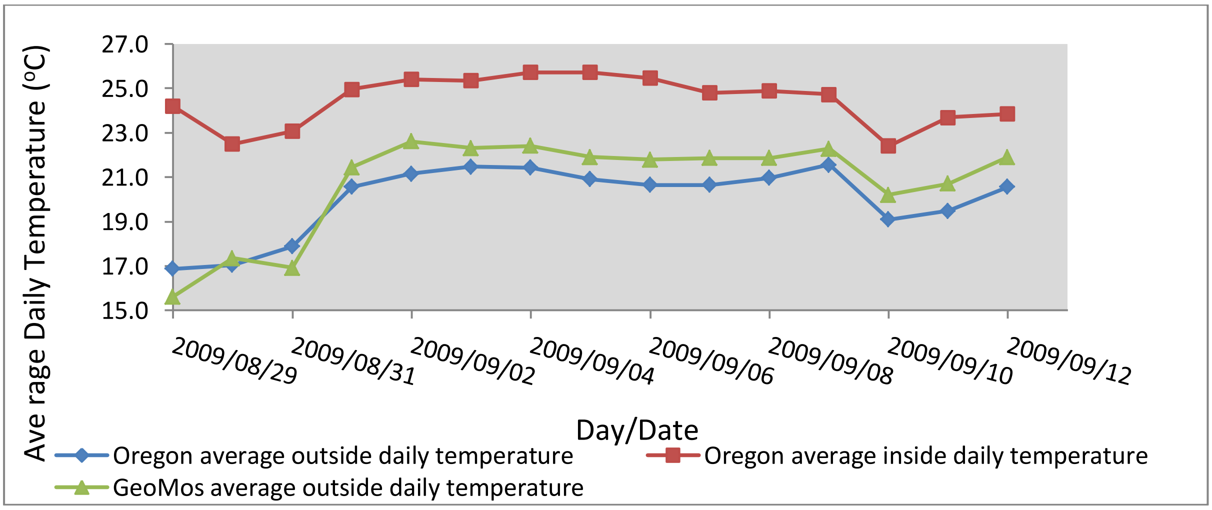

Figure C.3: Average daily temperature readings (short distance)

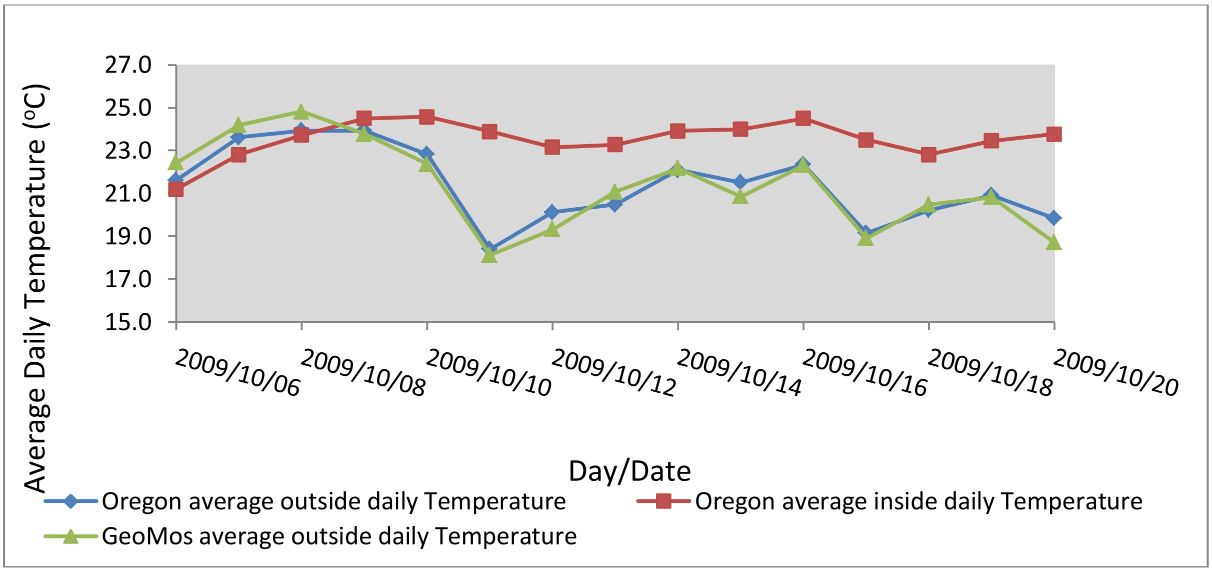

Figure C.4: Average daily temperature readings (long distance)

The results of the average daily temperature readings during short and long distances monitoring are presented in Figures C.3 and C.4. The graphs reveal that the temperature readings from both the Oregon average outside and the GeoMos average outside readings were nearly the same. The similarity was more pronounced during the long-distance monitoring as shown in figure C.4 than during the short-distance monitoring as shown in figure C.3.

Pressure

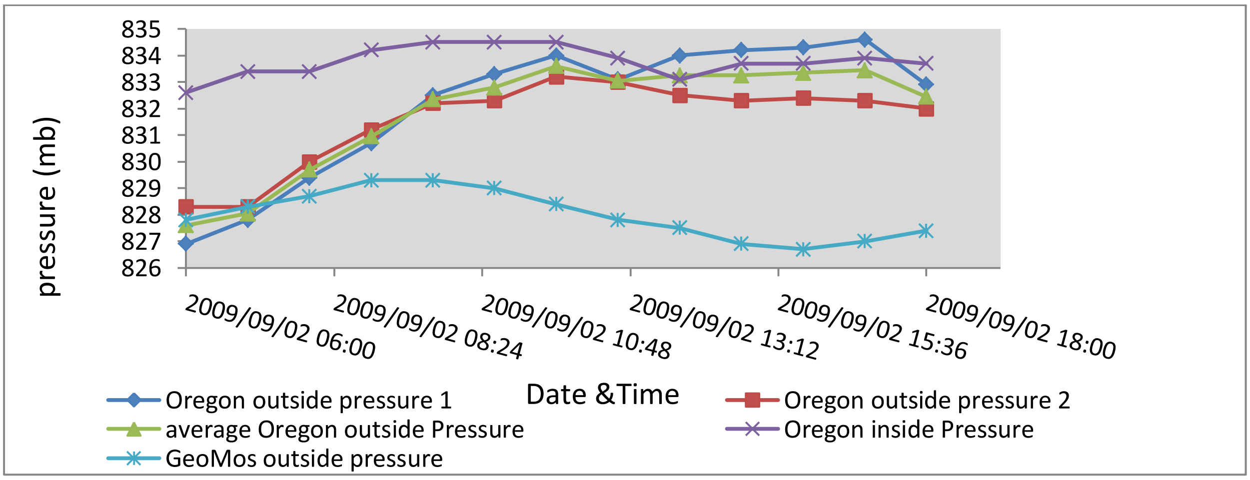

Figure C.5: A day pressure readings (short distance)

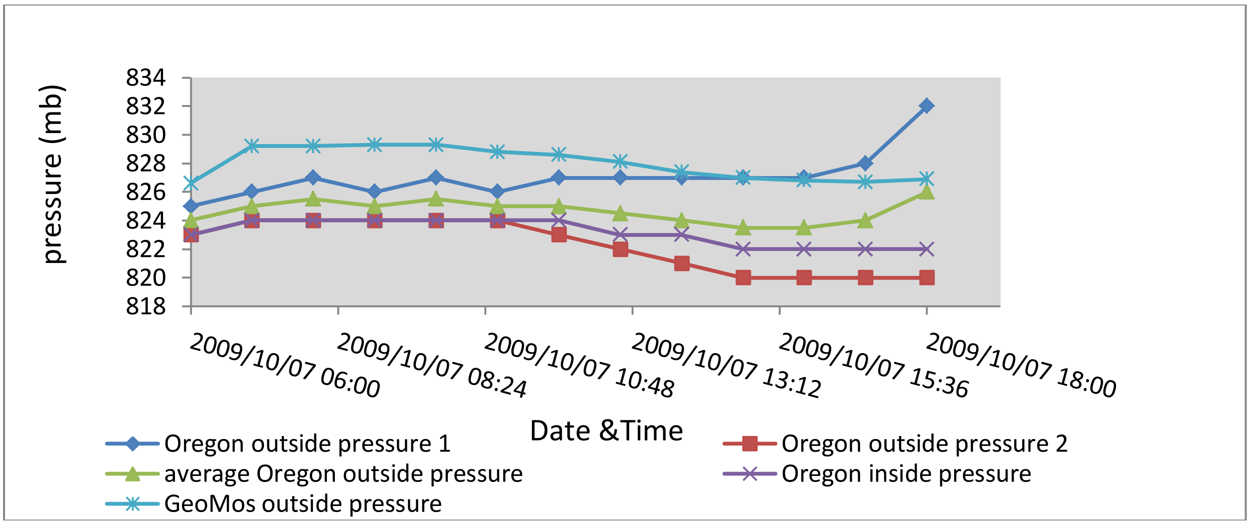

Figure C.6: A day pressure readings (long distance)

Figures C.5 and C.6 show the sample graphs for a day's pressure readings during short- and long-distances monitoring. Both graphs show steady or fairly constant inside pressure readings. The variations shown in the Oregon average outside pressure and the GeoMos outside pressure readings could be as a result of difference in the positions of the two sensors. In fact, the Oregon average outside pressure readings was the average of outside pressure readings at the instrument station and at the target station. Both are not at the same height (or the same weather condition) unlike the GeoMos pressure reading that was measured at the instrument station alone. Figure C.5 reveals that the inside pressure readings trend recorded on 2nd of September, 2009 are above other outside pressure readings while Figure C.6 reveals that the inside pressure readings taken on 07th of October, 2009 are below other outside pressure readings.

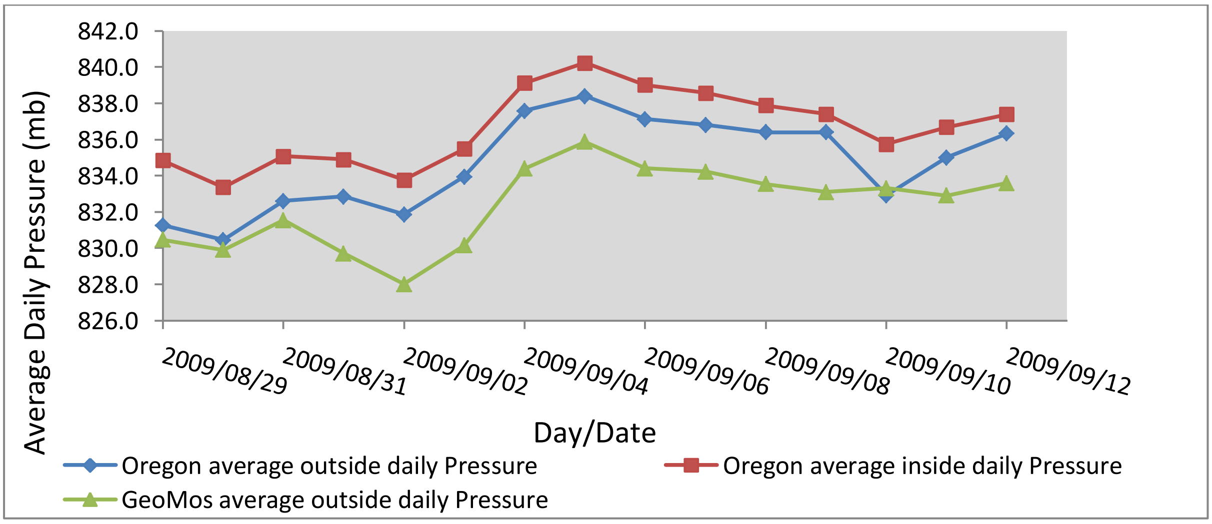

Figure C.7: Average daily pressure readings (short distance)

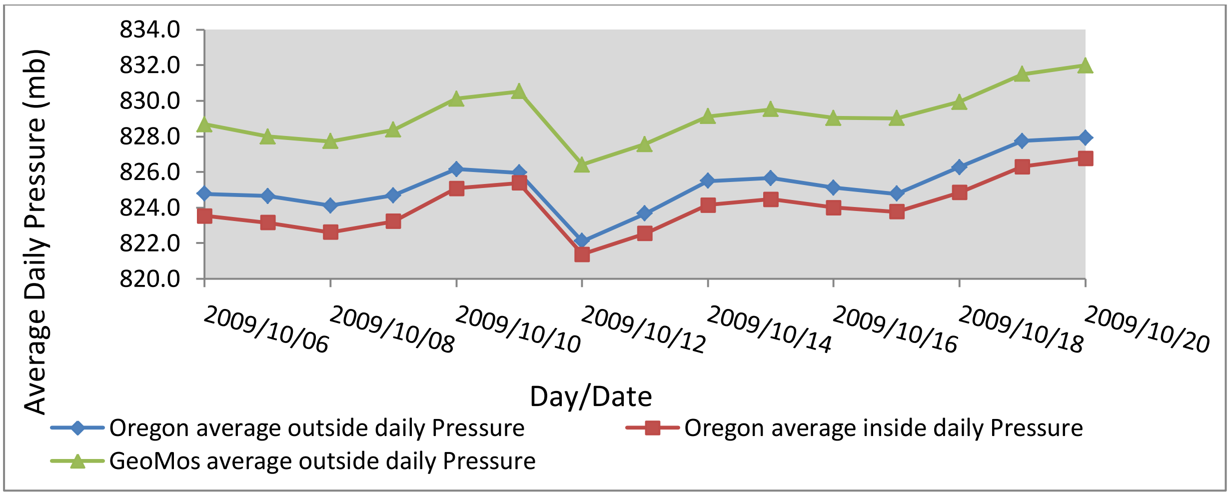

Figure C.8: Average daily pressure readings (long distance)

The results of average daily pressure readings during short- and long-distances monitoring are presented in Figures C.7 and C.8 respectively. In figures C.7 and C.8, there are clear differences between the three average pressure trends (i.e. Oregon average inside daily pressure, Oregon outside daily pressure and GeoMos average outside daily pressure). In figure C.7, the GeoMos average outside reading is above other pressure readings while in figure C.8, the average GeoMos outside reading is below other pressure readings.

Humidity

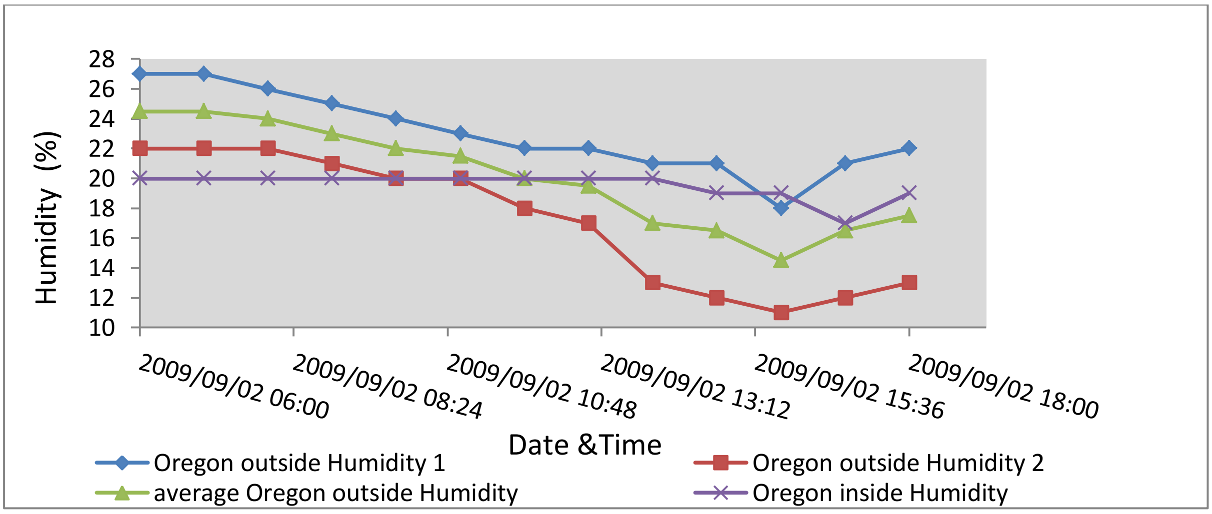

Figure C.9: A day humidity readings (short distance)

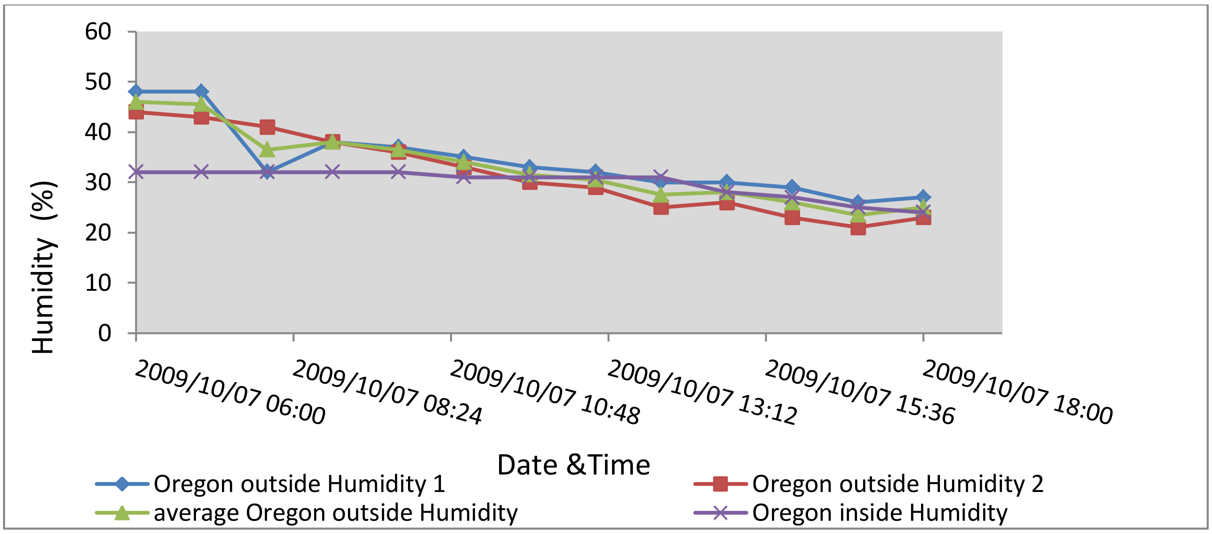

Figure C.10: A day humidity readings (long distance)

Figures C.9 and C.10 show the sample graphs for a day's humidity readings during short- and long-distances monitoring. Both graphs show steady and nearly constant readings in the inside humidity readings on both days (i.e between 17 – 20% during short distance monitoring and 24 – 32% during long distance monitoring). The graphs show the same trend i.e. high humidity readings in the morning and low humidity readings in the afternoon and tend to go up again in the evening. The GeoMos has no humidity sensor; consequently, there is no humidity reading recorded from it.

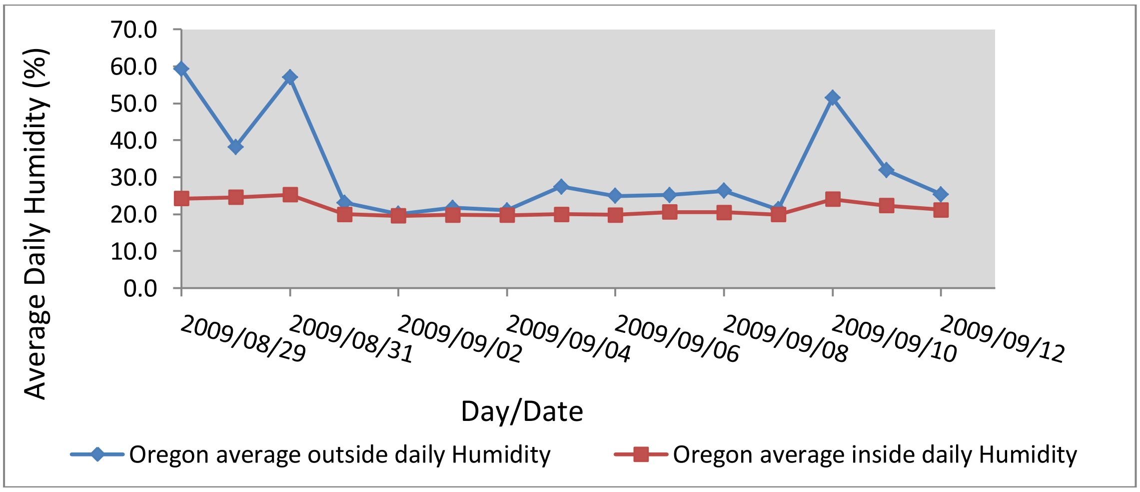

Figure C.11: Average daily humidity readings (short distance)

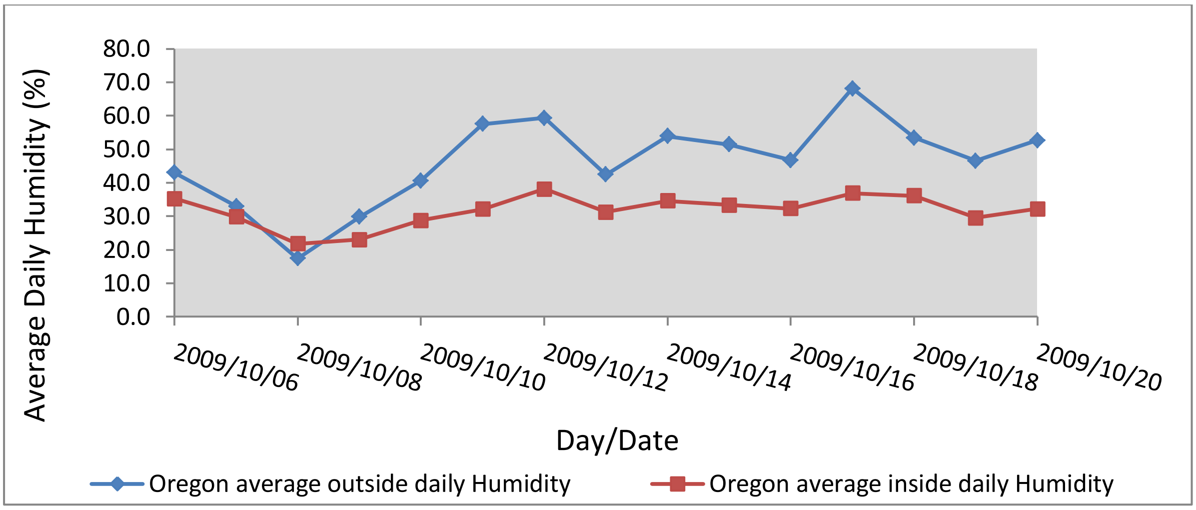

Figure C.12: Average daily humidity readings (long distance)

The results of average daily humidity readings during short- and long-distances monitoring are presented in Figures C.11 and C.12 respectively. The Oregon average inside humidity readings ranged between 19.5 – 25.3% and 21.8 – 38.2% during short- and long-distances monitoring. These figures translate into a 5.8% variation during short-distance monitoring and 16.4% variations during long-distance monitoring. The Oregon average outside humidity ranges between 20.1 – 59.3% during short-distance monitoring and 17.5 – 68.2% during long-distance monitoring (i.e. 39.2% variation during short-distance monitoring and 50.7% variation during long-distance monitoring).

CONCLUSION

In conclusion, the atmospheric parameters data analyzed revealed that outside temperature variations between 4.4^{o}C and 5.5^{o}C were encountered during the monitoring exercise while the inside temperature variations were between 3.3^{o}C and 3.4^{o}C. The outside pressure variations between 5.8 mb (i.e. 5.8 millibar) and 7.9 mb and inside pressure variations between 5.4 mb and 6.8 mb were also experienced during the exercise. Another factor encountered was outside humidity variations between 39.2% and 50.7% and inside humidity variation between 5.8% and 16.4%. These variations indicated the need for atmospheric correction as established in section 2.8 of chapter two of this report. Table C.1 summarizes the variations in atmospheric parameters during short and long distances monitoring as presented in Figures C.3, C.4, C.7, C.8, C.11 and C.12.

Table C.1: Summary of average atmospheric parameters variations during the short- and long-distance monitoring.

Date /Parameters	**Short HD Monitoring**					
29/08/2009 to 12/09/2009	Oregon average outside	variation	Oregon average inside	Variation	Geomos average outside	Variation
Temperature (^oC)	16.1 – 21.6	5.5^{o}C	22.4 – 25.7	3.3^{o}C	15.6 – 22.6	7.0^{o}C
Pressure (mb)	830.5 – 838.4	7.9 mb	833.4 – 840.2	6.8 mb	828.0 – 835.9	7.9 mb
Humidity (%)	20.1 – 59.3	39.2%	19.5 – 25.3	5.8%	NM	NM
	Long HD Monitoring					
06/10/2009 to 20/10/2009	Average Oregon out	variation	Average Oregon In	Variation	Average Geomos out	Variation
Temperature (^oC)	19.8 – 24.2	4.4 ^{o}C	21.2 – 24.6	3.4^{o}C	18.1 – 24.8	6.7^{o}C
Pressure (mb)	822.1 – 827.9	5.8 mb	821 – 826.8	5.4 mb	826.4 – 830.5	4.1 mb
Humidity (%)	17.5 – 68.2	50.7%	21.8 – 38.8	16.4%	NM	NM

NM means not measured

Appendix C.3

During data processing, before embarked on using the average daily readings of all the distance readings acquired, a variability test was carried out on the hourly distance readings per day. Standard deviation method was used to measure the variability or diversity in the daily distance readings. The method helped to ascertain how much variation or dispersion are the hourly distance readings from the average daily distance reading (i.e. the mean). The results of the standard deviation are presented in table C.2

The standard deviation of HD and VD daily readings during short and long distance measurements were very low (i.e. within 2.0 mm before atmospheric corrections and below 1 .0 mm after atmospheric corrections). The results were the same for HD and VD measurements to both mini and circular prisms. The only few exceptional cases were in HD and VD measurements to the sticker during long distance monitoring. This clearly revealed that visible red laser light is more affected by atmospheric variations as distance measurement increases (nevertheless, the standard deviation of the daily distance readings the sticker were a little above 2.0 mm after atmospheric corrections). The results revealed that the hourly distance readings per day were very close to the mean (i.e. the daily average distance readings). It also revealed the efficiency and sensitivity of the total station TCR 201+ used in the data collection. This is an indication that the hourly distance measurements were well observed without outliers. Based on these findings, the average daily distance readings were used in the data analyzed in this report.

Table C. 2: **Results of standard deviation test performed on hourly distance readings**

Standard deviation of daily HD measurements corrected for prism constant and scale factors but not corrected for atmospheric variation - short distance monitoring.

Table C.2.1: Standard deviation of hourly HD measurements to the mini prism per day before atmospheric corrections - short distance monitoring.

Day Date	Std Dev of HD to Mini Prism without glass	Std Dev of HD to Mini Prism with glass @ 45°	Std Dev of HD to Mini Prism with glass @ 60°	Std Dev of HD to Mini Prism with glass @ 90°
8/29/2009	0.0001	0.0001	0.0002	0.0002
8/30/2009	0.0004	0.0002	0.0003	0.0002
8/31/2009	0.0002	0.0002	0.0002	0.0002
9/1/2009	0.0005	0.0006	0.0005	0.0005
9/2/2009	0.0005	0.0005	0.0004	0.0006
9/3/2009	0.0002	0.0003	0.0002	0.0003
9/4/2009	0.0005	0.0006	0.0006	0.0005
9/5/2009	0.0003	0.0003	0.0004	0.0004
9/6/2009	0.0004	0.0004	0.0004	0.0004
9/7/2009	0.0002	0.0007	0.0006	0.0006
9/8/2009	0.0002	0.0006	0.0006	0.0006
9/9/2009	0.0008	0.0005	0.0006	0.0005
9/10/2009	0.0006	0.0008	0.0009	NM
9/11/2009	0.0006	0.0007	0.0007	NM
9/12/2009	0.0005	0.0008	0.0008	NM

Note: NM means not measured

Table C.2.2: Standard deviation of hourly HD measurements to the circular prism per day before atmospheric corrections - short distance monitoring.

Day Date	Std Dev of HD to Circular Prism without glass	Std Dev of HD to Circular Prism with glass @ 45°	Std Dev of HD to Circular Prism with glass @ 60°	Std Dev of HD to Circular Prism with glass @ 90°
8/29/2009	0.0002	0.0002	0.0002	0.0003
8/30/2009	0.0002	0.0003	0.0002	0.0002
8/31/2009	0.0001	0.0002	0.0002	0.0001
9/1/2009	0.0004	0.0002	0.0004	0.0004
9/2/2009	0.0004	0.0004	0.0004	0.0005
9/3/2009	0.0004	0.0004	0.0004	0.0003
9/4/2009	0.0004	0.0005	0.0005	0.0004
9/5/2009	0.0003	0.0003	0.0004	0.0003
9/6/2009	0.0004	0.0002	0.0003	0.0003
9/7/2009	0.0002	0.0006	0.0004	0.0006
9/8/2009	0.0003	0.0005	0.0003	0.0004
9/9/2009	0.0002	0.0005	0.0003	0.0004
9/10/2009	0.0007	0.0007	0.0008	NM
9/11/2009	0.0005	0.0007	0.0007	NM
9/12/2009	0.0004	0.0006	0.0008	NM

Table C.2.3: Standard deviation of hourly HD measurements to the sticker per day before atmospheric corrections - short distance monitoring.

Day Date	Std Dev of HD to Sticker without glass	Std Dev of HD to Sticker with glass @ 45o	Std Dev of HD to Sticker with glass @60o	Std Dev of HD to Sticker with glass @90o
8/29/2009	0.0003	0.0007	0.0008	0.0007
8/30/2009	0.0004	0.0006	0.0004	0.0005
8/31/2009	0.0003	0.0005	0.0005	0.0004
9/1/2009	0.0006	0.0006	0.0006	0.0007
9/2/2009	0.0006	0.0008	0.0008	0.0005
9/3/2009	0.0005	0.0005	0.0004	0.0004
9/4/2009	0.0007	0.0011	0.0008	0.0008
9/5/2009	0.0008	0.0010	0.0009	0.0008
9/6/2009	0.0008	0.0008	0.0009	0.0009
9/7/2009	0.0005	0.0012	0.0010	0.0007
9/8/2009	0.0009	0.0010	0.0010	0.0010
9/9/2009	0.0013	0.0013	0.0013	0.0014
9/10/2009	0.0015	0.0013	0.0013	NM
9/11/2009	0.0011	0.0008	0.0012	NM
9/12/2009	0.0006	0.0015	0.0008	NM

Standard deviation of daily HD measurements corrected for prism constant, scale factors and atmospheric variations corrections - short distance monitoring.

Table C.2.4: Standard deviation of hourly HD measurements to the mini prism per day after atmospheric corrections - distance monitoring.

Day Date	**Std Dev of HD to Mini Prism without glass**	**Std Dev of HD to Mini Prism with glass @ 45°**	**Std Dev of HD to Mini Prism with glass @ 60°**	**Std Dev of HD to Mini Prism with glass @ 90°**
8/29/2009	0.0001	0.0001	0.0002	0.0002
8/30/2009	0.0003	0.0002	0.0003	0.0002
8/31/2009	0.0002	0.0003	0.0001	0.0002
9/1/2009	0.0004	0.0005	0.0004	0.0004
9/2/2009	0.0004	0.0005	0.0004	0.0005
9/3/2009	0.0001	0.0003	0.0002	0.0003
9/4/2009	0.0004	0.0005	0.0005	0.0004
9/5/2009	0.0002	0.0002	0.0003	0.0003
9/6/2009	0.0003	0.0003	0.0003	0.0003
9/7/2009	0.0003	0.0006	0.0006	0.0006
9/8/2009	0.0002	0.0005	0.0005	0.0005
9/9/2009	0.0007	0.0004	0.0005	0.0004
9/10/2009	0.0005	0.0007	0.0008	NM
9/11/2009	0.0005	0.0007	0.0006	NM
9/12/2009	0.0005	0.0007	0.0007	NM

Table C.2.5: Standard deviation of hourly HD measurements to the circular prism per day after atmospheric corrections - short distance monitoring.

Day Date	Std Dev of HD to Circular Prism without glass	Std Dev of HD to Circular Prism with glass @ 45°	Std Dev of HD to Circular Prism with glass @ 60°	Std Dev of HD to Circular Prism with glass @ 90°
8/29/2009	0.0002	0.0002	0.0002	0.0003
8/30/2009	0.0002	0.0003	0.0002	0.0002
8/31/2009	0.0001	0.0003	0.0002	0.0002
9/1/2009	0.0004	0.0002	0.0003	0.0003
9/2/2009	0.0004	0.0003	0.0004	0.0004
9/3/2009	0.0003	0.0004	0.0004	0.0003
9/4/2009	0.0003	0.0004	0.0004	0.0003
9/5/2009	0.0003	0.0003	0.0004	0.0003
9/6/2009	0.0003	0.0002	0.0002	0.0003
9/7/2009	0.0002	0.0005	0.0003	0.0005
9/8/2009	0.0003	0.0004	0.0003	0.0003
9/9/2009	0.0002	0.0005	0.0003	0.0003
9/10/2009	0.0007	0.0006	0.0006	NM
9/11/2009	0.0005	0.0006	0.0006	NM
9/12/2009	0.0004	0.0006	0.0007	NM

Table C.2.6: Standard deviation of hourly HD measurements to the sticker per day after atmospheric corrections - short distance monitoring.

Day Date	Std Dev of HD to Sticker without glass	Std Dev of HD to Sticker with glass @ 45o	Std Dev of HD to Sticker with glass @60o	Std Dev of HD to Sticker with glass @90o
8/29/2009	0.0004	0.0007	0.0009	0.0007
8/30/2009	0.0003	0.0005	0.0004	0.0005
8/31/2009	0.0003	0.0005	0.0005	0.0004
9/1/2009	0.0006	0.0005	0.0005	0.0007
9/2/2009	0.0005	0.0008	0.0007	0.0004
9/3/2009	0.0005	0.0005	0.0004	0.0004
9/4/2009	0.0007	0.0010	0.0007	0.0007
9/5/2009	0.0007	0.0009	0.0008	0.0008
9/6/2009	0.0007	0.0007	0.0008	0.0008
9/7/2009	0.0005	0.0012	0.0009	0.0007
9/8/2009	0.0009	0.0010	0.0011	0.0010
9/9/2009	0.0012	0.0013	0.0012	0.0013
9/10/2009	0.0014	0.0013	0.0012	NM
9/11/2009	0.0011	0.0008	0.0012	NM
9/12/2009	0.0005	0.0014	0.0007	NM

Standard deviation of daily HD measurements corrected for prism constant, scale factors and atmospheric variations corrections - long distance monitoring.

Table C.2.7: Standard deviation of hourly HD measurements to the mini prism per day before atmospheric corrections - long distance monitoring.

Day Date	Std Dev of HD to Mini Prism without glass	Std Dev of HD to Mini Prism with glass @ 45°	Std Dev of HD to Mini Prism with glass @ 60°	Std Dev of HD to Mini Prism with glass @ 90°
10/6/2009	0.0023	0.0021	0.0023	0.0023
10/7/2009	0.0026	0.0024	0.0024	0.0025
10/8/2009	0.0028	0.0027	0.0028	0.0027
10/9/2009	0.0017	0.0017	0.0019	0.0018
10/10/2009	0.0021	0.0018	0.0019	0.0019
10/11/2009	0.0010	0.0009	0.0009	0.0009
10/12/2009	0.0019	0.0018	0.0019	0.0019
10/13/2009	0.0025	0.0025	0.0027	0.0026
10/14/2009	0.0020	0.0023	0.0023	0.0021
10/15/2009	0.0026	0.0027	0.0026	0.0025
10/16/2009	0.0012	0.0013	0.0013	0.0014
10/17/2009	0.0019	0.0023	0.0024	0.0033
10/18/2009	0.0022	0.0024	0.0026	0.0025
10/19/2009	0.0023	0.0024	0.0024	0.0023
10/20/2009	0.0023	0.0025	0.0025	0.0024

Table C.2.8: Standard deviation of hourly HD measurements to the circular prism per day before atmospheric corrections - long distance monitoring.

Day Date	Std Dev of HD to Circular Prism without glass	Std Dev of HD to Circular Prism with glass @ 45°	Std Dev of HD to Circular Prism with glass @ 60°	Std Dev of HD to Circular Prism with glass @ 90°
10/6/2009	0.0018	0.0019	0.0020	0.0018
10/7/2009	0.0019	0.0020	0.0020	0.0020
10/8/2009	0.0025	0.0024	0.0025	0.0025
10/9/2009	0.0014	0.0015	0.0015	0.0016
10/10/2009	0.0016	0.0016	0.0016	0.0016
10/11/2009	0.0010	0.0010	0.0010	0.0010
10/12/2009	0.0019	0.0020	0.0019	0.0018
10/13/2009	0.0023	0.0023	0.0024	0.0023
10/14/2009	0.0020	0.0021	0.0020	0.0020
10/15/2009	0.0023	0.0021	0.0022	0.0021
10/16/2009	0.0012	0.0012	0.0012	0.0012
10/17/2009	0.0018	0.0017	0.0019	0.0018
10/18/2009	0.0020	0.0021	0.0021	0.0021
10/19/2009	0.0024	0.0026	0.0026	0.0024
10/20/2009	0.0023	0.0023	0.0023	0.0022

Table C.2.9: Standard deviation of hourly HD measurements to the sticker prism per day before atmospheric corrections - long distance monitoring.

Day Date	Std Dev of HD to Sticker without glass	Std Dev of HD to Sticker with glass @ 60°
10/6/2009	0.0019	0.0017
10/7/2009	0.0016	0.0022
10/8/2009	0.0024	0.0028
10/9/2009	0.0012	0.0019
10/10/2009	0.0013	0.0013
10/11/2009	0.0011	0.0017
10/12/2009	0.0018	0.0019
10/13/2009	0.0027	0.0025
10/14/2009	0.0018	0.0021
10/15/2009	0.0020	0.0021
10/16/2009	0.0016	0.0014
10/17/2009	0.0021	0.0024
10/18/2009	0.0028	0.0023
10/19/2009	0.0029	0.0027
10/20/2009	0.0027	0.0021

Standard deviation of daily HD measurements corrected for prism constant, scale factors and atmospheric variations corrections - long distance monitoring.

Table C.2.10: Standard deviation of hourly HD measurements to the mini prism per day after atmospheric corrections - long distance monitoring.

Day Date	Std Dev of HD to Mini Prism without glass	Std Dev of HD to Mini Prism with glass @ 45°	Std Dev of HD to Mini Prism with glass @ 60°	Std Dev of HD to Mini Prism with glass @ 90°
10/6/2009	0.0007	0.0006	0.0008	0.0007
10/7/2009	0.0009	0.0007	0.0007	0.0009
10/8/2009	0.0008	0.0008	0.0009	0.0008
10/9/2009	0.0005	0.0006	0.0007	0.0007
10/10/2009	0.0004	0.0003	0.0003	0.0004
10/11/2009	0.0002	0.0003	0.0002	0.0003
10/12/2009	0.0004	0.0004	0.0004	0.0004
10/13/2009	0.0008	0.0009	0.0009	0.0008
10/14/2009	0.0005	0.0006	0.0006	0.0005
10/15/2009	0.0006	0.0007	0.0007	0.0005
10/16/2009	0.0004	0.0005	0.0004	0.0004
10/17/2009	0.0007	0.0009	0.0006	0.0005
10/18/2009	0.0004	0.0006	0.0008	0.0007
10/19/2009	0.0006	0.0009	0.0007	0.0007
10/20/2009	0.0005	0.0008	0.0007	0.0006

Table C.2.11: Standard deviation of hourly HD measurements to the circular prism per day after atmospheric corrections - long distance monitoring.

Day Date	Std Dev of HD to Circular Prism without glass	Std Dev of HD to Circular Prism with glass @ 45°	Std Dev of HD to Circular Prism with glass @ 60°	Std Dev of HD to Circular Prism with glass @ 90°
10/6/2009	0.0005	0.0006	0.0006	0.0005
10/7/2009	0.0003	0.0005	0.0005	0.0005
10/8/2009	0.0005	0.0005	0.0006	0.0005
10/9/2009	0.0004	0.0004	0.0003	0.0004
10/10/2009	0.0006	0.0004	0.0004	0.0004
10/11/2009	0.0003	0.0003	0.0004	0.0003
10/12/2009	0.0003	0.0004	0.0003	0.0003
10/13/2009	0.0005	0.0005	0.0006	0.0006
10/14/2009	0.0004	0.0004	0.0004	0.0004
10/15/2009	0.0004	0.0004	0.0003	0.0003
10/16/2009	0.0003	0.0004	0.0003	0.0004
10/17/2009	0.0007	0.0005	0.0009	0.0007
10/18/2009	0.0002	0.0003	0.0003	0.0003
10/19/2009	0.0005	0.0006	0.0005	0.0005
10/20/2009	0.0006	0.0005	0.0006	0.0004

Table C.2.12: Standard deviation of hourly HD measurements to the sticker prism per day after atmospheric corrections - long distance monitoring.

Day Date	Std Dev of HD to Sticker without glass	Std Dev of HD to Sticker with glass @ 60°
10/6/2009	0.0007	0.0012
10/7/2009	0.0008	0.0010
10/8/2009	0.0007	0.0009
10/9/2009	0.0004	0.0009
10/10/2009	0.0008	0.0010
10/11/2009	0.0003	0.0013
10/12/2009	0.0005	0.0010
10/13/2009	0.0008	0.0010
10/14/2009	0.0008	0.0011
10/15/2009	0.0011	0.0009
10/16/2009	0.0010	0.0008
10/17/2009	0.0013	0.0017
10/18/2009	0.0013	0.0021
10/19/2009	0.0009	0.0019
10/20/2009	0.0010	0.0012

Standard deviation of daily VD measurements corrected for prism constant and scale factors but not corrected for atmospheric variation - short distance monitoring.

Table C.2.13: Standard deviation of hourly VD measurements to the mini prism per day before atmospheric corrections - short distance monitoring.

Day Date	Std Dev of VD to Mini Prism without glass	Std Dev of VD to Mini Prism with glass @ 45°	Std Dev of VD to Mini Prism with glass @ 60°	Std Dev of VD to Mini Prism with glass @ 90°
8/29/2009	0.0004	0.0008	0.0005	0.0008
8/30/2009	0.0010	0.0010	0.0009	0.0009
8/31/2009	0.0012	0.0013	0.0011	0.0013
9/1/2009	0.0008	0.0009	0.0009	0.0007
9/2/2009	0.0010	0.0013	0.0011	0.0011
9/3/2009	0.0009	0.0013	0.0012	0.0011
9/4/2009	0.0009	0.0014	0.0013	0.0013
9/5/2009	0.0009	0.0012	0.0009	0.0010
9/6/2009	0.0008	0.0008	0.0008	0.0010
9/7/2009	0.0019	0.0017	0.0017	0.0017
9/8/2009	0.0016	0.0013	0.0017	0.0014
9/9/2009	0.0015	0.0011	0.0011	0.0009
9/10/2009	0.0014	0.0014	0.0015	NM
9/11/2009	0.0015	0.0013	0.0013	NM
9/12/2009	0.0009	0.0013	0.0013	NM

Table C.2.14: Standard deviation of hourly VD measurements to the circular prism per day before atmospheric corrections - short distance monitoring.

Day Date	Std Dev of VD to Circular prism without glass	Std Dev of VD to Circular prism with glass @ 45°	Std Dev of VD to Circular prism with glass @ 60°	Std Dev of VD to Circular prism with glass @ 90°
8/29/2009	0.0009	0.0009	0.0010	0.0009
8/30/2009	0.0010	0.0012	0.0008	0.0010
8/31/2009	0.0011	0.0017	0.0012	0.0013
9/1/2009	0.0014	0.0013	0.0013	0.0015
9/2/2009	0.0010	0.0010	0.0011	0.0009
9/3/2009	0.0006	0.0009	0.0007	0.0007
9/4/2009	0.0013	0.0012	0.0013	0.0011
9/5/2009	0.0011	0.0012	0.0012	0.0012
9/6/2009	0.0010	0.0009	0.0010	0.0011
9/7/2009	0.0012	0.0014	0.0013	0.0016
9/8/2009	0.0014	0.0013	0.0011	0.0010
9/9/2009	0.0015	0.0014	0.0012	0.0010
9/10/2009	0.0011	0.0016	0.0015	NM
9/11/2009	0.0013	0.0013	0.0014	NM
9/12/2009	0.0014	0.0011	0.0015	NM

Table C.2.15: Standard deviation of hourly VD measurements to the sticker per day before atmospheric corrections during - distance monitoring.

Day Date	Std Dev of VD to Sticker without glass	Std Dev of VD to Sticker with glass @ 45°	Std Dev of VD to Sticker with glass @ 60°	Std Dev of VD to Sticker with glass @ 90°
8/29/2009	0.0009	0.0010	0.0011	0.0014
8/30/2009	0.0009	0.0013	0.0010	0.0010
8/31/2009	0.0008	0.0022	0.0021	0.0012
9/1/2009	0.0008	0.0010	0.0011	0.0012
9/2/2009	0.0013	0.0015	0.0015	0.0016
9/3/2009	0.0008	0.0013	0.0013	0.0009
9/4/2009	0.0009	0.0014	0.0020	0.0012
9/5/2009	0.0007	0.0007	0.0007	0.0005
9/6/2009	0.0010	0.0013	0.0014	0.0011
9/7/2009	0.0020	0.0021	0.0020	0.0021
9/8/2009	0.0024	0.0019	0.0016	0.0019
9/9/2009	0.0020	0.0015	0.0011	0.0023
9/10/2009	0.0018	0.0018	0.0020	NM
9/11/2009	0.0014	0.0010	0.0016	NM
9/12/2009	0.0013	0.0010	0.0015	NM

Standard deviation of daily VD measurements corrected for prism constant, scale factors and atmospheric variations corrections - short distance monitoring.

Table C.2.16: Standard deviation of hourly VD measurements to the mini prism per day after atmospheric corrections - short distance monitoring.

Day Date	Std Dev of VD to Mini Prism without glass	Std Dev of VD to Mini Prism with glass @ 45°	Std Dev of VD to Mini Prism with glass @ 60°	Std Dev of VD to Mini Prism with glass @ 90°
8/29/2009	0.0004	0.0008	0.0005	0.0008
8/30/2009	0.0010	0.0010	0.0009	0.0009
8/31/2009	0.0011	0.0012	0.0011	0.0013
9/1/2009	0.0008	0.0009	0.0009	0.0007
9/2/2009	0.0010	0.0013	0.0011	0.0011
9/3/2009	0.0008	0.0012	0.0011	0.0011
9/4/2009	0.0009	0.0014	0.0013	0.0013
9/5/2009	0.0008	0.0012	0.0009	0.0010
9/6/2009	0.0007	0.0008	0.0008	0.0009
9/7/2009	0.0018	0.0017	0.0017	0.0017
9/8/2009	0.0016	0.0013	0.0017	0.0014
9/9/2009	0.0015	0.0011	0.0011	0.0009
9/10/2009	0.0014	0.0014	0.0016	NM
9/11/2009	0.0015	0.0013	0.0013	NM
9/12/2009	0.0009	0.0013	0.0014	NM

Table C.2.17: Standard deviation of hourly VD measurements to the circular prism per day after atmospheric corrections - short distance monitoring.

Day Date	Std Dev of VD to Circular prism without glass	Std Dev of VD to Circular prism with glass @ 45°	Std Dev of VD to Circular prism with glass @ 60°	Std Dev of VD to Circular prism with glass @ 90°
8/29/2009	0.0009	0.0009	0.0010	0.0009
8/30/2009	0.0010	0.0012	0.0008	0.0010
8/31/2009	0.0011	0.0017	0.0012	0.0013
9/1/2009	0.0014	0.0013	0.0013	0.0015
9/2/2009	0.0010	0.0010	0.0011	0.0009
9/3/2009	0.0006	0.0009	0.0007	0.0007
9/4/2009	0.0013	0.0012	0.0013	0.0011
9/5/2009	0.0011	0.0012	0.0012	0.0012
9/6/2009	0.0010	0.0009	0.0010	0.0011
9/7/2009	0.0012	0.0014	0.0013	0.0016
9/8/2009	0.0014	0.0013	0.0011	0.0010
9/9/2009	0.0015	0.0014	0.0012	0.0010
9/10/2009	0.0011	0.0016	0.0015	NM
9/11/2009	0.0013	0.0013	0.0014	NM
9/12/2009	0.0014	0.0011	0.0015	NM

Table C.2.18: Standard deviation of hourly VD measurements to the sticker per day after atmospheric corrections - short distance monitoring.

Day Date	Std Dev of VD to Sticker without glass	Std Dev of VD to Sticker with glass @ 45°	Std Dev of VD to Sticker with glass @ 60°	Std Dev of VD to Sticker with glass @ 90°
8/29/2009	0.0009	0.0010	0.0011	0.0014
8/30/2009	0.0009	0.0013	0.0010	0.0010
8/31/2009	0.0008	0.0022	0.0021	0.0012
9/1/2009	0.0008	0.0010	0.0011	0.0012
9/2/2009	0.0013	0.0015	0.0015	0.0016
9/3/2009	0.0008	0.0013	0.0013	0.0009
9/4/2009	0.0009	0.0014	0.0020	0.0012
9/5/2009	0.0007	0.0007	0.0007	0.0005
9/6/2009	0.0010	0.0013	0.0014	0.0011
9/7/2009	0.0020	0.0021	0.0020	0.0021
9/8/2009	0.0024	0.0019	0.0016	0.0019
9/9/2009	0.0020	0.0015	0.0011	0.0023
9/10/2009	0.0018	0.0018	0.0020	NM
9/11/2009	0.0014	0.0010	0.0016	NM
9/12/2009	0.0013	0.0010	0.0015	NM

Standard deviation of daily VD measurements corrected for prism constant and scale factors but not corrected for atmospheric variation - long distance monitoring.

Table C.2.19: Standard deviation of hourly VD measurements to the mini prism per day before atmospheric corrections - long distance monitoring.

Day Date	Std Dev of VD to Mini Prism without glass	Std Dev of VD to Mini Prism with glass @ 45°	Std Dev of VD to Mini Prism with glass @ 60°	Std Dev of VD to Mini Prism with glass @ 90°
10/6/2009	0.0011	0.0008	0.0010	0.0010
10/7/2009	0.0011	0.0011	0.0009	0.0010
10/8/2009	0.0013	0.0013	0.0011	0.0012
10/9/2009	0.0010	0.0010	0.0011	0.0010
10/10/2009	0.0012	0.0012	0.0008	0.0010
10/11/2009	0.0013	0.0010	0.0011	0.0009
10/12/2009	0.0012	0.0012	0.0010	0.0012
10/13/2009	0.0010	0.0010	0.0010	0.0011
10/14/2009	0.0011	0.0011	0.0011	0.0011
10/15/2009	0.0011	0.0007	0.0008	0.0009
10/16/2009	0.0012	0.0010	0.0012	0.0012
10/17/2009	0.0009	0.0009	0.0011	0.0009
10/18/2009	0.0011	0.0011	0.0011	0.0012
10/19/2009	0.0010	0.0009	0.0010	0.0010
10/20/2009	0.0011	0.0011	0.0010	0.0011

Table C.2.20: Standard deviation of hourly VD measurements to the circular prism per day before atmospheric corrections - long distance monitoring.

Day Date	Std Dev of VD to Circular Prism without glass	Std Dev of VD to Circular prism with glass @ 45°	Std Dev of VD to Circular prism with glass @ 60°	Std Dev of VD to Circular prism with glass @ 90°
10/6/2009	0.0013	0.0009	0.0011	0.0010
10/7/2009	0.0011	0.0011	0.0011	0.0011
10/8/2009	0.0011	0.0010	0.0011	0.0012
10/9/2009	0.0010	0.0010	0.0010	0.0010
10/10/2009	0.0012	0.0008	0.0012	0.0010
10/11/2009	0.0011	0.0010	0.0011	0.0011
10/12/2009	0.0013	0.0013	0.0013	0.0013
10/13/2009	0.0010	0.0010	0.0010	0.0012
10/14/2009	0.0010	0.0009	0.0010	0.0010
10/15/2009	0.0010	0.0010	0.0011	0.0010
10/16/2009	0.0013	0.0012	0.0011	0.0012
10/17/2009	0.0008	0.0008	0.0010	0.0008
10/18/2009	0.0010	0.0009	0.0010	0.0010
10/19/2009	0.0009	0.0011	0.0010	0.0010
10/20/2009	0.0012	0.0011	0.0012	0.0012

Table C.2.21: Standard deviation of hourly VD measurements to the sticker per day before atmospheric corrections - long distance monitoring.

Day Date	Std Dev of VD to Sticker without glass	Std Dev of VD to Sticker with glass @ 60°
10/6/2009	0.0071	0.0079
10/7/2009	0.0091	0.009
10/8/2009	0.0096	0.0065
10/9/2009	0.0069	0.0087
10/10/2009	0.0022	0.0074
10/11/2009	0.0039	0.0052
10/12/2009	0.0023	0.0041
10/13/2009	0.0027	0.0037
10/14/2009	0.0023	0.003
10/15/2009	0.0035	0.0097
10/16/2009	0.0035	0.0043
10/17/2009	0.0037	0.0046
10/18/2009	0.0031	0.0043
10/19/2009	0.0037	0.0037
10/20/2009	0.0041	0.0049

Standard deviation of daily VD measurements corrected for prism constant, scale factors and atmospheric variations corrections - long distance monitoring.

Table C.2.22: Standard deviation of hourly VD measurements to the mini prism per day after atmospheric corrections - long distance monitoring.

Day Date	Std Dev of VD to Mini Prism without glass	Std Dev of VD to Mini Prism with glass @ 45°	Std Dev of VD to Mini Prism with glass @ 60°	Std Dev of VD to Mini Prism with glass @ 90°
10/6/2009	0.0011	0.0008	0.0010	0.0010
10/7/2009	0.0011	0.0011	0.0009	0.0010
10/8/2009	0.0013	0.0013	0.0011	0.0012
10/9/2009	0.0010	0.0010	0.0011	0.0010
10/10/2009	0.0012	0.0012	0.0008	0.0010
10/11/2009	0.0013	0.0010	0.0011	0.0009
10/12/2009	0.0012	0.0012	0.0010	0.0012
10/13/2009	0.0010	0.0010	0.0010	0.0011
10/14/2009	0.0011	0.0011	0.0011	0.0011
10/15/2009	0.0011	0.0007	0.0008	0.0009
10/16/2009	0.0012	0.0010	0.0012	0.0012
10/17/2009	0.0009	0.0009	0.0011	0.0009
10/18/2009	0.0011	0.0011	0.0011	0.0012
10/19/2009	0.0010	0.0009	0.0010	0.0010
10/20/2009	0.0011	0.0011	0.0010	0.0011

Table C.2.23: Standard deviation of hourly VD measurements to the circular prism per day after atmospheric corrections - long distance monitoring.

Day Date	Std Dev of VD to Circular Prism without glass	Std Dev of VD to Circular prism with glass @ 45°	Std Dev of VD to Circular prism with glass @ 60°	Std Dev of VD to Circular prism with glass @ 90°
10/6/2009	0.0013	0.0009	0.0011	0.0010
10/7/2009	0.0011	0.0011	0.0011	0.0011
10/8/2009	0.0011	0.0010	0.0011	0.0012
10/9/2009	0.0010	0.0010	0.0010	0.0010
10/10/2009	0.0012	0.0008	0.0012	0.0010
10/11/2009	0.0011	0.0010	0.0011	0.0011
10/12/2009	0.0013	0.0013	0.0013	0.0013
10/13/2009	0.0010	0.0010	0.0010	0.0012
10/14/2009	0.0010	0.0009	0.0010	0.0010
10/15/2009	0.0010	0.0010	0.0011	0.0010
10/16/2009	0.0013	0.0012	0.0011	0.0012
10/17/2009	0.0008	0.0008	0.0010	0.0008
10/18/2009	0.0010	0.0009	0.0010	0.0010
10/19/2009	0.0009	0.0011	0.0010	0.0010
10/20/2009	0.0012	0.0011	0.0012	0.0012

Table C.2.24: Standard deviation of hourly VD measurements to the sticker per day after atmospheric corrections - long distance monitoring.

Day Date	Std Dev of VD to Sticker without glass	Std Dev of VD to Sticker with glass @ 60°
10/6/2009	0.0071	0.0079
10/7/2009	0.0091	0.009
10/8/2009	0.0096	0.0065
10/9/2009	0.0069	0.0087
10/10/2009	0.0022	0.0074
10/11/2009	0.0039	0.0052
10/12/2009	0.0023	0.0041
10/13/2009	0.0027	0.0037
10/14/2009	0.0023	0.003
10/15/2009	0.0035	0.0097
10/16/2009	0.0035	0.0043
10/17/2009	0.0037	0.0046
10/18/2009	0.0031	0.0043
10/19/2009	0.0037	0.0037
10/20/2009	0.0041	0.0049

Appendix C.4

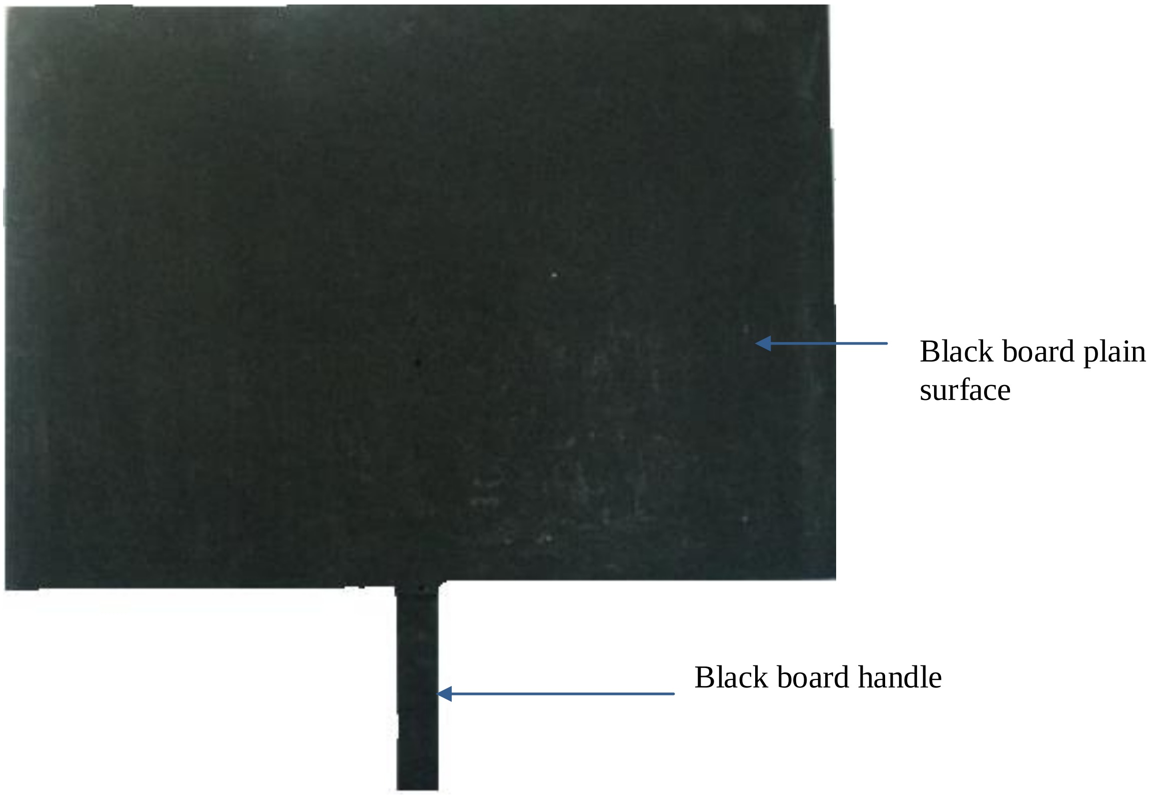

Figure C.4.1: Picture of black board

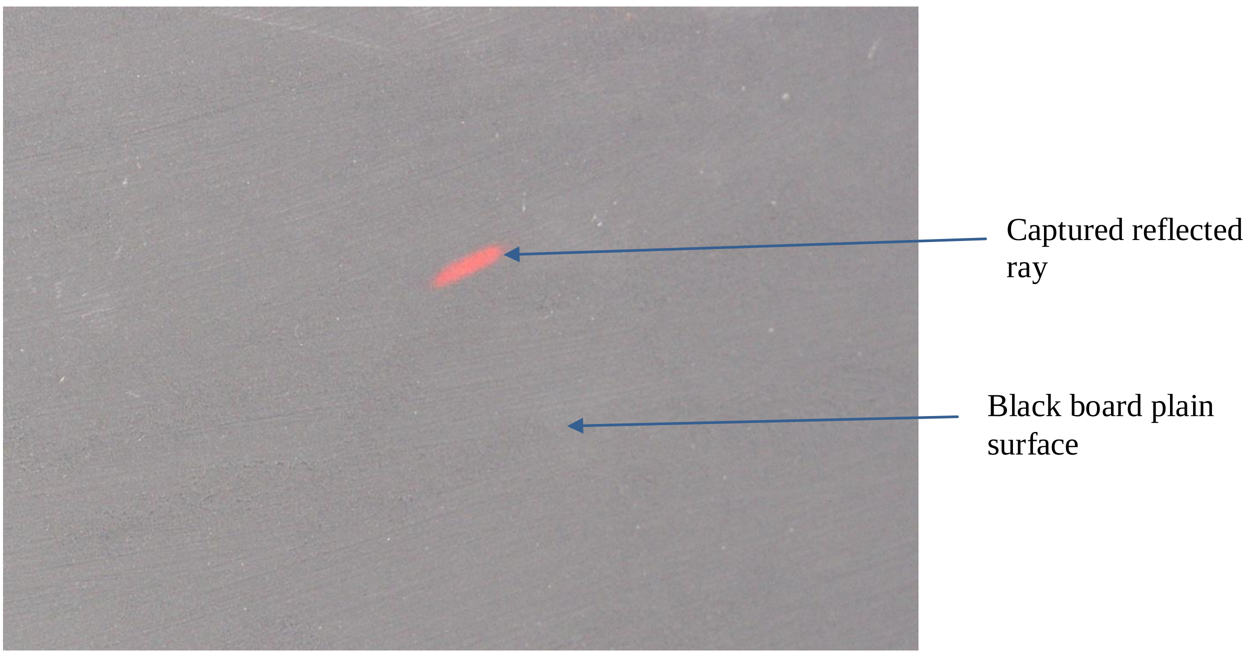

Figure C.4.2: Picture of reflected ray captured on a black board

Table C. 3: Summary of distance variations during short- and long-distance monitoring

Glass Thickness (mm)	Target	Type of Distance	Range before atmospheric correction (mm)	Range after atmospheric correction (mm)	Deviation (mm)	Monitoring type
2.0	Mini prism	HD	1.00 and 1.20	1.00 and 1.20	0.20	Short distance
3.0			1.40 and 1.70	1.40 and 1.70	0.30	
4.0			2.00 and 2.40	2.00 and 2.40	0.40	
5.0			1.90 and 2.30	1.90 and 2.30	0.40	
6.38			2.90 and 3.50	2.90 and 3.50	0.60	
2.0	Circular prism	HD	1.00 and 1.30	1.00 and 1.30	0.30	Short distance
3.0			1.40 and 1.80	1.40 and 1.80	0.40	
4.0			1.90 and 2.30	1.90 and 2.30	0.40	
5.0			1.60 and 2.50	1.60 and 2.50	0.90	
6.38			2.40 and 3.10	2.40 and 3.10	0.70	
2.0	Sticker	HD	0.90 and 1.80	0.90 and 1.80	0.90	Short distance
3.0			3.60 and 4.10	3.60 and 4.10	0.50	
4.0			1.80 and 4.20	1.80 and 4.20	2.40	
5.0			2.20 and 4.60	2.20 and 4.60	2.40	
6.38			3.50 and 5.40	3.50 and 5.40	1.90	
2.0	Mini prism	HD	0.90 and 1.30	0.90 and 1.30	0.40	Long distance
3.0			1.50 and 1.90	1.50 and 1.90	0.40	
4.0			2.10 and 2.70	2.10 and 2.70	0.60	
5.0			3.10 and 4.50	3.10 and 4.50	1.40	
6.38			3.20 and 4.20	3.20 and 4.20	1.00	
2.0	Circular prism	HD	0.80 and 1.20	0.80 and 1.20	0.40	Long distance
3.0			1.30 and 1.80	1.30 and 1.80	0.50	
4.0			1.90 and 2.40	1.90 and 2.40	0.50	
5.0			2.60 and 3.30	2.60 and 3.30	0.70	
6.38			3.10 and 4.30	3.10 and 4.30	1.20	
2.0	Sticker	HD	1.20 and 1.30	1.20 and 1.30	0.10	Long distance
3.0			1.40 and 1.70	1.40 and 1.70	0.30	
4.0			1.20 and 2.50	1.20 and 2.50	1.30	
5.0			2.70 and 4.90	2.70 and 4.90	2.20	
6.38			3.50 and 9.00	3.50 and 9.00	4.50	
2.0	Mini prism	VD	-0.60 and 0.20	-0.60 and 0.20	0.80	Short distance
3.0			-0.40 and 0.10	-0.40 and 0.10	0.50	
4.0			-1.10 and -0.20	-1.10 and -0.20	0.90	
5.0			-3.20 and -2.50	-3.20 and -2.50	0.70	
6.38			-2.20 and -1.40	-2.20 and -1.40	0.80	
2.0	Circular prism	VD	-1.00 and 0.00	-1.00 and 0.00	1.00	Short distance
3.0			-0.70 and 0.10	-0.70 and 0.10	0.80	
4.0			-3.50 and 1.10	-3.50 and 1.10	4.60	
5.0			-3.30 and -1.90	-3.30 and -1.90	1.40	
6.38			-4.10 and -0.60	-4.10 and -0.60	3.50	

Table C.3: Summary of distance variations during short- and long-distance monitoring continue……

Glass Thickness (mm)	Target	Type of Distance	Range before atmospheric correction (mm)	Range after atmospheric correction (mm)	Deviation (mm)	Monitoring type
2.0	Sticker	VD	-0.40 and 0.20	-0.40 and 0.20	0.60	Short distance
3.0			-1.40 and -0.40	-1.40 and -0.40	1.00	
4.0			-1.30 and -0.30	-1.30 and -0.30	1.00	
5.0			-2.70 and -0.20	-2.70 and -0.20	2.50	
6.38			-2.50 and -0.90	-2.50 and -0.90	1.60	
2.0	Mini prism	VD	0.10 and 13.60	0.10 and 13.60	13.50	Long distance
3.0			-8.30 and 7.50	-8.30 and 7.50	15.80	
4.0			1.10 and 7.40	1.10 and 7.40	6.30	
5.0			-1.90 and 0.00	-1.90 and 0.00	1.90	
6.38			-1.30 and 1.00	-1.30 and 1.00	2.30	
2.0	Circular prism	VD	-11.20 and -4.50	-11.20 and -4.50	6.70	Long distance
3.0			-7.70 and 5.80	-7.70 and 5.80	13.50	
4.0			-2.20 and 1.30	-2.20 and 1.30	3.50	
5.0			-1.30 and 1.50	-1.30 and 1.50	2.80	
6.38			-2.50 and 1.60	-2.50 and 1.60	4.10	
2.0	Sticker	VD	-12.70 and 2.70	-12.70 and 2.70	15.40	Long distance
3.0			-9.60 and -3.00	-9.60 and -3.00	6.60	
4.0			-1.00 and 1.10	-1.00 and 1.10	2.10	
5.0			-1.80 and 0.20	-1.80 and 0.20	2.00	
6.38			-1.00 and 3.10	-1.00 and 3.10	4.10	

Table C. 4: Summary of angular variations during short- and long-distance monitoring

Glass Thickness (mm)	Target	Type of angle	Angular constant	Deviation range (“)	Monitoring type
2.0	Mini prism	Hz	$290^o00'$	-01 to 00	Short distance
3.0				-01 to 00	
4.0				00 to 01	
5.0				-05 to 01	
6.38				-09 to 01	
2.0	Circular prism	Hz	$290^o00'$	-01 to 00	Short distance
3.0				-01 to 00	
4.0				-01 to 01	
5.0				-05 to -01	
6.38				-09 to 01	
2.0	Sticker	Hz	$290^o00'$	-01 to 00	Short distance
3.0				-01 to 00	
4.0				-01 to 01	
5.0				-02 to 01	
6.38				-09 to 01	
2.0	Mini prism	Hz	$257^o04'$	-05 to 00	Long distance
3.0				00 to 02	
4.0				00 to 01	
5.0				-01 to 00	
6.38				-01 to 00	
2.0	Circular prism	Hz	$257^o04'$	-05 to 00	Long distance
3.0				00 to 02	
4.0				00	
5.0				-01 to 00	
6.38				00	
2.0	Sticker	Hz	$257^o04'$	-03 to -01	Long distance
3.0				03 to 04	
4.0				00	
5.0				00	
6.38				00	
2.0	Mini prism	V	$-16^o00'$	-01 to 03	Short distance
3.0				-02 to 01	
4.0				-02 to 02	
5.0				05 to 10	
6.38				03 to 07	
2.0	Circular prism	V	$-16^o38'$	-01 to 00	Short distance
3.0				-02 to 01	
4.0				-01 to 01	
5.0				05 to 14	
6.38				02 to 12	

Table C.4: Summary of angular variations during short- and long-distance monitoring continued

Glass Thickness (mm)	Target	Type of angle	Angular constant	Deviation range (“)	Monitoring type
2.0	Sticker	V	-17°14’	-04 to 01	Short distance
3.0				-03 to 01	
4.0				-01 to 01	
5.0				-04 to 06	
6.38				01 to 06	
2.0	Mini prism	V	-02°07’	-04 to 00	Long distance
3.0				-01 to 03	
4.0				-01 to 00	
5.0				-01 to 01	
6.38				00	
2.0	Circular prism	V	-02°10’	-01 to 00	Long distance
3.0				-01 to 00	
4.0				-01 to 01	
5.0				-01 to 01	
6.38				-01 to 00	
2.0	Sticker	V	-02°13’	-01 to 01	Long distance
3.0				00 to 01	
4.0				00 to 01	
5.0				-01 to 00	
6.38				00	

APPENDIX E

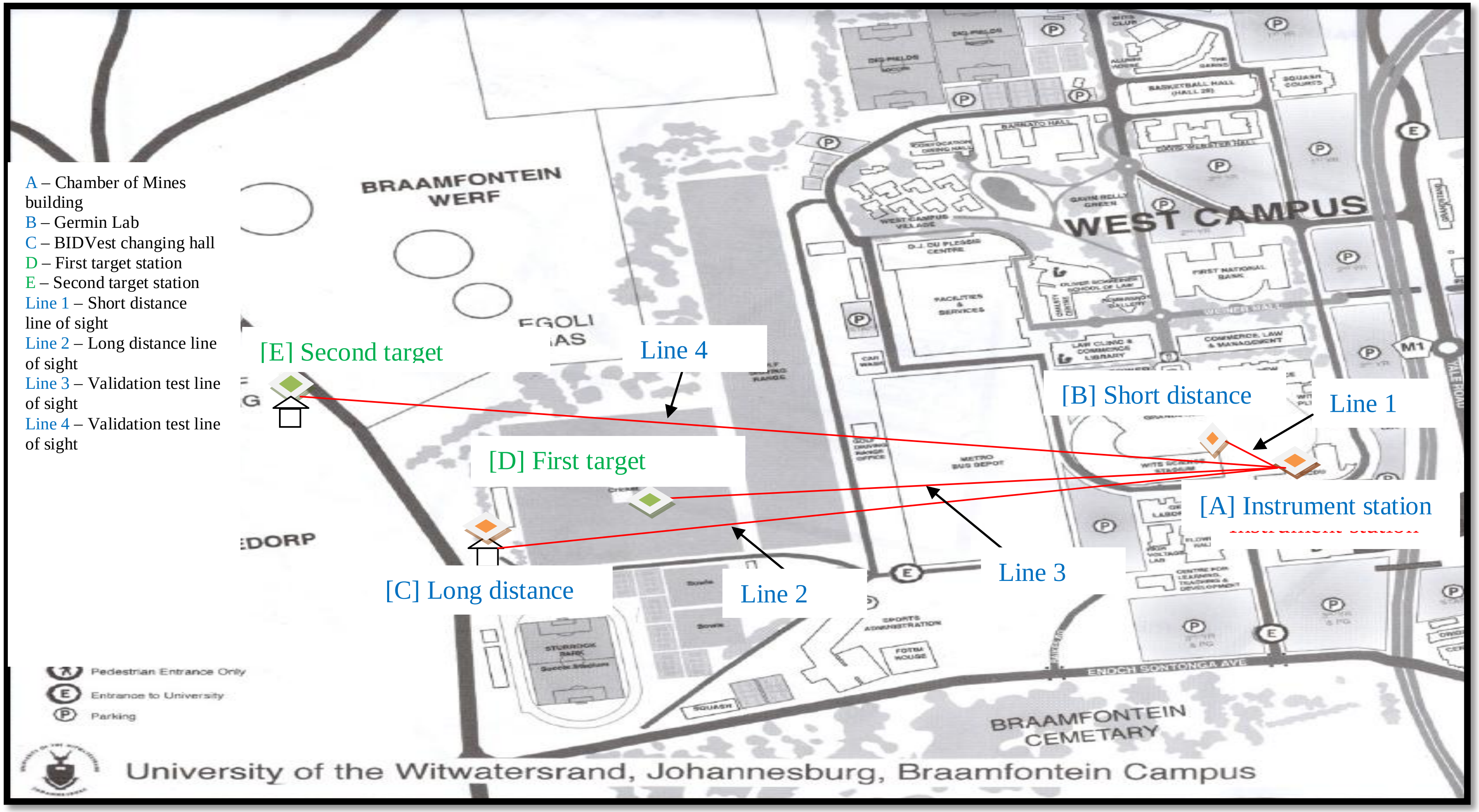

Figure E.1: Map showing campus observation stations and the two new target positions used for validation tests (adapted from WITs map)

Appendix E.2

<u>Instructions on Software Usage</u>

1. There are two ways of inputting data onto the software; the first is the normal way of inputting data **manually** to calculate a single distance correction. The other way is to import/read a file onto the software.

2. It should be noted that the imported file should follow the exact same structure as the attached file (**DataSample.xls**). In other words the text on cell A2 should always be a **date**, the text/number on cell A3 should always be **thickness** typed in the exact same manner (i.e. ##.## mm, there should be a space between a number and ***mm***). The date must always be followed by a distance, temperature, pressure and humidity (in that order). See appendix E.2.1.

3. The imported file should always be an "xls" file not an "xlsx" file. which means that the file should always be in "***Compatibility Mode***" (i.e. Excel 97-2003).

4. It should be ensured that in order for the software to read the value of "No glass" entry, the number on the time column should always be in the form "#.00" (i.e. a number should always be followed by '.00') . Any other text on this field should be removed and one should not put texts like 'Ng' in front to identify no glass. The software already knows by reading the '.00' input.

5. Every 'No Glass' entry should be followed by at least 'one' glass entry. This procedure must be standard. In other words, if one has 2 glass entries (example, 45° & 60°), the same should apply for the rest of the other 'no glass' entries with the same names. For example, in the attached file (**DataSample.xls**), every 'no glass' entry is followed by 4 glass entries and they are standard (i.e. 90°, 60°, 45°, 30°). The sample of DataSample.xls Microsoft Excel format is shown in appendix D.1.1 below.

6. The software can work on raw distance readings collected without glass barrier or with glass barrier at any angle.

7. Finally, the software assumes prism constant and scale factor correction has been performed by the total station or the operator on the distance readings before subjecting it to *Agcomo*.

Appendix E.2.1: Sample of Microsoft Excel import, read and plot file

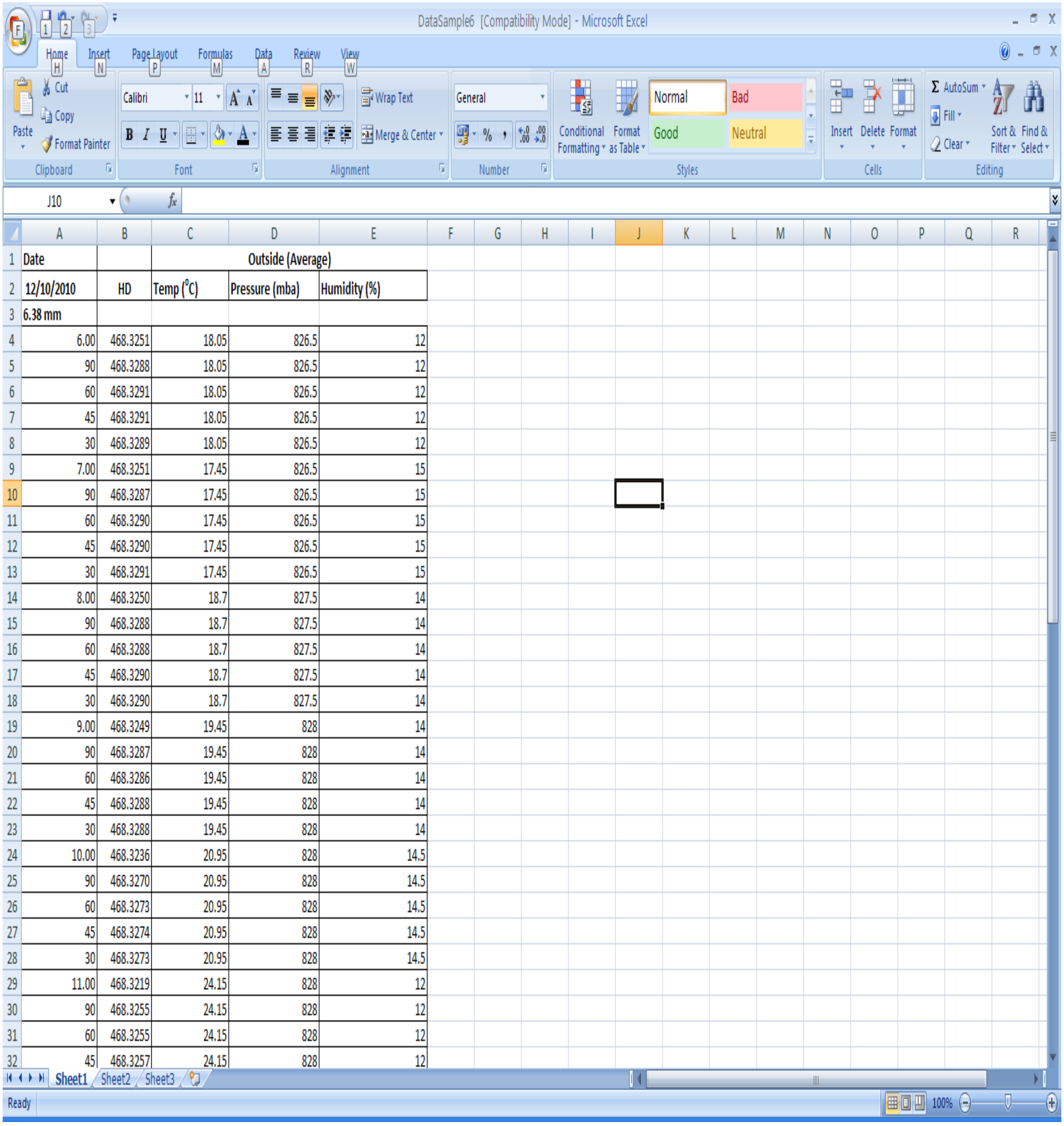

A	B	C	D	E
Date		Outside (Average)		
12/10/2010	HD	Temp (^{o}C)	Pressure (mba)	Humidity (%)
6.38 mm				
6.00	468.3251	18.05	826.5	12
90	468.3288	18.05	826.5	12
60	468.3291	18.05	826.5	12
45	468.3291	18.05	826.5	12
30	468.3289	18.05	826.5	12
7.00	468.3251	17.45	826.5	15
90	468.3287	17.45	826.5	15
60	468.3290	17.45	826.5	15
45	468.3290	17.45	826.5	15
30	468.3291	17.45	826.5	15
8.00	468.3250	18.7	827.5	14
90	468.3288	18.7	827.5	14
60	468.3288	18.7	827.5	14
45	468.3290	18.7	827.5	14
30	468.3290	18.7	827.5	14
9.00	468.3249	19.45	828	14
90	468.3287	19.45	828	14
60	468.3286	19.45	828	14
45	468.3288	19.45	828	14
30	468.3288	19.45	828	14
10.00	468.3236	20.95	828	14.5
90	468.3270	20.95	828	14.5
60	468.3273	20.95	828	14.5
45	468.3274	20.95	828	14.5
30	468.3273	20.95	828	14.5
11.00	468.3219	24.15	828	12
90	468.3255	24.15	828	12
60	468.3255	24.15	828	12
45	468.3257	24.15	828	12

It should be noted that the software will not run if any of the above instructions is violated. One should always sure that one has to check meticulously.

Table E.1: Raw HD readings captured on 12th October 2010

	Measured HD					Atmospheric parameters		
Date with Time	HD to Mini Prism without glass	HD to Mini Prism with 6.38 mm glass @ 30°	HD to Mini Prism with 6.38 mm glass @ 45°	HD to Mini Prism with 6.38 mm glass @ 60°	HD to Mini Prism with 6.38 mm glass @ 90°	Average Temperature °C	Average Pressure (mba)	Average Humidity (%)
2010/10/12 06:00	468.3251	468.3289	468.3291	468.3291	468.3288	18.05	826.50	12.00
2010/10/12 07:00	468.3251	468.3291	468.3290	468.3290	468.3287	17.45	826.50	12.00
2010/10/12 08:00	468.3250	468.3290	468.3290	468.3288	468.3288	18.45	827.50	14.00
2010/10/12 09:00	468.3249	468.3288	468.3288	468.3286	468.3287	19.45	828.00	14.00
2010/10/12 10:00	468.3236	468.3273	468.3274	468.3273	468.3270	20.95	828.00	14.50
2010/10/12 11:00	468.3219	468.3256	468.3257	468.3255	468.3255	24.15	828.00	12.00
2010/10/12 12:00	468.3212	468.3251	468.3252	468.3253	468.3250	25.70	828.00	10.00
2010/10/12 13:00	468.3206	468.3246	468.3243	468.3243	468.3245	27.20	827.00	8.50
2010/10/12 14:00	468.3204	468.3244	468.3243	468.3241	468.3241	28.50	827.00	7.50
2010/10/12 15:00	468.3195	468.3235	468.3232	468.3233	468.3232	30.05	827.00	7.00
2010/10/12 16:00	468.3201	468.3239	468.3240	468.3240	468.3239	28.50	827.00	7.50
2010/10/12 17:00	468.3203	468.3241	468.3243	468.3241	468.3242	27.95	827.00	7.50
2010/10/12 18:00	468.3216	468.3255	468.3254	468.3251	468.3251	26.75	827.00	8.50

Table E. 2: True HD readings captured on 12th October 2010 as calculated with *Agcomo* software

	HD after atmospheric and glass corrections				
Date with Time	**HD to Mini Prism without glass**	**HD to Mini Prism with 6.38 mm glass @ 30°**	**HD to Mini Prism with 6.38 mm glass @ 45°**	**HD to Mini Prism with 6.38 mm glass @ 60°**	**HD to Mini Prism with 6.38 mm glass @ 90°**
2010/10/12 06:00	468.3517	468.3517	468.3519	468.3519	468.3516
2010/10/12 07:00	468.3515	468.3517	468.3516	468.3516	468.3513
2010/10/12 08:00	468.3517	468.3519	468.3519	468.3517	468.3517
2010/10/12 09:00	468.3518	468.3519	468.3519	468.3517	468.3518
2010/10/12 10:00	468.3511	468.3510	468.3511	468.3510	468.3505
2010/10/12 11:00	468.3505	468.3504	468.3505	468.3503	468.3503
2010/10/12 12:00	468.3503	468.3504	468.3505	468.3506	468.3503
2010/10/12 13:00	468.3504	468.3505	468.3503	468.3503	468.3504
2010/10/12 14:00	468.3506	468.3508	468.3507	468.3505	468.3505
2010/10/12 15:00	468.3504	468.3506	468.3503	468.3504	468.3503
2010/10/12 16:00	468.3503	468.3503	468.3504	468.3504	468.3503
2010/10/12 17:00	468.3503	468.3503	468.3505	468.3503	468.3504
2010/10/12 18:00	468.3516	468.3517	468.3516	468.3513	468.3513

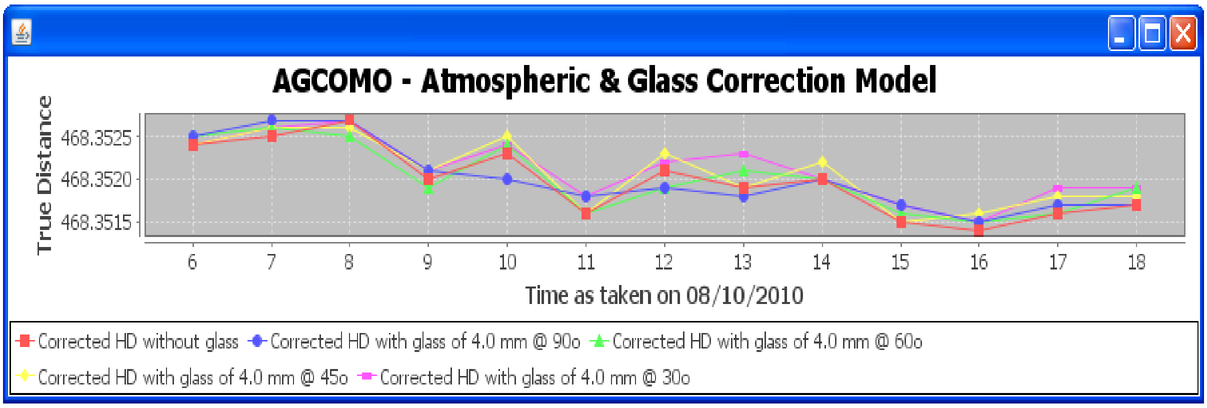

Figure E.2: Read from file and plot sample graph – transparent 4.0 mm glass

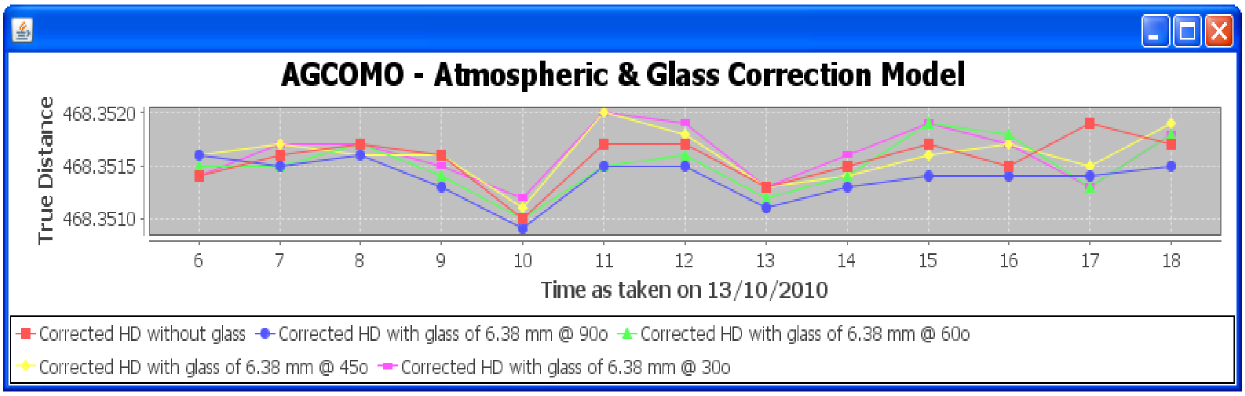

Figure E.3: Read from file and plot sample graph – transparent 6.38 mm glass

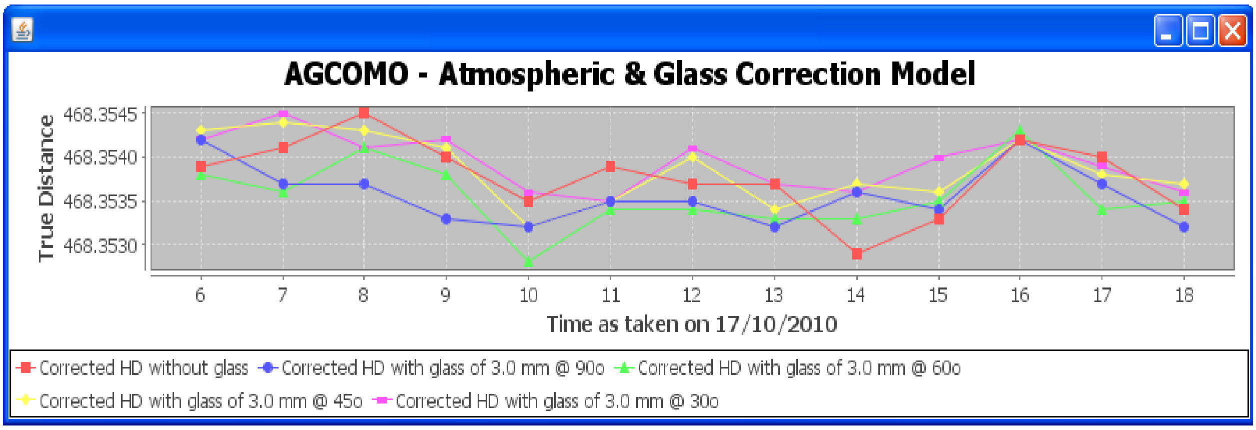

Figure E.4: Read from file and plot sample graph – dark-tinted 3.0 mm glass

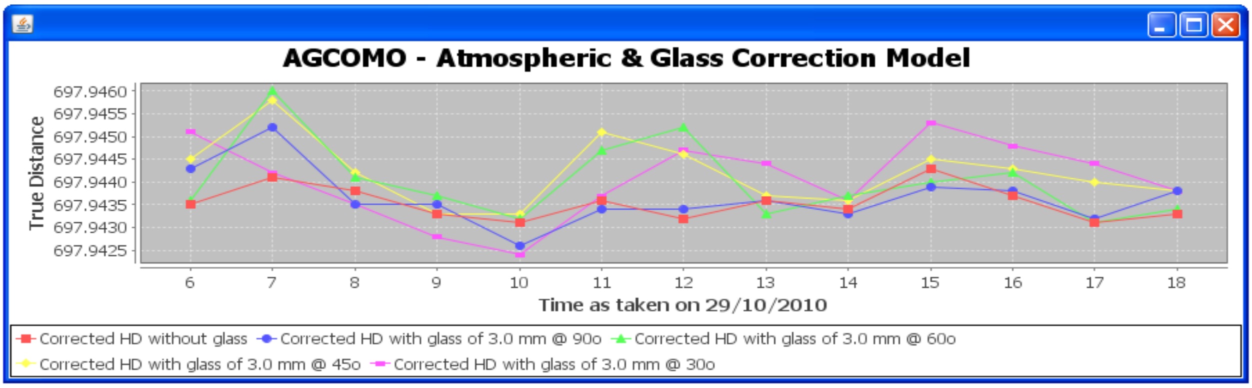

Figure E.5: Read from file and plot sample graph – light-tinted 3.0 mm glass